MULTI-SLICE COMPUTED TOMOGRAPHY OF CORONARY ARTERIES

Francesca Pugliese

ISBN:

Lay-out: Ton Everaers
Cover: Ton Everaers and Francesca Pugliese
Illustrations: Francesca Pugliese

Financial support by the Department of Radiology of Erasmus MC University Medical Centre Rotterdam, and by Bracco Diagnostics is gratefully acknowledged.

Printed by Ipskamp Print Partners

MULTI-SLICE COMPUTED TOMOGRAPHY OF CORONARY ARTERIES

MULTI-SLICE COMPUTER TOMOGRAFIE VAN DE KRANSSLAGADEREN

PROEFSCHRIFT

ter verkrijging van de graad van doctor aan de
Erasmus Universiteit Rotterdam
op gezag van de
rector magnificus

Prof. dr. S.W.J. Lamberts

en volgens besluit van het College voor Promoties

De openbare verededigingzal plaatvinden op
woensdag 29 Oktober 2008 om 09.45 uur

door

FRANCESCA PUGLIESE
geboren te Savona, Italië

ERASMUS UNIVERSITEIT ROTTERDAM

PROMOTIE COMMISSIE

Promotoren:

Prof. dr. G.P. Krestin

Prof. dr. P.J. de Feyter

Overige leden:

Prof. dr. M.G.M. Hunink

Prof. dr. D. Poldermans

Prof. dr. J.J. Bax

Co-promotor(en):

Dr. N.R. Mollet

Contents

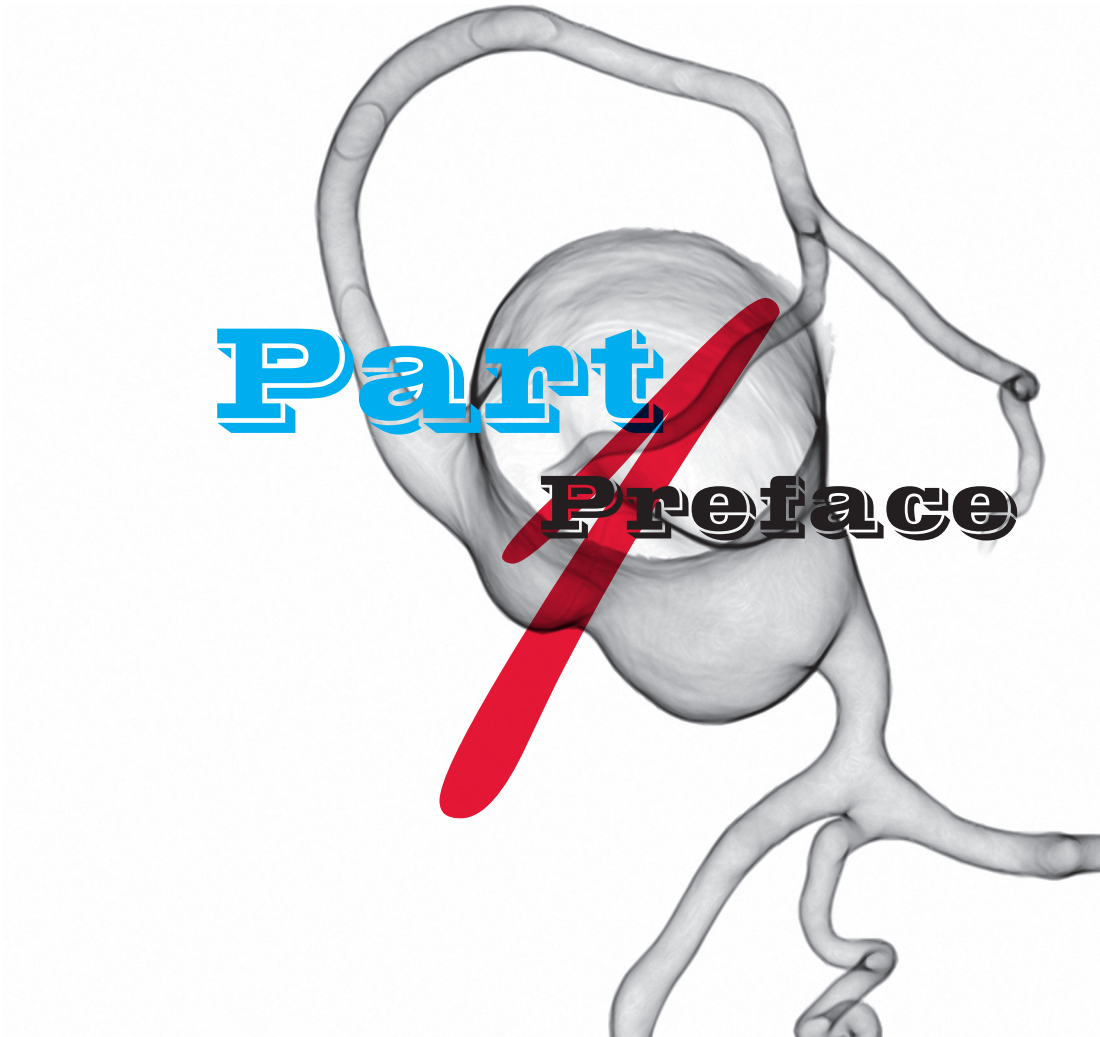

Part 1
Preface

CHAPTER 1

Introduction and thesis outline

Atherosclerosis is the number one cause of mortality in Western countries [1, 2]. Atherosclerosis is a progressive systemic disorder affecting large and medium-sized arteries. Although the atherosclerotic process starts in the 2nd and 3rd decades of life, symptoms do not usually occur during these early stages of disease. Decades later, when an atherosclerotic plaque causes an obstruction at the level of the coronary arteries which causes significant reduction of the oxygen supply to the heart, chest pain may occur. Chronic chest pain (angina pectoris) typically occurs during exercise or emotions when the higher oxygen demand of the heart is not matched by an increased supply. Chronic chest pain is relieved by a short period of rest or by the administration of nitrates. Advanced atherosclerotic lesions (e.g., plaques with a large necrotic core and a thin fibrous cap) may also rupture causing thrombus formation. As a result, diminished blood supply due to complete or partial blockage may cause acute myocardial infarction or sudden death.

Conventional coronary angiography, introduced in 1959, is still the reference technique for the evaluation of the coronary arteries. This technique requires the puncture of a peripheral artery, the advancement of a catheter towards the heart and selective injection of contrast agent into the coronary arteries. During this procedure, conventional x-ray images are obtained which display the lumen of coronary arteries. Catheter-based tech-

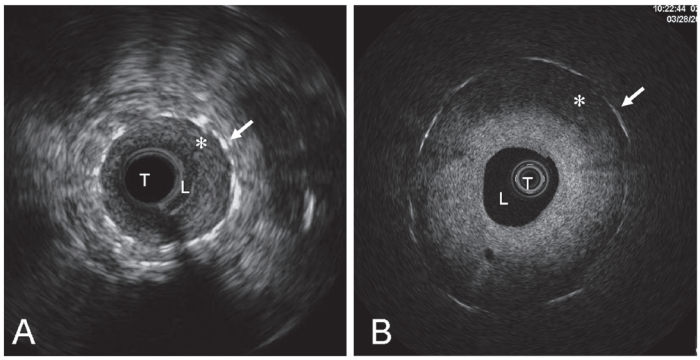

FIGURE 1 Catheter-based coronary artery imaging. Intravascular ultrasound (A) and optical coherence tomography (B) images in a patient with a coronary stent previously implanted in the left anterior descending artery show in-stent restenosis (asterisks). Arrows = stent struts. T = transducer; L = vessel lumen.

niques can be applied to determine the haemodynamic significance of coronary lesions (e.g., coronary flow velocity and pressure gradient measurement) and to assess the morphology of the vessel wall (e.g., intravascular ultrasound and optical coherence tomography - figure 1). Conventional angiography is however a costly technique and is associated with a small but not negligible risk of procedure-related complications [3, 4]. This prompted the development of techniques for the non-invasive visualization of coronary arteries.

Non-invasive imaging of the coronary arteries is technically very demanding. The lumen of clinically important coronary branches can be very small (2-4 mm) requiring a high spatial resolution. Heart contraction and breathing may cause significant motion artifacts which may be improved by the use of high temporal resolution techniques. Moreover, there needs to be synchronization of data acquisition with the electrocardiogram (ECG) in order to identify the phase of the cardiac cycle with the least amount of motion.

Several imaging modalities can be used to image coronary arteries non-invasively, e.g., electron-beam computed tomography (EBCT), magnetic resonance imaging (MRI) and multislice computed tomography (MSCT). Computed tomography (CT) was developed in the early '70 by G. Hounsfield and A. M. Mc Cormack, who were awarded the Nobel Prize in 1979. EBCT was the first CT scanner dedicated to cardiac imaging. EBCT has a high temporal resolution but a limited spatial resolution along the patient's longitudinal axis, which makes this technique suboptimal for the visualization of coronary arteries. Similarly, MRI has a high temporal resolution, but with current technology this modality is associated with relatively long acquisition times and limited spatial resolution. The feasibility of coronary artery imaging with CT depended on several further developments of the technology: spiral or helical CT was introduced in the early '90 by W.A. Kalender, which permitted to scan extended body regions in short times. MSCT was introduced in 1998 allowing acquisition of multiple cross sections in one gantry rotation. The first generation of MSCT scanner with spatial and temporal resolutions suitable for imaging coronary arteries was capable of acquiring 4 slices simultaneously (4-MSCT) [5]. From that moment, MSCT evolved at an extraordinary speed [6-8] with the introduction of 16-MSCT (2002), 64-MSCT (2004), dual source CT (2006), 128- and 256-MSCT (2007) and 320-MSCT (2008).

This thesis will focus on 64-MSCT and dual source CT, which require a single breath hold of approximately 12 seconds and <10 seconds, respectively, to scan the entire heart. These scanners have a spatial resolution of 0.4 mm in all direc-

tions and a temporal resolution which is sufficient to visualize the entire coronary tree in patients with heart rates <65-70 beats/minute. Patients with higher heart rates receive oral or intravenous ß-blockers to lower the heart rate thus minimizing the occurrence of motion artifacts. Dual source CT, with two x-ray tubes placed in the CT gantry, has an improved temporal resolution and provides images of excellent quality even at heart rates >70 beats/minutes, which obviates the need of administering ß-blockers before the scan.

MSCT visualizes the coronary artery lumen and wall, and provides information regarding several manifestations of coronary atherosclerosis, e.g., luminal narrowing, coronary artery calcification, non-calcified plaque, positive wall remodeling as well as in-stent restenosis and graft pathology. An overview of the technique and its clinical applications is given in **Chapter 2. Chapters 3-6** contain studies related to the technical optimization of coronary MSCT angiography, in particular the administration of contrast agent, the choice of the best pulsing window, and image reconstruction in patients with varying heart rates during the scan. **Chapter 7** focuses on the role played by observer experience in the diagnostic performance of MSCT coronary angiography. **Chapter 8** introduces the use of coronary MSCT angiography as a support to magnetically-assisted coronary intervention. **Chapter 9** evaluates prevalence and type of coronary anomalies observed with MSCT-CA. The diagnostic performance of 64-MSCT angiography in the detection of coronary stenosis in comparison to conventional angiography is discussed in **Chapters 10-13. Chapter 14** focuses on the analysis of coronary artery lesion calcification to improve the ability to predict underlying significant coronary stenosis. Finally, **Chapters 15-19** emphasize the difficulties encountered when MSCT is used for the detection of in-stent restenosis in coronary arteries, or in patients with bypass grafts.

References

1. World Health Organization - The ten causes of death by broad income group (2002). Fact sheet updated February 2007. Available at http://www.who.int/mediacentre/factsheets/fs310.pdf. Accessed on 14 April 2008.
2. Rosamond W, Flegal K, Furie K, Go A, Greenlund K, Haase N, Hailpern SM, Ho M, Howard V, Kissela B, Kittner S, Lloyd-Jones D, McDermott M, Meigs J, Moy C, Nichol G, O'Donnell C, Roger V, Sorlie P, Steinberger J, Thom T, Wilson M, Hong Y (2008) Heart disease and stroke statistics--2008 update: a report from the American Heart Association Statistics Committee and Stroke Statistics Subcommittee. Circulation 117:e25-146.
3. Kennedy JW, Baxley WA, Bunnel IL, Gensini GG, Messer JV, Mudd JG, Noto TJ, Paulin S, Pichard AD, Sheldon WC, Cohen M (1982) Mortality related to cardiac catheterization and angiography. Cathet Cardiovasc Diagn 8:323-40.
4. Kennedy JW (1982) Complications associated with cardiac catheterization and angiography. Cathet Cardiovasc Diagn 8:5-11.
5. Nieman K, Oudkerk M, Rensing BJ, van Ooijen P, Munne A, van Geuns RJ, de Feyter PJ (2001) Coronary angiography with multi-slice computed tomography. Lancet 357:599-603.
6. Mollet NR, Cademartiri F, Nieman K, Saia F, Lemos PA, McFadden EP, Pattynama PM, Serruys PW, Krestin GP, de Feyter PJ (2004) Multislice spiral computed tomography coronary angiography in patients with stable angina pectoris. J Am Coll Cardiol 43:2265-70.
7. Meijboom WB, van Mieghem CA, Mollet NR, Pugliese F, Weustink AC, van Pelt N, Cademartiri F, Nieman K, Boersma E, de Jaegere P, Krestin GP, de Feyter PJ (2007) 64-slice computed tomography coronary angiography in patients with high, intermediate, or low pretest probability of significant coronary artery disease. J Am Coll Cardiol 50:1469-75.
8. Weustink AC, Meijboom WB, Mollet NR, Otsuka M, Pugliese F, van Mieghem C, Malago R, van Pelt N, Dijkshoorn ML, Cademartiri F, Krestin GP, de Feyter PJ (2007) Reliable high-speed coronary computed tomography in symptomatic patients. J Am Coll Cardiol 50:786-94.

CHAPTER 2

Multi-slice computed tomography of coronary arteries

Francesca Pugliese
Pim J. de Feyter

In Di Mario C, Dangas G, Barlis P (ed). Interventional cardiology: principles and practice. Wiley-Blackwell Ed, Oxford. In press.

Summary

Multislice computed tomography (MSCT) can be used to image the heart and coronary arteries non-invasively. Because the heart is in continuous motion, this task is technically very demanding. Knowledge of the technical principles of cardiac MSCT and how to optimize the scan parameters are key in order to perform successful MSCT studies of the heart. This chapter will review the basic principles of cardiac MSCT. The most common clinical applications of this technique will also be discussed.

Introduction

The introduction of 4-slice CT in 2000 was followed by rapid and revolutionary advances in multislice computed tomography (MSCT) technology. Nowadays, 64-MSCT and dual source computed tomography (DSCT) are considered state-of-the-art for cardiac MSCT imaging.

Non contrast-enhanced MSCT scans allow visualization of cardiac and coronary artery calcification. After intravenous injection of iodinated contrast agent, MSCT can delineate cardiac chambers, great cardiac vessels and coronary arteries (Figure 1).

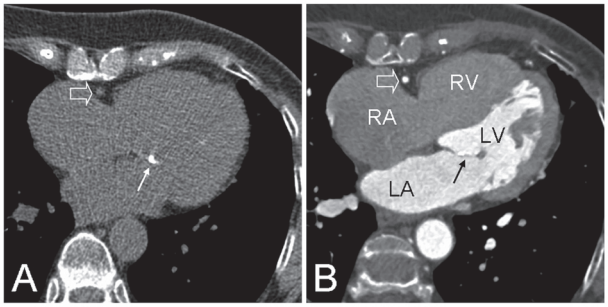

FIGURE 1. Axial images provide four-chamber views of the heart without (A) and with (B) injection of contrast agent. LA: left atrium; LV: left ventricle; RA: right atrium; RV: right ventricle; void arrow: right coronary artery; arrow: mild calcification of the mitral valve.

The evaluation of general cardiac morphology is usually performed by echocardiography and/or magnetic resonance

imaging (MRI) without the need for contrast injection or radiation exposure. Nevertheless, MSCT can be clinically helpful in a variety of situations, including the need for cross-sectional imaging in the event of inconclusive findings at echocardiography or in patients with pacemakers or other devices precluding MRI. Importantly, the main clinical focus of MSCT in cardiac imaging is the evaluation of coronary arteries.

Coronary MSCT Angiography - Technique

Basic Principles

In MSCT scanners, the X-rays are generated by an X-ray tube mounted on a rotating gantry. The patient is centered within the bore of the gantry such that the array of detectors is positioned to record incident photons after they have traversed the patient. MSCT differs from single detector CT principally by the design of the detector array, which allows the acquisition of multiple adjacent sections simultaneously.

MSCT systems have 2 principal modes of scanning (Figure 2). The first mode is sequential scanning, also known as "step-and-shoot", in which the table is advanced in a step-wise fashion. In this mode, the X-rays are generated during an imaging window positioned at a predetermined offset from the R wave (prospective ECG triggering; Figure 2, A) while the table is stationary. The diastolic phase of the cardiac cycle is usually chosen because cardiac motion is reduced in diastole. Sequential scanning is the current mode for measuring coronary calcium at most centers using MSCT.

The second mode is spiral or helical scanning, in which the table moves continu-

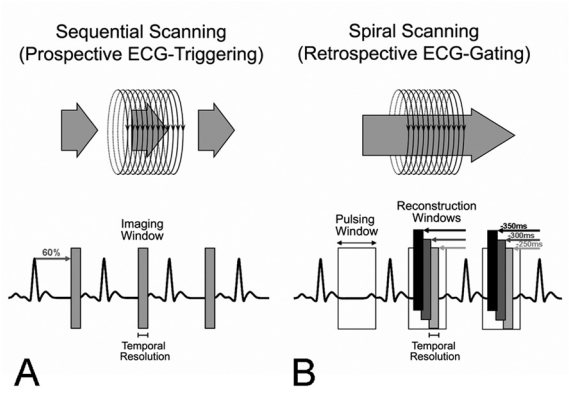

FIGURE 2. In sequential scanning, data for one axial slice are acquired, after which the table is advanced to the next position (A). Sequential scan protocols use prospective ECG-triggering to synchronize the data acquisition to the motion of the heart. Based on the measured duration of previous heart cycles, the scan of one slice is initiated at a pre-specified moment after the R-wave. Diastole is commonly chosen to ensure the least motion artifacts, e.g., 60% of the previous R-R interval. Spiral scanners acquire data continuously and record the patient's ECG while the table moves at a constant speed (B). Images are reconstructed using retrospective ECG-gating. This mode is more flexible to minimize motion artifacts because reconstruction window can be positioned arbitrarily within the R-R interval. If X-ray tube modulation is used, the full output occurs only during an interval of the cardiac cycle (pulsing window) which can eventually be used for image reconstruction.

ously at a fixed speed relative to the gantry rotation. The ECG trace of the patient is recorded during the scan. After data acquisition, the optimal reconstruction window is chosen among all available time positions to minimize motion artifacts (retrospective ECG gating; Figure 2, B). Spiral scanning is the current mode for performing coronary MSCT angiography because it allows flexibility in the position of reconstruction windows, which is helpful to ensure the least motion artifacts. However, spiral scanning is associated with a higher X-ray radiation exposure than sequential scanning.

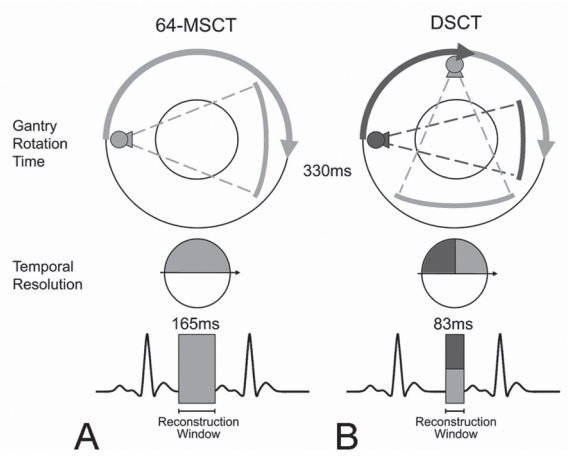

FIGURE 3. Reconstruction of MSCT images uses data acquired over 180°, thus temporal resolution equals half of the gantry rotation time. Because the shortest gantry rotation time currently achievable by a 64-MSCT scanner is 330ms, the corresponding temporal resolution is 165ms. Temporal resolution corresponds to the width of reconstruction window. In DSCT, two X-ray sources and two corresponding detector arrays are mounted at an angle of 90°, therefore only 90° rotation is needed to provide data from 180°. In DSCT, temporal resolution is equal to a quarter of the gantry rotation time, i.e. 330/4 = 83ms.

In order to reduce radiation exposure in spiral scanning, the X-ray tube current can be modulated prospectively: guided by the ECG, the full output occurs only during an interval of the cardiac cycle which will be used for image reconstruction (e.g., diastole), whereas the X-ray output will be reduced during the remaining cardiac cycle (Figure 2, B).

Temporal resolution is the time for acquiring the data needed for the reconstruction of one image. Temporal resolution depends primarily on gantry rotation time. In particular, because reconstruction of MSCT images requires data acquired over half gantry rotation (180°), temporal resolution equals half of the gantry rotation time (Figure 3, A). Temporal resolution corresponds to the width of the reconstruction window; MSCT images display the average cardiac motion over the reconstruction window. The shortest gantry rotation time currently achievable by a 64-MSCT scanner is 330ms and the corresponding temporal resolution is therefore 165ms. The latest development to improve temporal resolution and omit the need to lower patients' heart rates by pre-medication has been the introduction of MSCT scanners with two X-ray sources acquiring different projections simultane-

ously [1]. In dual-source computed tomography (DSCT), the two X-ray sources are mounted at an angle of 90°, therefore temporal resolution is equal to a quarter of the gantry rotation time, i.e. 330/4 = 83ms (Figure 3, B and Figure 4).

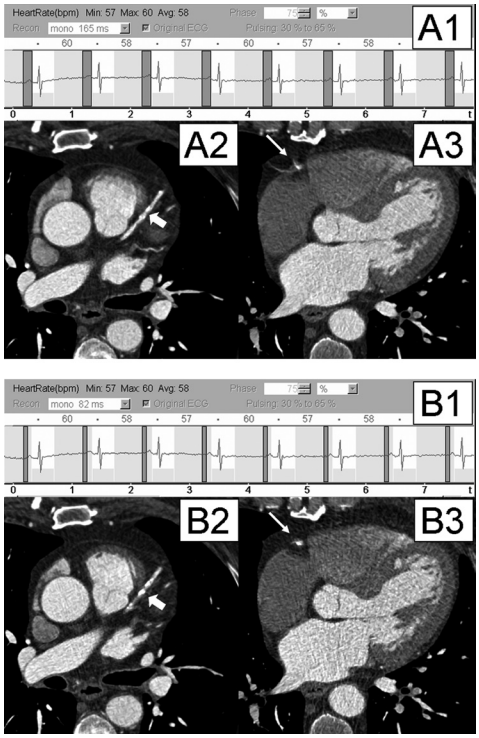

FIGURE 4. MSCT images display the average cardiac motion over the reconstruction window. A 165mm-wide reconstruction window (A1-A3) averages MSCT views obtained during 180° gantry rotation. This is the reconstruction algorithm employed in 64-MSCT. An 83mm-wide reconstruction window (B1-B3) averages MSCT views obtained (by 2 detector arrays) during 90° gantry rotation. This is the reconstruction algorithm employed in DSCT. Reconstruction using 180° data (A2) might improve image contrast when compared to reconstruction using 90° data (B2) because more MSCT views are averaged for the reconstruction of the same image (gross arrow=LAD). However, a wider reconstruction window worsens temporal resolution and may cause more blurring (A3) than the use of the narrowest reconstruction window (B3) (thin arrow=RCA)
(A full color version of this illustration can be found in the color section)

Coronary arteries have a diameter of 2-4mm in their proximal tract and taper distally, therefore high spatial resolution is another prerequisite for MSCT coronary imaging. Spatial resolution of MSCT on the transverse plane (x, y) is $0.4\times0.4mm^2$ [1]. Spatial resolution along patient's longitudinal axis (z-axis) is determined mainly by the individual detector width, which varies between 0.5-0.625mm depending on the manufacturer. These features permit reconstruction of high quality images with similar sub-millimeter resolution along the x, y, and z axis. Although catheter angiography has a bi-dimensional spatial resolution of $0.2\times0.2mm^2$, a major advantage of MSCT over catheter angiography is the ability to perform multi-planar reconstructed images (see below). Quality of multi-planar reconstruction strictly depends on the so-called "isotropic data", i.e., datasets where spatial resolution is equal in the x, y and z directions.

An overview of major image parameters, patient preparation and contrast administration in catheter angiography, 64-MSCT and DSCT is given in Table 1.

Contrast Enhancement

Good contrast enhancement in coronary arteries is essential for the detection of atherosclerotic changes and luminal stenosis. An iodine flow in the range from 1.2-2g/s is recommended [2]. This can

TABLE 1. Overview of image parameters, patient preparation and contrast administration

	Catheter Angiography	64-MSCT	DSCT
Spatial resolution	0.2x0.2mm^2	0.4x0.4x0.4mm^3	0.4x0.4x0.4mm^3
Temporal resolution	8ms	165ms	83ms
Preparation			
beta-blockers	no	• if heart rate ≥65 beats/min, metoprolol 100mg orally 1hr before scan or/and 5-15mg i.v. • in patients with aortic valve stenosis, severe hypotension, Mobitz heart block consider calcium channel blockers	(optional)
nitroglycerine	intracoronary	(optional – sublingual)	(optional – sublingual)
Contrast	80-100ml intracoronary	100ml intravenous	60-100ml intravenous

be achieved by either injecting low-concentration contrast material at high flow rates or by injection of high concentration contrast material at lower flow rates. However, it is standard practice to inject contrast agent at rates of at least 5ml/s. Total contrast volume is determined by contrast injection rate multiplied by the scan time required to cover the heart. Typical injection volumes are in the range 60-100ml.

Dual injection, i.e., iodinated contrast followed by saline (30-50ml) is recommended for MSCT of the heart. Saline is helpful to avoid dense opacification of the right cardiac chambers and consequent artifacts which might limit the interpretation of the right coronary artery.

Two major techniques are available to synchronize the arrival of contrast agent in coronary arteries and the beginning of the scan: bolus tracking and test bolus. In bolus tracking, the bolus is "tracked" in the ascending aorta just above coronary ostia. Roughly 7-10s after the contrast injection has begun, the scanner starts to monitor attenuation changes in a region of interest (ROI) positioned in the ascending aorta. Once enhancement reaches a preset attenuation threshold, e.g., 100HU above baseline attenuation of blood, the

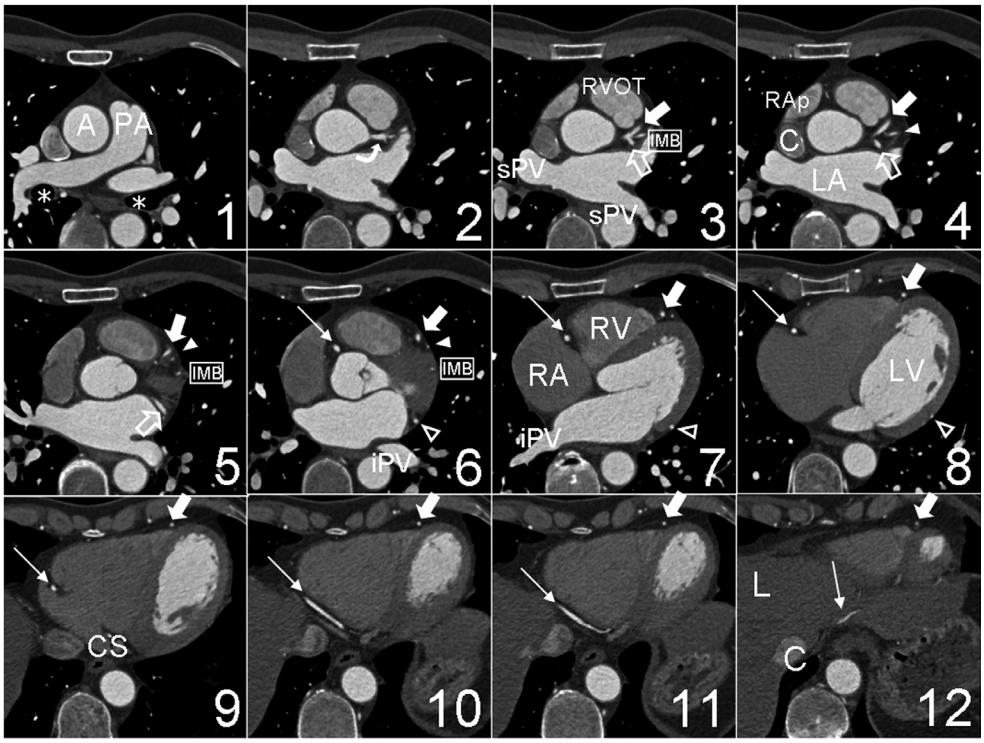

FIGURE 5A (1-12). The basic information of MSCT is the axial images (A1-A12). Scrolling through them in the cranial to caudal direction shows any structure in the axial plane. The scan starts at the level of the tracheal bifurcation (A1) therefore the main bronchi (asterisks), the ascending aorta (A) and pulmonary artery (PA) are shown. As we scroll caudally, the origin of the left main coronary artery (A2, curved arrow) and its trifurcation (A3) into left anterior descending artery (gross arrow), circumflex artery (void arrow) and intermediate branch (IMB) are seen. The left anterior descending artery (A3-A12, gross arrow) courses along the superior inter-ventricular groove and can be followed down to the apex of the heart. A diagonal branch is also seen (A4-A6, gross arrowhead). The left circumflex artery (A3-A5, void arrow) courses in the left atrio-ventricular groove and gives an obtuse marginal branch (A6-A8, void arrowhead). The proximal right coronary artery (A6, thin arrow) has a short horizontal course. Then the vessel courses caudally (A7-A9, thin arrow) in the right atrio-ventricular groove. The inferior inter-ventricular groove contains the posterior descending artery (A12, thin arrow).
Abbreviations: A=aorta; PA=pulmonary artery; asterisks=main bronchi; RVOT=right ventricular outflow tract; sPV=superior pulmonary veins; RAp=right appendage; C=cava; LA=left atrium; IMB=intermediate branch; iPV=inferior pulmonary veins; RA=right atrium; RV=right ventricle; LV=left ventricle; CS=coronary sinus; L=liver.

patient is instructed to hold his/her breath and the scan is initiated.

Test bolus needs a separate test contrast injection to time the main contrast injection. A ROI is positioned in the ascending aorta. Low dose scans separated by 1s are used to plot enhancement versus time after injection of the test bolus (10-12ml). Time to peak enhancement is used to determine the optimal scan delay.

Image Post-Processing

With image post-processing, the source axial images are modified and made useful for the observer [3] (Figure 5). With

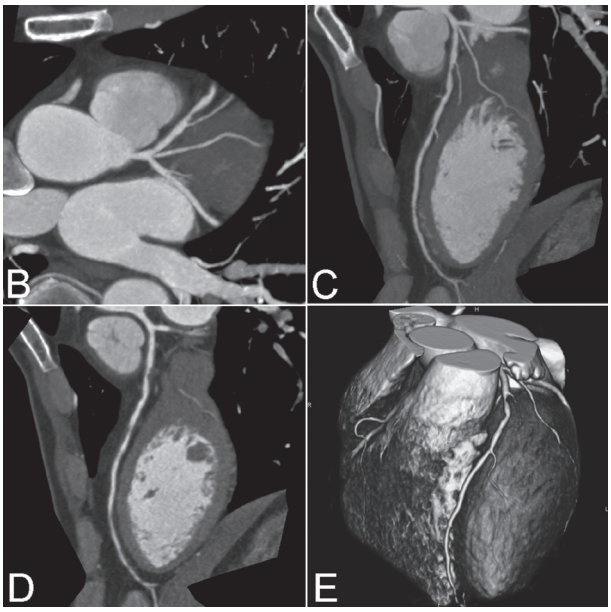

FIGURE 5B-E. Axial images are reconstructed to form a volume. Post-processing is performed on this volume data set. Multiplanar reconstructions (B) cut this volume according to planes arbitrarily tilted in any orientation. When the cut plane is not flat but curved, the result is a curved multiplanar reconstruction (C, D). This image is a flattened representation of the curved plane (D). Maximum intensity projection is an algorithm that visualizes only the structures with the highest attenuation along the observation line (C). Volume rendering (E) displays the volume based on the density of the structures. Color attribution is arbitrary, therefore the appearance will change when the operator changes the colors of the algorithm.
(A full color version of this illustration can be found in the color section)

isotropic resolution, multiplanar reformats (MPR) and maximum intensity projections (MIP) along the course of the coronary arteries are the routinely methods for assessment of coronaries from MSCT datasets. Three-dimensional volume rendering technique (VRT) provides a helpful overview, e.g., in cases of complex anatomy such as coronary artery bypass grafts (CABG) or anomalous coronary arteries [4]. However, axial images may be best for the detection of coronary stenoses.

Typical Artifacts

It is important to recognize a few typical MSCT artifacts which may lead to image misinterpretation. Motion artifacts (Figure 6) typically blur the contours of the heart and coronary arteries. Inconsistent triggering or arrhythmias will lead to misalignment of adjacent image stacks. Partial voluming occurs when a pixel (i.e., smallest portion of an image) contains more than one type of tissue. In this setting, the attenuation value assigned to the pixel is the weighted average of the different attenuation values. Thus, when a pixel is only partially filled by a structure of very high attenuation (e.g., metal or bone), a high

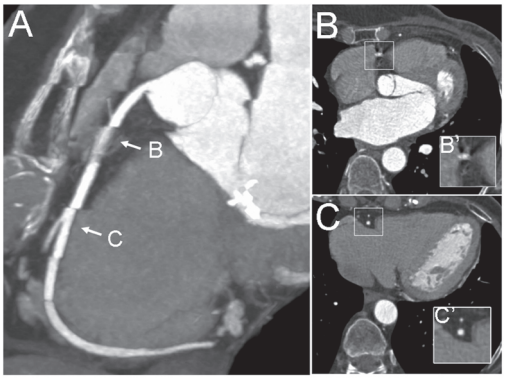

FIGURE 6. Typical artifacts in cardiac MSCT (A) include motion artifacts (B) and stack misalignment due to heart rate variations or slight arrhythmia (C). Whereas motion artifacts cause blurring (B), images within a misaligned stack are not blurred (C).

CT number is assigned to the complete pixel, which will thus appear bright on the image. This may lead to overestimation of the size of high-attenuation objects (e.g., coronary calcifications and stents) (Figure 7).

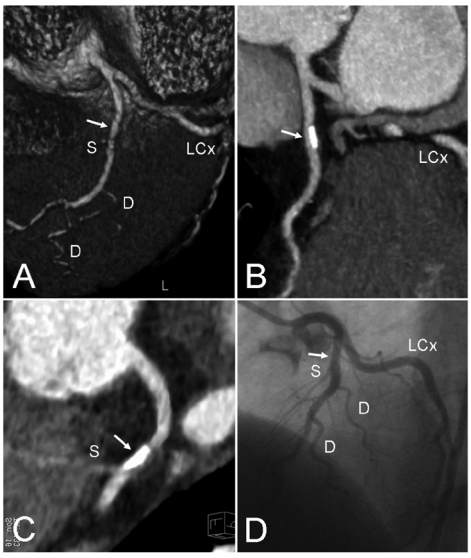

FIGURE 7. Volume rendered image (A), curved maximum intensity projection (B) and multiplanar reconstruction (C) show a calcified plaque (arrow) located in the LAD just proximal to the origin of a septal branch (S). The size of structures with high X-ray attenuation such as calcifications is overestimated in MSCT due to partial voluming. This calcification superimposes most of the coronary artery lumen. The conventional angiogram (D) shows a normal LAD. *(A full color version of this illustration can be found in the color section)*

Coronary MSCT Angiography – Clinical Applications

Stenosis Detection

Although conventional coronary angiography is still regarded as the reference standard for the detection and quantification of coronary artery stenosis, there are situations where sufficient information may be acquired by a non-invasive technique with benefits in terms of cost, patient risk and discomfort.

Since 1999, when the first studies on MSCT coronary angiography were published, the development of MSCT technology has been tremendous. Numerous studies [5-21] have compared the accuracy of MSCT in the detection of coronary artery stenosis versus invasive coronary angiography (Table 2). While sensitivity and specificity remained similar comparing 16-MSCT and 64-MSCT, 64-MSCT and DSCT became more robust for imaging the coronaries: in the segmental analysis, a decrease was shown for the number of coronary segments that had to be excluded due to insufficient image quality [22] (Figure 8, Table 2). Importantly, in the per-patient analysis, which is clinically relevant because it explores the ability of MSCT to identify patients with or without significant CAD, the negative predictive value was consistently found to be high, in the range 92-100% (Table 2). These findings led to the hypothesis that a normal MSCT may obviate the need for invasive angiography in properly selected clinical circumstances. The reported positive predictive values were lower, indicating the tendency of MSCT to overestimate the severity of disease in comparison to invasive coronary angiography. Especially

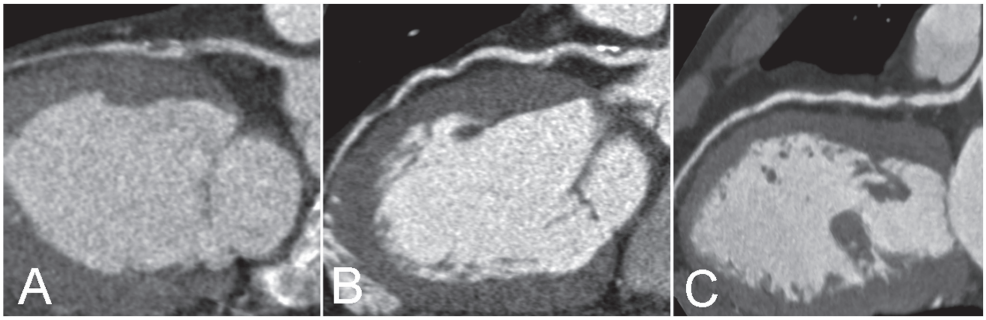

FIGURE 8. Curved multiplanar reconstructions of the LM and LAD arteries obtained in three different patients with 16-MSCT (A), 64-MSCT (B) and DSCT (C) show progressive improvement in image quality. All the patients had heart rates during the scan comprised between 62 and 65 beats/minute.

in the presence of coronary calcifications and residual motion in the dataset, MSCT is presently limited to accurately grade lesion severity (percentage of stenosis). However, MSCT has a notably high sensitivity and negative predictive value for the detection of significant CAD, thus it may be well suited to clinical situations in which exclusion of CAD is of paramount concern, e.g., in patients with low to intermediate pretest likelihood of disease [23]. The evolving indications of MSCT of the heart, with emphasis on the evaluation of coronary arteries, are shown in Table 3.

Bifurcations and Ostial Lesions

The angiographic evaluation of bifurcation lesions may be hindered by projectional foreshortening, vessels overlap and insufficient vessel opacification; for these reasons, the assessment of the side branch ostium can be particularly challenging. Errors in diagnosis may lead to consequences for patient management: when CABG surgery is the treatment of choice, underestimation of a side branch lesion may result in the side branch not being grafted; when PCI is preferred, detailed anatomic information will permit to better define intervention strategy. Moreover, conventional angiography does not provide sufficient information on the plaque burden at the level of the bifurcation. In the presence of a high plaque burden, initial treatment of both the main and side branches (e.g. crush or culottes techniques) should be preferred over main branch stenting first followed by provisional balloon angioplasty (with or without stenting) of the side branch. This approach may be preferable to reduce the occurrence of post-PCI plaque shift compromising the side branch lumen.

Van Mieghem et al. [24] compared MSCT to conventional angiography for

TABLE 2. Detection of coronary stenosis - diagnostic performance of MSCT versus conventional angiography

		Per segment					Per patient			
	No. patients	Unevaluable segments (%)	Sensitivity (%)	Specificity (%)	PPV (%)	NPV (%)	Sensitivity (%)	Specificity (%)	PPV (%)	NPV (%)
16-MSCT										
Mollet [13]	128	7	92	95	79	98	100	86	97	100
Hoffman [9]	103	6	95	98	87	99	97	87	90	95
Achenbach [5]	50	4	94	96	69	99	100	83	100	86
Mollet [12]	51	0	95	98	87	99	97	84	89	95
Garcia [7]	187	29	85	91	36	99	98	55	50	99
Dewey [6]	129	9	83	86	90	95	93	74	93	92
Hausleiter [8]	129	11	93	87	46	99	.	.	.	.
64-MSCT										
Leschka [11]	53	0	94	97	87	99	100	100	100	100
Raff [18]	70	12	86	95	66	98	95	90	93	93
Leber [10]	59	0	88	97	.	99	94	.	.	.
Pugliese [17]	35	0	99	96	78	99	100	90	96	100
Mollet [14]	52	2	99	95	76	99	100	92	97	100
Ropers [19]	82	4	95	93	56	99	96	91	83	98
Nikolaou [15]	72	10	86	95	72	97	97	72	83	95
Hausleiter [8]	114	8	92	92	54	99	99	75	74	99
DSCT										
Nikolaou [16]	20	4	95	93	79	98	.	.	.	.
Scheffel [20]	30	1	96	98	86	99	.	.	.	.
Weustink [21]	100	0	95	95	75	99	99	87	96	95

TABLE 3. Evolving indications of MSCT of the heart [23] with emphasis on the evaluation of coronary arteries

Detection of CAD in symptomatic patients

1. Intermediate pre-test probability of CAD + equivocal ECG/unable to exercise
2. Equivocal exercise tests, perfusion imaging, stress echo
3. Evaluation of coronary arteries in patients with heart failure of new onset to assess etiology

Coronary anomalies

Exclusion of CAD prior to cardiac valve surgery/major non-cardiac surgery

Patients with recurrent chest pain after PCI with low probability of in-stent restenosis and large stents (≥3mm)

Coronary bypass grafts

Acute chest pain

1. Non-ST segment elevation and initial troponin negative
2. Intermediate probability of aortic dissection/aneurysm, pulmonary emboli, obstructive CAD (triple rule out)

the detection and classification of coronary bifurcation lesions. In keeping with the available literature on non-bifurcation lesions, they reported 96% sensitivity, 97% specificity, 63% positive predictive value and 99% negative predictive value for the detection of bifurcation lesions (Figure 9). MSCT was found to be accurate also in classifying bifurcation lesions according to the Medina classification system [25]. Furthermore, thanks to the three-dimensional nature of MSCT data, the bifurcation angle between the main vessel and the side branch could be measured accurately. In situations where both branches needed to be stented, information regarding the bifurcation angle was used to support the choice of the stenting technique.

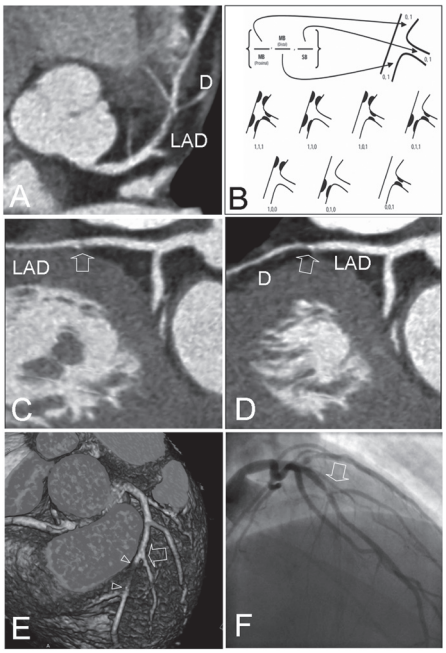

FIGURE 9. The DSCT multiplanar reconstruction (A) shows a proximal bifurcation lesion (arrows) in the LAD artery, also seen on the curved multiplanar reconstructions of the LAD (C) and diagonal branch (E). The lesion is confirmed by the conventional angiogram (F). According the Medina classification system (B), the lesion involves proximal main branch and side branch whereas the distal main branch is unremarkable (1,0,1). The lesion is not clearly detectable in the volume rendered image (E); distally to the bifurcation, the LAD has intramyocardial course (arrowheads).
(A full color version of this illustration can be found in the color section)

The visualization of ostial lesions (Figure 10) may equally be affected by projectional limitations in conventional angiography. Occasionally, ostial lesions can be

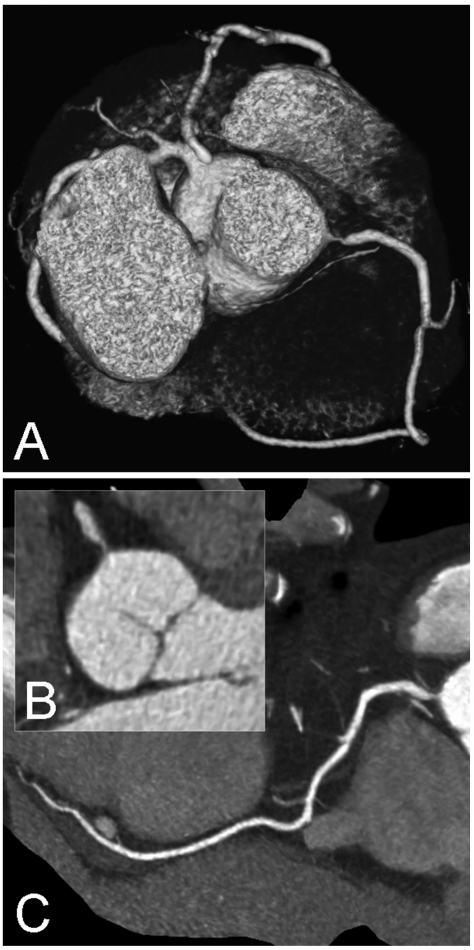

FIGURE 10. The volume rendered view after removal of the right atrium (A), axial image (B) and curved multiplanar reconstruction (C) demonstrate an ostial lesion of the RCA. *(A full color version of this illustration can be found in the color section)*

masked by the engagement of the catheter tip beyond the lesion. At a pre-interventional stage, MSCT can provide information on three-dimensional anatomy of ostial lesions and vessel take-off angle [26].

Chronic Total Occlusion

In the diagnostic work-up of patients with chronically occluded coronary arteries, MSCT can add important information to conventional angiography. Measurement of the length of the occluded segment, which has long been identified as a predictor of failed PCI, can be limited in conventional angiography by foreshort-

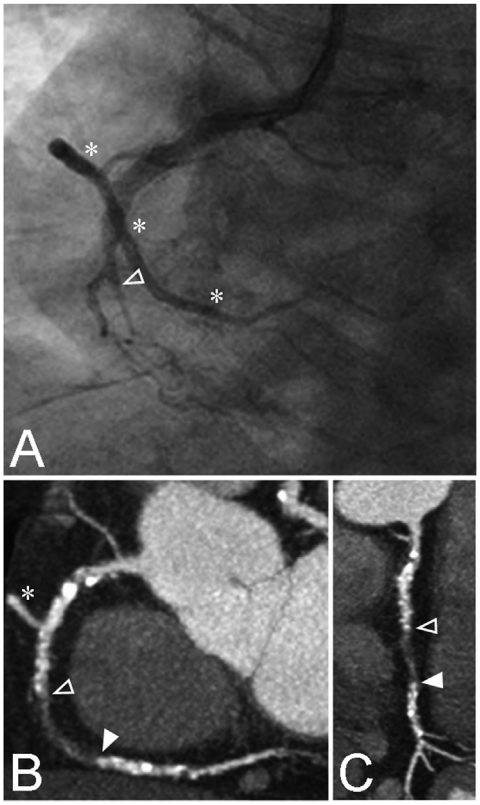

FIGURE 11. Occlusion of the RCA (void arrowheads) is demonstrated by the conventional angiogram (A), DSCT multiplanar reconstruction (B) and curved multiplanar reconstruction (C) of the vessel. The distal patent RCA is not sharply visualized on the angiogram (A). The multiplanar reconstruction (B) and curved multiplanar reconstruction (C) of the RCA permit better visualization of the distal patent vessel (solid arrowheads) and thus of the actual occlusion length. Asterisks: right ventricular branch.

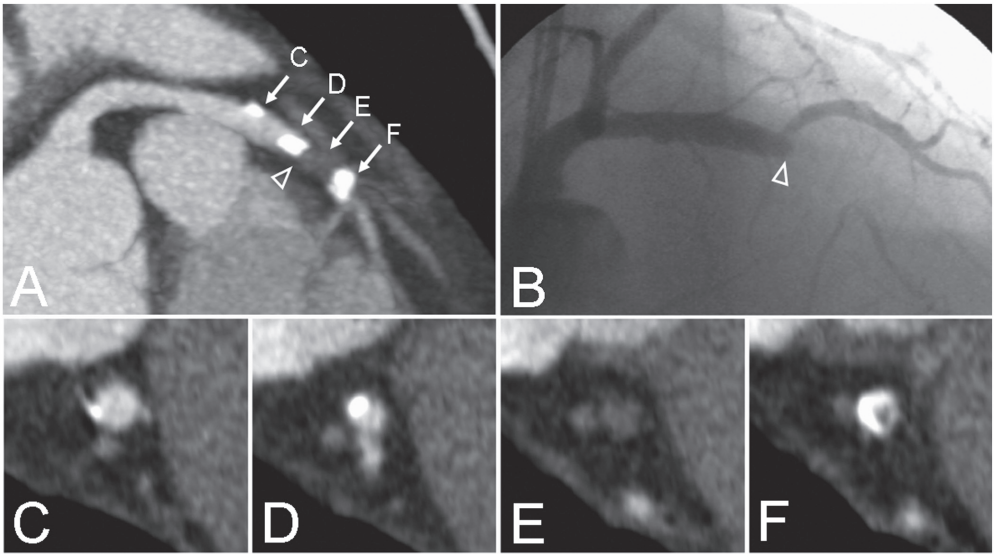

FIGURE 12. Occlusion of the proximal LAD (arrowheads) is demonstrated by the DSCT maximum intensity projection image (A) and conventional angiogram (B). The DSCT cross sections (C-F), obtained as indicated in A, provide information on the severity of lesion calcification. Bulky calcifications are present proximally to the occlusion (C), at the level of the stump (D) and more distally (F).

ening, calibration limitations and lack of collateral filling (Figure 11). Conversely, MSCT is a three-dimensional technique which allows reliable length measurement of coronary segments. Likewise, MSCT permits to evaluate the proximal entry port, the severity of calcification (Figure 12) and to delineate occlusion trajectory. Therefore, MSCT may improve the ability to predict the success rate of PCI. Mollet et al. [27] found that a blunt entry point, an occlusion length >15mm and severe calcification, all determined by MSCT, were independent predictors of procedural failure.

Stents

Coronary stents are notoriously difficult to assess by MSCT. Partial voluming artifacts (see above) enlarge the apparent size of the stent; this is particularly disturbing in smaller stents, where the in-stent lumen might be completely obscured, and in overlapping and bifurcation stents due to an excess of metal. As demonstrated in vitro, types of metal and strut thickness also play an important role for in-stent lumen assessability [28]; generally, stents with thinner struts (e.g., 0.14mm) are less problematic than stents with thicker struts (e.g., 0.15mm and above).

In the evaluation of coronary stents, the finding of contrast-enhancement distal

TABLE 4. Detection of in-stent restenosis - diagnostic performance of MSCT versus conventional angiography

	Unevaluable stents (%)	Sensitivity (%)	Specificity (%)	PPV(%)	NPV(%)
16-MSCT					
Gilard [30]					
All diameters	36	.	.	.	.
>3mm	19	86	100	100	99
≤3mm	49	54	100	100	94
40-MSCT					
Gaspar [31]					
All diameters	5	89	81	47	97
64-MSCT					
Rixe [34]					
All diameters	42	86	98	86	98
>3mm	22	100	100	100	100
3mm	42	83	96	83	96
*<3mm**	92	.	100	.	100
Ehara [33]					
All diameters	12	92	81	54	98
Cademartiri [32]					
All diameters	7	90	86	44	98
DSCT					
Pugliese [35]					
All diameters	5	94	92	77	98
≥3.5mm	0	100	100	100	100
3mm	0	100	97	91	100
≤2.75mm	22	84	64	52	90

*only 1 stent available, without in-stent restenosis

to the stent is not fool-proof for stent patency, because collateral pathways may fill the vessel retrogradely; if the stent is being evaluated for the presence of non-occlusive in-stent restenosis, direct visualization of the in-stent lumen becomes the mandatory criterion.

Technical requirements for coronary stent imaging are 64-slice MSCT scanners with thin detectors in order to optimize spatial resolution and decrease partial voluming. The use of sharper convolution kernels may be beneficial to decrease the entity of high density artifacts and is therefore recommendable for coronary stent imaging. High temporal resolution is also important because high density artifacts are exacerbated by the presence of residual motion in the MSCT dataset [29].

Clinical studies compared different generations of MSCT scanners to conventional angiography for the detection of in-stent restenosis, defined as ≥50% luminal narrowing (Table 4). Studies performed using 16-MSCT [30], 40-MSCT [31] and 64-MSCT [32-34] reported promising results with variable percentages of unassessable stents. Using DSCT [35], the percentage of unassessable stents was found to be low; whereas the diagnostic performance did not vary significantly between different stent configurations (i.e., single stents versus overlapping/bifurcation stenting), the results were influenced importantly by the stent diameter. In particular, the ability of DSCT to exclude with certainty in-stent restenosis in stents with diameters ≤2.75mm was significantly lower than that observed in larger stents.

Ideally, the stent type and diameter are known prior to the scan, therefore in-stent lumen accessibility in a particular patient could be predicted from the available in-vitro and in-vivo data. However, MSCT was shown to have a constantly high negative predictive value, therefore it may be useful in patients with clinical symptoms but low pre-test probability for in-stent restenosis.

Stent implantation in the LM and proximal LAD/CX provides a suitable scenario for the use of MSCT in the detection of in-stent restenosis. This is mainly due to the relatively large size of stents implanted in the LM and proximal LAD/CX; moreover, this part of the coronary tree is relatively protected from motion artifacts. Although CABG surgery is still recommended in patients with LM disease, PCI is increasingly performed on the unprotected LM coronary artery in the drug-eluting stent (DES) era. However, in-stent restenosis still occurs with DES and may cause fatal myocardial infarction or sudden death [36], therefore surveillance with routinely angiography 6 months after PCI for left main stem is highly recommended [37]. A study by Van Mieghem et

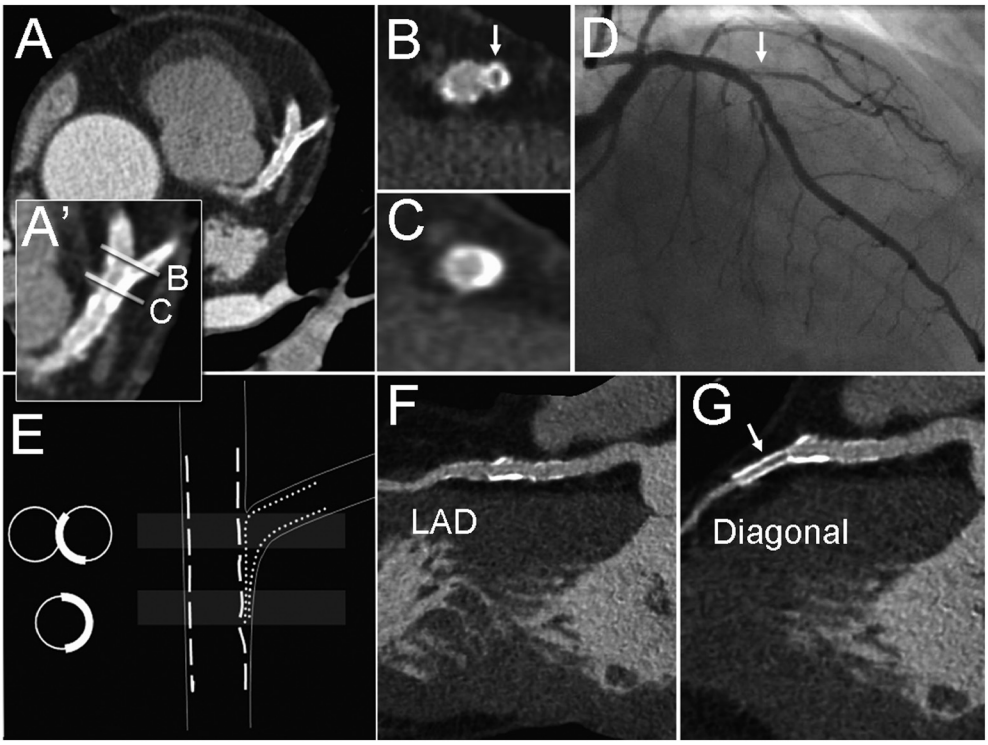

FIGURE 13. The DSCT axial image (A), its magnification (A'), the cross-sectional views (B, C) and the diagram (E) show the typical appearance of the crush stenting technique, characterized by three layers of metal crushed against the ostium of the side branch. The DSCT cross-section obtained at the level of the carina (B) and the curved multiplanar reconstruction of the diagonal branch (G) demonstrate in-stent restenosis in the diagonal branch stent (arrow). The LAD (main branch) is patent (F). The conventional angiogram (D) confirms the findings.

al. [38] showed that MSCT was safe and reliable in excluding in-stent restenosis in patients with LM and proximal LAD/CX stents; this study suggested that MSCT might be an acceptable first-line alternative to conventional angiography for the follow-up of patients after unprotected LM stenting.

MSCT also visualizes the configuration of bifurcation/overlapping stents (Figure 13) and the position of stents implanted in ostial lesions. Tissue prolapses, stent malapposition and underexpansion are generally not clearly visualized by MSCT. It is conceivable that stents with thinner struts, absorbable and non-metallic stents (Figure 14) will be less affected by high-density artifacts; the introduction of these new devices might increase the utility of MSCT in patients after PCI.

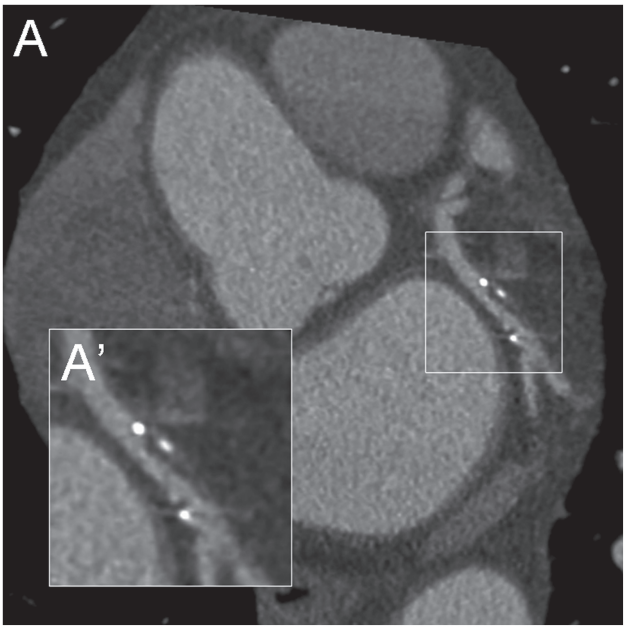

FIGURE 14. The DSCT multiplanar reconstruction (A) and its magnification (A') show a bioabsorbable stent placed in the LCx artery. The stent is radiolucent with radiopaque markers at the stent edges.

Coronary Artery Bypass Grafts

General Issues

Patients with prior coronary artery bypass graft (CABG) surgery usually present with co-morbidity and have a higher prevalence of valve disease and ventricular dysfunction compared with non-CABG patients. They have a higher incidence of complications during invasive procedures, including cardiac catheterization, and may therefore benefit from non-invasive coronary angiography performed by MSCT.

Generally, bypass grafts are well visualized by MSCT due to their large diameter, limited calcification and relative immobility. Surgical opaque material, such as vascular clips, sternal wires and graft orifice indicators may however hinder the evaluability of coronary grafts (Figure 15).

Clinical Performance and Limitations

64-MSCT permits to evaluate graft patency with a sensitivity approaching 100% in both arterial and venous grafts and without exclusion of grafts due to insufficient image quality [39-42]. However, ischemic symptoms in patients after CABG surgery can be caused by obstruction of bypass grafts or by disease progression in native coronary arteries. Comprehensive evaluation post-CABG surgery should also include the native coronary tree; assessment of the native coronary arteries can be difficult in these patients owing to the diffuse nature of the disease and the presence of severe calcifications [39].

Valve Disease

Whereas the visualization of the tricuspid and pulmonary valves is generally incon-

sistent, the mitral and aortic valves can reliably be depicted in contrast-enhanced MSCT scans. While MSCT cannot provide measurements of transvalvular flow and pressure gradients, dynamic imaging of the open and closed valve is possible (Figure 16). For the normal and stenotic aortic valve, recent studies have demonstrated the ability of MSCT to measure the orifice area with close correlation to transesophageal echocardiography and invasive assessment of the aortic orifice area [43, 44]. However, in the setting of severely calcified stenosis, measurements of the opening area by CT may become unreliable. Non-enhanced CT scans can be used to quantify aortic valve calcium [45].

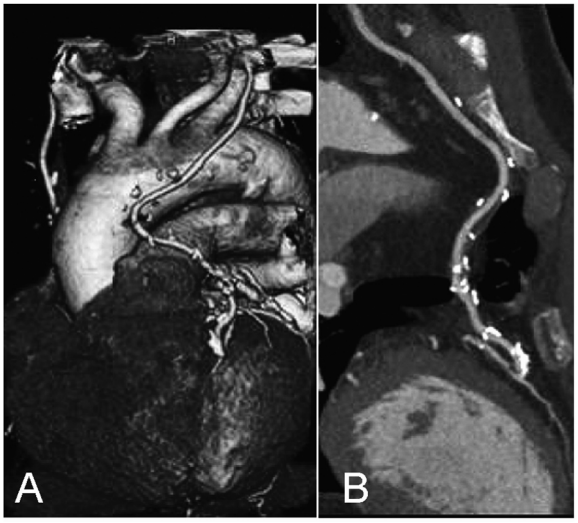

FIGURE 15. In a patient after coronary artery bypass graft surgery, the DSCT volume rendered image (A) and the curved multiplanar reconstruction (B) show patency of the left internal mammary artery graft and of the anastomosis of the graft onto the LAD. Notice the hyper-dense appearance of the surgical clips.
(A full color version of this illustration can be found in the color section)

FIGURE 16. The MSCT multiplanar images were obtained in 2 different patients (A and B) parallel to the aortic valve. Images in the upper row (A1, B1) were obtained during diastole. Images in the lower row (A2, B2) were obtained in systole. In patient A, the cusps adapt during diastole (A1) and open during systole (A2); the aortic valve is normal. In patient B, aortic cusps are thickened and calcified (B1, B2). Opening is incomplete during systole (B2); the patient has aortic valve stenosis.

Coronary Anomalies

It may sometimes be difficult during invasive coronary angiography to define the origin and course of anomalous coronary arteries. MSCT is extremely reliable to visualize the origin and course of anomalous coronary vessels and is well-suited for investigating patients with known or suspected congenital coronary artery anomalies. MSCT permits morphological analysis with very high resolution; moreover, this technique is not restricted by "echo windows" or by implanted de-

vices such as pacemakers or implantable cardioverter defibrillators, which are frequently encountered in patients with congenital heart disease.

References

1. Flohr TG, McCollough CH, Bruder H, Petersilka M, Gruber K, Suss C, Grasruck M, Stierstorfer K, Krauss B, Raupach R, Primak AN, Kuttner A, Achenbach S, Becker C, Kopp A, Ohnesorge BM (2006) First performance evaluation of a dual-source CT (DSCT) system. Eur Radiol 16:256-68.
2. Cademartiri F, Mollet NR, van der Lugt A, McFadden EP, Stijnen T, de Feyter PJ, Krestin GP (2005) Intravenous contrast material administration at helical 16-detector row CT coronary angiography: effect of iodine concentration on vascular attenuation. Radiology 236:661-5.
3. Fishman EK, Magid D, Ney DR, Chaney EL, Pizer SM, Rosenman JG, Levin DN, Vannier MW, Kuhlman JE, Robertson DD (1991) Three-dimensional imaging. Radiology 181:321-37.
4. Vogl TJ, Abolmaali ND, Diebold T, Engelmann K, Ay M, Dogan S, Wimmer-Greinecker G, Moritz A, Herzog C (2002) Techniques for the detection of coronary atherosclerosis: multi-detector row CT coronary angiography. Radiology 223:212-20.
5. Achenbach S, Ropers D, Pohle FK, Raaz D, von Erffa J, Yilmaz A, Muschiol G, Daniel WG (2005) Detection of coronary artery stenoses using multi-detector CT with 16 x 0.75 collimation and 375 ms rotation. Eur Heart J 26:1978-86.
6. Dewey M, Teige F, Schnapauff D, Laule M, Borges AC, Wernecke KD, Schink T, Baumann G, Rutsch W, Rogalla P, Taupitz M, Hamm B (2006) Noninvasive detection of coronary artery stenoses with multislice computed tomography or magnetic resonance imaging. Ann Intern Med 145:407-15.
7. Garcia MJ, Lessick J, Hoffmann MH (2006) Accuracy of 16-row multidetector computed tomography for the assessment of coronary artery stenosis. Jama 296:403-11.
8. Hausleiter J, Meyer T, Hadamitzky M, Zankl M, Gerein P, Dorrler K, Kastrati A, Martinoff S, Schomig A (2007) Non-invasive coronary computed tomographic angiography for patients with suspected coronary artery disease: the Coronary Angiography by Computed Tomography with the Use of a Submillimeter resolution (CACTUS) trial. Eur Heart J

9. Hoffmann MH, Shi H, Schmitz BL, Schmid FT, Lieberknecht M, Schulze R, Ludwig B, Kroschel U, Jahnke N, Haerer W, Brambs HJ, Aschoff AJ (2005) Noninvasive coronary angiography with multislice computed tomography. Jama 293:2471-8.
10. Leber AW, Knez A, von Ziegler F, Becker A, Nikolaou K, Paul S, Wintersperger B, Reiser M, Becker CR, Steinbeck G, Boekstegers P (2005) Quantification of obstructive and nonobstructive coronary lesions by 64-slice computed tomography: a comparative study with quantitative coronary angiography and intravascular ultrasound. J Am Coll Cardiol 46:147-54.
11. Leschka S, Alkadhi H, Plass A, Desbiolles L, Grunenfelder J, Marincek B, Wildermuth S (2005) Accuracy of MSCT coronary angiography with 64-slice technology: first experience. Eur Heart J 26:1482-7.
12. Mollet NR, Cademartiri F, Krestin GP, McFadden EP, Arampatzis CA, Serruys PW, de Feyter PJ (2005) Improved diagnostic accuracy with 16-row multi-slice computed tomography coronary angiography. J Am Coll Cardiol 45:128-32.
13. Mollet NR, Cademartiri F, Nieman K, Saia F, Lemos PA, McFadden EP, Pattynama PM, Serruys PW, Krestin GP, de Feyter PJ (2004) Multislice spiral computed tomography coronary angiography in patients with stable angina pectoris. J Am Coll Cardiol 43:2265-70.
14. Mollet NR, Cademartiri F, van Mieghem CA, Runza G, McFadden EP, Baks T, Serruys PW, Krestin GP, de Feyter PJ (2005) High-resolution spiral computed tomography coronary angiography in patients referred for diagnostic conventional coronary angiography. Circulation 112:2318-23.
15. Nikolaou K, Knez A, Rist C, Wintersperger BJ, Leber A, Johnson T, Reiser MF, Becker CR (2006) Accuracy of 64-MDCT in the diagnosis of ischemic heart disease. AJR Am J Roentgenol 187:111-7.
16. Nikolaou K, Saam T, Rist C, Johnson T, Vogt F, Oberhoffer M, Reichart B, Reiser MF, Becker CR (2007) [Pre- and postsurgical diagnostics with dual-source computed tomography in cardiac surgery]. Radiologe 47:310-8.
17. Pugliese F, Mollet NR, Runza G, van Mieghem C, Meijboom WB, Malagutti P, Baks T, Krestin GP, deFeyter PJ, Cademartiri F (2006) Diagnostic accuracy of non-invasive 64-slice CT coronary angiography in patients with stable angina pectoris. Eur Radiol 16:575-82.
18. Raff GL, Gallagher MJ, O'Neill WW, Goldstein JA (2005) Diagnostic accuracy of noninvasive coronary angiography using 64-slice spiral computed tomography. J Am Coll Cardiol 46:552-7.
19. Ropers D, Rixe J, Anders K, Kuttner A, Baum U, Bautz W, Daniel WG, Achenbach S (2006) Usefulness of multidetector row spiral computed tomography with 64- x 0.6-mm collimation and 330-ms rotation for the noninvasive detection of significant coronary artery stenoses. Am J Cardiol 97:343-8.
20. Scheffel H, Alkadhi H, Plass A, Vachenauer R, Desbiolles L, Gaemperli O, Schepis T, Frauenfelder T, Schertler T, Husmann L,

Grunenfelder J, Genoni M, Kaufmann PA, Marincek B, Leschka S (2006) Accuracy of dual-source CT coronary angiography: First experience in a high pre-test probability population without heart rate control. Eur Radiol 16:2739-47.

21. Weustink AC, Meijboom WB, Mollet NR, Otsuka M, Pugliese F, van Mieghem C, Malago R, van Pelt N, Dijkshoorn ML, Cademartiri F, Krestin GP, de Feyter PJ (2007) Reliable high-speed coronary computed tomography in symptomatic patients. J Am Coll Cardiol 50:786-94.
22. Pugliese F, Mollet NR, Hunink MG, Cademartiri F, Nieman K, van Domburg R, Meijboom WB, Van Mieghem C, Weustink AC, Dijkshoorn ML, de Feyter PJ, Krestin GP Diagnostic performance of computed tomography coronary angiography using different generation multislice scanners. Single-centre experience. Radiology. In press
23. Hendel RC, Patel MR, Kramer CM, Poon M, Hendel RC, Carr JC, Gerstad NA, Gillam LD, Hodgson JM, Kim RJ, Kramer CM, Lesser JR, Martin ET, Messer JV, Redberg RF, Rubin GD, Rumsfeld JS, Taylor AJ, Weigold WG, Woodard PK, Brindis RG, Hendel RC, Douglas PS, Peterson ED, Wolk MJ, Allen JM, Patel MR (2006) ACCF/ACR/SCCT/SCMR/ASNC/NASCI/SCAI/SIR 2006 appropriateness criteria for cardiac computed tomography and cardiac magnetic resonance imaging: a report of the American College of Cardiology Foundation Quality Strategic Directions Committee Appropriateness Criteria Working Group, American College of Radiology, Society of Cardiovascular Computed Tomography, Society for Cardiovascular Magnetic Resonance, American Society of Nuclear Cardiology, North American Society for Cardiac Imaging, Society for Cardiovascular Angiography and Interventions, and Society of Interventional Radiology. J Am Coll Cardiol 48:1475-97.
24. Van Mieghem CA, Thury A, Meijboom WB, Cademartiri F, Mollet NR, Weustink AC, Sianos G, de Jaegere PP, Serruys PW, de Feyter P (2007) Detection and characterization of coronary bifurcation lesions with 64-slice computed tomography coronary angiography. Eur Heart J 28:1968-76.
25. Medina A, Suarez de Lezo J, Pan M (2006) [A new classification of coronary bifurcation lesions]. Rev Esp Cardiol 59:183.
26. Aviram G, Shmilovich H, Finkelstein A, Rosen G, Banai S, Graif M, Keren G (2006) Coronary ostium-straight tube or funnel-shaped? A computerized tomographic coronary angiography study. Acute Card Care 8:224-8.
27. Mollet NR, Hoye A, Lemos PA, Cademartiri F, Sianos G, McFadden EP, Krestin GP, Serruys PW, de Feyter PJ (2005) Value of preprocedure multislice computed tomographic coronary angiography to predict the outcome of percutaneous recanalization of chronic total occlusions. Am J Cardiol 95:240-3.
28. Maintz D, Seifarth H, Raupach R, Flohr T, Rink M, Sommer T, Ozgun M, Heindel W, Fischbach R (2006) 64-slice multidetector coronary CT angiography: in vitro evaluation

of 68 different stents. Eur Radiol 16:818-26.

29. Pugliese F, Cademartiri F, van Mieghem C, Meijboom WB, Malagutti P, Mollet NR, Martinoli C, de Feyter PJ, Krestin GP (2006) Multidetector CT for visualization of coronary stents. Radiographics 26:887-904.
30. Gilard M, Cornily JC, Pennec PY, Le Gal G, Nonent M, Mansourati J, Blanc JJ, Boschat J (2006) Assessment of coronary artery stents by 16 slice computed tomography. Heart 92:58-61.
31. Gaspar T, Halon DA, Lewis BS, Adawi S, Schliamser JE, Rubinshtein R, Flugelman MY, Peled N (2005) Diagnosis of coronary in-stent restenosis with multidetector row spiral computed tomography. J Am Coll Cardiol 46:1573-9.
32. Cademartiri F, Schuijf JD, Pugliese F, Mollet NR, Jukema JW, Maffei E, Kroft LJ, Palumbo A, Ardissino D, Serruys PW, Krestin GP, Van der Wall EE, de Feyter PJ, Bax JJ (2007) Usefulness of 64-slice multislice computed tomography coronary angiography to assess in-stent restenosis. J Am Coll Cardiol 49:2204-10.
33. Ehara M, Kawai M, Surmely JF, Matsubara T, Terashima M, Tsuchikane E, Kinoshita Y, Ito T, Takeda Y, Nasu K, Tanaka N, Murata A, Fujita H, Sato K, Kodama A, Katoh O, Suzuki T (2007) Diagnostic accuracy of coronary in-stent restenosis using 64-slice computed tomography: comparison with invasive coronary angiography. J Am Coll Cardiol 49:951-9.
34. Rixe J, Achenbach S, Ropers D, Baum U, Kuettner A, Ropers U, Bautz W, Daniel WG, Anders K (2006) Assessment of coronary artery stent restenosis by 64-slice multi-detector computed tomography. Eur Heart J 27:2567-72.
35. Pugliese F, Weustink AC, Van Mieghem C, Alberghina F, Otsuka M, Meijboom WB, Van Pelt N, Mollet NR, Cademartiri F, Krestin GP, Hunink MG, de Feyter PJ (2007. doi:10.1136/hrt.2007.126474. Available online at http://heart.bmj.com/cgi/content/abstract/hrt.2007.126474v1?papetoc.

Accessed 25 September 2007) Dual-source coronary computed tomography angiography for detecting in-stent restenosis. Heart
36. Takagi T, Stankovic G, Finci L, Toutouzas K, Chieffo A, Spanos V, Liistro F, Briguori C, Corvaja N, Albero R, Sivieri G, Paloschi R, Di Mario C, Colombo A (2002) Results and long-term predictors of adverse clinical events after elective percutaneous interventions on unprotected left main coronary artery. Circulation 106:698-702.
37. Smith SC, Jr., Feldman TE, Hirshfeld JW, Jr., Jacobs AK, Kern MJ, King SB, 3rd, Morrison DA, O'Neill WW, Schaff HV, Whitlow PL, Williams DO, Antman EM, Adams CD, Anderson JL, Faxon DP, Fuster V, Halperin JL, Hiratzka LF, Hunt SA, Nishimura R, Ornato JP, Page RL, Riegel B (2006) ACC/AHA/SCAI 2005 Guideline Update for Percutaneous Coronary Intervention--summary article: a report of the American College of Cardiology/American Heart Association Task Force on Practice Guidelines (ACC/AHA/SCAI Writing Committee to Update the 2001 Guidelines for Percutaneous Coronary Intervention).

Circulation 113:156-75.

38. Van Mieghem CA, Cademartiri F, Mollet NR, Malagutti P, Valgimigli M, Meijboom WB, Pugliese F, McFadden EP, Ligthart J, Runza G, Bruining N, Smits PC, Regar E, van der Giessen WJ, Sianos G, van Domburg R, de Jaegere P, Krestin GP, Serruys PW, de Feyter PJ (2006) Multislice spiral computed tomography for the evaluation of stent patency after left main coronary artery stenting: a comparison with conventional coronary angiography and intravascular ultrasound. Circulation 114:645-53.
39. Malagutti P, Nieman K, Meijboom WB, van Mieghem CA, Pugliese F, Cademartiri F, Mollet NR, Boersma E, de Jaegere PP, de Feyter PJ (2007) Use of 64-slice CT in symptomatic patients after coronary bypass surgery: evaluation of grafts and coronary arteries. Eur Heart J 28:1879-85.
40. Meyer TS, Martinoff S, Hadamitzky M, Will A, Kastrati A, Schomig A, Hausleiter J (2007) Improved noninvasive assessment of coronary artery bypass grafts with 64-slice computed tomographic angiography in an unselected patient population. J Am Coll Cardiol 49:946-50.
41. Pache G, Saueressig U, Frydrychowicz A, Foell D, Ghanem N, Kotter E, Geibel-Zehender A, Bode C, Langer M, Bley T (2006) Initial experience with 64-slice cardiac CT: non-invasive visualization of coronary artery bypass grafts. Eur Heart J 27:976-80.
42. Ropers D, Pohle FK, Kuettner A, Pflederer T, Anders K, Daniel WG, Bautz W, Baum U, Achenbach S (2006) Diagnostic accuracy of noninvasive coronary angiography in patients after bypass surgery using 64-slice spiral computed tomography with 330-ms gantry rotation. Circulation 114:2334-41; quiz 2334.
43. Alkadhi H, Wildermuth S, Plass A, Bettex D, Baumert B, Leschka S, Desbiolles LM, Marincek B, Boehm T (2006) Aortic stenosis: comparative evaluation of 16-detector row CT and echocardiography. Radiology 240:47-55.
44. Feuchtner GM, Dichtl W, Friedrich GJ, Frick M, Alber H, Schachner T, Bonatti J, Mallouhi A, Frede T, Pachinger O, zur Nedden D, Muller S (2006) Multislice computed tomography for detection of patients with aortic valve stenosis and quantification of severity. J Am Coll Cardiol 47:1410-7.
45. Willmann JK, Weishaupt D, Lachat M, Kobza R, Roos JE, Seifert B, Luscher TF, Marincek B, Hilfiker PR (2002) Electrocardiographically gated multi-detector row CT for assessment of valvular morphology and calcification in aortic stenosis. Radiology 225:120-8.

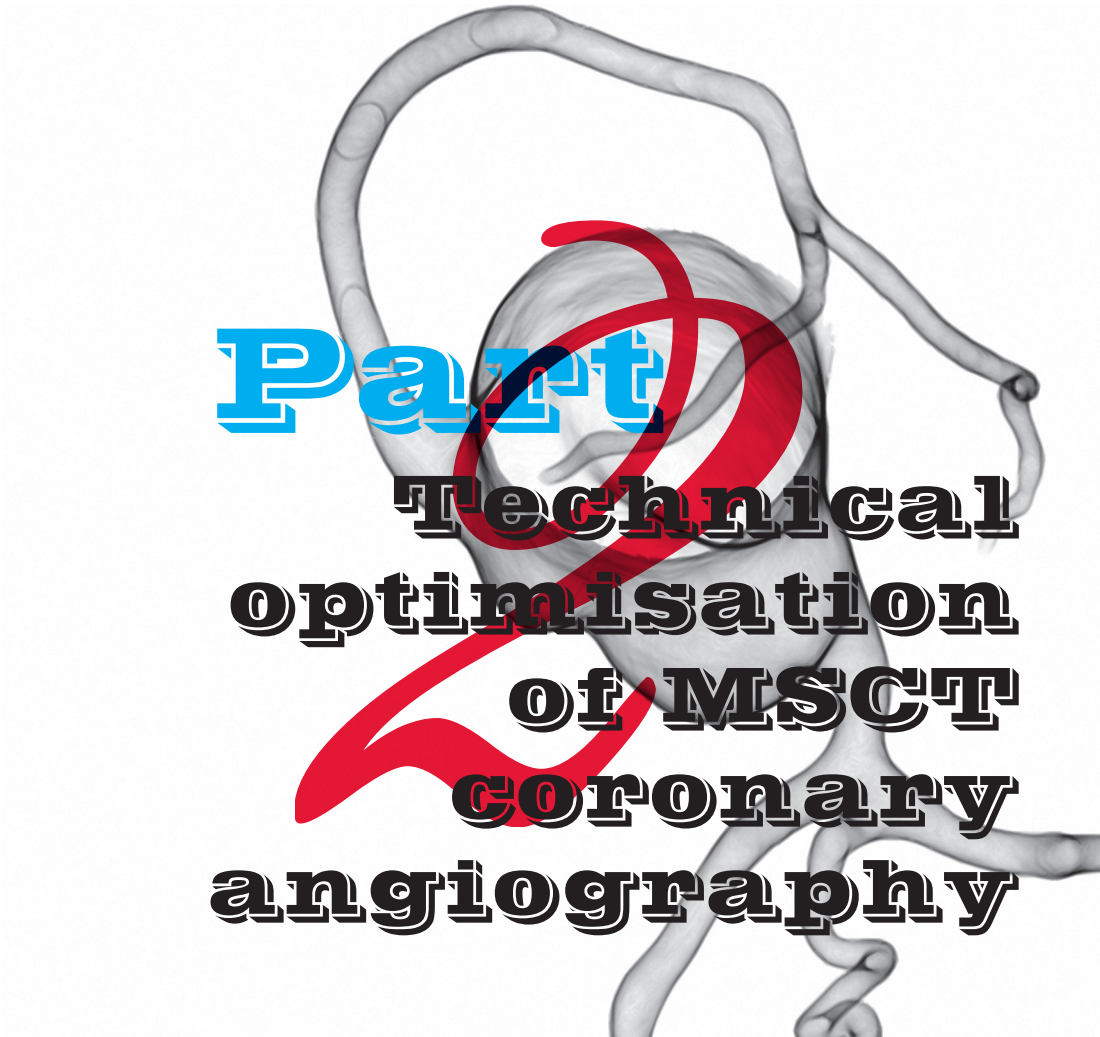

Part 2

Technical optimisation of MSCT coronary angiography

CHAPTER 3

Intravenous contrast material administration at coronary CT angiography: a review

Pugliese F, Cademartiri F, Mollet N, de Feyter P, Krestin G

In: de Feyter, Schoenhagen, Hammrtstingl, Feragalli (eds.) Advances in MDCT-Cardiac Imaging, volume 2, 2005.

Summary

A prerequisite for successful CT angiography is good contrast enhancement within the coronary arteries. In order to achieve this, there needs to be optimization of the injection parameters, e.g., contrast agent concentration, volume and injection rate. It is also mandatory to use appropriate techniques to synchronize the passage of contrast agent in the coronary vessels and the CT scan.

Introduction

Multi–detector technology has created new dimensions in spatial and temporal resolution in CT scanning. Multislice computed tomography scanners allow noninvasive coronary angiography within a single breath-hold by use of faster gantry rotation times and sophisticated algorithms for retrospective electrocardiographic gating [1]. Four-rows CT scanners had shown promising results [2] even if with a scan time of approximately 40 seconds, and suboptimal spatial and temporal resolution. Owing to the increased number of detector rows and faster gantry rotation, the introduction of 16-row scanners has decreased the time needed to image the entire heart to approximately 20 seconds, and thus enabled to obtain consistent images of the coronary arteries at CT angiography. Improved sensitivity of this technique in the detection of significant coronary artery stenoses has been reported [3, 4].

A prerequisite for successful CT angiography is prominent vascular enhancement. In order to achieve this, injection parameters must be accurately chosen and associated to synchronization protocols between the arterial passage of contrast agent and CT data acquisition. The introduction of multi-detector row CT technology requires even further optimization

and synchronization, due to the shorter acquisition times [5].

Contrast Enhancement in Coronary CT Angiography

The pattern of enhancement in a given vessel of interest can be described as a curve obtained by plotting attenuation values within the vessel against time, after intravascular injection of contrast material. This curve is also known as bolus geometry, and its shape resembles temporal changes in attenuation within the vessel (Figure 1). As it is observed in clinical practice with a fixed injection rate, this curve typically has a quite low upslope, a delay to reach a plateau rather than a peak, and eventually a slow decrease of the enhancement. Being aware of the attenuation changes in time is not trivial, since CT angiography is based on fast acquisition of data during the arterial phase of contrast passage. In order to image coronary arteries optimally, the timing and duration of CT scanning should be synchronized to the timing and duration of the actual enhancement curve, in particular to the portion resembling high and relatively homogenous attenuation.

Modality of Contrast Material Administration (parameters affecting bolus geometry)

The pattern of arterial enhancement (bolus geometry) in patients is influenced in first instance by parameters such as their age, body weight and cardiac output,

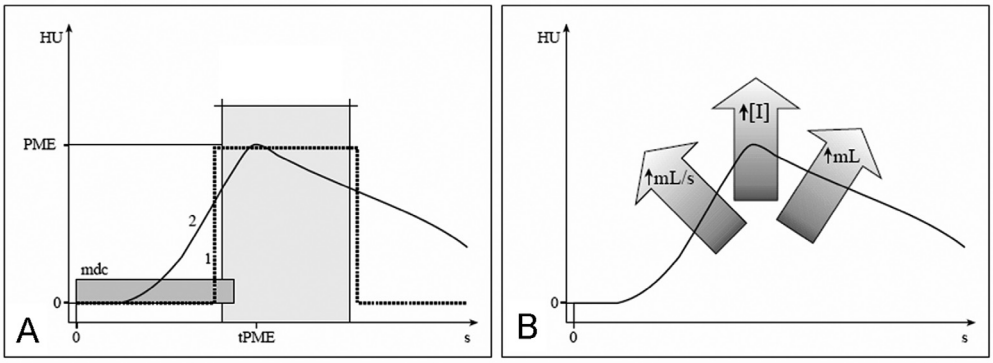

FIGURE 1. Attenuation-time curves after contrast agent injection at CT coronary angiography. (A) In ideal settings, the bolus geometry (dotted line, 1) has a rectangular shape and overlaps the CT imaging window (light grey rectangle). The actual enhancement curve (continuous line, 2) has a steep upslope, a rounded peak and a wash-out downslope. Portions of all the three enhancement phases are imaged. tPME= time to peak of maximum enhancement. PME= peak of maximum enhancement. (B) Contrast material volume, injection rate and concentration affect bolus geometry by elevating the peak of enhancement. The time to peak is delayed by an increase in volume, is made earlier by an increase in concentration whereas it stays unaffected by changes in iodine concentration [31].

which are not under operator control. Other parameters affecting bolus geometry such as (a) volume, (b) injection rate and (c) iodine concentration are related to the modality of contrast material administration, and thus are operator controlled [6, 7].

Contrast Material Volume

Ideally, a volume of contrast material normalized for a patient's body weight will result in a predictable degree of arterial enhancement. On the other hand, it is conceivable that an increase in contrast material volume will produce a proportional increase in arterial enhancement. In clinical practice, a fixed amount of contrast material is generally applied [8]. Since it is mandatory to obtain good coronary artery enhancement for the whole duration of the CT scan, an injection volume of approximately 100ml at 4ml/sec will take approximately 25 seconds to be administered, that is to say just a little longer than the average scan time of a 16-row CT imager [6]. In order to contain the dose of iodine and the risk of contrast material nephropathy, combined methods of contrast material bolus followed by saline solution flush have been applied to coronary CT angiography. Previous studies in the literature have described the injection of a saline solution in patients undergoing thoracic CT in order to push a decreased volume of contrast material, which allowed a 20% decrease of contrast material volume with a similar degree of tissue enhancement [9, 30]. More recently, the use of a saline solution injected intravenously immediately after the contrast material main bolus, also known as bolus chaser, has been tested in noninvasive 16-row CT coronary angiography, and has been compared to conventional contrast material protocols without bolus chaser [10]. The ´low volume' protocol with bolus chaser showed comparable enhancement at the level of coronary arteries with a 35% decrease in contrast material volume.

Injection Rate

In order to evaluate the relative effect of injection rate in vascular and hepatic enhancement during CT, some authors performed simultaneous and dynamic measurements of aortic, portal and hepatic attenuation in animal models and concluded that a higher injection rate has prominent effects on arterial enhancement without a consistent effect on venous and parenchymal (i.e. liver) enhancement [11]. Claussen et al. [12] reported that, in a patient population and with a peripheral injection site, below a threshold of 8ml/sec the peak aortic enhancement depended mainly on the injection rate, so that the elevation of the injection rate led to a proportional increase in arterial enhancement regardless of iodine concentration and injection volume [13]. The higher chance of renal

dysfunction associated with higher iodine load led to the development of strategies for improving the homogeneity of the arterial enhnacement to fit the imaging window, so that the overall amount of contrast material to be injected could be reduced. In particular, multiphasic protocols have been tested in which the injection rate is decreased during the contrast injection [14, 15, 16]. A higher injection rate at the beginning of the injection and a lower rate in the second part of the injection produce a prolongation of the plateau of enhancement. Such a change in bolus geometry was meant to allow the collection of the CT data set from the entire field of view with a constant level of arterial enhancement, while less contrast material volume is administered. The use of a multiphasic protocol for the administration of contrast material in 16-row coronary CT angiography does not provide significant advantages over a monophasic protocol in terms of vessel attenuation [17], since the faster scan time (faster gantry rotation + increased number of detector rows) makes the potential benefit for data acquisition of a longer plateau of enhancement worthless.The injection rates used in clinical coronary CT angiography range between 4 and 5ml/sec [6]. A large and proximal antecubital vein is commonly used in CT coronary angiography and 18-20 gauge cannulas allow the injection rate to be achieved without complications.

Iodine Concentration

Mathematical models for the description of contrast enhancement of blood vessels have been developed based on physiological data and pharmacokinetic rules. According to these approaches contrast enhancement of blood vessels follows the rules of a one-compartment model and depends on the volume of the vessel compartment, the flow rate within the vessel, the contrast material concentration and the time [18]. In animal series with given injection rate and volume, changes in contrast material concentration proved to have a prominent effect on arterial enhancement, whereas venous and parenchimal (i.e. liver) enhancement were affected much less prominently [11, 13]. Fenchel et al. [19] determined the influence of two different iodine concentrations of contrast material (400mg/ml vs. 300mg/ml) on contrast enhancement in abdominal multislice CT in a study performed on a patient population. According to these authors, the early enhancement of aorta, coeliac trunk and superior mesenteric artery is significantly higher when the 400mg/ml contrast material was used, thus allowing an excellent evaluability of splanchnic arteries [19, 20]. Similarly, there is clinical consent that effective opacification of the thoracic aorta is better achieved injecting high concentration contrast materials at injection rates of 3ml/sec or more [21]. The ideal iodine concentration for high vascular en-

hancement in coronary CT angiography is reported to be 350-400mg/ml [6].

CT Scan Synchronization (prediction of bolus geometry)

Synchronization of the scan with maximum enhancement of the vessels under investigation (imaging window) is the ultimate step required, not less important, in order to perform robust coronary CT angiography. Optimal acquisition timing is even more crucial when evaluation about patency of an in-stent coronary artery lumen is attempted on the basis of measured contrast enhancement, as reported in early papers [22, 23]. In general, for helical CT or multi–detector row helical CT, the most frequently used bolus timing techniques are (a) a fixed delay technique, (b) bolus-tracking, and (c) determination of the transit time by means of a test bolus injection.

Fixed delay Technique

Although the synchronization of contrast material administration is becoming increasingly important secondary to the introduction of faster multidetector CT scanners, controversies still remain on the use of these techniques. On the basis of experience and related to angiographic data, a fixed delay of 25 seconds was used to image the abdominal aorta after intravenous injection of 150ml of contrast material. In such series, 98% of the attenuation measurements were judged adequate for angiographic evaluation [24].

Bolus-Tracking Technique

This technique is based on real-time monitoring of the angiographic bolus with the acquisition of a series of dynamic low-dose monitoring scans at the level of the vessel of interest, during injection. It is possible to start the main scanning manually or automatically with a trigger threshold. The advantages of tracking the contrast agent bolus over the use of a fixed scan delay were assessed at dual-phase helical CT of the liver by Kopka et al. [25] Heavy and severely diseased patients represent the only limitation to this approach in that the attenuation threshold in tissues is often not achieved [26]. A method based on the interactive determination of the scanning delay at multidetector CT imaging of abdominal aortic aneurisms has also been published [27]. Low-radiation monitoring images were acquired in a single transverse section cephalad to the body region under investigation. The diagnostic portion of the scan was triggered manually and the power injector stopped as soon as contrast enhancement in the monitoring section could be qualitatively assessed. According to this study, a 29% decrease in contrast agent dose could be achieved with no enhancement loss

at the level of aorto-iliac arteries [27]. A protocol for optimal visualization of the pulmonary arteries in the diagnosis of pulmonary embolism was developed with the injection of a small bolus at slow injection rate, the passage of which was monitored at the level of pulmonary veins and triggered the injection of the main bolus [28]. This was meant to reduce high density artifacts arising from pooling of contrast agent in the right sections of the heart and allow better evaluation of the pulmonary arteries. In a recent study, the efficacy of the bolus-tracking technique was compared to that of test bolus at coronary CT angiography [5]. The authors report that the bolus-tracking group had more homogenous and steady enhancement compared with the test bolus group.

Test Bolus Technique

This technique is based on the calculation of the scan delay time by means of the intravenous injection of a small amount of contrast material (20 ml, or 15%–20% of the main bolus) during the acquisition of a series of dynamic, low-dose monitoring scans at the level of the vessel of interest [5]. The calculated delay time is eventually exerted between the commencement of the contrast main bolus injection and the start of CT data acquisition. Bolus-tracking was revealed to be superior to the test bolus technique in optimizing coronary artery opacification in 16-detector row CT coronary angiography [5].

Discussion

An overview of the literature attempting to optimize contrast injection parameters and scanning synchronization techniques is reported in Table 1. Some authors have focused on CT angiography in patient populations. Although others have experimented on animals or have primarily considered parenchymal (i.e. liver, pancreas) enhancement patterns, data on aortic enhancement are nevertheless available from these studies. Being aware of the x-ray attenuation changes in time within the vessels under investigation is not trivial, since CT angiography is strictly based on fast acquisition of data during the arterial phase of contrast passage, and most of these works test and express their efforts of optimizing contrast enhancement for CT angiography by means of measurements of vascular attenuation over time. The attenuation values sampled are distributed and described according to bolus geometry (and its changes). The bolus geometry and dynamics resemble the temporal changes of contrast enhancement within the vessels of interest (Fig. 1A). A rectangular profile that overlaps the imaging window is an ideal setting for bolus geometry. In practice, the enhancement curve has an upslope, a smooth peak re-

TABLE 1. Summary of the literature on the parameters affecting the bolus geometry and techniques of CT scanning synchronization. Changes in peak aortic attenuation are reported. The parameters tested in each study are **bolded.**

	Volume (ml)	Injection rate (ml/sec)	Concentration (mgI/ml)	Measured peak aortic attenuation (average, HU)
Yamashita et al. [29]	**1.5ml/kg**	3.0	300	238
	2.5ml/kg			270
Han et al. [13]	3ml/kg	**0.5**	300	262
		2		545
Fenchel et al. [19]	130	5.0	**300**	260
	98		**400**	365
Garcia et al. [11]	**1.5ml/kg**	**6**	280	388
	2ml/kg	**3**		288
Cademartiri et al.[5]	**20+100 test bolus**	4.0	320	306
	100 bolus tracking			328
Ho et al.[27]	**107±20 (interactive delay protocol)**	4.0	300	285
	150			288
Haage et al. [30]	**75**	3.0	370	240
	60+30 saline			238
Cademartiri et al. [10]	**140**	4.0	320	325
	100+40 saline			327

sembling a plateau and a wash-out portion. The shape of the bolus geometry can be manipulated in order to provide adequate contrast enhancement, both in terms of peak height and duration. The volume, injection rate and iodine concentration of the contrast material are the parameters that should be adjusted in order to optimize the attenuation of vessels. Such an effort can neglect neither the technical performance of the scanner such as gantry rotation time and number of detector rows (= scanning time), nor the size of the vascular territory to be imaged, since synchronization of the data acquisition with robust enhancement in the entire field of view must be achieved. An increase in contrast material volume increases arterial enhancement and delays the maximum enhancement peak (Fig. 1B). A higher injection rate also produces an increase in arterial enhance-

ment. The enhancement peak will also be earlier (Fig. 1B). Both the latest features are desirable in coronary CT angiography, so that high-injection rates are used. Nevertheless, in clinical practice such effects are limited by a higher chance of contrast material extravasation. Theoretically, administering the injection at decreasing rates acts on bolus geometry and prolongs the plateau phase, which is the imaging phase and allows the contrast agent dose to be reduced by minimizing the vessel enhancement in nondiagnostic phases. With the advent and widespread diffusion of 16-detector rows CT scanners this strategy is not even required anymore, owing to the faster coverage of the body region to be imaged at maximum enhancement, which automatically contains the contrast dose needed. The attenuation accomplished in vessels is also proportional to the iodine concentration of the contrast agent, whereas the time to peak remains unaffected by changes in concentration (Fig. 1B). Thus the use of high-concentration contrast agents is preferred over low-concentration ones. Conversely, one has to be aware that the influx of contrast of very high concentration may cause a combination of motion and high-density artifacts when imaged at CT. Moreover, it is well known that viscosity increases with iodine concentration and decreases with rising temperatures. Hence high concentration contrast materials (monomeric ≥ 350mg/ml or dimeric 320mg/ml) should be administered only after appropriate heating at 38°C. It has been pointed out that contrast material volume shares the effect of elevating the peak of enhancement with the other injection parameters. Nevertheless, at a fixed concentration and injection rate, a very high contrast volume would also increase the overall iodine load. In clinical practice, adequate enhancement during the imaging window is generally fulfilled through the use of fixed amounts of contrast material according to the temporal performance of the CT scanner. In our experience, provided that adequate concentration and injection rate are feasible for robust CT angiography in the first instance, the latter parameter is ultimately adjusted to a trade-off depending on the diagnostic question and patient habitus. For example, a larger field of view and a longer scan time are usually required for full coverage of bypass graft surgery. In these circumstances, no deterioration of image quality occurs with a slight reduction in the injection rate. A larger blood pool and higher x-ray attenuation may be partly associated with poorer vascular enhancement in heavier patients. As a rule of thumb, if the patient`s weight is over 90kg, a 20% increase in contrast material volume might be advisable.

Optimizing bolus geometry ultimately means tailoring the enhancement within

the vessels under study (which is a dynamic effect of contrast material administration) to the acquisition performance of the CT scanner. Once that the injection parameters have been adjusted and robust enhancement is predictable in the vascular bed, the CT data acquisition must be accurately synchronized to the most homogenous phase of enhancement. In other words, it would be worthless to obtain good contrast enhancement that does not correspond to the imaging window. To this purpose, several options are available. The imaging delay can be calculated by means of the test bolus technique by detecting the time for a small tester injection to travel to the vessels under study. Bolus-tracking is a synchronization technique in which, after one single contrast injection, a monitoring acquisition phase triggers the diagnostic acquisition phase as soon as the attenuation in the territory to be imaged reaches a threshold, visually or automatically assessed. Both a test bolus and a bolus-tracking can be advantageously applied to coronary CT angiography. A paper by Cademartiri et al.[5] tested the efficiency of both methods at 16-detector row CT and assessed a more homogenous and steady enhancement with the bolus-tracking technique, in particular at the level of left coronary branches. The analysis of the aortic bolus geometry revealed that the scan was performed during the plateau of enhancement in this group. In contrast, since the calculated scan delay was slightly shorter in the test bolus group, such patients were imaged when the contrast material in ascending aorta was still increasing (upslope of attenuation/time curve). Should a 4 detector-row CT imager be used to perform coronary angiography, hyperventilation may be necessary prior to the start of the data acquisition, owing to the relatively long scanning time. The wide respiratory movements in hyperventilation may not allow a reliable monitoring sequence for bolus-tracking at the level of ascending aorta. In these settings, the choice of bolus test over bolus-tracking may be mandatory.

References

1. Nieman K, Oudkerk M, Rensing BJ, et al. Coronary angiography with multi-slice computed tomography. Lancet 2001; 357:599-603.
2. Knez A, Becker CR, Leber A, at al. Uselfulness of multislice spiral computed tomography angiography for determination of coronary artery stenoses. Am J Cardiol 2001; 88:1191-1194.
3. Nieman K, Cademartiri F, Lemos PA, et al. Reliable noninvasive coronary angiography with fast submillimeter multislice spiral computed tomography. Circulation 2002; 106:2051-2054.
4. Ropers D, Baum U, Pohle K, et al. Detection of coronary artery stenoses with thin-slice multi-detector row spiral computed tomography and multiplanar reconstruction. Circulation 2003; 107:664-666.
5. Cademartiri F, Nieman K, van der Lugt A, et al. Intravenous contrast material administration at 16-detector row helical CT coronary angiography: test bolus versus bolus tracking technique. Radiology 2004; 233:817-823.
6. De Feyter PJ, Krestin GP (Eds.). Computed tomography of the coronary arteries. Chapter 19. Taylor and Francis Ed., Abingdon (UK) 2005.
7. Brink JA. Contrast optimization and scan timing for single and multidetector-row computed tomography. J Comput Assist Tomogr 2003; 27:S3-8.
8. Cademartiri F, van der Lugt A, Luccichenti G, Pavone P, Krestin GP. Parameters affecting bolus geometry in CTA: a review. J Comput Assist Tomogr 2002; 26:598-607.
9. Hopper KD, Mosher TJ, Kasales CJ, et al. Thoracic spiral CT: delivery of contrast material pushed with injectable saline solution in a power injector. Radiology 1997; 205:269-271.
10. Cademartiri F, Mollet N, van der Lugt A, et al. Non-invasive 16-row multislice coronary angiography: usefulness of saline chaser. Eur Radiol 2004; 14:178-183.
11. Garcia P, Genin G, Bret PM, et al. Hepatic CT enhancement: effect of the rate and volume of contrast medium injection in an animal model. Abdom Imag 1999; 24:597-603.
12. Claussen CD, Banzer D, Pfretzschner C, Kalender WA, Schorner W. Bolus geometry and dynamics after intravenous contrast medium injection. Radiology 1984; 153:365-368.
13. Han JK, Kim AY, Lee KY, et al. Factors influencing vascular and hepatic enhancement at CT: experimental study on injection protocol using a canine model. J Comput Assist Tomogr 2000; 24;400-406.
14. Hittmair K, Fleischmann D. Accuracy of predicting and controlling time-dependent aortic enhancement from a test bolus injection. J Comput Assist Tomogr 2001; 23; 474-484.

15. Fleischmann D, Hittmair K. Mathematical analysis of arterial enhancement and optimization of bolus geometry for CT angiography using the discrete Fourier transform. J Comput Assist Tomogr 1999; 23:474-484.
16. Fleischmann D, Rubin GD, Bankier AA, et al. Improved uniformity of aortic enhancement with customized contrast medium injection protocols at CT angiography. Radiology 2000; 214: 363-371.
17. Cademartiri F, Luccichenti G, Marano R, et al. Comparison of monophasic vs biphasic administration of contrast material in non-invasive coronary angiography using 16-row multislice computed tomography. Rad Med 2004; 107:489-496.
18. Bae KT, Heiken JP, Brink JA. Aortic and hepatic contrast medium enhancement at CT. Part I. Prediction with a computer model. Radiology 1998; 207: 647-655.
19. Fenchel S, Fleiter TR, Aschoff AJ, van Gessel R, Brambs HJ, Merkle EM. Effect of iodine concentration of contrast media on contrast enhancement in multislice CT of the pancreas. Br J Radiol 2004; 77:821-830.
20. Tsurusaki M, Sugimoto K, Fujii M, Sugimura K. Multi-detector row helical CT of the liver: quantitative assessment of iodine concentration of intravenous contrast material on multiphasic CT--a prospective randomized study. Radiat Med 2004; 22:239-245.
21. Storto ML, Ciccotosto C, Patea RL, Spinazzi A, Bonomo L. Spiral CT of the mediastinum: optimization of contrast medium use. Eur J Radiol 1994; 18:S83-87.
22. Hong C, Chrysant GS, Woodard PK, Bae KT. Coronary artery stent patency assessed with in-stent contrast enhancement measured at multi-detector row CT angiography: initial experience. Radiology 2004; 233:286-291.
23. Nieman K, Cademartiri F, Raaijmakers R, Pattynama P, de Feyter P. Noninvasive angiographic evaluation of coronary stents with multi-slice spiral computed tomography. Herz 2003; 28:136-142.
24. Macari M, Israel GM, Berman P, et al. Infrarenal abdominal aortic aneurism at multi-detector row CT angiography: intravascular enhancement without a timing acquisition. Radiology 2001; 220:519-523.
25. Kopka L, Rodenwaldt J, Fischer U, Mueller DW, Oestman JW, Grabbe E. Dual-phase helical CT of the liver: effects of bolus tracking and different volumes of contrast material. Radiology 1996; 201:321-326.
26. Paulson EK, Fisher AJ, DeLong DM, Parker DD, Nelson RC. Helical liver CT with computer-assisted bolus-tracking technology: is it possible to predict which patients will not achieve a threshold of enhancement? Radiology 1998; 209:787-792.
27. Ho LM, Nelson RC, Gimenez EI, DeLong DM. Abdominal aortic aneurysms at multi-detector row helical CT: optimization with interactive determination of scanning delay and contrast medium dose. Radiology 2004; 232:854-859.

28. Gattoni F, Tagliaferri B, Scali P, Brioschi S, Boioli F. Contrast medium injection optimisation in spiral CT for the diagnosis of pulmonary embolism. Radiol Med 2003; 105:416-424.
29. Yamashita Y, Komohara Y, Takahashi M et al. Abdominal helical CT : evaluation of optimal doses of intravenous contrast material-a prospective randomized study. Radiology 2000; 216:718-723.
30. Haage P, Schmotz-Rode T, Hubner D et al. Reduction of contrast material dose and artifacts by a saline flush using a double power injector in helical CT of the thorax Am J Roentgenol 2000; 174:1049-1053.
31. Cademartiri F, Luccichenti G, Marano R et al. Spiral CT-angiography with one, four, and sixteen slice scanners. Technical note. Radiol Med 2003; 106:269-283

CHAPTER 4

High iodine concentration contrast material for non-invasive MSCT coronary angiography: iopromide versus iomeprol 400

Cademartiri F, de Monye C, Pugliese F, Mollet NR, Runza G, van der Lugt A, Midiri M, de Feyter PJ, Lagalla R, Krestin G.

Investigative Radiology 2006; 41:349-353

Summary

Purpose: The objective of this study was to compare intracoronary attenuation on 16-row multislice computed tomography (16-MSCT) coronary angiography using 2 contrast materials (CM) with high iodine concentration.

Materials and Methods: Forty consecutive patients (29 male, 11 female; mean age, 61 ± 11 years) with suspected coronary artery disease were randomized to 2 groups to receive 100mL of either iopromide 370 (group 1: Ultravist 370, 370 mg iodine/mL; Schering AG, Berlin, Germany) or iomeprol 400 (group 2: Iomeron 400, 400 mg iodine/mL; Bracco Imaging SpA, Milan, Italy). Both CM were administered at a rate of 4 mL/s. All patients underwent 16-MSCT coronary angiography (Sensation 16; Siemens, Germany) with collimation 16 x 0.75 mm and rotation time 375ms. The attenuation in Hounsfield units (HU) achieved after each CM was determined at regions of interest (ROIs) placed at the origin of coronary arteries and on the ascending aorta, descending aorta, and pulmonary artery. Differences in mean attenuation in the coronary arteries and on the ascending aorta, descending aorta, and pulmonary artery were evaluated using Student t test.

Results: The mean attenuation achieved at each anatomic site was consistently greater after iomeprol 400 than after iopromide 370. At the origin of coronary arteries, the mean attenuation

after iomeprol 400 (340 ± 53 HU) was greater ($P < 0.05$) than that after iopromide 370 (313 ± 42 HU). Similar findings were noted for the mean attenuation in the ascending aorta, descending aorta, and pulmonary artery.

Conclusion: The intravenous administration of iomeprol 400 provides higher attenuation of the coronary arteries and of the great arteries of the thorax as compared with iopromide 370 using the same injection parameters.

Introduction

Current data suggest that significant coronary artery stenosis can be detected with 16-row multidetector computed tomography (16-MDCT) angiography [1–7]. The increased number of detector rows and faster gantry rotation with 16-MDCT compared with the previous 4-MDCT generation have improved the diagnostic performance of the technique and reduced the time needed to cover the entire heart to approximately 20 seconds [3]. The type and iodine concentration of contrast media (CM) used in CT angiography (CTA) have assumed increasing importance because the attenuation that can be achieved in vessels greatly affects image quality and thus diagnostic yield [8–10]. These considerations are even more important for imaging the coronary arteries because of the small caliber and tortuous anatomy of these vessels, and because of the presence of often extensive vessel wall disease.

The attenuation achievable in vessels can be improved by optimizing synchronization between the arterial passage of the CM and CT data acquisition and by modifying the injection parameters for intravenous (IV) administration of CM [8]. Whereas various bolus-tracking techniques are available to improve synchronization [11], modification of the injection parameters to increase vascular attenuation might involve altering the rate of CM injection, the volume injected, and/or the iodine concentration of the CM used [8]. Recently, we have demonstrated that CM with higher iodine concentrations yields significantly higher attenuation in the coronary arteries and descending aorta [12]. Although several iodinated CM are available on the market, very few are formulated to contain a high or very high concentration of iodine (ie, >350 mgI/mL). The purpose of the present study was to prospectively compare 2 different CM, one with a high concentration of iodine (iopromide 370 mgI/mL) and one with a very high concentration of iodine (iomeprol 400 mgI/mL), in terms of the attenuation obtained in an extended territory comprising the coronary arteries as well as the ascending and descending thoracic aorta and pulmonary arteries.

CHAPTER 4

Materials and Methods

Patient Population

A total of 40 patients (29 men, 11 women; mean age, 61 ± 11 years; age range, 34–79 years) referred for noninvasive MSCT coronary angiography for suspected coronary artery disease were enrolled prospectively. Exclusion criteria for coronary CTA were irregular heart rate, previous allergic reaction to iodine contrast media, renal insufficiency (serum creatinine >120 mmol/L), pregnancy, respiratory impairment, unstable clinical status, or marked heart failure. Institutional Review Board approval was received and all patients gave informed consent to participate in the study.

Patients were assigned randomly to 2 groups to receive either 100 mL of iopromide 370 (Ultravist 370; Schering AG, Berlin, Germany; 370 mg iodine/mL) (group 1) or 100 mL of iomeprol 400 (Iomeron 400; Bracco Imaging SpA, Milan Italy; 400 mg iodine/mL) (group 2). Patients with a pre-examination heart rate equal to or greater than 65 beats per minute (bpm) were given 100 mg of metoprolol orally 1 hour before the scan. The heart rate during the examination was recorded continuously.

Multislice Computed Tomography Examination Protocol

MSCT coronary angiography was performed on a 16-row detector system (Sensation 16; Siemens, Forchheim, Germany) in the craniocaudal direction. The scan parameters were as follows: number of detector rows: 16, individual detector width: 0.75 mm, gantry rotation time: 375 ms, tube voltage: 120 kV, tube current: 600–700 mAs, feed/rotation: 3.0 mm, scan range: 120–140 mm.

CM administration was performed intravenously (antecubital vein) using a prototype double-head power injector (Stellant; MedRAD, Pittsburgh, PA) through an 18-G Venflon needle. All CM administrations were performed intravenously at a rate of 4 mL/s and were followed by 40 mL of saline flush at the same rate. The resulting iodine administration rate was 1.48 g iodine/s for group 1 and 1.6 g iodine/s for group 2.

Synchronization between the passage of contrast material and data acquisition was achieved with real-time bolus tracking (CARE bolus; Siemens, Forchheim, Germany) using a region of interest (ROI) positioned on the ascending aorta. Automatic triggering of the scan acquisition occurred at a threshold attenuation of +100 Hounsfield units (HU) above baseline average attenuation.

Data Collection

Data collection and analysis was performed using previously reported methodology with some modifications [13]. Two datasets were reconstructed using retrospective electrocardiographic gating with a time window beginning 400 ms before the next R wave. The first dataset was reconstructed for the purpose of coronary artery attenuation assessment. Reconstruction of this dataset was performed with the following parameters: effective slice width: 1 mm, reconstruction interval: 0.5 mm (50% overlap), field of view (FOV): 160 mm, and convolution filter: medium-smooth (Siemens Medical Solutions; factory filter: B30f). The second dataset was reconstructed to assess the vessels of the thorax. Reconstruction of this dataset was performed with the following parameters: effective slice width: 3 mm, reconstruction interval: 3 mm, FOV: 200 mm, and convolution filter: medium-smooth.

Measurements of Attenuation

Coronary Arteries

Axial slices in the first dataset were scrolled to find the best location to measure the attenuation (HU) at the origin of the 4 main coronary arteries (right coronary artery [RCA], left main artery [LM], left anterior descending artery [LAD], circumflex [CX]) (Figure 1). The ROIs were drawn as large as possible on the vessels with care taken to avoid calcifications, plaques, and stenoses.

Great Vessels

The attenuation was determined at ROIs positioned on consecutive slices (at inter-

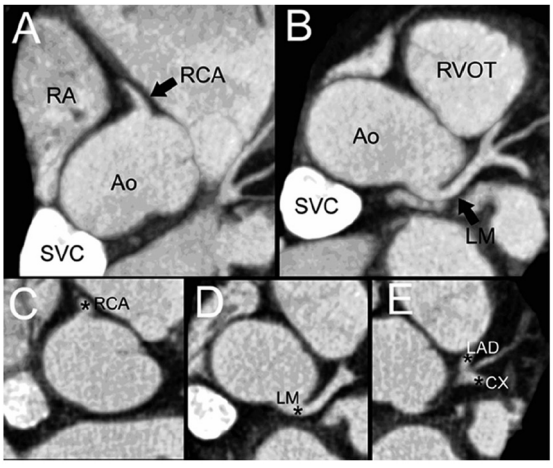

FIGURE 1. Assessment of attenuation at the origin of coronary vessels. In A and B, 2 oblique para-axial maximum-intensity projection reconstructions show the ascending aorta (Ao) and the origin of the right coronary artery (RCA) and left main coronary artery (LM). The superior vena cava (SVC) is also shown with very high attenuation. The assessments of attenuation at the origin of the main coronary arteries are performed for RCA, for LM, for the left anterior descending (LAD) artery and for the circumflex (CX), as shown in C, D, and E, respectively.

vals of approximately 1 second) on the ascending aorta through to the left ventricle (ROI1), the descending aorta (ROI2), and the pulmonary artery through to the right ventricle (ROI3). A fourth ROI (ROI4) was positioned on the superior vena cava (Figure 2). The attenuation after each CM and the bolus geometry of the CM in each vessel were determined.

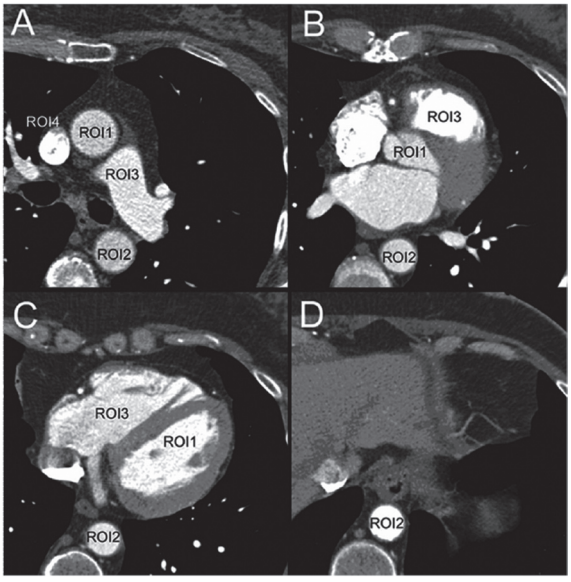

FIGURE 2. Assessment of bolus geometry through the dataset. The assessment of bolus geometry in the great vessels of the thorax was performed using regions of interest (ROI) positioned on each vessel on consecutive slices. ROIs on the ascending aorta (ROI1) were positioned at the beginning of the scan (A and B) and at the point of entry of contrast material into the left ventricle (C). ROIs on the descending aorta (ROI2) were positioned on consecutive slices throughout the dataset (A–D). ROIs on the pulmonary artery (ROI3) were positioned at the beginning of the scan (A), at the right ventricle outflow tract (B), and in the right ventricle (C). A fourth (ROI4) was positioned on the superior vena cava at the beginning of the scan (A).

Data Analysis

The attenuation values of the 4 coronary arteries were averaged for all patients in each group, and the overall average was used to compare the 2 groups.

The attenuation values obtained from the ROIs positioned on the ascending and descending aorta and pulmonary artery in each patient were averaged at each time point to generate average time/density curves. The average vascular attenuation in these vessels indicated quantitatively the amount of CM present in the vessel during the scan. Two additional parameters were considered descriptive of vascular attenuation in the great vessels of the thorax: the attenuation at the beginning of the scan (time 0) and the maximum enhancement value (MEV; peak of attenuation) determined from the time/density curve.

Significant differences between the 2 groups were assessed using a Student t test. A P-value <0.05 was considered significant.

Results

The mean (± standard deviation) age, body weight, and heart rate (HR) of patients in each group are shown in Table 1 along with the mean scan delay and mean scan time of the MSCT examinations. No significant

TABLE 1. Demographic data

	Group 1	Group 2
No. patients	20	20
Male/female	15/5	14/6
Age (yrs)	59 ± 12	63 ± 10
Weight (kg)	73 ± 9	75 ± 11
Heart rate (beats/min)	61 ± 7	60 ± 8
Mean scan delay (sec)	21.7 ± 1.9	20.6 ± 2.3
Mean scan time (sec)	18.0 ± 2.1	18.5 ± 2.4

differences (P >0.05) in any parameter were apparent between the groups. Of the 40 patients enrolled for the study, 22 (55%) were already on long-term beta-blockers. A total of 28 of 40 (70%) patients received additional oral beta-blockers before the scan. The average heart rate at patient presentation for the scan was 69 ± 11 bpm, which dropped to 57 ± 8 bpm after beta-blocker administration.

All examinations and bolus timing procedures were successfully completed in all patients. No significant adverse reactions to contrast material were observed in any patient and no changes in heart rate were noted either during the administration of contrast material or during the MSCT examination itself.

Coronary Artery Attenuation

The mean attenuation at the origin of the 4 coronary arteries was always higher after Iomeron 400 (340 ± 53 HU) than after iopromide 370 (313 ± 42 HU) (Table 2; Figure 3).

Comparison of the mean overall difference between the 2 groups revealed significantly (P <0.05) higher mean attenuation after Iomeron 400 than after iopromide 370.

Great Vessel Attenuation

The average attenuation was in all cases significantly (P <0.05) higher after Iomeron 400 than after iopromide 370 (ascending aorta: 353 ± 59 HU vs 312 ± 47 HU; descending aorta: 350 ± 55 HU vs 307 ± 48 HU; pulmonary artery: 317 ± 72 HU vs 282 ± 52 HU, respectively)

TABLE 2. Attenuation at Origin of Coronary Arteries

Vessel - HU	Group 1	Group 2	Δ
RCA	315 ± 58	357 ± 66	+42
LM	322 ± 45	350 ± 52	+28
LAD	295 ± 57	321 ± 65	+34
CX	287 ± 46	331 ± 60	+44
Average*	313 ± 42	340 ± 53	+27

* The average attenuation at the origin of coronary arteries was significantly lower for group 1 (Ultravist 370) compared with group 2 (Iomeron 400) (P <0.05).
SD, standard deviation; Δ = relative difference (group 2 average HU - group 1 average HU).

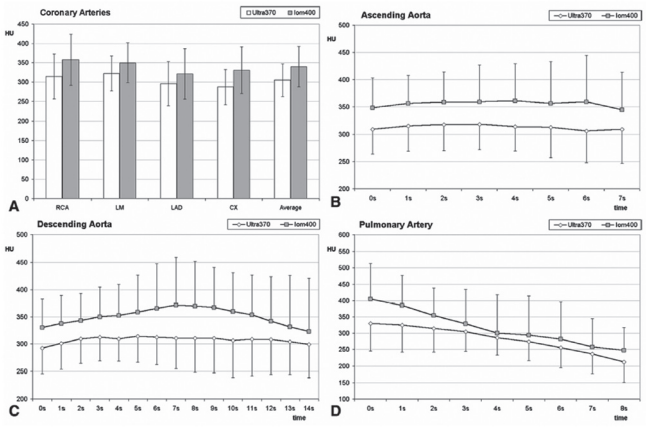

FIGURE 3. Results of attenuation assessment of coronary arteries and great thoracic vessels. The results of the attenuation assessment at the level of coronary arteries show slightly lower values for group 1 but not significantly different in all 4 sample regions (A). The average time/density curves in the ascending aorta and descending aorta are almost identical for groups 1 and group 2 (B and C). For the pulmonary artery, instead, group 1 shows more "pooling" of contrast material in the right chambers of the heart (D).

(Table 3; Figure 3). Similar findings were obtained for the attenuation at time zero. Determinations of the MEV revealed significantly ($P < 0.05$) greater attenuation with Iomeron 400 in the ascending and descending aorta but not in the pulmonary artery.

Discussion

Imaging of the coronary arteries is hampered by their small size and tortuous course and, when a stenosis or obstruction is present, by reduced blood flow. Improved visualization of these vessels can be achieved by increasing the iodine administration rate either by increasing the injection rate to provide a progressively higher vascular attenuation or by increasing the iodine concentration of the administered CM [14]. Although increasing the injection rate is possibly a more readily feasible approach than increasing the iodine concentration of the CM, the injection rates used in routine clinical practice for coronary artery imaging are already typically 4 to 5 mL/s. To increase the injection rate further would require larger needles and larger veins and more time to set the intravenous supply. Moreover, the risk of CM extravasation would also increase. The use of a CM with higher iodine concentration may thus be an attractive alternative, particularly for the improved visualization of vessels that contain a smaller volume of blood [9,10].

A number of reports have discussed the role of CM with high iodine concentration for CT angiography [12,14,15]. In a recent study comparing several contrast agents with differing iodine concentrations (iohexol 300 mgI/mL, iodixanol 320 mgI/mL, iohexol 350 mgI/mL, iomeprol 350 mgI/mL, and iomeprol 400 mdI/mL) for MSCT of the coronary arteries, we

TABLE 3. Bolus Geometry in the Great Vessels of the Thorax

	Ascending Aorta				Descending Aorta				Pulmonary Artery			
	Group 1	Group 2	Δ	P	Group 1	Group 2	Δ	P	Group 1	Group 2	Δ	P
Average (HU)	312 ± 47	353 ± 59	+41	<0.05	307 ± 48	350 ± 55	+43	<0.05	282 ± 52	317 ± 72	+35	<0.05
Time 0 (HU)	309 ± 45	348 ± 55	+39	<0.05	292 ± 47	330 ± 53	+38	<0.05	330 ± 85	405 ± 109	+75	<0.05
MEV (HU)	339 ± 48	390 ± 70	+51	<0.05	341 ± 49	408 ± 73	+67	<0.05	317 ± 52	352 ± 100	+35	0.17

Measurements of vascular attenuation for the main vessels of the thorax are displayed for group 1 (Ultravist 370) and group 2 (Iomeron 400).
Δ , relative difference (group 2 average HU - group 1 average HU).

have shown that significantly higher vascular attenuation is achieved with the highest iodine concentration and that significantly lower attenuation is achieved with the lowest iodine concentration [12]. Our findings support the findings of an earlier study by Becker et al [16] in which 2 different iodine concentrations (iomeprol 300 and 400 mgI/mL) were compared at 2 different injection rates (2.5 and 3.5 mL/s) for 4-MSCT angiography of coronary arteries. Their conclusion was that the vascular attenuation achieved with 400 mgI/mL and 3.5 mL/s was significantly higher than the other protocols and that 300 mgI/mL and 2.5 mL/s provides significantly lower attenuation. More recently, a study by Rist et al has shown that 63 mL of a CM with high iodine concentration (Iomeron 400) injected at a rate of 2.5 mL/s provides equivalent attenuation to that achieved after injection of 83 mL of a CM with standard iodine concentration (Iomeron 300) at a rate of 3.3 mL/s [Rist, personal communication].

Our prospective study was aimed at further defining the benefits of CM with high iodine concentration by comparing the attenuation achieved in the coronary arteries and great vessels of the thorax after administration of 2 CM with high iodine concentration (iopromide 370 and Iomeron 400). Along with iopamidol 370 (Isovue 370; Bracco Diagnostics, Princeton, NJ), these 2 CM contain the highest con-

centrations of iodine of any CM currently available on the market. With all other injection variables (volume, injection rate) and examination parameters kept constant, significantly higher attenuation was found in all vessels with the CM with the highest concentration of iodine (400 mg/mL). These findings suggest that modest increases in the concentration of iodine can lead to significant increases in the attenuation observed and thereby improve the visualization of the vessels of interest.

With the advent of newer, faster 16- and 64-slice CT scanners with considerably more rapid acquisition times, there is a greater need to achieve high attenuation in a shorter period time without a concomitant increase in CM volume. Although one way to achieve this is by modifying the iodine administration rate through alteration of the CM injection rate, a more practical way might entail the use of a CM with higher iodine concentration. Given the greater attenuation seen in the present study with Iomeron 400, and the fact that no differences were observed in either the incidence of adverse events or the heart rate before and after injection, the CM with the highest concentration of iodine can be recommended for CT angiography of small arteries.

In conclusion, our study has demonstrated that the use of CM with higher iodine concentration provides higher vascular attenuation in the coronary arteries as well as in the ascending and descending thoracic aorta and pulmonary arteries.

References

1. Nieman K, Cademartiri F, Lemos PA, et al. Reliable noninvasive coronary angiography with fast submillimeter multislice spiral computed tomography. Circulation. 2002; 106:2051–2054.
2. Ropers D, Baum U, Pohle K, et al. Detection of coronary artery stenoses with thin-slice multi-detector row spiral computed tomography and multiplanar reconstruction. Circulation. 2003; 107:664–666.
3. Heuschmid M, Kuttner A, Flohr T, et al. Visualization of coronary arteries in CT as assessed by a new 16 slice technology and reduced gantry rotation time: first experiences. Rofo. 2002; 174:721–724.
4. Flohr T, Stierstorfer K, Bruder H, et al. New technical developments in multislice CT—part 1: approaching isotropic resolution with sub-millimeter 16-slice scanning. Rofo. 2002; 174:839–845.

5. Flohr T, Bruder H, Stierstorfer K, et al. New technical developments in multislice CT, part 2: sub-millimeter 16-slice scanning and increased gantry rotation speed for cardiac imaging. Rofo. 2002; 174:1022–1027.
6. Gerber TC, Stratman BP, Kuzo RS, et al. Effect of acquisition technique on radiation dose and image quality in multidetector row computed tomography coronary angiography with submillimeter collimation. Invest Radiol. 2005; 40:556–563.
7. Sanz J, Rius T, Kuschnir, et al. The importance of end-systole for optimal reconstruction protocol of coronary angiography with 16-slice multidetector computed tomography. Invest Radiol. 2005; 40:155–163.
8. Cademartiri F, van der Lugt A, Luccichenti G, et al. Parameters affecting bolus geometry in CTA: a review. J Comput Assist Tomogr. 2002; 26:596–607.
9. Bae KT, Heiken JP, Brink JA. Aortic and hepatic peak enhancement at CT: effect of contrast medium injection rate—pharmacokinetic analysis and experimental porcine model. Radiology. 1998; 206:455– 464.
10. Fleischmann D, Rubin GD, Bankier AA, et al. Improved uniformity of aortic enhancement with customized contrast medium injection protocols at CT angiography. Radiology. 2000; 214:363–371.
11. Cademartiri F, Nieman K, van der Lugt A, et al. Intravenous contrast material administration at helical 16-multidetector-row helical CT: test bolus vs bolus tracking. Radiology. 2004; 233:817– 823.
12. Cademartiri F, Mollet NR, van der lugt A, et al. Intravenous contrast material administration at helical 16-detector row CT coronary angiography: effect of iodine concentration on vascular attenuation. Radiology. 2005; 236:661– 665.
13. Cademartiri F, Mollet N, van der Lugt A, et al. Non-invasive 16-row multislice CT coronary angiography: usefulness of saline chaser. Eur Radiol. 2004;14: 178 –183.
14. Fleischmann D. Use of high concentration contrast media: principles and rationale—vascular district. Eur J Radiol. 2003; 45(suppl 1):S88 –S93.
15. Brink JA. Use of high concentration contrast media (HCCM): principles and rationale—body CT. Eur J Radiol. 2003; 45(suppl 1): S53–S58.
16. Becker CR, Hong C, Knez A, et al. Optimal contrast application for cardiac 4-detector-row computed tomography. Invest Radiol. 2003; 38:690–694.

CHAPTER 5

Post-processing using MSCT coronary angiography improves image interpretability in patients with fast heart rates and heart rate variations

Pugliese F, Alberghina F, Meijboom WB, Malago' R, Gopalan D, de Feyter PJ.

Journal of Cardiovascular Medicine 2007; 8:1088-1090.

Summary

In coronary computed tomography (CT) angiography, the patient's electrocardiogram (ECG) is used

a) to modulate the emission of high-energy x-rays during a portion the R-R interval (pulsing window) in order to reduce the x-ray exposure to patients, and b) to select the CT data acquired during the same portion of the R-R interval over multiple cardiac cycles (reconstruction window) in order to minimize motion artifacts.

The application of a modulation interval (pulsing window) appropriate to the patient's heart rate and the combination of several different datasets (reconstruction windows) provides a robust method for obtaining diagnostic information with coronary CT angiography in patients with heart rate variations during the scan.

Introduction

Coronary computed tomography (CT) angiography is becoming a practical alternative to coronary catheterization in selected patient groups [1]. However, the literature reports that image quality is inversely related to heart rate [2]; diagnostic accuracy is higher at lower heart rates and deteriorates at higher heart rates [3]. Likewise, heart rate variation during the

scan may impair image quality heavily. We demonstrate how we obtained diagnostic image quality of the right coronary artery (RCA) with 64-slice CT angiography in a patient whose heart rate ranged from 81 to 111 beats/min during the scan. The average heart rate was 99 beats/min.

Materials and Methods

The patient was a 42-year-old obese woman, with Kawasaki disease diagnosed at 2 years of age and mental retardation, who presented with exertional palpitations. Rest electrocardiogram (ECG) and stress testing were inconclusive for recent ischemia. Non-invasive study of coronary arteries was performed with CT angiography. The patient had sinus heart rhythm and average heart rate was 88 beats/min before preparation. One hour before the CT study, the patient received 100mg metoprolol orally and medication to reduce anxiety. Five milligrams of atenolol were injected i.v. just before the scan. Nevertheless, the average heart rate during scan was 99 beats/min, ranging from 81 to 111 beats/min (Figure 1).

When the patient received instructions before the scan and the breath hold was rehearsed, we noted that the heart rate was subject to changes in frequency. Thus, we increased the interval during which maximum tube output was given from the routine 55–70% of the cardiac cycle to 25–70%.

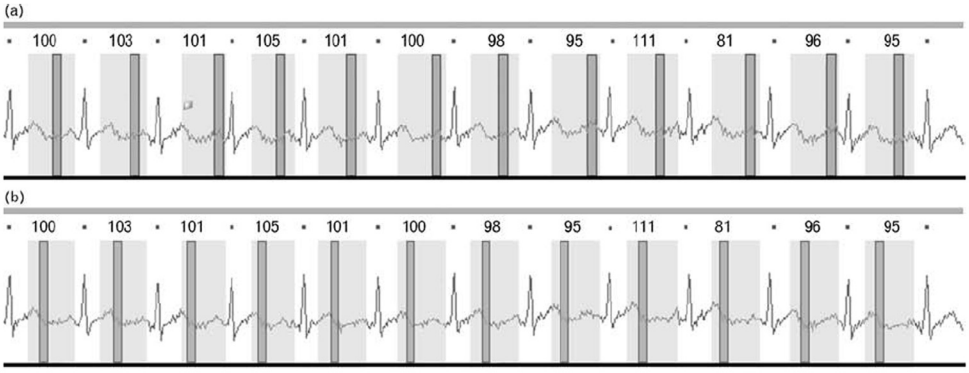

FIGURE 1. Electrocardiogram registered during the computed tomography scan. Maximal X-ray tube output is given from 25–70% of cardiac cycle (light boxes) so that data acquired during diastole (a) and systole (b) can be used for image reconstruction.

Coronary CT angiography was performed with a 64-slice scanner (Siemens Sensation 64, Erlangen, Germany). Gantry rotation time was 330 ms, detector size

was 2x32x0.6mm (z-flying focal spot technology). These parameters translated into a temporal resolution of 165 ms and a spatial resolution of isotropic 0.4mm3. Contrast agent (Iomeron, 400 mgI/ml, Bracco, Milan, Italy) was injected into the antecubital vein at a flow rate of 5.0 ml/s.

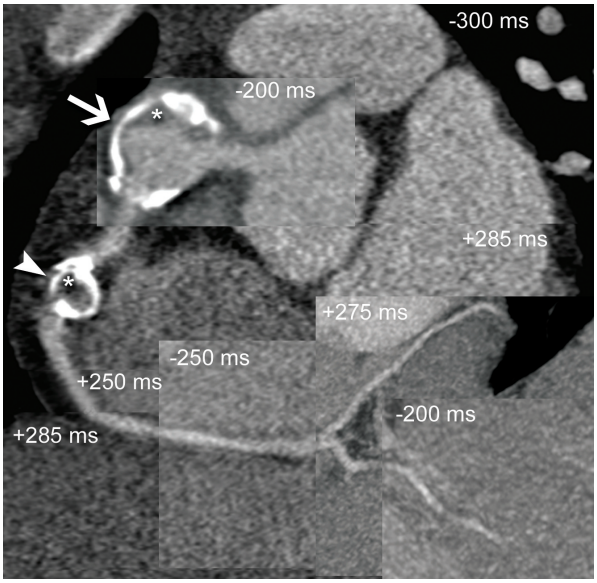

FIGURE 2. 'Panoramic' multiplanar computed tomography view of the right coronary artery (RCA) obtained by combination of datasets from different phases of the cardiac cycle. A giant calcified aneurysm is seen proximally (arrow). A second calcified aneurysm is localized in the mid-tract of the RCA (arrowhead). Hypodense material consistent with thrombus is visible in both aneurysms (asterisks). However, the lumen is patent.

First, we reconstructed two datasets 300 ms before the R wave with monosegmental and bisegmental reconstruction algorithms, respectively. Because the latter did not result in better image quality, we proceeded by reconstructing multiple datasets using the monosegmental algorithm. Both diastolic (Figure 1a) and systolic (Figure 1b) reconstruction windows were used. Reconstructed slice thickness was 0.75mm with an increment of 0.4mm.

Results

Tracts of the RCA could be visualized by diagnostic image quality in different datasets. By combining multiplanar views on an offline computer, the RCA could be visualized in its entirety (Figure 2). The left coronary artery was less affected by motion artefacts and was unremarkable. Despite the high heart rate of the patient, diagnostic image quality was obtained due to the enhanced temporal resolution of 64-slice CT compared to previous-generation CT scanners.

Two partially calcified coronary aneurysms were seen in the RCA. The proximal, larger aneurysm (Figure 2, arrow) was patent with a small amount of thrombus (Figure 2, asterisk) layered on its walls. The aneurysm localized in the mid-RCA (Figure 2, arrowhead) was partially filled with thrombus (asterisk). At this level, two experienced readers (FP, WBM)

scored in consensus the severity of luminal narrowing as <50%. The total time needed for preparation of the datasets and their evaluation was 20 min. The patient eventually underwent conventional angiography (Figure 3). Fractional flow reserve measurement in the mid-RCA yielded a value <0.75, confirming the CT findings.

Discussion

Coronary CT angiography is a fast, non-invasive diagnostic modality where data for image formation can be acquired over the entire cardiac cycle or over a portion of the R-R interval. The latter acquisition technique is called ECG-controlled dose modulation. ECG-controlled dose modulation involves maximal X-ray tube output during diastole accompanied by a decrease in tube output during systole. The result is a total dose reduction of 30–50%, depending on the patient's heart rate [4]. Therefore, the use of dose modulation is always recommended. However, when the patient's heart rate is high and refractory to b-blockers, reconstructions in the systolic phase are often necessary, especially for visualization of the middle RCA.

By widening the maximal tube output interval to 25–70%, we used data acquired in both systole and diastole for image formation. A wider pulsing interval also allows manual editing of the position of reconstruction windows along the cardiac cycle to compensate for heart rate changes during the scan. After analysing the RCA segment by segment in different datasets, we selected the best images from each dataset and provided an inter-

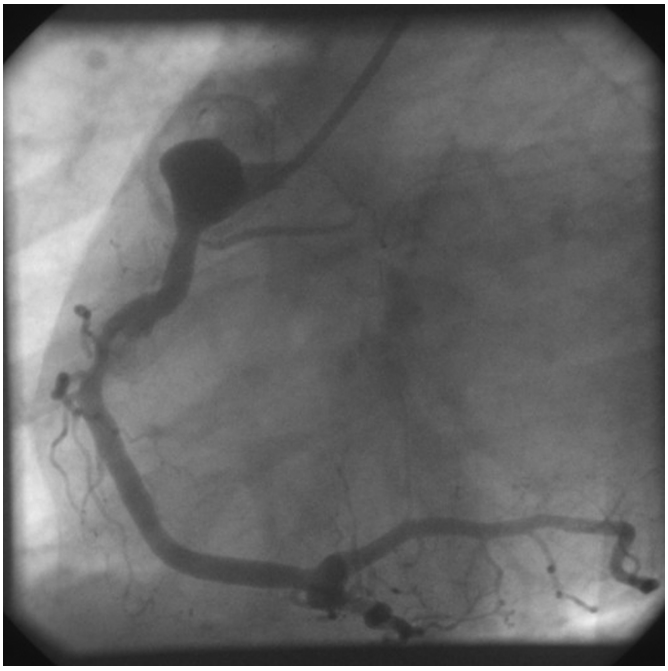

FIGURE 3. Conventional angiogram of the right coronary artery confirms the computed tomography findings.

pretable view of the entire RCA (Figure 2).

It could be argued that increasing the interval of maximal tube output increases X-ray exposure. However, a percentage increase of the modulation interval does not imply an absolute increase in patient X-ray exposure when the patient's heart rate is very high. Moreover, it has been reported that, at heart rates less than 85 beats/min, the best image quality is obtained in diastole whereas, with higher heart rates, the best reconstruction phase shifts to end-systole [5]. Setting the maximal tube output to the end-systole might therefore reduce the radiation exposure without decreasing image quality in patients with high heart rates.

If the acquisition protocol is flexible and adapted to a patient's heart rate, coronary CT angiography has advantages over other non-invasive coronary imaging modalities (e.g. magnetic resonance imaging; MRI). In uncooperative patients, CT is easier than MRI because it is faster and one single breath-hold is required. The capability to intervene with customized image reconstruction and expert post-processing to minimize motion artefacts is an additional tool for improving the clinical reliability of coronary CT angiography.

References

1. Pugliese F, Mollet NR, Runza G, van Mieghem C, Meijboom WB, Malagutti P, et al. Diagnostic accuracy of non-invasive 64-slice CT coronary angiography in patients with stable angina pectoris. Eur Radiol 2006; 6:575–582.
2. Hong C, Becker CR, Huber A. ECG-gated reconstructed multi-detector row CT coronary angiography: effect of varying trigger delay on image quality. Radiology 2001; 220:712–717.
3. Nieman K, Rensing BJ, van Geuns RJ, Vos J, Pattynama PM, KrestinGP, et al. Non-invasive coronary angiography with multislice spiral computed tomography: impact of heart rate. Heart 2002; 88:470–474.
4. Hausleiter J, Meyer T, Hadamitzky M, Huber E, Zankl M, Martinoff S, et al. Radiation dose estimates from cardiac multislice computed tomography in daily practice: impact of different scanning protocols on effective dose estimates. Circulation 2006; 113:1305–1310.
5. Leschka S, Wildermuth S, Boehm T, Desbiolles L, Husmann L, Plass A, et al. Noninvasive coronary angiography with 64-section CT:

effect of average heart rate and heart rate variability on image quality. Radiology 2006; 241:378–385.

CHAPTER 6

Optimal ECG pulsing windows in relation to heart rate: effect on image quality and radiation exposure in dual source computed tomography coronary angiography

Weustink AC, Mollet NR, Pugliese F, Flohr T, Meijboom WB, Dijkshoorn ML, ten Kate G-J, de Feyter PJ, Krestin GP.

Radiology, manuscript in press.

Summary

Purpose: To determine the optimal width and timing of the ECG pulsing window within the cardiac cycle in relation to heart rate (HR), image quality and radiation exposure in patients with suspected coronary artery disease.

Materials and Methods: The institutional review board approved the study and all patients gave informed consent.

Dual Source CT was performed in 301 patients (mean HR 70.1±13.3; range: 43-112 bpm) using a wide ECG pulsing window (25-70% of the R-R-interval). Datasets were reconstructed every 5% from 20%-75% of RR-interval. Image quality was assessed by two observers on a per segment level and classified as good or impaired. High quality datasets were those with each segment being of good quality. The width and timing of the image reconstruction window was calculated. Based on these findings, an optimal HR dependent ECG pulsing protocol was designed and the potential dose-saving effect on effective dose (in mSv) was calculated.

Results: At low HR (≤65 bpm), high-quality datasets were obtained during ED, at high HR (≥80 bpm) during ES and at intermediate HR (66-79 bpm) during both

ES and ED. The optimal ECG pulsing windows for low, intermediate and high HR were at 60-76%, 30-77% and 31-47% of the R-R-interval, which decreases the effective dose at low HR from 18.7 to 6.8 mSv, at intermediate HR from 14.7 to 13.4 mSv and at high HR from 11.3 to 4.2 mSv, respectively.

Conclusion: Optimal ECG pulsing can reduce radiation exposure to the patient, in particular in low and high heart rates with preservation of image quality.

Introduction

CT coronary angiography has emerged as a non-invasive diagnostic modality that reliably excludes the presence of significant coronary artery disease (1-8). However, the radiation exposure associated with CT-scanning is high (9) as compared to conventional coronary angiography, and may restrict clinical use.

Technological improvements are required to reduce radiation exposure, while preserving CT image quality. The Dual Source CT (DSCT) scanner is equipped with two X-ray sources resulting in an improved temporal resolution of 83 ms allowing scanning at higher heart rates (10-14). The radiation exposure is primarily reduced due to the increased pitch, and thus shorter scan times in patients with higher heart rates. An additional cardiac bowtie filter and a smaller field-of-view of the second detector further reduce radiation exposure (14).

In addition, DSCT is equipped with electrocardiographically (ECG)-triggered X-ray tube modulation or "ECG pulsing". Prior to the scan, the operator can manually select the width and timing of the ECG pulsing window in the R-R-interval during which full tube current is given. The ECG pulsing window is preferably positioned within the cardiac cycle when the heart moves less, e.g. end-systole and end-diastole, to obtain motion-free images of the coronary arteries. The tube current outside the pulsing window can be set at 20% (functional analysis possible) or 4% of nominal tube current and hence the total radiation exposure can be greatly reduced.

The aim of this study was to determine the optimal width and timing of the ECG pulsing window within the cardiac cycle in relation to heart rate (HR), image quality and radiation exposure in patients suspected for coronary artery disease.

CHAPTER 6

Materials and Methods

Patients, Scan Protocol, and Image Reconstruction

Authors who are not employees of or consultants for Siemens Medical Solutions (Forchheim, Germany) had control of inclusion of any data and information that might present a conflict of interest for the author (T.G.F.) who is an employee of that company.

During a period from July 2006 to June 2007, we included 362 consecutive symptomatic patients suspected of having coronary artery disease scheduled for conventional coronary angiography (CCA). Only patients in sinus rhythm without a previous history of percutaneous intervention or bypass surgery were included. Excluded were patients with known allergy to Iodinated contrast material (n=11), impaired renal function (serum creatinine>120 μmol/l) (n=18), persistent arrhythmias (n=17) or logistic inability to perform a CT scan before CCA (n=15). Thus, the study population comprised 301 patients (215 male, 86 female, mean age 63.6±10.6; range 25-89 years). The institutional review board approved the study and all patients gave informed consent. No oral or intravenous ß-blockers were administered prior to the scan. All patients received nitroglycerin (0.4 mg) sublingually just before scanning.

Patient age, sex, body mass index was recorded. All patients were scanned using a DSCT scanner (Somatom Definition, Siemens Medical Solutions, Forchheim, Germany).

The system is equipped with two X-ray tubes and two corresponding detectors mounted on a single gantry with an angular offset of 90° and a gantry rotation time of 330 ms (15).

DSCT scan parameters were: number of X-ray sources 2, detector collimation 32 x 0.6 mm with double sampling by rapid alteration of the focal spot in the longitudinal direction (z-axis flying focal spot), rotation time 330 ms, tube voltage 120 kV. The pitch varied between 0.2 for low heart (<40 beats/minute) rates and 0.53 for high heart rates (>100 bpm), with individually adapted pitch values for heart rates >40 and <100 bpm. Each tube provided 412 mAs/rot (625 mA), and full X-ray tube current (100%) was given from 25 to 70% of the RR-interval to include both the end-systolic (ES) and end-diastolic (ED) phase. The tube current was reduced to 20% of maximum tube current outside the ECG pulsing window. A bolus of Iodinated contrast material (Ultravist ® 370, Schering, AG, Germany) which varied between 60-100 ml depending on the expected scan time, was injected at a flow rate of 5.5 ml/s in an antecubital vein followed by a saline

bolus chaser at 5.0 ml/s. A bolus tracking technique was applied to synchronize the data acquisition with the arrival of contrast in coronary arteries. All CT coronary angiography datasets were reconstructed using a single-segmental reconstruction algorithm: slice thickness 0.75 mm; increment 0.4 mm; medium-to-smooth convolution kernel (B26f); resulting in a spatial resolution of 0.6-0.7 mm in-plane and 0.5 mm through-plane (15). Average HR, scan length (cm), scan time, pitch, and contrast load were recorded. For each patient, 12 datasets were reconstructed in 5% steps from 20% to 75% of the R-R-interval.

Image Quality

All images were transferred to a dedicated workstation (Multi-Modality Workstation, Siemens Medical Solutions, Forchheim, Germany).

During a three month period, two observers (A.W. with 3 years of experience in cardiovascular imaging, and N.M. with 7 years of experience) independently evaluated image quality on a per segment level in all 12 datasets. The images were sequentially presented to the observers. Coronary segments were classified according to a 17-segment modified American Heart Association (AHA) classification (16). The grading criteria for image quality were as follows:

1. Good image quality (no or mild coronary motion artifact present; confident image evaluation)
2. Impaired image quality (extensive coronary motion artifact present; impairment of diagnostic evaluation)

The image quality was assessed for each segment with a vessel diameter of at least 1.5 mm. Axial views, maximum intensity projections (MIP) and (curved) multiplanar reformations (MPR) were used to identify coronary motion artifacts. Three months after the initial evaluation, one observer (A.W.) re-analyzed a randomly selected set of 100 datasets to determine the intra-observer agreement. Both observers (A.W. and N.M) independently selected the best end-systolic (ES) and end-diastolic (ED) datasets providing the largest number of segments with good image quality. The selected dataset was defined as "high quality" if all segments demonstrated good image quality. Inter-observer disagreements were resolved by consensus in a joint session.

Classification into Heart Rate Groups

After plotting the heart rate against the frequency of high quality datasets reconstructed during ES and/or ED, patients were divided into low, intermediate, and high heart rates (Figure 1, 'Results').

FIGURE 1. Distribution of high quality end-systolic (ES) and end-diastolic (ED) datasets in relation to heart rate

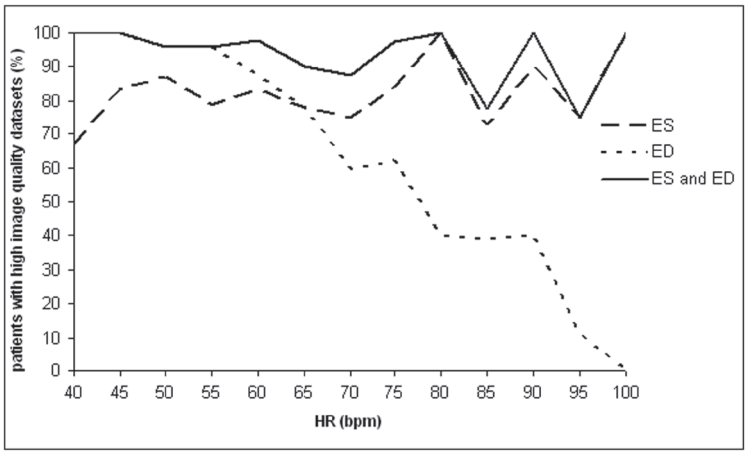

ECG pulsing window

For each HR group, the optimal width of the image reconstruction window during ED and ES, respectively, was calculated including exact 95% confidence intervals. The optimal timing (during ES/ED or both) of the ECG pulsing window was determined by evaluating the differences in occurrence of high-quality ES and ED datasets in each HR group. The optimal width of the ECG pulsing window (in percentage) corresponded to the calculated width of the image reconstruction window for each HR group.

Effective dose

The effective dose for DSCT coronary angiography was estimated using Monte Carlo estimations (ImPACT®, version 0.99x, St. George's Hospital, Tooting, London, UK) and derived from CTDIvol measurements obtained from the CT scanner console. The CTDIvol estimates the average radiation within the scanned volume based on a standardized phantom (17).

For each HR group, the potential effect of the optimal ECG pulsing window on the effective dose was calculated using the following equation:

$$((0.45 * Emax) + (0.55 * Emax / T)) = Epat$$

$$Eopt = ((W * Emax) + (1 - W)) / T$$

Emax calculated dose using maximum tube current throughout the en tire cardiac cycle

Epat effective dose based on the Mon te Carlo estimations in each patient

Eopt calculated effective dose using optimized ECG pulsing

W width of the optimal pulsing window

T tube current outside the pulsing window as a percentage the nominal tube current;
T 20%= 5, T 4%= 25

Statistical Analysis

Statistical analysis was performed using SPSS software (12.0.1, Chicago, IL). Continuous variables were reported as means and SDs and categorical variables as frequencies or percentages. Comparison between HR groups for age and BMI was calculated using the ANOVA test and for gender the Chi-square test. Inter- and intra-observer variability for the evaluation of image quality was determined by k-statistics. The McNemar Test was used to evaluate the difference between the frequency of high quality datasets reconstructed in ED and ES. An additional agreement analysis was performed after random selection of a single segment per dataset in each patient to explore the effect of nesting.

Results

Image Quality

A total of 4406 coronary artery segments were evaluated (Table 1). The k-statistics of the inter-and intra-observer agreement for the evaluation of image quality was 0.73 and 0.81, respectively. The agreement analysis exploring the effect of the clustered nature of the data demonstrated practically identical k-statistics (0.75) indicating that there was a negligible correlation between observations within each patient.

TABLE 1. Percentage of good image quality on a per segment- and per patient-level

		N	ED, %	ES, %	ED + ES, %
Patient level		301	71	81	93
Segment level	All	4406	95	98	99
	Proximal	1192	98	99	100
	Mid	900	94	96	99
	Distal	1089	94	97	99
	Side	1225	97	99	100

N indicates number; ED, end-diastole; ES, end-systole; proximal segments, 1,5,6,11; mid segments, 2,7,13; distal segments, 3,4,815; side segments: 9,10,12,14,16,17

A "high quality" dataset was found during ES in 81.1% (244/301) of patients and in ED in 71.1% (214/301) of patients, respectively. The k-statistics of the inter-observer agreement for the selection of high quality datasets was 0.88.

Classification into Heart Rate Groups

Patients were divided into low (HR≤65 bpm), intermediate (HR 66-79 bpm), and high (≥80 bpm) heart rates based on two cut-off values (Figure 1).

TABLE 2. Patient demographics

	Overall	Group 1 HR ≤65	Group 2 HR 65-79	Group 3 HR ≥80	p-values group 1_2	p-values group 1_3	p-values group 2_3
No. of patients	301	127	109	65	P<0.001	P<0.001	P<0.001
Age (yr)	63.6 ± 10.6	64.1 ± 9.4	63.0 ± 9.8	66.3 ± 11.4	0.537	0.056	0.018
Male sex	215 (71%)	92 (72%)	77 (71%)	46 (71%)	0.447	0.412	0.201
Body Mass Index, kg/m^2	26.1 ± 3.4	26.4 ± 3.2	25.8 ± 4.0	25.7 ± 2.9	0.488	0.411	0.169
Average HR, bpm	70.1 ± 13.3	55.4 ± 4.2	64.8 ± 2.5	90.3 ± 7.3	P<0.001	P<0.001	P<0.001
Scan length, cm	12.0 ± 1.9	12.4 ± 2.1	12.0 ± 1.5	12.0 ± 1.1	0.022	P<0.001	P<0.05
Scan time, sec	8.4 ± 1.9	9.8 ± 1.4	8.1 ± 0.8	6.6 ± 0.8	P<0.001	P<0.001	P<0.001
Pitch	0.30	0.24	0.27	0.39	P<0.001	P<0.001	P<0.001
Contrast load, ml	74.0 ± 11.3	81.7 ± 7.6	72.9 ± 4.2	63.8 ± 4.4	P<0.001	P<0.001	P<0.001
CTDIvol, mGy	65.3 ± 17.2	75.7±14.5	67.9 ± 16.1	53.5 ± 17.9	P<0.001	P<0.001	P<0.001

TABLE 3. Image reconstruction windows (95 CI%) in three heart rate (HR) groups

HR	ES, % R-R-interval	ED, % R-R-interval
≤65 bpm	25-39%	60-76%
65-79 bpm	30-44%	61-77%
≥80 bpm	31-47%	65-75%

ES indicates end-systole; ED, end-diastole

ECG Pulsing Window

Patient characteristics are listed in Table 2. The timing of the image reconstruction windows in ED and ES varied within the R-R interval (Table 3). In low heart rates, ED reconstructions provided high-quality datasets in 92.9% (118/127) without significant improvement (p=0.13) by adding ES reconstructions. In intermediate heart rates, ES reconstructions provided high-quality datasets in 78.9% (86/109) and ED reconstructions in 68.8 % (75/109). The availability of both ES and ED reconstructions significant improved (p<0.001) the number of high-quality datasets (90.8%, 99/109). In high heart rates, ES reconstructions provided high-quality datasets in 83.1% (54/65) without significant improvement (p=0.45) by adding ED reconstructions (Figure 2).

FIGURE 2. Frequency of high quality datasets in three HR groups in end-diastole (ED) and/or end-systole (ES) on a per patient level

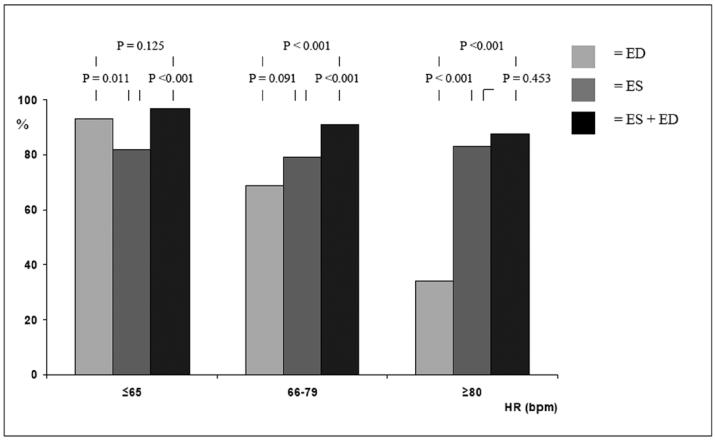

Based on these observations, the optimal timing and width of the ECG pulsing window was determined for each HR group: 60-76% of R-R-interval for low heart rates, 30-77% of R-R interval for intermediate heart rates and 31-47% of R-R interval for high heart rates (Figure 3). This is in agreement with the results of a study of Husmann et al (18) who investigated coronary artery motion at different cardiac phases in relation to heart rate and found that with increasing heart rate, best image quality shifts to earlier percentage phases of the R-R-interval.

Effective Dose

Instead of a fixed ECG pulsing window (25-70% of R-R interval), an optimized HR dependent ECG pulsing protocol can reduce the effective dose of the CT examination by 41% (18.7 to 11.0 mSv) in low heart rates and 37% (11.3 to 7.1 mSv) in high heart rates (Table 4). The use of a reduced tube current outside the ECG pulsing window of 4% instead of 20% would have resulted in a further dose reduction of 38% (11.0 to 6.8 mSv) in low heart rates and 41% (7.1 to 4.2

TABLE 4. Effective dose (mSv) in Dual Source CT Coronary Angiography

ECG pulsing (% of R-R interval)	Tube current outside pulsing window	E (mSv) All HR	E (mSv) HR≤65 bpm	E (mSv HR 66-79 bpm	E (mSv) HR ≥80 bpm
No pulsing	-	27.7	33.4	26.3	20.2
Wide pulsing (25-70%)	20%	15.7*	18.7*	14.7*	11.3*
Wide pulsing (25-70%)	4%	13.2	15.8	12.4	9.5
Optimal pulsing (**)	20%	11.8	11.0	15.6	7.1
Optimal pulsing (**)	4%	8.6	6.8	13.4	4.2

HR indicates heart rate; E, estimated effective dose;
* based on Monte Carlo estimations using CTDIvol in each patient;
* * Optimal ECG pulsing windows: 60-76% (HR ≤65 bpm); 30-77% (HR 66-79 bpm); 31-47% (HR ≥80 bpm)

mSv) in high heart rates. In intermediate heart rates, the width of the ECG pulsing window could not be narrowed without affecting image quality. However, the effective dose can be reduced by 9% (14.7 to 13.4 mSv) with reduced tube current outside ECG pulsing window of 4%.

Discussion

With the growth of cardiac CT use worldwide, concern has been raised about the rather high radiation exposure associated with CT coronary angiography (CTCA) (18, 19). Optimization of scan protocols is therefore mandatory to keep the radiation exposure "as low as reasonably achievable (ALARA)''. It is important that referring physians and operators are familiar with dose saving algorithms that can be applied in CTCA. The tube current and voltage can be optimized according to patient's habitus. Prospectively electrocardiographically (ECG)-controlled X-ray tube modulation or "ECG pulsing" represents another effective tool to reduce the radiation exposure (20, 21).

Hausleiter et al. demonstrated that the combination of a 100-kV scan protocol with ECG pulsing reduced patient dose by 53% and 64% in 16- and 64-slice CTCA, respectively (22).

In our study we used a DSCT scanner equipped with ECG pulsing. The DSCT scanner allows high-quality scanning of patients with higher heart rates due to the improved temporal resolution (10, 11, 12, 13). Because data were lacking on the potential effects of the width and timing of the ECG pulsing window on image quality and radiation exposure, we choose to use a relative wide ECG pulsing window of 25-70% of the cardiac cycle. This allowed us to study the optimal tim-

ing and width of the ECG pulsing window in different heart rates without compromising image quality.

Our results show that in patients with a low heart rate (≤65 bpm), high-quality motion-free end-diastolic datasets were obtained in the large majority (93%) of the patients. This allows us to safely use of a narrow ECG pulsing window (60-76% of the RR-interval) without affecting image quality. In patients with an intermediate heart rate (between 66 and 79 bpm), the use of both ES and ED datasets resulted in the majority of patients (91%) with high-quality datasets. Therefore, narrow ECG pulsing during either ES or ED is not optimal. In this case, the use of a wide ECG pulsing window (29-77%), encompassing both the end-systole and end-diastole is required to obtain high quality images.

In patients with high heart rates (≥80 bpm), the ES datasets provided high quality motion-free datasets in 83% of patients. Additional end-diastolic datasets did not improve the number of patients with high-quality datasets. This can be explained by the relative short diastolic phase during higher heart rates and therefore absence of a motion-free period during early and late diastolic filling phase and subsequent immediate atrial kick all of which cause continuous displacement of the coronary arteries. Thus, ECG pulsing can be optimized in patients with high heart rates by narrowing the ECG pulsing window width (31-47% of the R-R-interval). This is in agreement with the results of a study by Husmann et al (23) who investigated coronary artery motion at different cardiac phases in relation to heart rate and found that with increasing heart rate, best image quality shifts to earlier phases of the R-R-interval.

FIGURE 3. Width and timing of ECG pulsing windows in the RR-interval in low (≤65 bpm), intermediate (66-79 bpm) and high (≥80 bpm) heart rates

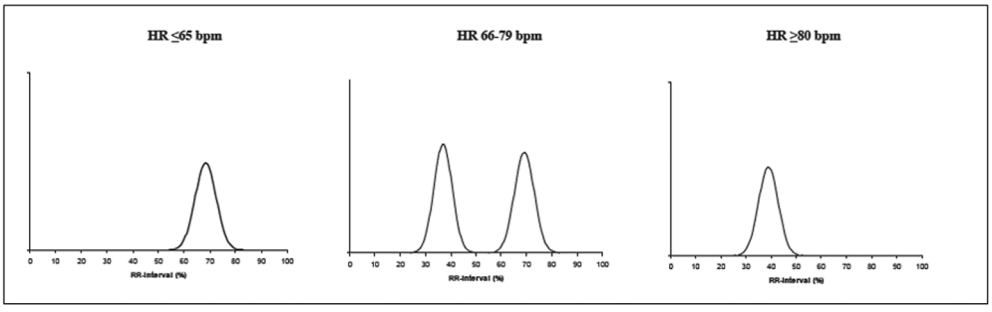

The reduction in radiation exposure was considerable if one could use a narrow ECG pulsing window according to the heart rate. In patients with low heart rates (≤65 bpm), the radiation exposure was reduced to an effective dose of 11.0 mSv with reduced tube current outside the pulsing window of 20% of nominal value to 6.8 mSv in case of reduced tube current outside pulsing window of 4% of nominal value. It is of note that in patients with low heart rates the use of a narrow pulsing window is very effective to reduce patient dose because of the relatively long "low dose" period of the long R-R interval.

In patients with intermediate heart rates (65-79 bpm), reduction in radiation exposure can only be achieved by using a reduced tube current at 4% of maximum value in combination with a wide ECG pulsing window. However, the radiation exposure can be further reduced in patients with intermediate heart rates because our data showed that there are potentially two narrow pulsing windows to acquire the data, of 29-44% and 61-77% of the R-R-interval, which would allow CT scanners equipped with the possibility of double pulsing (2 peaks of nominal tube current during a single heart beat) to use this scan protocol. For double pulsing, scanner technology should allow fast tube current transitions from nominal to low tube current and visa versa. To date double pulsing is not yet clinically applicable in CT coronary angiography.

In patients with high heart rates (≥80 bpm), optimized ECG pulsing can lower the effective dose to 7.1 or 4.2 mSv, respectively, in case of reduced tube current outside the pulsing window of 20% or 4% of maximum value. In this case the reduction in radiation exposure is mainly the result of the high pitch and hence short scan time to cover the heart (14).

Study Limitations

For the image quality evaluation, we only took into account the presence of coronary motion artifacts. Other image degrading artifacts, such as low signal-to-noise or calcium-related blooming were not evaluated.

Our results show that the use of optimal ECG pulsing windows in relation to heart rate would result in a significant decrease in radiation exposure in DSCT coronary angiography. However, our findings were based on calculations and therefore assumptions only. Nevertheless, these assumptions appear reasonable and are taken from the technical properties of the DSCT scanner, which allow selection of narrow ECG pulsing windows in any phase of the cardiac cycle. However, prospective selection of these narrow pulsing windows in low and high heart rates re-

quire testing in the real clinical situation to demonstrate that these settings indeed do not compromise image quality.

In addition, prospective studies should provide evidence that the sensitivity and specificity to detect or rule out significant coronary artery disease is not negatively affected by the use of narrow ECG pulsing windows.

We did not evaluate the effect of other dose saving algorithms, e.g. lower tube voltage of current on image quality. It is expected that lower mAs or kV values in slim patients will further patient dose estimates. Our results apply only to DSCT scanners, and may be different for other systems.

In particular the temporal resolution of 83 ms of the DSCT scanner allows the use of relatively smaller pulsing windows in high heart rates as compared to other scanners.

Conclusion

The optimal phase of image reconstruction within the cardiac cycle strongly depends on the heart rate of the patient. Our results suggest that an optimized ECG pulsing strategy can greatly reduce radiation exposure while preserving image quality, in particular in low and high heart rates.

References

1. Nieman K, Oudkerk M, Rensing BJ: Coronary angiography with multi-slice computed tomography. Lancet 2001; 357:599-603.
2. Knez A, Becker CR, Leber A: Usefulness of multislice spiral computed tomography angiography for determination of coronary artery stenoses. Am J Cardiol 2001; 88:1191-1194.
3. Achenbach S, Ropers D, Pohle FK: Detection of coronary artery stenoses using multi-detector CT with 16 x 0.75 collimation and 375 ms rotation. Eur Heart J 2005; 26:1978-1986.
4. Garcia MJ, Lessick J, Hoffmann MH: Accuracy of 16-row multidetector computed tomography for the assessment of coronary artery stenosis. Jama 2006; 296:403-411.
5. Heuschmid M, Kuettner A, Schroeder S: ECG-gated 16-MDCT of the coronary arteries: assessment of image quality and accuracy in detecting stenoses. AJR Am J Roentgenol 2005; 184:1413-1419.

6. Ropers D, Baum U, Pohle K: Detection of coronary artery stenoses with thin-slice multi-detector row spiral computed tomography and multiplanar reconstruction. Circulation 2003; 107:664-666.
7. Mollet NR, Cademartiri F, van Mieghem CA: High-resolution spiral computed tomography coronary angiography in patients referred for diagnostic conventional coronary angiography. Circulation 2005; 112:2318-2323.
8. Leschka S, Alkadhi H, Plass A: Accuracy of MSCT coronary angiography with 64-slice technology: first experience. Eur Heart J 2005; 26:1482-1487.
9. Einstein AJ, Moser KW, Thompson RC: Radiation dose to patients from cardiac diagnostic imaging. Circulation 2007; 116:1290-1305.
10. Achenbach S, Ropers D, Kuettner A: Contrast-enhanced coronary artery visualization by dual-source computed tomography--initial experience. Eur J Radiol 2006; 57:331-335.
11. Leber AW, Johnson T, Becker A: Diagnostic accuracy of dual-source multi-slice CT-coronary angiography in patients with an intermediate pretest likelihood for coronary artery disease. Eur Heart J 2007.
12. Johnson TR, Nikolaou K, Wintersperger BJ: Dual-source CT cardiac imaging: initial experience. Eur Radiol 2006.
13. Weustink AC, Meijboom WB, Mollet NR: Reliable high-speed coronary computed tomography in symptomatic patients. J Am Coll Cardiol 2007; 50:786-794.
14. McCollough CH, Primak AN, Saba O: Dose performance of a 64-channel dual-source CT scanner. Radiology 2007; 243:775-784.
15. Flohr TG, McCollough CH, Bruder H: First performance evaluation of a dual-source CT (DSCT) system. Eur Radiol 2006; 16:256-268.
16. Austen WG, Edwards JE, Frye RL: A reporting system on patients evaluated for coronary artery disease. Report of the Ad Hoc Committee for Grading of Coronary Artery Disease, Council on Cardiovascular Surgery, American Heart Association. Circulation 1975; 51:5-40.
17. McCollough CH: Patient dose in cardiac computed tomography. Herz 2003; 28:1-6.
18. Einstein AJ, Henzlova MJ, Rajagopalan S: Estimating risk of cancer associated with radiation exposure from 64-slice computed tomography coronary angiography. Jama 2007; 298:317-323.
19. Brenner DJ, Hall EJ: Computed tomography--an increasing source of radiation exposure. N Engl J Med 2007; 357:2277-2284.
20. Jakobs TF, Becker CR, Ohnesorge B: Multislice helical CT of the heart with retrospective ECG gating: reduction of radiation exposure by ECG-controlled tube current modulation. Eur Radiol 2002; 12:1081-1086.
21. Stolzmann P, Scheffel H, Schertler T: Radiation dose estimates in dual-source computed tomography coronary angiography. Eur Radiol 2007.
22. Hausleiter J, Meyer T, Hadamitzky M: Radiation dose estimates from cardiac multislice computed tomography in daily practice: impact of different scanning

protocols on effective dose estimates. Circulation 2006; 113:1305-1310.

23. Husmann L, Leschka S, Desbiolles L: Coronary Artery Motion and Cardiac Phases: Dependency on Heart Rate: Implications for CT Image Reconstruction. Radiology 2007; 245:568-576.

CHAPTER 7

Learning Curve for coronary CT angiography: what constitutes sufficient training?

Pugliese F, Hunink MGM, Gruszczynska K, Alberghina F, Malago'R, van Pelt N, Mollet NR, Cademartiri F, Weustink AC, Meijboom WB, Witteman C, de Feyter PJ, Krestin GP.

Radiology, manuscript accepted for publication.

Summary

Purpose: To prospectively evaluate the effect of experience with coronary computed tomography angiography (CTA) on the capability to detect ≥50% coronary stenoses.

Materials and Methods: The Institutional Review Board approved the study protocol. All patients consented to undergo CTA before conventional coroanry angiography (CCA) after being informed of the additional radiation dose. They also consented on the use of their data for future retrospective research. Three radiologists and 1 cardiologist inexperienced with coronary CTA attended our cardiac CT unit for a 1-year fellowship. Fellows were involved in the acquisition and interpretation of 12-15 coronary CTA per week (~600/year). To assess the progression in diagnostic performance, fellows ('readers') independently interpreted 50 CTA test cases in patients who also underwent CCA. Cases were repeatedly assigned in random order at baseline, 1, 2, 6 months and 1 year. The same cases were interpreted by 2 experts (consensus). We calculated sensitivity, specificity, and diagnostic odds ratios (DOR) compared to CCA.

Results: At baseline, the range across readers in sensitivity was 33-72%, specificity 70-94%, and DOR 3.8-8.1. After 6 months, sensitivity was 43-80%, specificity 71-88%, and DOR 8.8-15.2. After 1 year, sensitivity was 66-75%, specificity 87-92%, and DOR 14.7-25.8. The sensitivity of expert physicians was 95%, specificity 93% and DOR 255.9. Between baseline and 6 months: readers 1-3 showed improved sensitivities but not significantly while specificities remained similar; reader 4 improved specificity significantly while

sensitivity remained similar; all readers improved DOR but not significantly. Between baseline and 1 year: readers 1-2 improved sensitivity significantly but not specificity; reader 4 improved specificity significantly but not sensitivity; readers 1, 2, and 4 improved DOR significantly; reader 3 improved sensitivity, specificity, and DOR not significantly.

Conclusion: Increasing exposures to coronary CTA improved the diagnostic performance of inexperienced physicians. However, acquiring expertise in coronary CTA was slow, and may take >1year.

Introduction

Coronary computed tomography angiography (CTA) performs well in the detection of coronary stenoses (1-10). Most studies, however, were carried out in selected institutions by experienced physicians. The performance of coronary CTA may vary according to the level of expertise of the interpreting physician.

The American College of Radiology (ACR) position is that a trained radiologist is qualified to supervise and read the full set of images involved in coronary CTA (11, 12). Physicians entering practice in coronary CTA for the first time can follow the recommendations of the American College of Cardiology Foundation (ACCF)/American Heart Association (AHA) (13) and the Society of Cardiovascular Computed Tomography (14). It was hypothesized that the training necessary for achieving competence in coronary CTA would consist of minimum numbers of cases performed over time. One could pursue three levels of training through the mentored interpretation of 50 coronary CTA cases over a period of 4 weeks (Level 1), 150 CTA cases over 8 weeks (Level 2), and 300 CTA cases over 6 months (Level 3), respectively (13).

Although recommendations regarding case loads are widely used, no evidence exists to relate the increasing exposure to coronary CTA to the interpretation performance. We investigated the effects of increasing experience with coronary CTA on the interpretation performance of 3 radiologists and 1 cardiologist (without prior experience with coronary CTA) by prospectively evaluating the changes in their capability to detect ≥50% coronary stenoses during a 1-year fellowship in our cardiac CT unit. The threshold of ≥50% luminal narrowing was chosen for consistency with most coronary CTA studies (1-10).

Materials and Methods

Patients (test cases)

Between July and September 2004, 52 patients were recruited to a study at our institution comparing 64-slice coronary CTA with conventional coronary angiography (CCA). These patients were scheduled for diagnostic CCA, they were in sinus heart rhythm, able to hold breath for 15 seconds, and they had never undergone percutaneous coronary intervention or coronary bypass surgery. The Institutional Review Board approved the study protocol and the reading protocol. Particular attention was paid to the additional radiation dose. All patients consented to undergo CTA before CCA after being informed of the additional radiation dose. They also consented on the use of their data for future retrospective research.

Coronary CTA and Conventional Coronary Angiography (CCA) (Table 1)

All patients were scanned with a 64-slice CT scanner (Sensation 64, Siemens, Forchheim, Erlangen, Germany) and underwent CCA (15) within 2 weeks of CTA.

Readers and CTA Exposure

From April 2006 to July 2007, 2 radiologists in the last year of training (1.5-year experience with non-cardiac CT), 1 cardiologist in the last year of training (1.5-year experience with CCA), and 1 trained radiologist (>3-year experience with non-cardiac CT) attended our cardiac CT unit for a 1-year fellowship. None had prior experience with coronary CTA.

Two rotations were created; 2 fellows were assigned to each rotation. Each pair of fellows was involved in the acquisition and interpretation of 12-15 coronary CTA / week (~600 / year). The CTA scans were performed by a technologist, however both fellows were present during the scan activity. Patients were given metoprolol (when needed) by an attending independent cardiologist. It was then the fellows' responsibility to reconstruct images and select the best reconstruction windows ('phases') for interpretation. Subsequently, the fellows scored these coronary CTA studies for significant stenoses (≥50% diameter reduction) on an offline workstation (Multimodality Workplace VE20A, Siemens, Erlangen, Germany) using multi-planar reconstructions (MPR) and curved MPR (syngo 3D, Siemens). The fellows had to generate MPR/curved MPR images, classify coronary segments according to a modified 17-segment AHA model (15), and prepare a preliminary report. Lesions were scored visually. No lesion quantification software was used. Testing the efficacy of different types of post-processing (e.g., volume-

TABLE 1. Parameters for coronary CTA and CCA (n = 50 test cases)

Coronary CTA: inclusion criteria	Sinus heart rhythm
	Ability to hold the breath for 15 seconds
	No previous coronary revascularization with stent implantation or bypass graft surgery
Coronary CTA: patient preparation according to pre-scan heart rate (HR) (beats/min.)	
HR <70	None
70≤ HR <80	100mg metoprolol [a] orally 45 min. before the scan
HR ≥80	100mg metoprolol [a] plus 1mg lorazepam [b] orally 45 min. before the scan
Coronary CTA: scan parameters	
Detectors and width (no.x mm)	32x2x0.6
Rotation time (ms)	330
Tube current x time (mAs)	800-900
Tube voltage (kV)	120
Table feed per rotation (mm)	3.8
Scan time (s)	12-14
Coronary CTA: contrast agent	
Type	iomeprol [c]
Volume (ml)	100
Concentration (mgI/ml)	400
Injection rate (ml/s)	5 [d]
Synchronization technique	Bolus tracking
Coronary CTA: image reconstruction	
Reconstruction technique	Retrospectively ECG-gated monosegmental algorithm
Reconstruction thickness (mm)	0.75
Reconstruction increment (mm)	0.4
Convolution kernel	B30f
Reconstructed datasets ('phases')	Mid- to end-diastole and end-systole to optimize the visualization of all coronary segments
CCA	
Timing	Within 2 weeks of CTA
Operator	Independent experienced (>10-year) interventional cardiologist unaware of CTA findings
Coronary segment classification model	17-segment modified American Heart Association (AHA) model (15)
Lesion quantification	Quantitative coronary angiography (QCA) performed using validated software [e]
Definition of significant stenosis	Diameter reduction ≥50%

a: Selokeen, Astra Zeneca, London, UK, b: Temesta, Wyeth Pharmaceuticals, Collegeville, PA, c: Iomeron 400, Bracco, Milan, Italy , d: Contrast agent was injected into an antecubital vein, e: CAAS II®, Pie Medical, Maastricht, the Netherlands

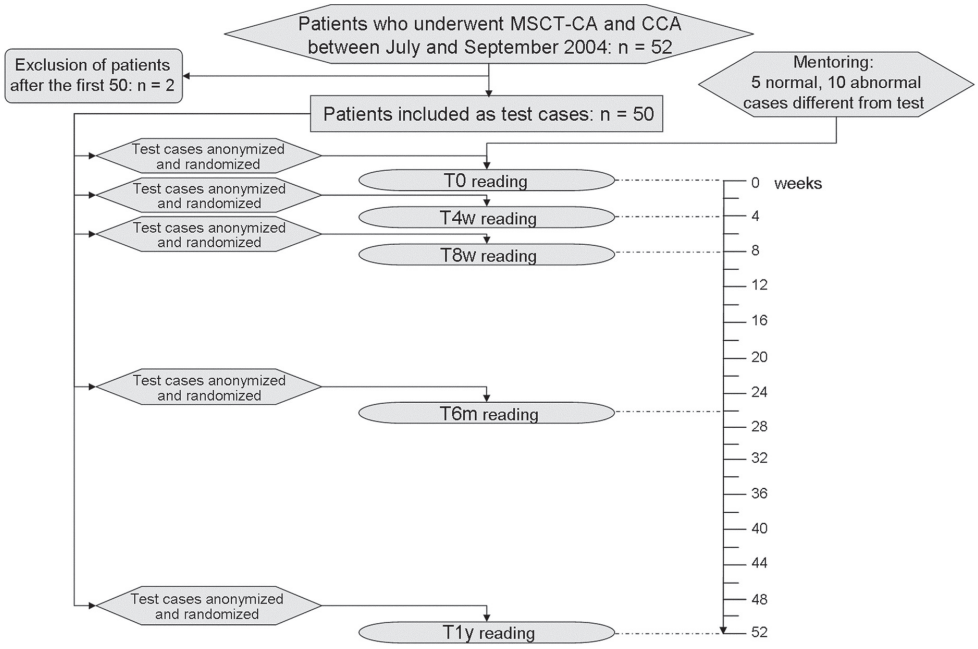

FIGURE 1. Selection of test cases and reading protocol. The first 50 consecutive patients who had undergone coronary CTA and CCA for an ongoing study comparing the 2 techniques were chosen as test cases. After receiving feedback on 5 normal and 10 abnormal CTA studies (different from the test cases), the readers evaluated independently and blindly the 50 test cases. The readings were done at baseline (T0), after 4 weeks (T4w), after 8 weeks (T8w), after 26 weeks, i.e., 6 months (T6m), and after 52 weeks, i.e., 1 year (T1y) of cumulative training.

rendering technique) was beyond our purpose, therefore the fellows used the same application (syngo 3D, Siemens) for all the duration of the study. Because two fellows were assigned to each rotation, they shared the responsibilities of reconstructing images and reporting in equal parts (50%). Individual fellows' involvement was documented in a log book (i.e., number and type of patients). Patient's symptoms and clinical history were available to the fellows for this activity. The fellows could seek clarification of any issues (e.g., technical, clinical) encountered during data acquisition and analysis, and could compare CTA with CCA and any other diagnostic tests. The CTA studies were reviewed under supervision of one in a team of 3 independent experienced physicians, i.e., 1 cardiologist (W. B. M) and two radiologists (F. P., N. R. M.) all with ≥3-year experience with coronary CTA, within a week from the scan date. The expert physician re-interpreted the coronary CTA studies and issued the official reports. This took circa 5-20 minutes per study. The fellows discussed their own findings

and received arguments for interpretation mistakes.

Selection of Test Cases and Reading Protocol

Before starting the study, the fellows received lectures on cardiac anatomy and coronary CTA technique. They also received feedback by one expert physician (N. R. M.) in the interpretation of 15 mentored cases (different from the test cases). These mentored cases consisted of 5 normal and 10 abnormal coronary CTA studies. The fellows were familiarized with the CT workstation by the experienced colleagues such that they were able to use the application (syngo 3D, Siemens) routinely used for reading coronary CTA at our institution.

One radiologist (non-observer) (F. P.) selected the first 50 consecutive CTA cases from the database of 52 patients to be used as 'test cases' (Figure 1). The fellows, or readers, were tested individually. They independently read the same 50 coronary CTA test cases at different stages of their fellowships: at the beginning of the fellowship (T0, i.e., baseline), after 4 weeks (T4w), after 8 weeks (T8w), after 26 weeks (T6m, i.e., 6 months), and after 52 weeks (T1y, i.e., 1 year) (Figure 1). The 4 weeks, 8 weeks and 26 weeks training periods correspond to the training Levels 1, 2 and 3, respectively, as described by the ACCF/AHA (13). Although the readers were aware that they were evaluating the same set of studies, the 50 test cases were anonymized and the order of evaluation was randomized for each reading using random number tables to prevent readers from remembering the cases and being biased by their own prior interpretations. The readers were unaware of patient's symptoms, risk factors, CCA and any other test results. All cases were evaluated on an offline workstation (Leonardo VB30A equipped with syngo 3D, Siemens) similar to that used for the evaluation of routine cases. Readers had 5 days to complete the tests cases. Two datasets for each patient (i.e., the best diastolic and systolic phases previously selected by an independent experienced radiologist, N. R. M.) were available to the readers. Each reader generated his/her own MPR/curved MPR images, and these reformatted images were not available to the others. The readers had to identify coronary segments on the reformatted images and classify them following the same 17-segment AHA model (15) used for CCA. Cases were then visually scored for the presence of significant stenoses using MPR and curved MPR images. Readers recorded their findings by filling in standardized score sheets. All identifiable segments (i.e., visible segments) had to be scored without excluding any due to poor image quality and/or calcifications. Only the segments that could not be identified (e.g., anatomically absent or

very small) were not scored. The evaluation time per case (including generation of MPR/curved MPR images, segment identification and detection of ≥50% stenoses) was also recorded.

CCA was used as standard of reference for the detection of significant stenoses and for the calculation of reader performance. One independent radiologist (non-observer) (F. P.) compared the coronary CTA score sheets from each reader with the Quantitative Coronary Angiography (QCA) results. The readers did not receive feedback about their diagnostic performances. The type of training was not individualized based on the level of performance acquired by each reader (i.e., deliberate practice), but remained the same throughout the study.

Expert Consensus Reading

One radiologist (F. P) and 1 cardiologist (W. B. M.) (both with ≥3-year experience) scored the same 50 coronary CTA test cases in a consensus reading using the same workstation (Leonardo VB30A equipped with syngo 3D, Siemens) used by the fellows. The expert physicians were unaware of patients' symptoms, angiographic findings, and fellows' diagnostic performances.

Statistical Analysis

Statistical analysis was performed using dedicated software (SPSS, version 12.1. SPSS Inc., Chicago, Ill., and STATA/SE 8.2, College Station, TX.). Results were reported according to the Standards for Reporting of Diagnostic Accuracy, or STARD, criteria (16). Quantitative variables were expressed as means (standard deviations) and categorical variables were expressed as frequencies or percentages. Logistic regression analysis was used to explore the relationship between the ability to identify coronary artery segments by CTA (dependent variable, dichotomous) and reader experience measured in weeks (independent variable) adjusting for the reader. The presence vs. absence of stenoses on CCA was determined for the non-identified segments separately to determine whether the non-identified segments may have biased the results of our analysis.

Reader performance in the detection of individual significant coronary stenoses (≥50% luminal narrowing) by CTA was compared to QCA. We calculated sensitivity, specificity, positive predictive value (PPV), negative predictive value (NPV), and the diagnostic odd ratios (DOR) with the corresponding 95% confidence intervals (CI's). The DOR is an overall measure of the discriminatory power of the test with DOR = (true positives * true

negatives) / (false positives * false negatives) (17-19). Comparisons of the sensitivity and specificity achieved by each reader in the different readings were performed by analysis of the CI's and hypothesis testing using Mc Nemar's test. Inter-observer agreement for the detection of significant coronary stenoses at CTA was determined by multiple rater k-statistics. Comparisons of k values were performed by analyzing the 95% CI's. To determine the intra-observer agreement in CCA interpretation, the same observer (P. J. F., >10-year experience with CCA) evaluated 30/50 (60%) CCA studies twice with a time interval of 2 years.

The data was clustered implying that potential correlation existed between the multiple (seventeen) segments analyzed per patient (20, 21). To adjust for the clustered nature of the data, we used a bootstrap approach for the analyses. We created 1000 replications of the dataset using sampling with replacement and treating all of a patient's observations as a cluster (implying an independent identical distribution at the patient level). Bias-corrected 95% confidence intervals were reported (21, 22).

Since this was an exploratory analysis, a significance level of 0.05 was used throughout in spite of the multiple comparisons so as to optimize the power of showing a difference if there is one.

Results

Test Cases (Table 2)

Twelve/50 (24%) patients had normal coronary arteries, 17/50 (34%) had 1-vessel disease and 21/50 (42%) had multiple-vessel disease. The mean (standard deviation) Agatston calcium score was 366 (437) (range 0-2013). None of the patient had coronary artery anomalies.

Reader Exposure to Coronary CTA (Table 3)

Table 3 describes the number and type of patients who underwent coronary CTA over time, constituting the fellows' annual case load. The fellows were exposed to ~600 coronary CTA studies in a year, and the case mixes in the 2 rotations were similar.

Reader Performance (Table 4)

From baseline to 1 year, the ability to identify coronary segments improved significantly in relation to experience (odds ratio = 1.09; CI: 1.03-1.70). On average, 93% (2704/2896) segments were identified at baseline, 94% (2720/2896) at 4 weeks, 91% (2621/2896) at 8 weeks, 96% (2773/2896) at 6 months, and 97% (2803/2896) at 1 year. The expert physicians identified 719/724 (99%) segments. Unidentified segments (i.e., scored as absent) were distal or side

No. of patients (test cases)	50
Demographics	
Average age (sd) a (years)	59 (10)
No. of men; average age (sd) a	38/50; 59 (9) b
No. of women; average age (sd) a	12/50; 58 (18) b
Cardiovascular risk factors: no. (%)	
Obesity (Body Mass Index ≥30 Kg/m^2)	14/50 (28%)
Smoking	13/50 (26%)
Hypertension	16/50 (32%)
Serum cholesterol >200 mg/dL (5.18 mmol/L)	25/50 (50%)
Diabetes mellitus	7/50 (14%)
Family history	11/50 (22%)
Number of risk factors: no. (%)	
0	11/50 (22%)
1	7/50 (14%)
2	15/50 (30%)
≥3	17/50 (34%)
Coronary segments visualized by CCA	724
Segments with ≥50% stenoses: no. (%)	95/724 (13%)
Severity of CAD: no. (%)	
No disease	12/50 (24%)
1-vessel	17/50 (34%)
2-vessel	13/50 (26%)
3-vessel	8/50 (16%)
Disease of left main artery: no. (%)	1/50 (2%)
Medication before CTA and heart rate	
Metoprolol: no. (%)	30/50 (60%)
Mean heart rate during scan (sd) a (beats/min.)	58 (7)
Agatston calcium score	
Mean (sd) a	366 (437)
Median	215
Range	0-2013
Categories: no. (%)	
0-10	12/50 (24%)
11-400	22/50 (44%)
401-1000	13/50 (26%)
>1000	3/50 (6%)

TABLE 2. Baseline characteristics and angiographic findings of the 50 test cases

a: sd = standard deviation
b: Average ages in men and women were similar (Wilcoxon rank sum test: p = 0.61)

TABLE 3. Reader exposure. Number and type of patients who underwent coronary CTA over time constituting the fellows' annual case load [a]

	Rotation A (2 fellows)	Rotation B (2 fellows)
Number of cases over time		
4 weeks	57	50
8 weeks	109	99
26 weeks (6 months)	327	312
52 weeks (1 year)	625	591
Case mix: no. (%)		
Suspected or known CAD	**342/625 (55%)**	**365/591 (62%)**
at least 1 significant stenosis	120/342 (35%)	142/365 (39%)
Exclusion CAD before valve surgery	**54/625 (9%)**	**49/591 (8%)**
at least 1 significant stenosis	13/54 (24%)	11/49 (22%)
Suspected coronary anomalies	**14/625 (2%)**	**10/591 (2%)**
at least 1 significant stenosis	1/14 (7%)	1/10 (10%)
Patients with coronary stents	**125/625 (20%)**	**98/591 (16%)**
at least 1 significant stenosis [b]	48/125 (38%)	29/98 (30%)
Patients with CABG grafts	**90/625 (14%)**	**69/591 (12%)**
at least 1 significant stenosis [b]	90/90 (100%)	69/69 (100%)

[a] The 50 coronary CTA studies used as test cases are not included in these numbers
[b] Numbers include stenoses in the native coronary arteries

branches ≤1.5mm in diameter. None of these segments contained significant stenoses, therefore they did not affect the computation of sensitivity. We did not include these segments as negative findings because this would have led to an overestimation of specificity. All identified segments were scored for the presence of stenoses irrespective of image quality and/or calcification.

The experts had a sensitivity of 95% (95% CI: 87-98), a specificity of 93% (91-95), and a DOR of 255.9. Sensitivities, specificities, and the DOR achieved by the fellows over time are compared in Table 4 and plotted in Figure 2. An example of a coronary lesion missed by all fellows but detected by the experts is given in Figure 3.

Reader 1 and reader 2 increased their sensitivities but not significantly between baseline and 6 months. Specificity did not increase significantly between baseline, 6 months and 1 year, thus the DOR

TABLE 4. Individual reader sensitivity, specificity and DOR

		TP	TN	FP	FN	**Sensitivity** (0.95 CI)	p-values [a]				**Specificity** (0.95 CI)	p-values [a]				DOR (0.95 CI)
							experts	T0	T4w	T8w	T6m		experts	T0	T4w	T8w	T6m	
experts		90	583	41	5	.90/95 **.95** (.87-.98)	-					583/624 **.93** (.91-.95)	-					52470/205 **255.9 (97.9-302.0)**
reader 1	**T0**	35	508	85	55	35/90 **.39** (.29-.50)	<0.001	-				508/593 **.86** (.83-.88)	<0.001	-				17780/4675 **3.8** (2.3-6.2)
	T4w	59	488	100	30	59/89 **.66** (.55-.76)	<0.001	0.002	-			488/588 **.83** (.80-.86)	<0.001	0.08	-			28792/3000 **9.6** (5.9-15.6)
	T8w	33	446	44	45	33/78 **.42** (.31-.54)	<0.001	0.26	<0.001	-		446/490 **.91** (.88-.93)	0.53	0.003	<0.001	-		14718/1980 **7.4** (4.3-12.8)
	T6m	50	538	71	43	50/93 **.54** (.43-.64)	<0.001	0.21	0.16	0.22	-	538/609 **.88** (.85-.91)	0.001	0.27	<0.001	0.41	-	26900/3053 8.**8** (5.5-14.0)
	T1y	68	550	63	23	68/91 **.75** (.64-.83)	0.001	<0.001	0.10	<0.001	0.001	550/613 **.90** (.87-.92)	0.019	0.099	<0.001	0.26	0.34	37400/1449 **25.8** (14.9-44.7)
reader 2	**T0**	30	569	35	60	30/90 **.33** (.24-.44)	<0.001	-				569/604 **.94** (.92-.96)	0.53	-				17070/2100 **8.1** (4.6-14.3)
	T4w	54	488	114	37	54/91 **.59** (.49-.69)	<0.001	<0.001	-			488/602 **.81** (.78-.84)	<0.001	<0.001	-			26352/4218 **6.2** (3.9-9.7)
	T8w	51	549	61	41	51/92 **.55** (.44-.66)	<0.001	<0.001	0.23	-		549/610 **.90** (.87-.92)	0.21	0.001	<0.001	-		27999/2501 **11.2** (6.9-18.4)
	T6m	40	574	39	53	40/93 **.43** (.32-.54)	<0.001	0.18	0.052	0.19	-	574/613 **.94** (.91-.95)	0.90	0.49	<0.001	0.002	-	22960/2067 **11.1** (6.6-18.9)
	T1y	62	566	52	32	62/94 **.66** (.55-.75)	<0.001	<0.001	0.16	0.21	<0.001	566/618 **.92** (.89-.94)	0.28	0.051	<0.001	0.34	0.15	35092/1664 **21.1** (12.9-35.2)

reader 3	**T0**	52	493	83	39	52/91 **.57** (.46-.67)	<0.001	-				493/576 **.86** (.82-.88)	<0.001	-				25636/3237 **7.9** (5.0-12.7)
	T4w	71	423	158	19	71/90 **.79** (.69-.87)	0.004	<0.001	-			423/581 **.73** (.69-.76)	<0.001	<0.001	-			30033/3002 **10.0** (5.8-17.3)
	T8w	70	445	129	21	70/91 **.77** (.67-.85)	0.002	0.001	1.0	-		445/574 **.78** (.74-.81)	<0.001	<0.001	0.012	-		31150/2709 **11.5** (6.8-19.5)
	T6m	72	418	170	18	72/90 **.80** (.70-.87)	0.007	0.049	0.84	0.078	-	418/588 **.71** (.67-.75)	<0.001	<0.001	0.31	0.051	-	30096/3060 **9.8** (5.6-17)
	T1y	61	519	77	28	61/89 **.69** (.58-.78)	<0.001	0.051	0.059	0.11	0.1	519/596 **.87** (.84-.90)	<0.001	0.29	<0.001	<0.001	<0.001	31659/2156 **14.7** (8.9-24.5)
reader 4	**T0**	62	401	173	24	62/86 **.72** (.61-.80)	0.001	-				401/572 **.70** (.65-.74)	<0.001	-				24862/4152 **6.0** (3.6-10.0)
	T4w	72	447	141	19	72/91 **.79** (.69-.87)	0.04	1.0	-			447/588 **.76** (.72-.79)	<0.001	0.003	-			32184/2679 **12.0** (6.9-20.7)
	T8w	70	455	138	23	70/93 **.75** (.65-.83)	0.001	0.35	0.30	-		455/593 **.77** (.73-.80)	<0.001	0.003	0.75	-		31850/3174 **10.0** (6.0-16.6)
	T6m	64	517	78	28	64/92 **.70** (.58-.79)	<0.001	0.46	0.26	0.61	-	517/595 **.87** (.84-.89)	0.001	<0.001	<0.001	<0.001	-	33088/2184 1**5.2** (9.1-25.3)
	T1y	63	545	65	29	63/92 **.68** (.57-.78)	<0.001	0.07	0.20	0.12	0.12	545/610 **.89** (.87-.91)	0.006	<0.001	<0.001	<0.001	0.11	34335/1885 1**8.2** (10.9-30.3)

a McNemar's test

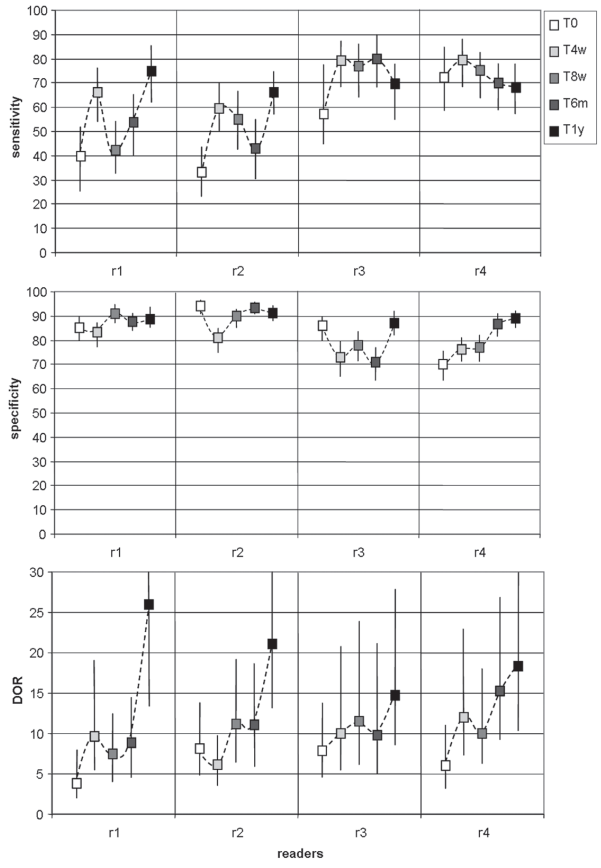

FIGURE 2: Sensitivity, specificity and the diagnostic odds ratios (DOR) obtained at T0 (white), T4w (light grey), T8w (grey), T6m (dark grey) and T1y (black) were plotted for each reader (r1-r4) with 95% confidence intervals. All readers had at least one drop in their overall performance, i.e. DOR, at an intermediate stage of the learning process, i.e., between 4 and 8 weeks for readers 1 and 4 and between 8 weeks and 6 months for readers 2 and 3. Reader 2 had an additional drop in performance between baseline and 4 weeks.

However, specificities at 1 year were significantly better than at 4 weeks. At 8 weeks, readers 1 and 2 achieved specificities similar to those of the experts; sensitivities were however significantly lower than those of the experts.

With reader 3, between baseline and 6 months sensitivity increased significantly whereas specificity decreased significantly, thus the DOR remained similar. Between 6 months and 1 year specificity increased significantly and sensitivity decreased non-significantly, thus the DOR increased but not significantly. The increase in DOR between baseline and 1 year was also not statistically significant. Although sensitivity and the DOR at 1 year were not significantly better than at 4 weeks, specificity was.

increased but not significantly between baseline and 6 months (overlapping CI's). A further significant increase in sensitivity occurred between 6 months and 1 year. With reader 1, the DOR improved significantly between baseline and 1 year. The sensitivities achieved by these readers at 4 weeks were similar to those at 1 year.

With reader 4, sensitivities at baseline, 6 months and 1 year were similar. Specificity increased significantly between baseline and 6 months, and further between 6 months and 1 year although not significantly. The DOR increased but not significantly between baseline and 6 months,

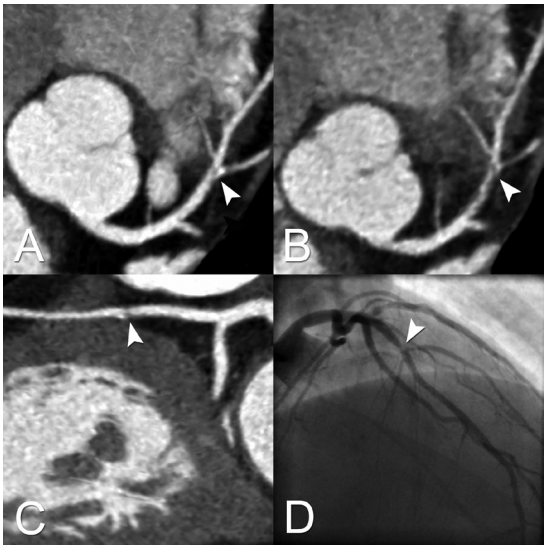

FIGURE 3: Two-mm-thick MIP (A), 0.75mm-thick MPR (B) and curved MPR (C) coronary CTA images (obtained by one of the experts) show a coronary lesion (arrowhead) causing significant narrowing of the middle LAD. This lesion was mis-classified by all the fellows at 1 year, but was correctly detected as significant by the experts. Conventional angiography (D) confirms the finding.

and between 6 months and 1 year. At 1 year, specificity and the DOR were significantly better than at baseline. The sensitivity at 4 weeks was similar to that at 1 year; however, specificity at 1 year was significantly better than at 4 weeks. Sensitivities and specificities achieved by readers 3 and 4 were always lower than those obtained by the experts.

The bootstrap analysis adjusting for the clustered nature of the data demonstrated that there was a negligible correlation between observations within each patient.

Evaluation Times

Evaluation times decreased significantly in relation to reader experience. Average (standard deviation) evaluation time in minutes was 20 (13) at baseline, 18 (8) at 4 weeks, 16 (10) at 8 weeks, 12 (4) at 6 months, and 13 (5) at 1 year. Average evaluation time (standard deviation) of the expert physicians was 10.0 (3.1) minutes. It took however additional 5 (2.2) minutes to achieve consensus. The experts were faster than all fellows at baseline, 4 weeks and 8 weeks (all p-values <0.05). At 6 months and 1 year, evaluation times of fellows and experts were similar (all p-values >0.05).

Inter- and Intra-Observer Agreement

The values for k (0.95 CI) were 0.32 (0.25-0.39) at baseline, 0.46 (0.42-0.52) at 4 weeks, 0.39 (0.33-0.45) at 8 weeks, 0.40 (0.34-0.46) at 6 months, and 0.48 (0.42-0.54) at 1 year. Between baseline and 6 months, and between 6 months and 1 year inter-observer agreement improved although not significantly (overlapping CI's). The improvement between baseline and 1 year was statistically significant (non-overlapping CI's). The k-value of intra-observer agreement in the interpretation of CCA was 0.95 (0.95 CI: 0.92-0.98).

CHAPTER 7

Discussion

Physicians inexperienced with coronary CTA improved their capability to detect significant coronary stenoses. The evaluation time also decreased with experience, which correlates with expertise and is relevant in clinical practice. However, none of the readers improved their DOR significantly between baseline and 6 months, and only two of them (readers 1 and 4) improved their DOR significantly between baseline and 1 year. Importantly, whereas the specificities achieved by the fellows were approaching those of the experts or reported in the literature (1-8), sensitivities were much lower. CTA had >90% sensitivity compared to CCA in most available studies (1-8). At the end of the learning curve reported here, sensitivity ranged from 66% to 75% (Figure 2).

Several explanations may account for this difference. Firstly, it was reported that ~10 years of preparation are needed to attain expertise in any domain (the 10-year rule) (23). Such amount of preparation may overlap with regular medical education so that it is difficult to determine a starting point. Nevertheless, the published research on diagnostic performance of coronary CTA was carried out by physicians with ≥3-year experience. It might therefore take more than 1 year for an inexperienced physician to become an 'expert' (Level 3). Secondly, published studies were designed in a way that two readers scored the CTA cases and eventually resolved any disagreement by consensus. Whereas the expert reading in our study was a consensus reading, we chose to determine individual performance among the fellows in order to study individual growing expertise which we feel is relevant for daily clinical practice. It might also be argued that there are objective differences between CCA and CTA, e.g., limited views, differences in systole versus diastole with CCA, inability to accurately image coronary arteries due to calcifications with CTA. However, CCA was the reference technique for most published studies, and the sensitivity and specificity obtained by our experts were similar to those of the literature. A high calcium score, in particular, may hinder the ability to estimate lesion severity with CTA introducing error in the estimation of sensitivity and specificity. The mean calcium score (366) of our test cases and the percentage of patients (~30%) with a calcium score >400 were however similar to most published studies (1-3, 5, 8).

It should be emphasized that the training offered in this study did not include the so-called deliberate practice, i.e., a type of training which is individualized based on the level of acquired performance through the administration of cases selected by a teacher (23). Fellows were not

confronted with their tendency to underestimate lesions. Had they been taught to be lenient in calling a lesion significant through explanation of the clinical consequences, they could potentially have further improved their sensitivity albeit at the expense of specificity. However, the development of a formal training course and individualized feedback was beyond the purpose of this study although probably worth considering in future fellowship programs (24).

Interestingly, we found that the diagnostic performance did not improve following a linear pattern. All readers had at least one drop in performance (Figure 2). This phenomenon was found in different areas of skill acquisition (25). When approaching a diagnostic task, beginners would lack knowledge and experience; intermediates would have knowledge but limited experience, practised physicians would have both knowledge and experience (26). Experience would shift the type of cognitive processing from deliberate to intuitive; with intermediates, neither of the two would be strong enough to yield good results (26). This U-shaped model of performance is known as the 'intermediate effect' (27-29). Readers at intermediate stage might also have had an overconfident approach to the task, whereas at initial/advanced stages they could have been more motivated to perform well.

Our study has limitations. Firstly, the number of participants was small. It was objectively difficult to engage physicians in full-time commitment for 1 year. Including participants with varying degrees of experience could have yielded more generalizable results. However, we aimed at evaluating the effect of increasing CTA exposure on the diagnostic performance of inexperienced physicians. Secondly, we did not calculate readers' diagnostic performance at the patient level because the population of 50 test cases was too small to provide robust results. The high number of patients with at least one significant stenosis (38/50, 76%) would have led to an overestimation of sensitivity. Instead, we computed the diagnostic performance at a segmental level consistent with the published literature, adjusting for clustering of observations within patients.

In conclusion, although inexperienced physicians improved their diagnostic performances through increasing exposures to coronary CTA, it may take a prolonged time to gain the expertise to read coronary CTA as an independent practitioner, which should have implications for training under existing guidelines.

CHAPTER 7

References

1. Leber AW, Knez A, von Ziegler F, et al. Quantification of obstructive and nonobstructive coronary lesions by 64-slice computed tomography: a comparative study with quantitative coronary angiography and intravascular ultrasound. J Am Coll Cardiol 2005; 46:147-154.
2. Meijboom WB, van Mieghem CA, Mollet NR, et al. 64-slice computed tomography coronary angiography in patients with high, intermediate, or low pretest probability of significant coronary artery disease. J Am Coll Cardiol 2007; 50:1469-1475.
3. Mollet NR, Cademartiri F, van Mieghem CA, et al. High-resolution spiral computed tomography coronary angiography in patients referred for diagnostic conventional coronary angiography. Circulation 2005; 112:2318-2323.
4. Nikolaou K, Knez A, Rist C, et al. Accuracy of 64-MDCT in the diagnosis of ischemic heart disease. AJR Am J Roentgenol 2006; 187:111-117.
5. Raff GL, Gallagher MJ, O'Neill WW, Goldstein JA. Diagnostic accuracy of noninvasive coronary angiography using 64-slice spiral computed tomography. J Am Coll Cardiol 2005; 46:552-557.
6. Ropers D, Rixe J, Anders K, et al. Usefulness of multidetector row spiral computed tomography with 64- x 0.6-mm collimation and 330-ms rotation for the noninvasive detection of significant coronary artery stenoses. Am J Cardiol 2006; 97:343-348.
7. Pugliese F, Mollet NR, Runza G, et al. Diagnostic accuracy of non-invasive 64-slice CT coronary angiography in patients with stable angina pectoris. Eur Radiol 2006; 16:575-582.
8. Weustink AC, Meijboom WB, Mollet NR, et al. Reliable high-speed coronary computed tomography in symptomatic patients. J Am Coll Cardiol 2007; 50:786-794.
9. Pugliese F, Mollet NR, Hunink MG, et al. Diagnostic performance of coronary CT angiography by using different generations of multisection scanners: single-center experience. Radiology 2008; 246:384-393.
10. Vanhoenacker PK, Heijenbrok-Kal MH, Van Heste R, et al. Diagnostic performance of multidetector CT angiography for assessment of coronary artery disease: meta-analysis. Radiology 2007; 244:419-428.
11. Jacobs JE, Boxt LM, Desjardins B, Fishman EK, Larson PA, Schoepf J. ACR practice guideline for the performance and interpretation of cardiac computed tomography (CT). J Am Coll Radiol 2006; 3:677-685.
12. Weinreb JC, Larson PA, Woodard PK, et al. American College of Radiology clinical statement on noninvasive cardiac imaging. Radiology 2005; 235:723-727.
13. Budoff MJ, Cohen MC, Garcia MJ, et al. ACCF/AHA clinical competence statement on cardiac imaging with computed tomography and magnetic resonance: a report of the American College of Cardiology Foundation/ American Heart Association/American

College of Physicians Task Force on Clinical Competence and Training. J Am Coll Cardiol 2005; 46:383-402.

14. Budoff MJ, Achenbach S, Fayad Z, et al. Task Force 12: training in advanced cardiovascular imaging (computed tomography): endorsed by the American Society of Nuclear Cardiology, Society for Cardiovascular Angiography and Interventions, Society of Atherosclerosis Imaging and Prevention, and Society of Cardiovascular Computed Tomography. J Am Coll Cardiol 2006; 47:915-920.
15. Austen WG, Edwards JE, Frye RL, et al. A reporting system on patients evaluated for coronary artery disease. Report of the Ad Hoc Committee for Grading of Coronary Artery Disease, Council on Cardiovascular Surgery, American Heart Association. Circulation 1975; 51:5-40.
16. Bossuyt PM, Reitsma JB, Bruns DE, et al. Towards complete and accurate reporting of studies of diagnostic accuracy: The STARD Initiative. Radiology 2003; 226:24-28.
17. Irwig L, Bossuyt P, Glasziou P, Gatsonis C, Lijmer J. Designing studies to ensure that estimates of test accuracy are transferable. BMJ 2002; 324:669-671.
18. Pepe MS, Janes H, Longton G, Leisenring W, Newcomb P. Limitations of the odds ratio in gauging the performance of a diagnostic, prognostic, or screening marker. Am J Epidemiol 2004; 159:882-890.
19. Hunink MGM, Glasziou P. Decision making in health and medicine. Cambridge, UK: Cambridge University Press, 2001; 145-146.
20. Fleiss JL, Levin B, Cho Paik M. Statistical Methods for Rates and Proportions. New York, NY: Wiley, 2003; 440-448, 462-486.
21. Zhou XH, Obuchowski NA, McClish DK. Statistical Methods in Diagnostic Medicine. New York, NY: Wiley, 2002; 157.
22. Efron B, Tibshirani RJ. An Introduction to the Bootstrap. New York, NY: Chapman & Hall, 1993; 47-48, 87, 125, 130-132, 164, 184-190.
23. Ericsson KA, Charness N. Expert performance. Its structure and acquisition. American psychologist 1994; 49:725-747.
24. Crowley AL, Patel MR, Bashore T, et al. Training cardiovascular specialists in imaging: a curriculum based on fundamental concepts required for multimodal imaging. Am Heart J 2007; 154:838-845.
25. Patel VL, Arocha JF, Zhang J. Thinking and reasoning in medicine. In: Holyoak KJ, Morrison RG, eds. The Cambridge handbook of thinking and reasoning Cambridge, UK: Cambridge University Press., 2005; 727-750.
26. Brammer R. Effects of experience and training on diagnostic accuracy. Psychol Assess 2002; 14:110-113.
27. Baylor AL. A U-shaped model for the development of intuition by level of expertise. . New Ideas in Psychology 2001; 19:237-244.
28. Brainerd CJ. Dropping the other U: An alternative approach to U-shaped developmental functions. Journal of Cognition and Development 2004; 5:81-88.
29. Witteman CLM, van den Bercken JHL. Intermediate effects in psychodiagnostic classification. European Journal of Psychological Assessment 2007; 23:56-61.

CHAPTER 8

Advanced magnetic navigation: multislice computed tomography-guided percutaneous coronary intervention in a patient with triple-vessel disease

Ramcharitar S, Pugliese F, Patterson M, van Geuns RJ, de Feyter PJ, Guiliguian D, Serruys PW.

Manuscript submitted for publication.

Summary

Magnetic navigation is a technology that allows the accurate guidance of a magnetically enabled guidewire through the use of external magnets generating a precisely directed magnetic field. This technology can be combined with MSCT. The pathway of the diseased coronary arteries can automatically be traced, even through chronic total occlusions. The operator has access to an endoluminal view that simulates looking through the vessel lumen and simultaneously to the corresponding MSCT image of the vessel cross-section.

Introduction

Multi-slice computed tomography (MSCT) is a rapidly evolving technology in the field of coronary artery imaging(1). Current 64-slice MSCT allows the delineation of coronary lumen and the visualization of the plaque burden through the attenuation of soft-tissue contrast and its high sensitivity for vessel calcification(2). At present, this technology is utilized for its diagnostic potential. However, it is now possible through the amalgamation of MSCT with the Niobe® Magnetic Navigation System MNS (Stereotaxis, St Louis, MO, USA) to use it for performing percutaneous coronary intervention (PCI)(3).

Magnetic navigation is a technology that allows the accurate guidance of a magnetically enabled guidewire through the use of external magnets that generate a precisely directed magnetic field. The coupling of this technology with MSCT was initially introduced in the Navigant® 2.10 software (Stereotaxis) as an innovative approach to manage chronic total occlusions (CTOs)(4). It allowed the user to segment out the 3D rendered MSCT volume and to identify the diseased vessel by manually marking points on the vessel surface. This generated a pathway used as a baseline to produce directional magnetic vectors, tangent to the pathway at the point where the guide-wire magnetic tip is placed.

With the recent upgrade to Navigant® 2.11, a segmented MSCT volume that only shows the coronary tree (Siemens Medical Solutions, Forchheim, Germany) can be imported into the software. The pathway of the diseased coronary arteries can automatically be traced, even through CTOs. The interventional cardiologist can hence request magnetic vectors that truly correspond to the patient anatomy. In addition, the operator has access to the endoluminal view (5) that simulates looking through the vessel lumen and simultaneously to the corresponding Multi-Planar Reconstruction (MPR) slice, as well as an automated update of the magnetic vector as the wire is advanced.

This case report illustrates the first use of this innovation - in a complex patient with triple-vessel disease.

Materials and Methods

A 56-year old diabetic woman presented unstable angina. Angiography performed at her referring hospital revealed significant three-vessel disease (Figure 1 a-c) with lesions in the proximal segments of both the right coronary artery (RCA) and the left anterior descent (LAD) as well as diffuse disease in the obtuse marginal (MO). As part of an angina protocol workup, she had an MSCT, which showed all three vessels having varying amounts of calcification (Figure 2).

Percutaneous Coronary Intervention was planned following a clinical consultation with our surgical colleagues. Standard six French catheters (4.0 Judkins Right and 3.5 CLS) were used to facilitate the MSCT guided Magnetic Assisted Intervention (MAI). The procedure of integrating the MSCT in Navigant® 2.11 (Pathway Planning) and crossing the lesion is detailed below.

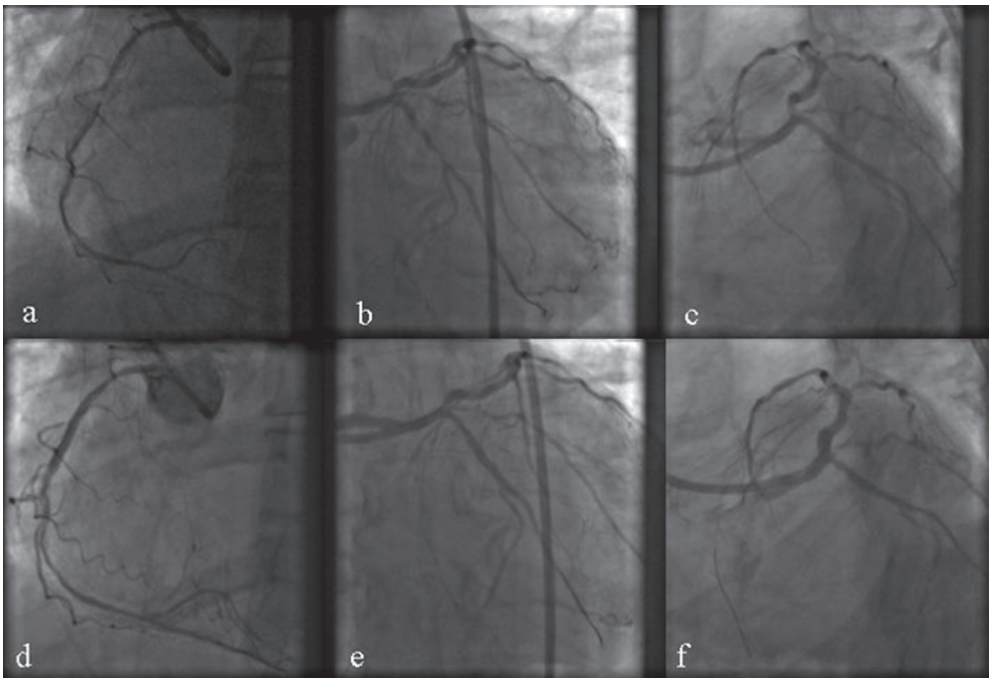

FIGURE 1. Angiographic views of the three diseased vessels pre- (a-c) and post (d-f) treatment.

Pathway Planning and Crossing

This is done in three steps:

1. Extraction of the coronary tree from the raw MSCT DICOM dataset (Siemens)
2. Automatic vessel centerline computation (Stereotaxis)
3. Sequenced magnetic guidewire navigation (Stereotaxis)

Coronary Tree Extraction

The Siemens Circulation™ (Circulation, version syngo CT 2007A, Siemens, Forchheim, Erlangen, Germany) allows the identification of the coronary tree from an MSCT angiogram (Figure 2). The package then performs a semi-automatic segmentation of the coronary tree based on a single seed point. This post-processing of the DICOM dataset can be imported into the Navigant® 2.11 software.

Pathway Planning

Once the coronary tree is imported into Navigant® 2.11, the user assesses the diseased vessels and asks the software to compute their centerlines: the trajectory in the middle of each vessel. This results in a pathway based on which the magnetic field – critical for directing the

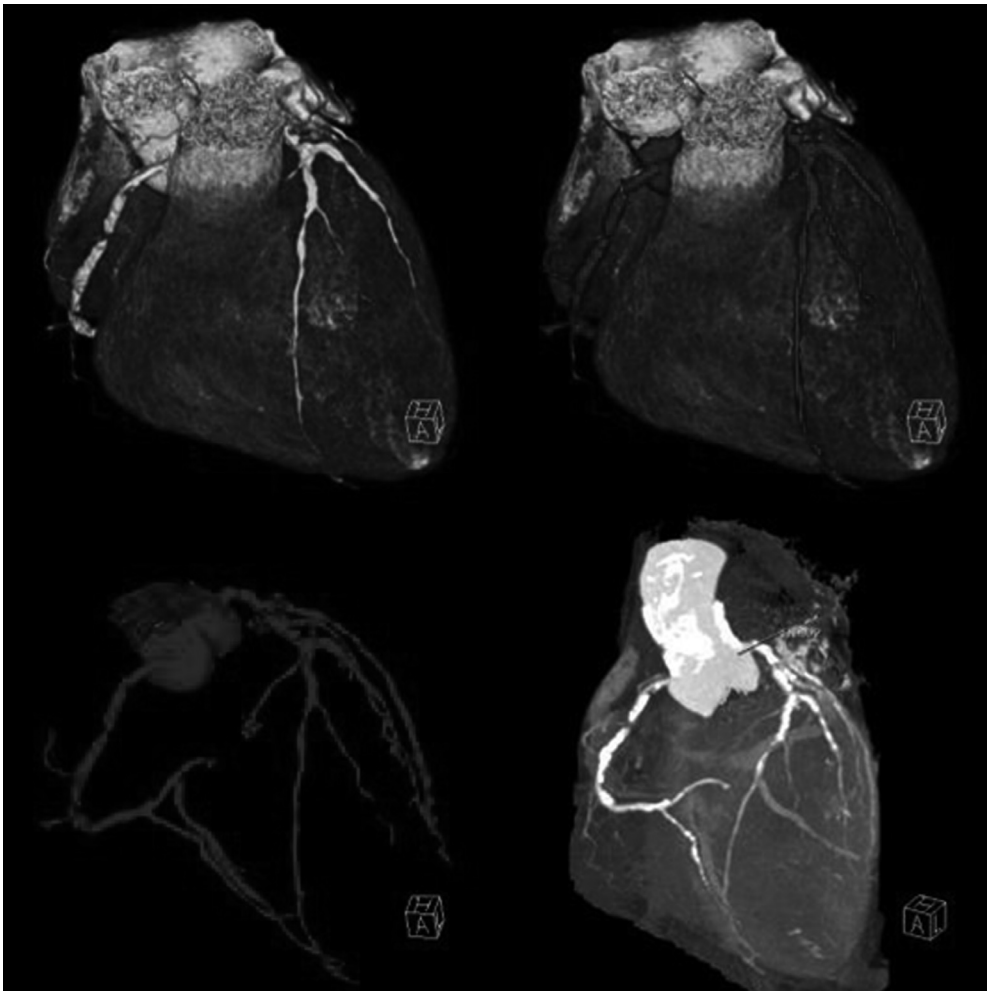

FIGURE 2. Volume-rendered MSCT image with coronary segmentation is displayed in blue with vessel calcification shown in bottom right image.
(A full color version of this illustration can be found in the color section)

guide-wire tip – will be generated. The magnetic vector will be tangent to the point in the vessel where the operator has chosen to navigate. It therefore defines the instantaneous advancement direction (Figure 3).

In addition to this, Navigant® 2.11 uses the data from the MSCT to generate an endoluminal view and an MPR slice. Hence, the interventionalist is provided with a forward-looking representation of the inside walls of the diseased coronaries. At the same time, the Hounsfield map of the transversal MPR slice is shown.

FIGURE 3. Volume-rendered coronary tree with the automatically computed pathway and the tangent magnetic vector.
(A full color version of this illustration can be found in the color section)

Magnetic Navigation

The navigation is performed after co-registration of the MSCT to two Xray images that are at least 30° apart and aligning the centerline/navigational path to the live fluoroscopy image. At each position along the navigational path all three corresponding magnetic vector, endoluminal view and MPR slice can be shown on a touch screen monitor. A novel feature that is unique to Navigant® 2.11 is that after registering a magnetic wire the physician is able to choose a step size (1 to 9mm) and a so-called sequencing rate (1 to 60sec) for the vector to automatically update along the vessel. This means that the operator can fully concentrate on the wire advancement guided by the moving vectors on the live fluoroscopy

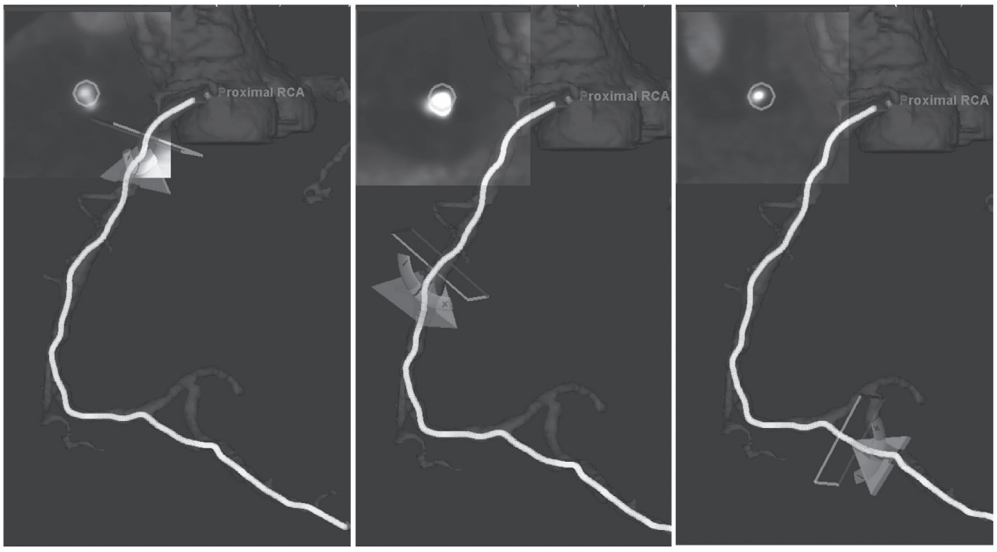

FIGURE 5. Volume-rendered automated vessel sequencing. MPR slices are in the upper left quadrants.
(A full color version of this illustration can be found in the color section)

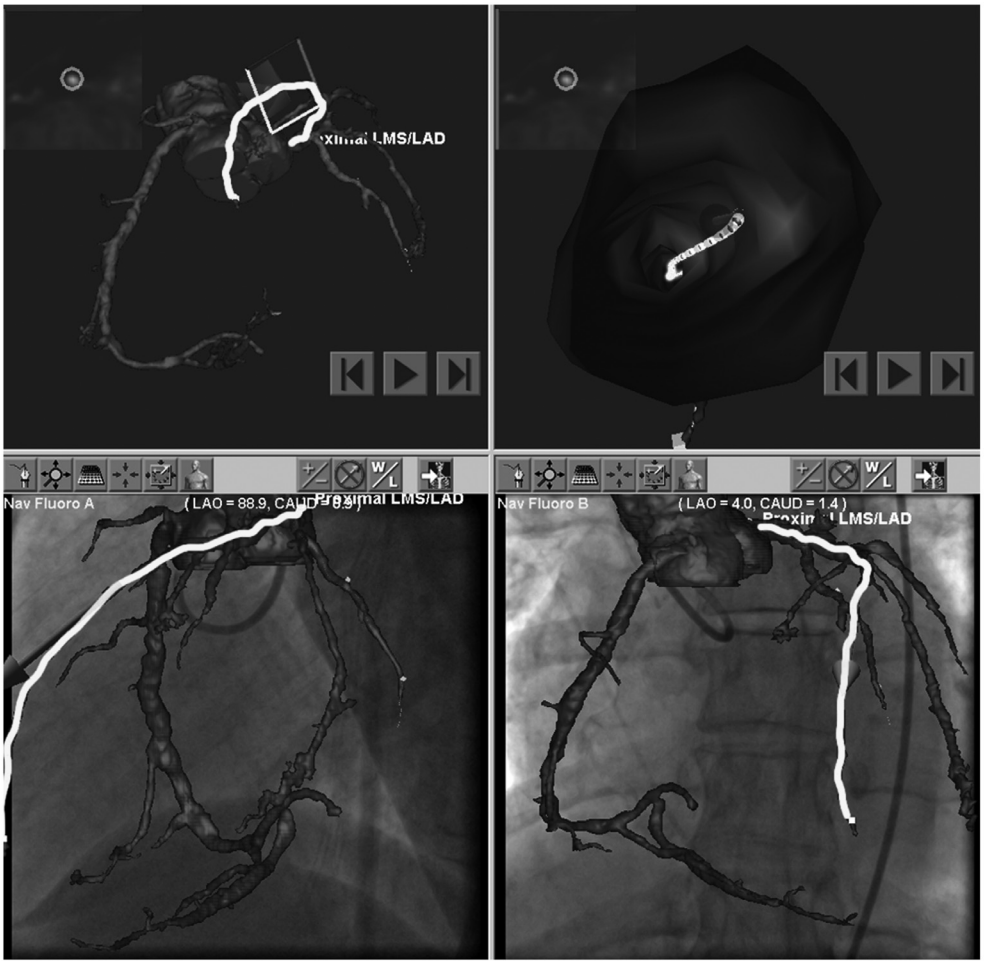

FIGURE 4. Volume-rendered navigation and tools for the operator.
(A full color version of this illustration can be found in the color section)

image (Figure 4). As the vector is sequentially updated so too are the MPR slices together with the endoluminal views. This automated sequencing can however be temporarily stopped at any desired time (Figure 5)

Results

Using the approach of automated wire advancement, the proximal lesion in the RCA was crossed with a Titan 3mm straight tip magnetic wire in 30 seconds with minimal contrast (8ml). The lesion was predilated with a Voyager 2.5x20mm balloon at 8 atmospheres following which

a Xience™ V stent (2.5x20mm) was implanted at 20 atmospheres. A similar magnetic wire was used to cross the lesions in the MO (20sec, 2ml contrast) and in the LAD (20sec, 2ml contrast) to permit the direct implantation of Xience™ V stents (2.5x15mm and 3.5x15mm) respectively. There was TIMI 3 flow in all three coronary arteries on angiography (Figure 1d-e) and she was discharged home after an uncomplicated 48h stay in hospital. She is requested to continue dual anti-platelet medication for one year.

Discussion

The MNS allows a full omni directional (360°) movement of a 2-3mm Neodymium magnet attached to the tip of a 0.014mm guide wire. Magnetic vectors created in Navigant® precisely control this movement so as to follow a 3-dimensional navigational path or road map of the coronary artery. The use of MSCT to create such a road map not only gives useful information about the plaque composition and eccentricity but more importantly it enables the direct visualization of occluded segments in a CTO. It is reported that the success in treating CTO can depend not only on the length of the occlusion but also on the amount of calcium within the occlusion. As such, the ability to directly visualize the MPR slices whilst simultaneously being aligned to the position of the vector that guides the wire is an extremely useful tool. This paper describes the first ever PCI where an interventionalist can visualize exactly what is being encountered ahead of a guidewire. The link with MNS gives the wire the ability to steer around eccentric plaque as highlighted in this case or to channel microvessels within an occlusion. It is worth pointing out that the endoluminal view is a display tool and the vectors generated are the same with or without this additional feature. However, by manually adjusting the vector to take into account subtle changes in the vascular anatomy while looking in the endoluminal view can offer a higher degree of navigational accuracy. The overall complexity of the case demonstrates that MAI is safe and feasible in patients with multi-vessel disease.

Conclusion

The incorporation of MSCT extracted coronary arteries in Navigant® 2.11 provide an innovative approach to facilitate PCI with its potential advantages of visualizing the MPR slice, the endoluminal view and automated segmental vector advancement.

References

1. Van Mieghem CA, Cademartiri F, Mollet NR, Malagutti P, Valgimigli M, Meijboom WB, Pugliese F, McFadden EP, Ligthart J, Runza G and others. Multislice spiral computed tomography for the evaluation of stent patency after left main coronary artery stenting: a comparison with conventional coronary angiography and intravascular ultrasound. Circulation 2006;114(7):645-53.
2. Sanz J, Dellegrottaglie S, Fuster V, Rajagopalan S. Calcium scoring and contrast-enhanced CT angiography. Curr Mol Med 2006;6(5):525-39.
3. Patterson MS, Schotten J, van Mieghem C, Kiemeneij F, Serruys PW. Magnetic navigation in percutaneous coronary intervention. J Interv Cardiol 2006;19(6):558-65.
4. Garcia-Garcia HM, Tsuchida K, van Mieghem C, Daemen J, van Weenen S, Patterson M, van der Ent M, van der Giessen WJ, Meulenbrug H, Sehra R and others. Multi-slice computed tomography and magnetic navigation-initial experience of cutting edge new technology in the treatment of chronic total occlusions. Eurointervention 2007.
5. Patterson M, Tanimoto S, Tsuchida K, PW. S. Magnetic Navigation with the Endo-Luminal View and the X-ray overlay - Major advances in novel technology. Eurointervention 2007;in press.

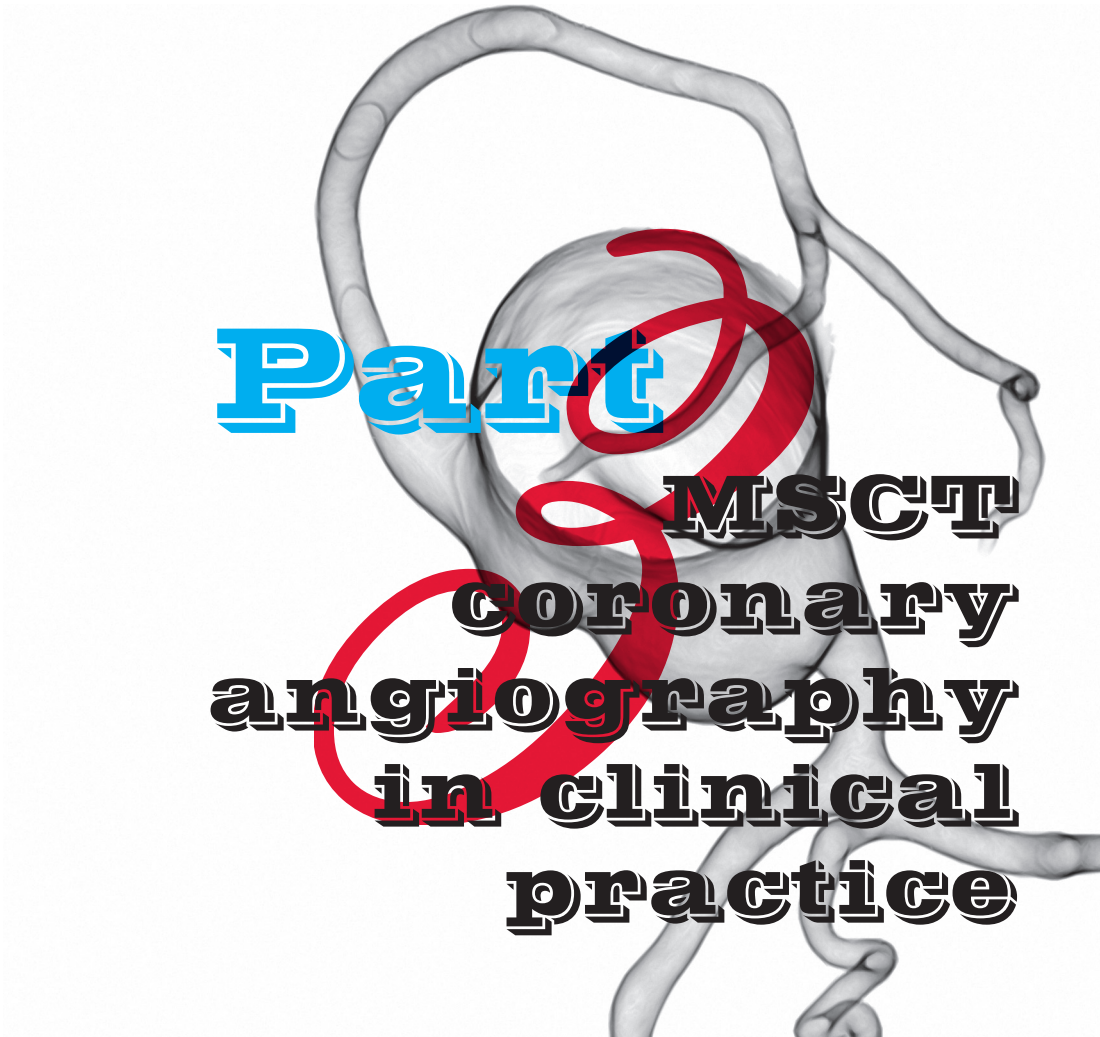

Part 2

MSCT coronary angiography in clinical practice

CHAPTER 9

Prevalence and characteristics of major and minor coronary artery anomalies in an adult population assessed by computed tomography coronary angiography

Rodriguez-Granillo GA, Rosales MA, Pugliese F, Fernandez-Pereira C, Doval H, Rodriguez AE.

EuroIntervention, manuscript accepted for publication.

Summary

Purpose: The global prevalence and characteristics of coronary artery anomalies (CAAs) remain debatable since populations between studies are widely different. Our purpose was to explore the prevalence and characteristics of major and minor CAAs using computed tomography coronary angiography (CCTA).

Materials and Methods: Consecutive patients in sinus rhythm referred for evaluation by CCTA were prospectively studied for the presence of CAAs. Scans were performed using 40-row and 64-row CT scanners.

Results: We studied 577 patients [mean age 61±11 years; 81% men]. Patients were studied either as control of stents, or due to the presence of multiple risk factors (53 %), or due to chest pain, equivalent symptoms or inconclusive stress tests (47 %). We identified CAAs in 121 (21.0 %) patients. Six (1.0 %) anomalous origination of a coronary artery from the opposite sinus (ACAOS) were identified. Coronary ectasia or aneurysm was present in 10 (1.7 %) patients. 109 intramuscular segments (MB) were found in 100 (17.3 %) patients. Coronary hypoplasia was identified in 3 patients, all involving the RCA, and 3 patients had an absent left main coronary artery. None of the segments with ACAOS (prox-

imal segment) or MB had atherosclerotic plaque.

Conclusion: CAAs were highly prevalent along the coronary tree, and anatomical characteristics that might help stratify the risk and guide therapy of CAAs could be easily identified with CCTA.

Introduction

During the past few years, several studies have explored the prevalence and characteristics of coronary artery anomalies (CAAs) by means of multiple diagnostic methods. Originally, CAAs have been reported in pathological studies, with its inherent limitations since its population is obviously biased (1),(2). Subsequently, echocardiographic and conventional selective angiographic studies have reported the prevalence of CAAs non-invasively and invasively, respectively, in in-vivo settings (3,4). Echocardiographic investigation, though, is limited for this purpose since it can only identify the anomalous origination of a coronary artery from the opposite sinus of Valsalva (ACAOS), without being able to describe the course of the coronary arteries or the territory involved, as well as other more frequent types of CAAs (5). Moreover, echocardiography, even in children with a good acustic window, can fail to detect some cases of ACAOS (3). In a prospective echocardiographic study of ACAOS in patients with preoperative angiographic confirmation, five out of eight patients with ACAOS and ostial stenosis were not diagnosed (6).

Conventional angiography, in addition to its invasive nature, is restricted for the detection of CAAs for numerous reasons. Angiography lacks the ability to differenciate between high (i.e. interarterial) and low (i.e. retroaortic) risk ACAOS, as well as the myocardial territory involved. Besides, myocardial bridging (MB) is largely underreported by conventional angiography (7), probably due to the ability of the technique to identify only MB that produce the typical "milking" phenomenon.

Several additional CAAs with different and heterogeneous presentations can be found, including coronary artery ectasia or aneurysms (CEA), which may induce myocardial ischemia even without concomitant atherosclerotic disease (8). The global prevalence of major and minor CAAs remains a matter of debate since populations between studies are widely different. In addition, methodological aspects and limitations natural to most techniques further influence the results.

Although it has been advocated that CAAs should be reported as a whole (9), few studies have reported the global incidence of these findings. The purpose of

the present study was therefore to explore the prevalence and characteristics of CAA using high resolution computed tomography coronary angiography (CCTA) in a consecutive series of 599 patients.

Materials and Methods

Between October 2005 and December 2007, consecutive patients in sinus rhythm, able to hold their breath for ≥ 15 seconds, without history of contrast related allergy, renal failure, arrhythmia, or hemodynamic instability, and referred for evaluation by computed tomography coronary angiography (CCTA) in our institution, were prospectively studied for the presence of CAAs. Patients with a heart rate > 70 bpm received beta-blockers either as a single oral dose (atenolol 50 mg) 1 hour before the scan, or intravenously (propranolol 1 mg/min) inmediately before the scan.

CCTA Acquisition and Analysis

Electrocardiographically gated scans were performed using 40-row (324 patients) and 64-row (253 patients) CT scanners (Brilliance 40 and Brilliance 64, Philips, the Netherlands). A bolus of 80-125 ml of iodinated contrast material (Optiray®, Ioversol 350 mg/ml, Mallinckrodt, St. Louis, U.S.A.) was injected through an arm vein at 5-6 ml/s. The scan parameters were a collimation either 40 x 0.625 mm or 64 x 0.625 mm, rotation time 0.4 seconds, tube voltage 120 kV, and mAs 600-1000. A bolus tracking technique was used to synchronize the arrival of contrast at the level of the coronary arteries with the start of acquisition.

Reconstructions were assessed using axial planes, multiplanar reconstructions, volume rendering techniques, curved multiplanar reconstructions, and maximum intensity projections. In all patients, images were reconstructed in end diastole (75 % of the R-R interval) and image quality was evaluated on a per segment basis. Where images were judged to be suboptimal, additional reconstruction windows (30 %, 40 %, 70 % and 80 %) were explored in order to achieve optimal quality images. Two experienced observers (GARG and MAR) evaluated all scans.

Definition of CAA

The classification scheme of Angelini et al. (10) was used to identify and categorize CAAs. ACAOS were identified and the type, path, and the presence of ostial stenosis and atherosclerosis were reported as previously described (10). Myocardial bridging (MB) was identified as an intramuscular segment of a coronary artery. As previously reported, segments covered by a thin layer of muscle were included since they may be compressed during

systole (11). The location (mid LAD, distal LAD, diagonal, obtuse marginal, intermediate branch), path (deep septal, superficial, right ventricle), length, and the presence of atherosclerosis within the host vessel and intramural segment were evaluated.

Coronary ectasias were defined as non-obstructive lesions of the epicardial coronary arteries with a dilation 1.5- to 2.0-fold of normal diameters, and coronary aneurysms were defined as a dilations exceeding 2.0-fold of normal diameters (12). Coronary ectasia or aneurysm (CEA) were classified as saccular when the transverse diameter was greater than the lenght, and fusiform when the longitudinal dilation was larger than the transverse diameter. Dilated coronaropathy was defined as bilateral fusiform CEA involving both the right and left coronary arteries (8).

Discrete variables are presented as counts and percentages. Continuous variables are presented as mean ± SD. Comparisons among groups were performed using X2 tests. Statistical analyses were performed with SPSS software, version 13.0 (Chicago, Illinois, USA).

Results

Five hundred and ninety nine consecutive patients referred for evaluation by CCTA were prospectively studied for the presence of CAAs. Twenty two patients (3.7 %) were excluded due to poor image quality and 1 (0.2 %) due to contrast extravasation, leading to a final study population of 577 patients. Patients were studied as control of stents or for screening due to the presence of multiple risk factors (53 %), or due to chest pain, equivalent symptoms or inconclusive stress tests (47 %). The mean age was 60.8±11.3 years and 81% were men. The mean heart rate immediately before the scan was 61.1±7.4 bpm (range 40 to 93 bpm). The right coronary artery was dominant in 87.1 % of cases, the left circumflex in 7.7 % and there was codominance in 5.2 % of cases.

Following the classification proposed by Angelini et al. (10), CAAs were identified in 121/577 (21.0 %) patients (Table 1). Twenty three percent of male patients had CAAs, whereas 12.6% of female patients had CAAs (p=0.02).

Six ACAOS (1.0 %) were detected, 3 right ACAOS (Figure 1) and 3 left ACAOS (Figure 2). Clinical and anatomical features of these patients are depicted in Table 2. The mean age of patients with ACAOS was 57±13 years. Most pa-

TABLE 1. Coronary artery anomalies, n (%)

Total	**121 / 577 (21.0 %)**
Anomalous origination on the contralateral sinus (ACAOS)	6 (1.0 %)
Ectasia or aneurysm (CEA)	10 (1.7 %)
Myocardial bridging (MB)	100 (17.3 %)
Coronary hypoplasia	3 (0.5 %)
Absent left main coronary artery	3 (0.5 %)
Other (fistula, split LAD)	2 (0.3 %)

One patient had simultaneous ACAOS and MB, and another patient had CEA and MB.

tients were males, clinical presentations were diverse, and concomitant atherosclerotic disease was rare. Half of the ACAOS had a retroaortic course and half an interarterial course (between the aorta and the pulmonary trunk). No patients had atherosclerotic disease at the proximal segment. A 40 year-old patient with no cardiovascular risk factors, atypical chest pain and positive thallium scan, who underwent a conventional angiogram in another center that was reported as normal, had the left circumflex ostium at the right sinus of Valsalva, with a retroaortic course and ostial stenosis without evidence of atherosclerosis. During the angiogram, a prominent diagonal had been taken as a normal LCX, since the latter had its ostium 1.5 mm caudal from ostium of the RCA (Figure 2) and was therefore never engaged during the angiogram.

Coronary ectasia or aneurysm (CEA) was identified in 10 (1.7 %) patients. Characteristics of patients with CEA are shown in Table 3. Ninety percent were males. In 2 patients, the CEA was saccular, in 4 patients was fusiform, in 1 patient was

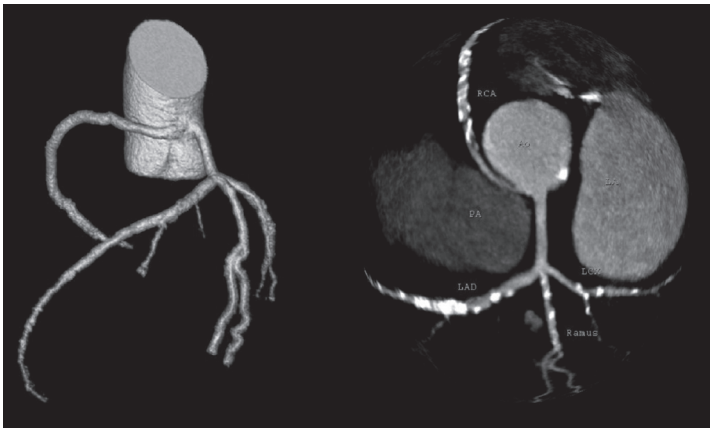

FIGURE 1. Right coronary artery arising from the left sinus of Valsalva, with a interarterial (between the aorta and the pulmonary artery) course, an acute angle take-off, and ostial stenosis without evidence of atherosclerosis at the proximal segment.
(A full color version of this illustration can be found in the color section)

TABLE 2. Patients with anomalous origination of a coronary artery from the opposite sinus

	#1	#2	#3	#4	#5	#6
Sex	M	M	M	M	M	F
Age	40	37	68	47	60	71
Asymptomatic	-	-	-	X	-	X
Chest pain, atypical	X	X	-	-	-	-
Chest pain, typical	-	-	X	-	X	-
LCX from RCA	-	-	-	-	X	-
LCX from right sinus	X	-	-	-	-	X
RCA from left sinus	-	X	X	X	-	-
Retroaortic course	X	-	-	-	X	X
Interarterial (between Ao and PA)	-	X	X	X	-	-
Acute angle take off	-	X	X	X	X	X
Intramural location	-	-	X	-	X	-
Ostial stenosis	65 %	60 %	70 %	35 %	0 %	75 %
Proximal atherosclerosis	No	No	No	No	No	No
Distal atherosclerosis	No	No	Yes	No	No	No
Non-target vessel disease	No	No	Yes	No	No	Yes

saccular bilateral, and in other 3 was fusiform bilateral ("dilated coronaropathy") (Figure 3). One patient had a history of cocaine use and bilateral aneurysms. Another patient was admitted to our hospital for surgical intervention of a retroperitoneal tumor and suffered a hypertensive crisis with signs of acute heart failure during surgery. A saccular aneurysm of 8.5 mm x 8.0 mm in the distal left main trunk affecting the ostium of the left anterior descending coronary artery, with no evidence of coronary atherosclerosis was detected by CCTA (Figure 3 b). Another patient suffered from an acute myocardial infarction

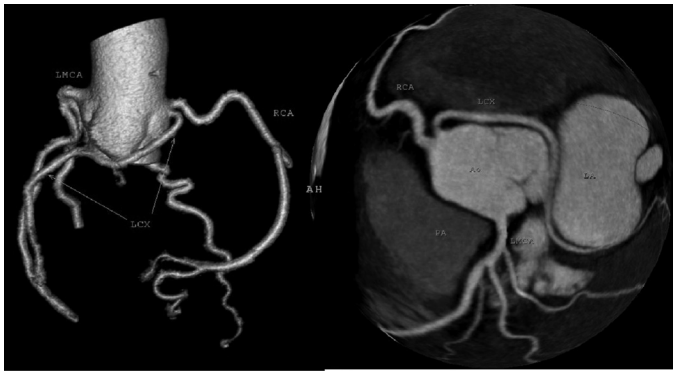

FIGURE 2. Left circumflex arising from the right sinus of Valsalva, with a retroartic course, ostial stenosis, and no evidence of coronary atherosclerosis along the coronary tree. This patient had a previous angiogram deemed as normal, where a prominent diagonal was probably mistaken with the left circumflex.
(A full color version of this illustration can be found in the color section)

TABLE 3. Patients with coronary ectasia or aneurysms (CEA)

	#1	#2	#3	#4	#5	#6	#7	#8	#9	#10
Sex	M	M	M	M	M	M	M	M	M	F
Age	41	51	63	66	59	38	50	48	73	32
Cocaine use	-	-	-	-	-	-	-	-	-	X
Asymptomatic	-	-	X	X	-	X	-	-	X	-
Control of non target vessel stents	X	-	-	-	-	-	-	-	-	-
Chest pain	-	X	-	-	X	-	X	X	-	X
Type	Sac	Fus	Fus	FB	Sac	Fus	Fus	FB	Fus	SB
Localization	RCA	RCA	RCA	3V	LM	RCA	LCX	3V	RCA	PV, LAD
Maximum diameter	8.1	6.6	7.9	6.4	8.7	5.7	6.3	7.2	6.6	5.3
Reference diameter	3.2	3.0	5.9	2.7	3.0	2.9	2.5	3.0	3.7	2.0
CEA atherosclerosis	No	No	Yes	No	No	No	Yes	No	No	No
Non-target lesion	Yes	Yes	Yes	No	No	No	Yes	No	No	Yes

Sac refers to saccular, fus to fusiform, SB to saccular bilateral and FB to bilateral fusiform ("dilated coronaropathy"). RCA refers to right coronary artery, 3V to 3-vessel, LM to left main, LCX to left circumflex, LAD to left anterior descending and PV refers to posteroventricular.

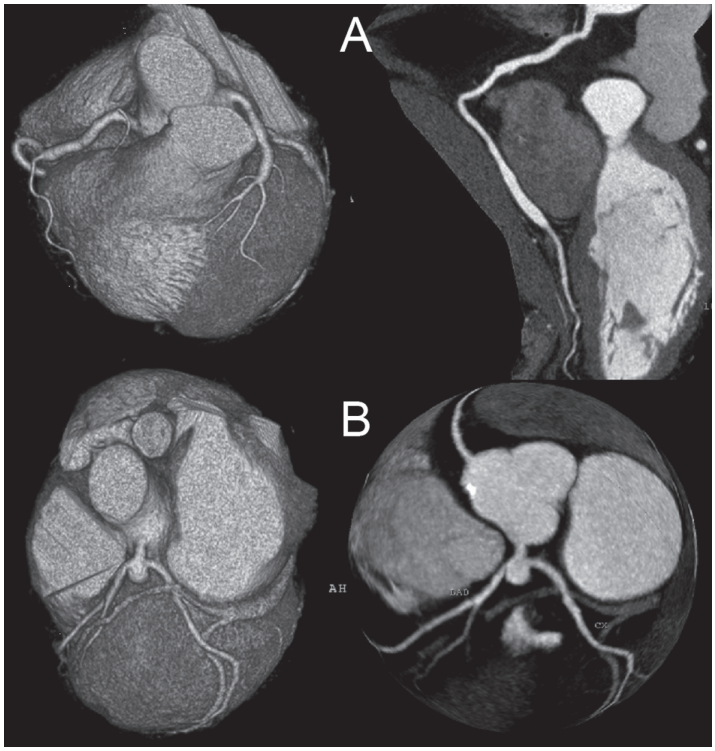

FIGURE 3. Coronary ectasia or aneurysms: A) Bilateral fusiform coronary ectasia ("dilated coronaropathy"). On the right panel, a curved multiplanar reconstruction shows difuse ectasia of the distal right coronary artery. B) Saccular aneurysm of the distal left main coronary artery with ostial stenosis of the left anterior descending.
(A full color version of this illustration can be found in the color section)

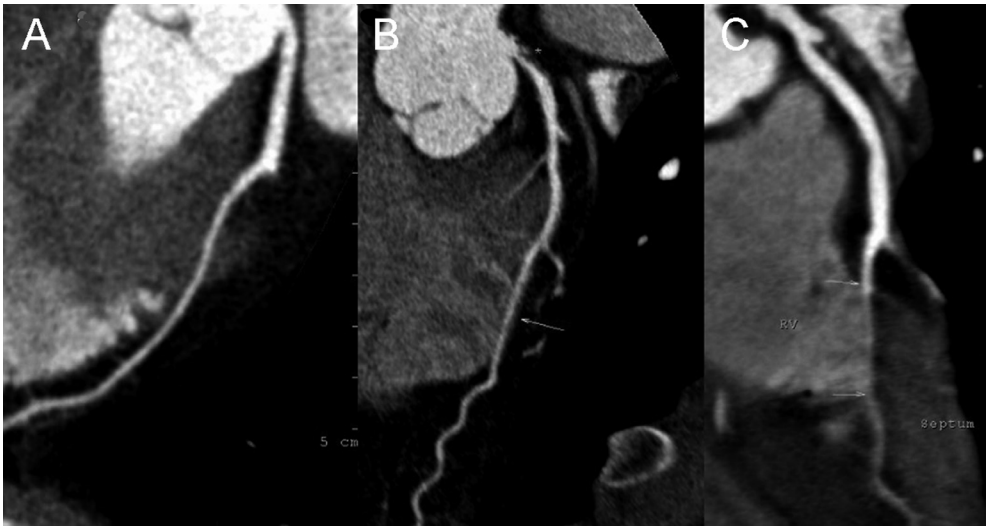

FIGURE 4. Myocardial bridging: A) deep septal type, B) superficial type, C) right ventricular type. In B, a severe non-calcified lesion, can be seen on the proximal left main coronary artery.

due to oclusion of a fusiform coronary artery aneurysm.

One hundred and nine intramuscular segments (myocardial bridging, MB) were identified in 100 (17.3 %) patients. Characteristics of the MB are displayed in Table 4 and Figure 4. MB was found in 88/466 (18.9 %) of male patients and in 12/111 (10.8 %) of female patients (p=0.04). Most intramuscular segments were located in the left anterior descending artery (67.0 %), whereas no MB was located at the right coronary artery. Although 71 (65.1%) patients had atherosclerotic disease in the "host" vessel, there was no evidence of atherosclerosis within any MB segment. Nevertheless, one patient had a previous stent in such segment due to ischemia.

Coronary hypoplasia was identified in 3 patients, all involving the RCA, with a large, dominant LCX (Figure 5). Three patients had an absent left main coronary artery (Figure 6).

Discussion

Although the medical community has been aware of the presence of coronary artery anomalies (CAAs) for a long time (1,2), the paucity of reports, the lack of prospective studies and the conflicting data regarding the prevalence of CAAs, has created confusion about the true prevalence as well as the clinical and haemodinamic implications of these findings. More recently, the ischemic mechanisms of CAAs have been explored with

more detail in angiographical and post mortem studies (10). With the advent of novel technologies such as magnetic resonance coronary angiography and CCTA, non-invasive detection of all CAAs can be accomplished with high precision. CCTA is an emerging technology that has a high sensitivity and specificity for the detection of significant epicardial coronary atherosclerosis, as well as an effective method to evaluate the extent and distribution of non-significant lesions in the coronary tree (13-15). In addition, CCTA can accurately characterize the sinus of Valsalva, the distal coronary beds, and the myocardium itself (16). Although a previous study has reported the prevalence and anatomical features of MB by means

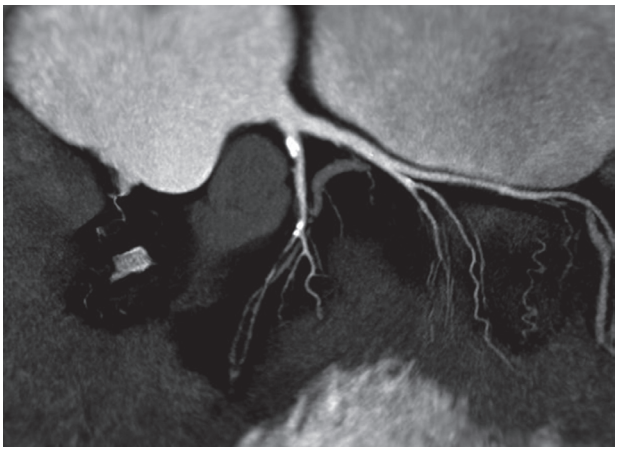

FIGURE 5. Coronary hypoplasia of the right coronary artery. A very large left circumflex is dominant. Note a severe lesion at the distal left anterior descending coronary artery.

TABLE 4. Myocardial bridging

Total	109 in 100 patients (17.3 %)
Location	
Mid LAD	49 (45.0 %)
Distal LAD	24 (22.0 %)
Obtuse marginal	20 (18.3 %)
Diagonal	12 (11.0 %)
Intermediate branch	4 (3.7 %)
Lenght	24.5±13.0 (range 7.0 to 71.4 mm)
MB without atherosclerosis, within diseased vessel	71 (65.1 %)
MB without atherosclerosis, within normal vessel	37 (33.9 %)
MB with atherosclerotic diasease or stent	1 (0.9 %)
Left anterior descending MB, Type	
Deep septal	16 (21.6 %)
Superficial	39 (52.7 %)
Right ventricle	19 (25.7 %)

FIGURE 6. Absence of left main coronary artery. The left anterior descending and the the left circumflex clearly arise from independent ostia at the left sinus of Valsalva.
(A full color version of this illustration can be found in the color section)

of CCTA (11), the present study reports for the first time the prevalence and characteristics of all (major and minor) CAAs in consecutive series of 577 adults using CCTA. Identification of CAAs was feasible and straightforward using CCTA. We found a high prevalence of CAAs (21 %), being MB the most frequent finding as expected.

Anomalous Origination of a Coronary Artery from the Opposite Sinus (ACAOS)

With a prevalence ranging from 0.2 to 1.0 % (17), the anomalous origination of a coronary artery from the opposite sinus of Valsalva (ACAOS), represents a common cause of sudden cardiac death in the young population, particularly in individuals that undergo strenuous exercise (18). Unfortunately, since most patients with ACAOS are asymptomatic (less than one third of patients develop chest pain, syncope, palpitations, dyspnea), the diagnosis is usually made post-mortem (19-21). In our series, similar to previous reports (10), the prevalence of ACAOS was 1 %, and 5 out of 6 patients were males. Of note, one patient had previously undergone a coronary angiography which was erroneously deemed as normal. Most segments with ACAOS displayed ostial stenosis. Nevertheless, none of the proximal segments of ACAOS had atherosclerosis. As proposed by Angelini et al.(9), such discordance might be explained by the coronary hypoplasia commonly seen in proximal segments of ACAOS.

CCTA evaluation allowed the identification of the ostium of the anomalous coronary arteries, the presence of atherosclerosis, intramural segments, ostial stenosis and/or acute angle take-off. In addition, we were able to differentiate between high (i.e. interarterial) and low (i.e. retroaortic) risk ACAOS.

The choice of therapy (medical, stent implantation or surgical repair) depends on

the ACAOS type (right or left), symptoms, presence of ostial stenosis, course, myocardial territory involved, and the presence of reversible ischemia (9). Accordingly, since CCTA can provide valuable information regarding the type, origin, stenosis, course and territory involved of ACAOS, this technique might be a useful tool to guide therapy in such patients.

Myocardial Bridging (MB)

MB has been recognized as minor CAA (10). Pathological and clinical studies are largely discordant regarding the prevalence of MB, ranging from 15 % to 85 % in post mortem series (22-24) and from 0.5% to 2.5% in angiographic series (7,25,26). Although MB is in most cases an incidental finding during coronary angiography, several authors have reported an association between MB and ischemic events, including myocardial infarction and sudden death (27).

In our study, MB was predominantly found in males, and the mid LAD was the most common location (45 %), although secondary branches were not uncommon. In line with previous reports, the right coronary artery was protected from MB (11,27). Of note, deep septal MB were the least common type. This might partially explain the underestimation of MB by conventional angiography. The prevalence of MB in our series would have been of 2.7 %, ie. similar to the prevalence reported in angiographic studies (7,25,26) if we had taken into account only deep septal MB. Experimental studies have shown that the length of a coronary narrowing has an impact on the hemodynamics (28). In our study, the mean length of the intramuscular segments was 24.5 mm. It is noteworthy that out of 109 intramuscular segments, none of them had atherosclerotic disease within the tunneled segment. Recently, a number of studies demonstrated that the average and maximal peak velocity measured by intracoronary Doppler within the tunneled segment was more than twice as high as the velocity at the proximal and distal segments (27). Accordingly, the lack of atherosclerosis might be potentially attributed to the high shear stress and, hence, laminar flow present within the tunneled segments. In turn, atherosclerosis has a tendency to arise more frequently in low-oscillatory shear stress regions, where there is a loss of the physiological flow-oriented alignment of the endothelial cells (29-31).

Coronary Ectasia or Aneurysms (CEA)

Even in angiographically normal coronary arteries, patients with CEA can develop myocardial ischemia and/or myocardial infarction. This has been shown by Kruger et al. (8), who demonstrated exercise-induced ischemia and insufficient vasoconstriction in patients with non-

atherosclerotic dilated coronaropathy, thus enforcing the concept of endothelial dysfunction associated with CEA. The angiographic incidence of CEA in diagnostic cardiac catheterizations has been found to vary between 0.3% and 4.9% (32-35). CEA are caused by atherosclerosis in 50 % of the cases, whereas 30 % are usually congenital and only 10 % to 20 % of CEA are related to inflammatory or connective tissue disorders (12,35). In our series, we identified 10 (1.7 %) patients with CEA (1.7 %), and only 20 % of CEA had evidence of atherosclerotic plaque by CCTA, although 50 % of the patients had atherosclerosis elsewhere along the coronary tree. In agreement to the available reports (2), CEA were largely (90 %) more frequent in males than females. Of note, the only female with CEA, with bilateral aneurysms, had a history of cocaine use. The association between cocaine use and CEA has been described recently by Satran et al. (2), who found that 30 % of cocaine users had coronary artery aneurysms, typically bilateral.

Clinical Implications

To our knowledge, the present study reports for the first time the prevalence and characteristics of all CAAs in a consecutive series of patients using CCTA. Identification of CAAs by CCTA was feasible, and anatomical characteristics that might help stratify the risk and guide therapy of CAAs could be easily identified. We found a high prevalence of CAAs along the coronary tree. With a worldwide increasingly growing use of CCTA for the detection of coronary artery stenosis and its indications in constant expansion, and since identification of CCAs does not require any modification from standard scan protocols, the findings of the present study should encourage CCTA specialists to routinely explore for the presence of CAAs. In turn, provided that scans would specifically be performed to search for CAAs, tube modulation techniques might be applied to reduce radiation dose to levels comparable to conventional angiography (36,37). It is noteworthy that none of the segments with ACAOS (n= 6) or MB (n=109) had proximal atherosclerosis. As aforementioned, this might potentially be due to the smaller reference diameter at such segments and hence increased shear stress, leading to protection from atherosclerosis. Given the paucity of data regarding the natural history of CAAs, large multicenter CCTA registries that provide unique prognostic information of CAAs are warranted.

Limitations

The present was an observational study, and the findings were not systematically confirmed by conventional angiography. However, CCTA has been validated as an accurate diagnostic tool to evaluate the coronary tree (13). Since the study population was mainly constituted by adult

patients referred for cardiovascular study, we cannot consider the sample as normal or unselected. Due to the observational nature of the study, we lack cause-effect mechanisms to explain the ethiology of coronary ectasia. Similarly, we did not systematically perform functional tests in order to evaluate the haemodinamic significance of the findings. Finally, despite CAAs seem to be more prevalent in males, we cannot completely rule out a possible influence of the under-representation of women in cardiovascular populations. Nevertheless, a similar trend was shown even in pediatric studies (3).

REFERENCES

1. Morgagni J. De Sedibus et Causis morborum. Venecutus Tom I, Epis 27, Art 28, 1761.
2. Gore I, Smith J, Clancy R. Congenital aneurysms of the coronary arteries with report of a case. Circulation 1959;19:221-7.
3. Davis JA, Cecchin F, Jones TK, Portman MA. Major coronary artery anomalies in a pediatric population: incidence and clinical importance. J Am Coll Cardiol 2001;37:593-7.
4. Engel HJ TC, Page HL. Major variations in anatomical origin of the coronary arteries: angiographic observations in 4250 patients without associated congenital heart disease. Cathet Cardiovasc Diagn 1975;1:157- 69.
5. Hejmadi A SD. What is the most effective method of detecting anomalous coronary origin in symptomatic patients? J Am Coll Cardiol 2003;42:155-7.
6. Frommelt PC, Frommelt MA, Tweddell JS, Jaquiss RD. Prospective echocardiographic diagnosis and surgical repair of anomalous origin of a coronary artery from the opposite sinus with an interarterial course. J Am Coll Cardiol 2003;42:148-54.
7. Noble J, Bourassa MG, Petitclerc R, Dyrda I. Myocardial bridging and milking effect of the left anterior descending coronary artery: normal variant or obstruction? Am J Cardiol 1976;37:993-9.
8. Kruger D, Stierle U, Herrmann G, Simon R, Sheikhzadeh A. Exercise-induced myocardial ischemia in isolated coronary artery ectasias and aneurysms ("dilated coronopathy"). J Am Coll Cardiol 1999;34:1461-70.
9. Angelini P. Coronary artery anomalies: an entity in search of an identity. Circulation 2007;115:1296-305.
10. Angelini P VS, Chan AV, Diez JG. Normal and anomalous coronary arteries in humans. In: Angelini P, ed. Coronary Artery Anomalies: A Comprehensive Approach. Philadelphia: Lippincott Williams & Wilkins 1999:27-150.

11. Konen E, Goitein O, Sternik L, Eshet Y, Shemesh J, Di Segni E. The prevalence and anatomical patterns of intramuscular coronary arteries: a coronary computed tomography angiographic study. J Am Coll Cardiol 2007;49:587-93.
12. Befeler B, Aranda MJ, Embi A, Mullin FL, El-Sherif N, Lazzara R. Coronary artery aneurysms: study of the etiology, clinical course and effect on left ventricular function and prognosis. Am J Med 1977;62:597-607.
13. Mollet N, Cademartiri F, van Mieghem CA, et al. High-resolution spiral CT coronary angiography in patients referred for diagnostic conventional coronary angiography. Circulation 2005;112:2318-2323.
14. Mollet NR, Cademartiri F, Nieman K, et al. Noninvasive assessment of coronary plaque burden using multislice computed tomography. Am J Cardiol 2005;95:1165-9.
15. Rodriguez-Granillo GA, Rosales MA, Degrossi E, Durbano I, Rodriguez AE. Multislice CT coronary angiography for the detection of burden, morphology and distribution of atherosclerotic plaques in the left main bifurcation. Int J Cardiovasc Imaging 2007;23:389-92.
16. Baks T, Cademartiri F, Moelker AD, et al. Multislice computed tomography and magnetic resonance imaging for the assessment of reperfused acute myocardial infarction. J Am Coll Cardiol 2006;48:144-52.
17. Yamanaka O, Hobbs RE. Coronary artery anomalies in 126,595 patients undergoing coronary arteriography. Cathet Cardiovasc Diagn 1990;21:28-40.
18. Basso C, Maron BJ, Corrado D, Thiene G. Clinical profile of congenital coronary artery anomalies with origin from the wrong aortic sinus leading to sudden death in young competitive athletes. J Am Coll Cardiol 2000;35:1493-501.
19. Kragel AH, Roberts WC. Anomalous origin of either the right or left main coronary artery from the aorta with subsequent coursing between aorta and pulmonary trunk: analysis of 32 necropsy cases. Am J Cardiol 1988;62:771-7.
20. Maron BJ, Shirani J, Poliac LC, Mathenge R, Roberts WC, Mueller FO. Sudden death in young competitive athletes. Clinical, demographic, and pathological profiles. Jama 1996;276:199-204.
21. Liberthson RR. Sudden death from cardiac causes in children and young adults. N Engl J Med 1996;334:1039-44.
22. Polacek P, Kralove H. Relation of myocardial bridges and loops on the coronary arteries to coronary occulsions. Am Heart J 1961;61:44-52.
23. Hansen BF. Myocardial covering on epicardial coronary arteries. Prevalence, localization and significance. Scand J Thorac Cardiovasc Surg 1982;16:151-5.
24. Ferreira AG, Jr., Trotter SE, Konig B, Jr., Decourt LV, Fox K, Olsen EG. Myocardial bridges: morphological and functional aspects. Br Heart J 1991;66:364-7.
25. Juilliere Y, Berder V, Suty-Selton C, Buffet P, Danchin N, Cherrier F. Isolated myocardial

bridges with angiographic milking of the left anterior descending coronary artery: a long-term follow-up study. Am Heart J 1995;129:663-5.

26. Angelini P, Trivellato M, Donis J, Leachman RD. Myocardial bridges: a review. Prog Cardiovasc Dis 1983;26:75-88.
27. Bourassa MG, Butnaru A, Lesperance J, Tardif JC. Symptomatic myocardial bridges: overview of ischemic mechanisms and current diagnostic and treatment strategies. J Am Coll Cardiol 2003;41:351-9.
28. Feldman RL, Nichols WW, Pepine CJ, Conti CR. Hemodynamic significance of the length of a coronary arterial narrowing. Am J Cardiol 1978;41:865-71.
29. Kornet L, Hoeks AP, Lambregts J, Reneman RS. In the femoral artery bifurcation, differences in mean wall shear stress within subjects are associated with different intima-media thicknesses. Arterioscler Thromb Vasc Biol 1999;19:2933-9.
30. Berceli SA, Warty VS, Sheppeck RA, Mandarino WA, Tanksale SK, Borovetz HS. Hemodynamics and low density lipoprotein metabolism. Rates of low density lipoprotein incorporation and degradation along medial and lateral walls of the rabbit aorto-iliac bifurcation. Arteriosclerosis 1990;10:686-94.
31. Rodriguez-Granillo GA, Garcia-Garcia HM, Wentzel J, et al. Plaque composition and its relationship with acknowledged shear stress patterns in coronary arteries. J Am Coll Cardiol 2006;47:884-5.
32. Hartnell GG, Parnell BM, Pridie RB. Coronary artery ectasia. Its prevalence and clinical significance in 4993 patients. Br Heart J 1985;54:392-5.
33. Markis JE, Joffe CD, Cohn PF, Feen DJ, Herman MV, Gorlin R. Clinical significance of coronary arterial ectasia. Am J Cardiol 1976;37:217-22.
34. Swaye PS, Fisher LD, Litwin P, et al. Aneurysmal coronary artery disease. Circulation 1983;67:134-8.
35. Falsetti HL, Carrol RJ. Coronary artery aneurysm. A review of the literature with a report of 11 new cases. Chest 1976;69:630-6.
36. Hausleiter J, Meyer T, Hadamitzky M, et al. Radiation dose estimates from cardiac multislice computed tomography in daily practice: impact of different scanning protocols on effective dose estimates. Circulation 2006;113:1305-10.
37. Husmann L, Valenta I, Gaemperli O, et al. Feasibility of low-dose coronary CT angiography: first experience with prospective ECG-gating. Eur Heart J 2008;29:191-7.

CHAPTER 10

Diagnostic performance of coronary computed tomography angiography by using different generations of multislice scanners. Single-centre experience

Pugliese F, Mollet NR, Hunink MGM, Cademartiri F, Nieman K, van Domburg R, Meijboom WB, Weustink AC, Dijkshoorn ML, de Feyter PJ.

Radiology 2008; 246:384-393.

Summary

Purpose: To retrospectively compare sensitivity and specificity of four generations of multidetector computed tomographic (CT) scanners for diagnosing significant (≥50%) coronary artery stenosis, with quantitative conventional coronary angiography as reference standard.

Materials and Methods: The institutional review board approved this study. All patients consented to undergo CT studies prior to conventional coronary angiography, after they were informed of the additional radiation dose, and to the use of their data for future retrospective research. Two hundred four patients (157 men, 47 women; mean age, 58 years ± 11 [standard deviation]), classified in four groups of 51 patients each, underwent coronary CT angiography with four-section, first- and second-generation 16-section, and 64-section CT scanners. Patients in sinus rhythm scheduled for conventional coronary angiography (stable angina, atypical chest pain) were included. Patients with bypass grafts and stents were excluded. Two readers unaware of results of conventional coronary angiography evaluated CT scans. Coro-

nary artery segments of 2 mm or larger in diameter were included for comparative evaluation with quantitative coronary angiography. Sensitivity, specificity, positive predictive value (PPV), and negative predictive value (NPV) for detection of significant stenoses (≥50% luminal diameter reduction) were calculated.

Results: Image quality was rated poor for the following percentages of coronary artery segments: 33.1% at four-section CT, 14.4% at first-generation 16-section CT, 6.3% at secondgeneration 16-section CT, and 2.6% at 64-section CT. Sensitivity, specificity, PPV, and NPV, respectively, were as follows: 57%, 91%, 60%, and 90% at four-section CT; 90%, 93%, 65%, and 99% at first-generation 16-section CT; 97%, 98%, 87%, and 100% at second-generation 16-section CT; and 99%, 96%, 80%, and 100% at 64-section CT. Diagnostic performance of four-section CT was significantly poorer than that of second-generation 16-section CT (odds ratio = 4.57) and 64-section CT (odds ratio = 2.89).

Conclusion: Diagnostic performance of coronary CT angiography varies among scanners of different generations. Earlier-generation scanners (four sections) had significantly poorer performance; performance of 16- compared with 64-section CT scanners showed progressive, although not significant, improvement.

Introduction

Coronary multidetector computed tomographic (CT) angiography is an emerging technique that allows noninvasive detection of significant coronary stenoses (≥50% luminal diameter reduction) (1,2). After the initial promising results obtained with four-section CT scanners, progressively higher temporal and spatial resolutions have been achieved by increasing gantry rotation speed and the number of detector rows and by reducing individual detector size (3–6). This achievement was obtained through various configurations, including six-, eight-, 10-, 12-, 16-, 32-, 40-, 64- and 256-section CT scanners. With the exception of 256-section CT, several studies have been published in which the diagnostic performance of each CT scanner is explored separately (7–22). The purpose of our study was to retrospectively compare the sensitivity and specificity of four generations of multidetector CT scanners for diagnosis of significant (≥50%) coronary artery stenosis by using quantitative conventional coronary angiography as the reference standard.

CHAPTER 10

Materials and Methods

General Study Design

This study was designed as a retrospective evaluation of the diagnostic performance of a four-section CT scanner (Somatom Plus 4 VolumeZoom; Siemens, Erlangen, Germany) from February 2000 to January 2002; a first-generation 16-section CT scanner (Somatom Sensation 16; Siemens) from April 2002 to May 2003, featuring 12 sections per rotation in cardiac protocols; a second-generation 16-section CT scanner (Somatom Sensation 16 Straton; Siemens) from July 2003 to April 2004; and a 64-section CT scanner (Somatom Sensation 64 Cardiac Configuration; Siemens) from May 2004 to March 2006. Multisection CT was performed to detect significant (≥50% luminal narrowing) coronary stenoses by using conventional coronary angiography with quantitative stenosis assessment (quantitative coronary angiography) as the reference standard (23). As a result of z-flying focal spot technology, with the 64-section system, 64 sections per rotation were acquired with a 32-row detector array.

The institutional review board approved our study and was made aware of the additional radiation dose. All patients consented to undergo the CT studies prior to conventional coronary angiography after they were informed of the additional radiation dose and its risks. They also consented to the use of their data for future retrospective research.

Patients

A total of 204 patients (157 men, 47 women; mean age, 58 years ± 11 [standard deviation]) with stable angina pectoris or atypical chest pain underwent coronary multidetector CT angiography a mean of 7 days ± 3 prior to conventional coronary angiography. The first 51 consecutive patients examined with each CT scanner were included in four equally sized groups and were scheduled for conventional coronary angiography on the basis of their clinical status (Figure 1). Patients with bypass grafts and coronary stents were excluded.

Patient Preparation

Patients without a contraindication to beta-adrenergic blocking agents (overt heart failure and atrioventricular conduction abnormalities) and with initial heart rates higher than 65 beats per minute received a single oral dose of 100 mg of metoprolol (Selokeen; Astra Zeneca, Zoetermeer, the Netherlands) 1 hour before CT.

Scan Protocol and Image Reconstruction

All patients underwent unenhanced CT for determination of calcium score before CT angiography, and the parameters

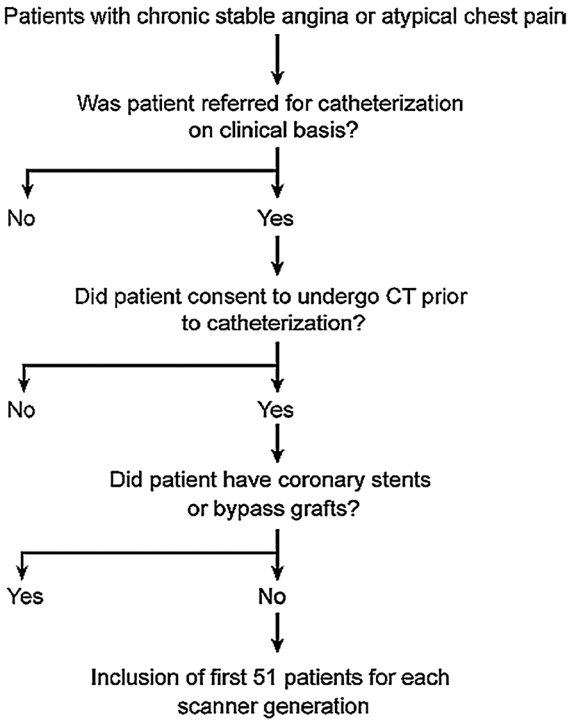

FIGURE 1. Flow diagram shows inclusion criteria for the study.

used with each scanner are presented in Table 1. Images were reconstructed by using a monosegmental electrocardiographically gated reconstruction algorithm. For this algorithm, data are used from a single heartbeat obtained during half-gantry rotation, resulting in a temporal resolution equal to half of the rotation time. Data sets were reconstructed during the interval between the mid- and end-diastolic phases (eg, 300, 350, 400, and 450 msec before the next R wave). We also reconstructed data sets during the end-systolic phase (between 25% and 35% of the R-R interval). Medium-sharp convolution kernels (B30f) were used for image reconstruction.

Quantitative Coronary Angiography

One observer (C.V.M., with 10 years of experience in coronary angiography) who was unaware of the CT results identified coronary artery segments on the conventional coronary angiogram by following a 17-segment modified American Heart Association classification model (24). These segments were as follows: The right coronary artery included segment 1, proximal segment; segment 2, middle segment; segment 3, distal segment; segment 4a, posterior descending coronary artery; and segment 4b, posterolateral artery. The left main coronary artery was segment 5. The left anterior descending coronary artery included segment 6, proximal segment; segment 7, middle segment; segment 8, distal segment; segment 9, first diagonal segment; and segment 10, second diagonal segment. The circumflex branch of the left coronary artery included segment 11, proximal segment; segment 12, first marginal segment; segment 13, middle segment; segment 14, second marginal

Table 1. Scan protocol with scanners of generations

	Four section scanner	1st generation 16section scanner	2nd generation 16-section scanner	64-section scanner
No. of detectors and section thickness (mm)	4x1	12x0.75	16x0.75	32x2x0.6
Rotation time (ms)	500	420	375	330
Tube current-time product (mAs)	300	400-450	500-600	800-900
Tube voltage (kV)	120	120	120	120
Table feed per rotation (mm)	1.5-2 [a]	3	3	3.8
Scan time (s)	35-45	19-22	18-20	12-14
Contrast agent	Iomeprol [b]	Iodixanol [c]	Iomeprol [b]	Iomeprol [b]
volume (ml)	150	120	100	100
concentration (mgI/ml)	350	320	400	400
injection rate (ml/s)	3.5	4	4	5
Reconstruction thickness (mm)	1.25	1.00	1.00	0.75
Reconstruction increment (mm)	0.6	0.5	0.5	0.4
Estimated exposure (mSv) [d]	5-8	8-9	11-16	15-20

a Table feed increased to 2 for HR>65 beats/minute
b Iomeron, Bracco , Milan, Italy
c Visipaque, GE Healthcare, Eindhoven, the Netherlands
d WinDose, Institute of Medical Physics, Erlangen, Germany

segment; segment 15, distal segment; and segment 16, intermediate branch. Stenoses were evaluated and classified as significant if the mean luminal narrowing was 50% or greater by using a validated quantitative coronary angiographic algorithm (Cardiovascular Angiography Analysis System, CAAS II; Pie Medical Imaging, Maastricht, the Netherlands).

CT Image Evaluation

Independent review of the CT scans was performed by two readers (N.R.M., F.C., with 3 years of experience each in cardiac radiology) who were blinded to the results of conventional coronary angiography and quantitative coronary angiography. All images from studies were evaluated at an off-line workstation (Leonardo VB30A; Siemens). Disagreement between both observers was resolved with consensus. All available coronary segments were identified by following the 17-segment American Heart Association model used for the evaluation of conventional angiograms (24). Image quality was classified as good (defined as the absence of any image-degrading artifacts related to motion, calcification, or noise), adequate (defined as the presence of image-degrading

artefacts but with evaluation possible with moderate confidence), poor (defined as the presence of image-degrading artefacts but with evaluation possible with low diagnostic confidence), or nonevaluable (defined as no evaluation possible).

CT images were visually classified for the presence of significant stenosis by using multiplanar reconstruction and curved multiplanar reconstruction; blood vessels with a diameter of 2 mm or larger were considered, because of their clinical relevance and because they are amenable to revascularization.

Statistical Analysis

Statistical analysis was performed by using commercially available software (Stata, version 8.2 for Windows; StataCorp, College Station, Tex). Results were reported in accordance with the Standards for Reporting of Diagnostic Accuracy, or STARD, criteria (23). Quantitative variables were expressed as means ± standard deviations, and categoric variables were expressed as frequencies or percentages. The percentages of significant stenoses and of cardiovascular risk factors were compared among the groups by using the chi squared test. The Kruskal-Wallis nonparametric test was used to compare ordinal variables, such as the number of risk factors and severity of coronary artery disease (defined as the number of blood vessels with significant stenoses). Analysis of variance was used to compare ages, heart rates, and log-transformed Agatston calcium scores. The log-transformed Agatston calcium scores were used because the calcium scores demonstrated a skewed distribution. A difference with $P < .01$ was used as the level of significance to account for multiple testing.

To compensate for uninterpretability bias caused by the presence of excluded segments (25, p 104), diagnostic performance in the four-section CT group was evaluated by using the multiple imputation function. Analysis of missing values was performed with the statistical package, and the results of coronary CT angiography in excluded segments were obtained as a function of the patient's age, sex, and available CT angiographic findings.

We calculated sensitivity, specificity, positive predictive value (PPV), and negative predictive value (NPV) of coronary CT angiography for the detection of significant coronary artery stenosis, with the corresponding 95% confidence intervals (CIs). These parameters were computed (a) per patient, (b) per segment, and (c) per location, that is, for proximal segments, middle segments, and distal segments or side branches. Segments 1, 5, 6, and 11 were defined as proximal segments; segments 2, 7, and 13 were defined as

middle segments; and segments 3, 4a, 4b, 8, 9, 10, 12, 14, 15, and 16 were defined as distal segments or side branches (24). Two additional sensitivity analyses were performed to explore the effect of the clustered nature of the data, in that the data consisted of multiple potentially correlated observations (ie, segments) per patient. First, we reanalyzed the results for all segments by using generalized estimating equations, with the assumption of a binomial distribution of the dependent variable, a logit-link function, the patient as cluster, an equal-correlation model within each cluster, and the robust sandwich estimator of the variance (25, p 157;26,27). Subsequently, we reanalyzed the data by using the bootstrap approach, with the patient as cluster, sampling with replacement, performing 1000 replications, and analyzing the bias-corrected 95% CI (25, p 168;28).

Finally, we used the generalized estimating equation approach with a logit-link function on segment data to explore the strength of association between conventional coronary angiography and coronary CT angiography adjusted according to the generation of the CT scanner. In this analysis, conventional coronary angiography was considered as the dependent variable, defined as one, meaning the presence of a 50% or greater luminal stenosis, and as zero, meaning the absence of a 50% or greater luminal stenosis; the CT scanner type was considered as the explanatory variable, and a difference with $P < .05$ was considered significant. Interobserver agreement for the detection of significant coronary stenosis was determined by calculating the k statistic. The k values that were less than 0.20 were considered to indicate poor agreement; those between 0.21 and 0.40 indicated fair agreement; those between 0.41 and 0.60 indicated moderate agreement; those between 0.61 and 0.80 indicated good agreement; and those greater than 0.81 indicated very good agreement.

Results

Clinical Data

No patients were excluded because of a high Agatston calcium score (Table 2). The overall agreement between observers in detecting significant coronary stenoses was good: k values were 0.65 for four-section CT scanners; 0.69 for first-generation 16-section CT scanners; 0.72 for second-generation 16-section CT scanners; and 0.73 for 64-section CT scanners.

Prevalence of Disease

The prevalence of disease was defined as the number of significant stenoses detected at conventional coronary angiography and was as follows: 0.13 lesion per segment in the four-section CT group, 0.13

TABLE 2. Clinical presentation, severity of coronary artery disease, heart rates and medication use in 51 patients per group

Characteristic	Four-section scanner group	First generation 16-scanner group	Second generation 16-scanner group	64-section scanner group	P value
Demographics					
Age (y) a	56 ± 10	59 ± 12	59 ± 10	59 ± 11	0.73 [b]
Sex					0.85 [c]
No. of men	40	41	37	39	
No. of women	11	10	14	12	
Cardiovascular risk factors					
Obesity [d]	13 (25)	14 (27)	10 (20)	14 (27)	0.79 [c]
Smoking	12 (24)	14 (27)	15 (29)	14 (27)	0.95 [c]
Hypertension	21 (41)	27 (53)	19 (37)	16 (31)	0.16 [c]
Serum cholesterol >200 mg/dL [e]	23 (45)	22 (43)	24 (47)	25 (49)	0.97 [c]
Diabetes mellitus	9 (18)	10 (20)	9 (18)	7 (14)	0.92 [c]
Family history	14 (27)	15 (29)	13 (25)	12 (24)	0.63 [c]
No. of risk factors					0.44 [f]
0	7 (14)	10 (20)	12 (24)	11 (22)	
1	12 (24)	10 (20)	15 (29)	7 (14)	
2	14 (27)	10 (20)	8 (16)	16 (31)	
≥3	18 (35)	21 (41)	16 (31)	17(33)	
No. of diseased blood vessels					0.95 [f]
0	13 (25)	13 (25)	13 (25)	12 (24)	
1	13 (25)	15 (29)	14 (27)	17 (33)	
2	16 (31)	14 (27)	15 (29)	13 (25)	
3	7 (14)	7(14)	5 (10)	8 (16)	
Disease of left main artery	3 (6)	2 (4)	5 (10)	1 (2)	0.42 [c]
Preparation and monitoring					
Use of beta-blockers before scanning	28(55)	31(61)	25(49)	31(61)	0.48 [c]
Heart rate during scanning a (beats/min)	57± 7	56 ± 6	57 ± 5	58 ± 7	0.47 [b]
Agatston calcium score [a]	412 ± 513	457 ± 445	397± 593	440 ± 589	0.34 [g]

Note - Data are numbers of patients except where indicated otherwise. Numbers in parentheses are percentages, which were calculated on the basis of 51 patients in each group and were rounded.

a Data are the mean ± standard deviation.
b One-way analysis of variance.
c Chi squared test.
d Obesity was defined as a body mass index of 30 kg/m^2 or greater.
e SI unit conversion for 200 mg/dL is 5.18 mmol/L.
f Kruskal-Wallis nonparametric test.
g One-way analysis of variance on log-transformed calcium scores.

TABLE 3. Causes of unevaluable segments and poor image quality.

Cause	Four-section scanner group	First generation 16-scanner group	Second generation 16-scanner group	64-section scanner group
Unevaluable segments [a]	**25.6** (136/532)	**0**	**0**	**0**
Segments with poor image quality [b]	**7.5** (40/532)	**14.4** (85/590)	**6.3** (38/607)	**2.6** (14/537)
Total % (ratio)	**33.1** (176/532)	**14.4** (85/590)	**6.3** (38/607)	**2.6** (14/537)
Calcification				
% (ratio)	**25.0** (44/176)	**55.3** (47/85)	**76.3** (29/38)	**85.7** (12/14)
Motion				
% (ratio)	**51.1** (90/176)	**27.1** (23/85)	**23.7** (9/38)	**14.3** (2/14)
Low Contrast-to-noise ratio				
% (ratio)	**23.9** (42/176)	**17.6** (15/85)	**0**	**0**

Note - Data are percentages. Numbers in parentheses were used to calculate the percentages.

a Segments were excluded from evaluation
b Segments were not excluded from evaluation

lesion per segment in the first-generation 16-section CT group, 0.12 lesion per segment in the second-generation 16-section CT group, and 0.16 lesion per segment in the 64-section CT group. No significant difference was found among the groups (P = .55).

Image Quality

One-fourth (25.6%, 136 of 532) of coronary segments with a diameter of 2 mm or larger were classified as unevaluable in the group examined with four-section CT scanners (Table 3, Figure 2). Of these 136 unevaluable segments, 34 (25%) were proximal segments (segments 1, 5, 6, and 11), 57 (42%) were middle segments (segments 2, 7, and 13), and 45 (33%) were distal segments or side branches (segments 3, 4a, 4b, 8, 9, 10, 12, 14, 15, and 16) (24). When newer-generation (16- and 64-section) scanners were used, no segments were judged unevaluable.

Diagnostic Performance

Four-section CT data were corrected for uninterpretability bias as described earlier (25, p 104) (Tables 4, 5; Figures 3, 4). Including vessels with a diameter smaller than 2 mm, the sensitivity, specificity, PPV, and NPV for 64-section CT calculated at a segmental level were 98%, 95%, 75%, and 99%, respectively; these values were 100%, 91%, 97%, and 100%, respectively, at a patient level. Results of the sensitivity analysis in which we explored the effect of the clustered nature of the data

FIGURE 2. Example of image quality obtained with scanners of various generations at heart rate of approximately 60 beats per minute. Transverse CT images obtained through the left main (arrowhead) and left anterior descending (arrow) arteries in (A) 60-year-old man with heart rate of 59 beats per minute examined with four-section CT scanner, with poor image quality; (B) 58-year-old man with same heart rate as patient in a examined with first-generation 16-section CT scanner, with adequate image quality; (C) 61-year-old man with heart rate of 60 beats per minute examined with second-generation 16-section CT scanner, with good image quality; and (D) 59-year-old man with same heart rate as patient in C examined with 64-section CT scanner, with good image quality.

demonstrated practically identical results (and 95% CIs), indicating that there was a negligible correlation between observations within each patient.

Discussion

Our study findings indicate that the diagnostic performance of coronary CT angiography with the use of newer-generation scanners (ie, performance with 64-section and second-generation 16-section CT scanners) is better than that with four-section CT scanners.

A surprising finding was that sensitivity, specificity, and NPV obtained with second-generation 16-section and 64-section CT scanners were similar. A possible explanation for this result is that our evaluation with 16-section coronary CT angiography was restricted to vessels of 2 mm or larger in diameter, and this result is in keeping with the findings reported by others (9–11,13,14,29).

Sixty-four-section CT, however, has been reported to have the capability for assessment of coronary branches smaller than 2 mm (16,18–20). In our study, we showed that, when the entire coronary tree was evaluated, the diagnostic performance was similar to the performance when only vessels of 2 mm or larger in diameter were included.

The absolute frequency of coronary segments affected by poor image quality, whatever its cause (ie, calcification, mo-

TABLE 4. Diagnostic Performance of Coronary CT Angiography with Different Generations of Scanners

	Four-section scanner group		First generation 16-scanner group		Second generation 16-scanner group		64-section scanner group	
Segments and Statistics	**Value**	**95% CI**	**Value**	**95% CI**	**Value**	**95% CI**	**Value**	**95% CI**
All segments with ≥2mm diameter								
No. available	532	…	590	…	607	….	537	…
Sensitivity	**57** (56/99)	46-66	**90** (66/73)	83-97	**97** (61/63)	92-100	**99** (80/81)	96-100
Specificity	**91** (395/433)	88-94	**93** (481/517)	90-95	**98** (535/544)	97-99	**96** (436/456)	93-97
PPV	**60** (56/94)	49-69	**65** (66/102)	55-73	**87** (61/70)	79-94	**80** (80/100)	72-87
NPV	**90** (395/438)	87-93	**99** (481/488)	97-99	**100** (535/537)	99-100	**1.0** (436/437)	99-100
Proximal segments								
No. available	204	…	192	…	201	…	202	…
Sensitivity	**78** (35/45)	62-88	**94** (30/32)	77-98	**92** (23/25)	72-98	**100** (30/30)	85-100
Specificity	**94** (152/161)	89-97	**93** (148/160)	86-95	**97** (170/176)	92-98	**97** (166/172)	92-98
PPV	**81** (35/43)	64-89	**71** (30/42)	55-83	**79** (23/29)	59-91	**83** (30/36)	66-93
NPV	**94** (152/161)	88-96	**99** (148/150)	94-99	**99** (170/172)	95-99	**100** (166/166)	97-100
Middle segments								
No. available	123	…	135	…	136	…	132	…
Sensitivity	**42** (8/19)	21-66	**93** (27/29)	75-98	**100** (23/23)	82-100	**96** (27/28)	79-99
Specificity	**93** (97/104)	86-97	**92** (97/106)	84-95	**97** (110/113)	91-99	**93** (97/104)	86-97

PPV	**53** (8/15)	27-77	**75** (27/36)	57-87	**88** (23/26)	68-96	**79** (27/34)	61-90
NPV	**90** (97/108)	82-94	**98** (97/99)	92-99	**100** (110/110)	95-100	**99** (97/98)	93-99
Distal segments or side branches								
No. available	205	…	263	…	270	…	203	…
Sensitivity	**34** (12/35)	19-52	**75** (9/12)	42-93	**100** (15/15)	74-100	**100** (23/23)	82-100
Specificity	**82** (137/168)	74-86	**94** (236/251)	90-96	**100** (255/255)	98-100	**96** (173/180)	91-98
PPV	**27** (12/44)	15-43	**38** (9/24)	19-59	**100** (15/15)	74-100	**77** (23/30)	57-89
NPV	**85** (137/161)	79-90	**99** (236/239)	96-99	**100** (255/255)	98-100	**100** (173/173)	97-100
Per-patient analysis								
No. of patients	51	…	51	…	51	…	51	…
Sensitivity	**72** (26/36)	54-85	**100** (41/41)	89-100	**100** (31/31)	86-100	**100** (38/38)	88-100
Specificity	**67** (10/15)	38-87	**60** (6/10)	27-86	**95** (19/20)	73-99	**100** (13/13)	71-100
PPV	**84** (26/31)	65-93	**91** (41/45)	77-97	**97** (31/32)	82-99	**100** (38/38)	88-100
NPV	**50** (10/20)	27-72	**100** (6/6)	51-100	**100** (19/19)	79-100	**100** (13/13)	71-100

Note - Data are percentages except where indicated otherwise. Percentages were rounded. Numbers in parentheses were used to calculate the percentages. Calculations were performed for segments with a diameter of 2 mm or greater; chronic total occlusions and segments distal to an occlusion were excluded. Therefore, in some patients, not all 17 segments were available for evaluation. Proximal segments = segments 1, 5, 6, 11; middle segments = segments 2, 7, 13; distal segments or side branches = segments 3, 4a, 4b, 8, 9, 10, 12, 14, 15, and 16, as numbered in reference 24.

TABLE 5. Strength of the Association between Conventional Angiography and CT Findings Corrected by the CT Methods Calculated by Using the Generalized Estimating Equation Approach

Method comparison	odds ratio	95% CI
64-section vs 4-section	2.89 [a]	1.34-6.23
Second-generation 16-section vs 4-section CT	4.57 [a]	1.81-11.5
First-generation 16-section vs 4-section CT	1.23	0.64-2.34

a Significant value

tion, or low contrast-to-noise ratio), decreased progressively as the number of sections of the scanners increased from four to 64. However, the decrease in motion and low contrast-to-noise ratio predominated over the decrease in calcifications. For this reason, the percentage of coronary calcification as a cause of poor image quality increased as the number of sections of the scanners increased from four to 64 as a consequence of the decrease in the percentage of motion and low contrast-to-noise ratio.

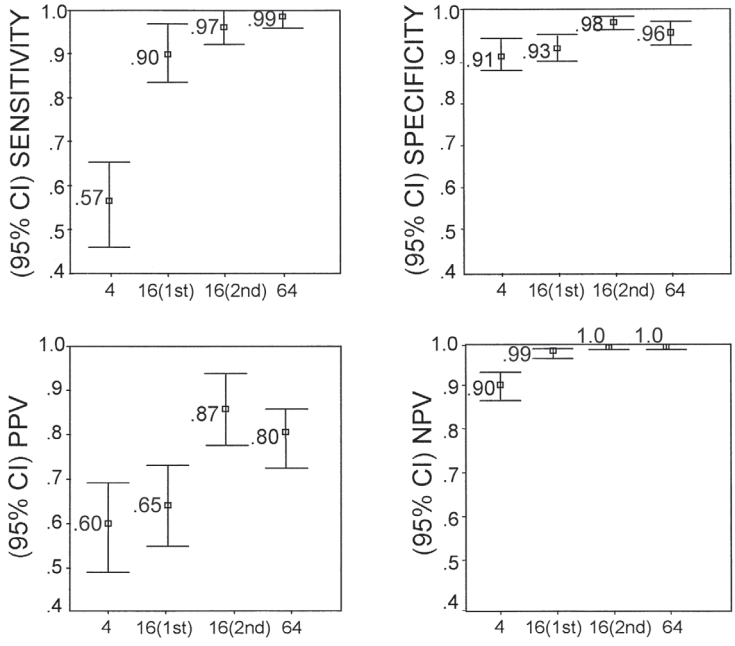

FIGURE 3. Diagnostic performance parameters calculated at segmental level (all segments ≥2mm in diameter). Segmental sensitivity, specificity, PPV, and NPV obtained with four-section, first-generation 16-section, second-generation 16-section, and 64-section CT scanners are plotted with 95% CIs (error bars). A general performance improvement is seen as the number of sections of the scanners increases from four to 64. Sensitivity and NPV of four-section CT scanner are significantly lower than those obtained with other scanners, as shown by nonoverlapping 95% CIs. PPV for four-section CT scanner is significantly lower than that for second-generation 16-section and 64-section CT scanners.

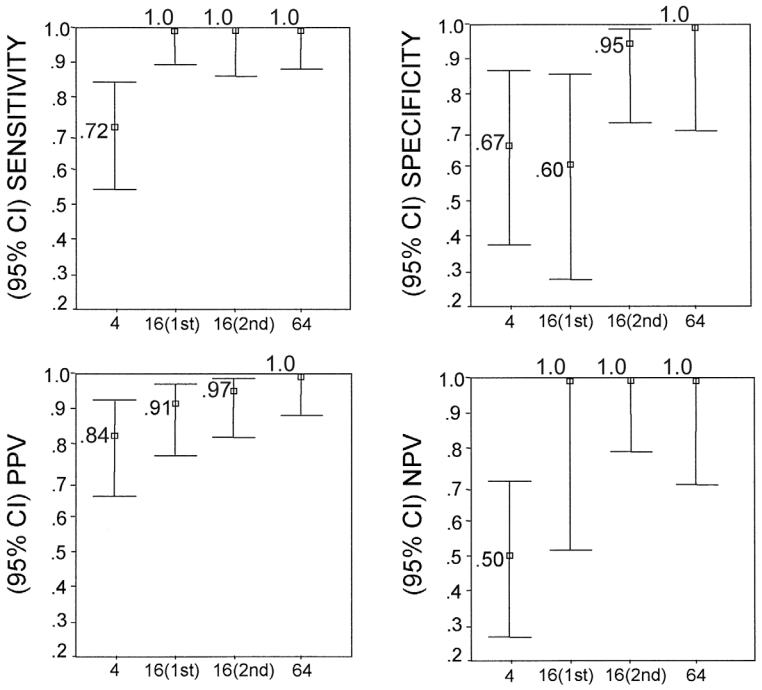

FIGURE 4. Diagnostic performance parameters calculated at patient level. Per-patient sensitivity, specificity, PPV, and NPV obtained with four-section, first-generation 16-section, second-generation 16-section, and 64-section CT scanners are plotted with 95% CIs (error bars). NPV of 16- and 64-section CT scanners is 100%. Sensitivity of four-section CT scanner is significantly lower than that obtained with other scanners, whereas some overlap of 95% CIs is observed for remaining parameters.

Previously, the trade-off for improved diagnostic performance and clinical reliability was increased radiation exposure (30,31). However, electrocardiographically controlled dose modulation is now available with all scanners. Dose modulation involves nominal tube output during diastole, accompanied by a reduction in tube output during systole. The result is a total dose reduction of 30%–50%, depending on the patient's heart rate. The introduction of dual-source CT scanners (32) heralds potential additional benefits with respect to a decrease in x-ray exposure as the pitch increases at higher heart rates, leading to a reduction in the examination time and the radiation dose to the patient. Moreover, the improved temporal resolution of these systems suggests that pharmacologic control of the heart rate will become unnecessary.

Our study had limitations. Because we included subjects referred for conventional angiography, it was inevitable that there would be a high prevalence of disease

in the groups available for comparison. Such a condition favors any test aiming for high sensitivity (33). Moreover, because there was a high prevalence of disease, the differences among the various generations of scanners may have been somewhat reduced.

Another limitation was that our study was conducted as a retrospective evaluation of data acquired over time about different patient cohorts. More important, however, the baseline characteristics (age, sex, heart rate, coronary calcium score, prevalence of obese subjects, comorbidity) and the prevalence of stenosis in the four groups included in the comparison were similar.

In conclusion, results of this study indicate that the diagnostic performance of coronary CT angiography with four-section CT is inferior to that with 16-section CT. The added value offered by 64-section CT is high diagnostic performance in the evaluation of the entire coronary tree.

References

1. Fox K, Garcia MA, Ardissino D, et al. Guidelines on the management of stable angina pectoris: executive summary—the Task Force on the Management of Stable Angina Pectoris of the European Society of Cardiology. Eur Heart J 2006;27:1341–1381.
2. Hendel RC, Patel MR, Kramer CM, et al. ACCF/ACR/SCCT/SCMR/ASNC/NASCI/SCAI/SIR 2006 appropriateness criteria for cardiac computed tomography and cardiac magnetic resonance imaging: a report of the American College of Cardiology Foundation Quality Strategic Directions Committee Appropriateness Criteria Working Group, American College of Radiology, Society of Cardiovascular Computed Tomography, Society for Cardiovascular Magnetic Resonance, American Society of Nuclear Cardiology, North American Society for Cardiac Imaging, Society for Cardiovascular Angiography and Interventions, and Society of Interventional Radiology. J Am Coll Cardiol 2006;48:1475–1497.
3. Flohr T, Kuttner A, Bruder H, et al. Performance evaluation of a multi-slice CT system with 16-slice detector and increased gantry rotation speed for isotropic submillimeter imaging of the heart. Herz 2003;28:7–19.
4. Ferencik M, Moselewski F, Ropers D, et al. Quantitative parameters of image quality in multidetector spiral computed tomographic

coronary imaging with submillimeter collimation. Am J Cardiol 2003;92:1257–1262.

5. Ohnesorge B, Flohr T, Becker C, et al. Cardiac imaging by means of electrocardiographically gated multisection spiral CT: initial experience. Radiology 2000;217:564–571.
6. Schoepf UJ, Becker CR, Ohnesorge BM, Yucel EK. CT of coronary artery disease. Radiology 2004;232:18–37.
7. Vogl TJ, Abolmaali ND, Diebold T, et al. Techniques for the detection of coronary atherosclerosis: multi-detector row CT coronary angiography. Radiology 2002;223:212–220.
8. Gerber BL, Coche E, Pasquet A, et al. Coronary artery stenosis: direct comparison of four-section multi-detector row CT and 3D navigator MR imaging for detection—initial results. Radiology 2005;234:98–108.
9. Mollet NR, Cademartiri F, Nieman K, et al. Multislice spiral computed tomography coronary angiography in patients with stable angina pectoris. J Am Coll Cardiol 2004;43: 2265–2270.
10. Mollet NR, Cademartiri F, Krestin GP, et al. Improved diagnostic accuracy with 16-row multi-slice computed tomography coronary angiography. J Am Coll Cardiol 2005;45:128–132.
11. Hoffmann MH, Shi H, Schmitz BL, et al. Noninvasive coronary angiography with multislice computed tomography. JAMA 2005; 293:2471–2478.
12. Nieman K, Rensing BJ, van Geuns RJ, et al. Usefulness of multislice computed tomography for detecting obstructive coronary artery disease. Am J Cardiol 2002;89:913–918.
13. Heuschmid M, Kuettner A, Schroeder S, et al. ECG-gated 16-MDCT of the coronary arteries: assessment of image quality and accuracy in detecting stenoses. AJR Am J Roentgenol 2005;184:1413–1419.
14. Achenbach S, Ropers D, Pohle FK, et al. Detection of coronary artery stenoses using multi-detector CT with 16 x 0.75 collimation and 375 ms rotation. Eur Heart J 2005;26: 1978–1986.
15. Achenbach S, Giesler T, Ropers D, et al. Detection of coronary artery stenoses by contrast-enhanced, retrospectively electrocardiographically-gated, multislice spiral computed tomography. Circulation 2001;103:2535–2538.
16. Leber AW, Knez A, von Ziegler F, et al. Quantification of obstructive and nonobstructive coronary lesions by 64-slice computed tomography: a comparative study with quantitative coronary angiography and intravascular ultrasound. J Am Coll Cardiol 2005; 46:147–154.
17. Leschka S, Alkadhi H, Plass A, et al. Accuracy of MSCT coronary angiography with 64-slice technology: first experience. Eur Heart J 2005;26:1482–1487.
18. Mollet NR, Cademartiri F, van Mieghem CA, et al. High-resolution spiral computed tomography coronary angiography in patients referred for diagnostic conventional coronary angiography. Circulation 2005;112:2318–2323.

19. Raff GL, Gallagher MJ, O'Neill WW, Goldstein JA. Diagnostic accuracy of noninvasive coronary angiography using 64-slice spiral computed tomography. J Am Coll Cardiol 2005;46:552–557.
20. Pugliese F, Mollet NR, Runza G, et al. Diagnostic accuracy of non-invasive 64-slice CT coronary angiography in patients with stable angina pectoris. Eur Radiol 2006;16:575–582.
21. Ropers D, Rixe J, Anders K, et al. Usefulness of multidetector row spiral computed tomography with 64- x 0.6-mm collimation and 330-ms rotation for the noninvasive detection of significant coronary artery stenoses. Am J Cardiol 2006;97:343–348.
22. Nikolaou K, Knez A, Rist C, et al. Accuracy of 64-MDCT in the diagnosis of ischemic heart disease. AJR Am J Roentgenol 2006;187:111–117.
23. Bossuyt PM, Reitsma JB, Bruns DE, et al. Towards complete and accurate reporting of studies of diagnostic accuracy: the STARD Initiative. Radiology 2003;226:24–28.
24. Austen WG, Edwards JE, Frye RL, et al. A reporting system on patients evaluated for coronary artery disease. Report of the Ad Hoc Committee for Grading of Coronary Artery Disease, Council on Cardiovascular Surgery, American Heart Association. Circulation 1975;51:5–40.
25. Zhou XH, Obuchowski NA, McClish DK. Statistical methods in diagnostic medicine. New York, NY: Wiley, 2002.
26. Fleiss JL, Levin B, Cho Paik M. Statistical methods for rates and proportions. 3rd ed. New York, NY: Wiley, 2003.
27. Smith PJ, Hadgu A. Sensitivity and specificity for correlated observations. Stat Med 1992; 11:1503–1509.
28. Efron B, Tibshirani RJ. An introduction to the bootstrap. New York, NY: Chapman & Hall, 1993.
29. Nieman K, Cademartiri F, Lemos PA, Raaijmakers R, Pattynama PM, de Feyter PJ. Reliable noninvasive coronary angiography with fast submillimeter multislice spiral computed tomography. Circulation 2002;106:2051–2054.
30. Gerber TC, Stratmann BP, Kuzo RS, Kantor B, Morin RL. Effect of acquisition technique on radiation dose and image quality in multidetector row computed tomography coronary angiography with submillimeter collimation. Invest Radiol 2005;40:556–563.
31 Hausleiter J, Meyer T, Hadamitzky M, et al. Radiation dose estimates from cardiac multislice computed tomography in daily practice: impact of different scanning protocols on effective dose estimates. Circulation 2006;113:1305–1310.
32. Flohr TG, McCollough CH, Bruder H, et al. First performance evaluation of a dual source CT (DSCT) system. Eur Radiol 2006;16:256–268.
33. Brenner H, Gefeller O. Variation of sensitivity, specificity, likelihood ratios and predictive values with disease prevalence. Stat Med 1997;16:981–991.

CHAPTER 11

Diagnostic performance of non-invasive 64-slice computed tomography coronary angiography in patients with stable angina pectoris

Pugliese F, Mollet NR, Runza G, van Mieghem C, Meijboom WB, Malagutti P, Baks T, Krestin GP, de Feyter PJ, Cademartiri F.

European Radiology 2006; 16:575-582.

Summary

Purpose: Multislice computed tomography (CT) is an emerging technique for the non-invasive detection of coronary stenoses. While the diagnostic accuracy of 4-slice scanners was limited, 16-slice CT imagers showed promising results due to increased temporal and spatial resolution. These technical advances prompted us to evaluate the diagnostic performance of 64-slice CT coronary angiography in the detection of significant stenoses (defined as ≥50% luminal diameter reduction) versus invasive quantitative coronary angiography (QCA).

Materials and methods: Thirty-five patients with stable angina pectoris underwent CT coronary angiography performed with a 64-slice scanner (gantry rotation time 330 ms, individual detector width 0.6 mm) prior to conventional coronary angiography. Patients with heart rates >70 beats/min received 100 mg metoprolol orally. One hundred millilitres of contrast agent with an iodine concentration of 400 mgI/ml were injected at a rate of 5 ml/s into the antecubital vein. The CT scan was triggered with the bolus tracking technique.

Results: The sensitivity, specificity and the positive and negative predictive values of 64-slice CT were 99%, 96%, 78% and

99%, respectively, on a per-segment basis. The values obtained on a per-patient basis were 100%, 90%, 96% and 100%, respectively.

Conclusion: When referral to catheterization is questionable, CT coronary angiography may identify subjects with normal angiograms and consistently decrease the number of unnecessary invasive procedures.

Introduction

Multislice computed tomography (CT) coronary angiography is an emerging technique that allows the non-invasive detection of significant coronary stenoses. Various studies have been published exploring the diagnostic performance of CT coronary angiography using different scanner generations [1–3]. Clinical application of 4-slice CT coronary angiography was limited, due to a considerable number of non-assessable vessels (up to 39% of the included vessels) [4] as a result of a limited resolution and a relatively long breath hold of approximately 40 s. Sixteen-slice CT coronary angiography showed an improved diagnostic accuracy for the detection of significant stenoses due to an increased temporal and spatial resolution and shorter breath-hold time (approximately 20 s) [5–11]. However, these studies only evaluated coronary vessels with a luminal diameter above 1.5 mm or 2.0 mm. Most recently, a new generation of CT scanners was introduced. These scanners render 64 slices per rotation and offer a temporal resolution of 165 ms and an unprecedented spatial resolution of isotropic 0.4 mm3 [12]. These technical advances prompted us to evaluate the diagnostic performance of 64-slice CT coronary angiography to detect significant stenoses (defined as ≥50% lumen diameter reduction) in the entire coronary tree in a patient cohort with stable angina pectoris.

Materials and Methods

Subjects

Thirty-five consecutive patients with stable angina pectoris (21 men; mean age±SD: 61±10 years, range: 46–80 years) underwent 64-slice CT coronary angiography within 15 days prior to coronary catheterisation. Patients exhibiting sinus heart rhythm capable of holding their breath for 15 s and without contraindications to the administration of iodinated contrast agents were prospectively included. Exclusion criteria were the presence of arrhythmias, previous bypass graft surgery or percutaneous coronary intervention with stent implantation. The study proto-

TABLE 1. Scan parameters and technique of contrast agent administration.

Scan parameters	
Gantry rotation time	330 ms
Number of slices per rotation	32 x 2
Individual detector width	0.6 mm
Table feed	3.8 mm/rotation
Tube voltage	120 kV
Tube current	900 mAs (no current modulation)
Contrast agent	iomeprol, Iomeron® 400
Volume	100 ml
Concentration	400 mgI/ml
Injection rate	5 ml/sec
Injection site	Antecubital vein
Synchronization technique	Bolus-tracking

col was approved by our institutional review board and all patients gave informed consent.

Patient Preparation Prior to CT

Patients with pre-scan heart rates above 70 beats/min received a single oral dose of 100 mg metoprolol 1 h prior to the CT scan.

CT Scan Protocol

All patients underwent CT coronary angiography using a 64-slice CT scanner (Sensation 64, Siemens, Forchheim, Germany). The scan parameters used for CT coronary angiography are detailed in Table 1. A bolus of 100 ml contrast material (iomeprol, Iomeron 400, Bracco, Milan, Italy) was injected into the antecubital vein (flow rate 5 ml/s) and the CT scan was triggered with a bolus tracking technique.

Radiation exposure associated to this scan protocol, calculated using a dedicated software package (WinDose, Institute of Medical Physics, Erlangen, Germany), was 15:20 mSv (male:female, respectively).

CT Image Reconstruction

A retrospective ECG-gated technique was used for image reconstruction. The images were reconstructed with data acquired during a single heartbeat. The data sets were reconstructed during the mid-to-end diastolic phase, with reconstruction windows set at −300 ms to −450 ms before the next R-wave or 60% to 70% of the R–R interval. In the case of insufficient image quality, additional reconstructions during the end-systolic phase (25% to 35% of the R–R interval) were performed. When mildly irregular heart rates were encountered, such as bundle branch blocks or premature beats, the temporal variability in the reconstruction phase were compensated for manually with ECG editing. Inaccurate detection of the R waves was corrected and temporal windows applied to premature beats were deleted, filling the next diastolic interval

with one or more temporal windows to avoid data gaps. The reconstructed slice thickness was 0.75 mm, with an increment of 0.4 mm. All of the CT data sets were filtered with a medium-soft convolution kernel.

CT Image Analysis

The CT scans were scored by two experienced readers independently and were blinded of the results of conventional coronary angiography. Inter-observer agreement was calculated. In the cases of diverging opinions, an agreement was reached by consensus.

The maximum intensity projections were used in order to provide an anatomical overview of the coronary arteries and to identify side branches. Multi-planar reformatted images were used to visually classify lesions as significant or non-significant.

The image quality was evaluated on a per-segment basis and classified as good (absence of image-degrading artefacts related to motion, calcification or noise), adequate (presence of artefacts but images still suitable for evaluation, albeit with moderate confidence) or poor (presence of severe image-degrading artefacts, resulting in low diagnostic confidence). Reasons accounting for poor image quality were identified in calcification of the vessel wall, motion artefacts and low contrast-to-noise ratio. Calcification was rated as absent, small and isolated, dense and eccentric or bulky. Motion artefacts were defined as any blurring of the vessel contour due to movement. A low contrast-to-noise ratio was recorded in cases with scarce vessel enhancement, resulting in noisy images.

Quantitative Coronary Angiography (QCA)

All coronary segments visualised at catheterisation were included for comparison with CT. The segments were classified according to a modified 17-segment American Heart Association (AHA) model [13]. A single observer blinded to the CT results quantitatively evaluated the coronary lumen of all coronary segments on two projections using dedicated software (CAAS, Pie Medical, Maastricht, The Netherlands). Stenoses were scored as significant in the case of a mean lumen diameter reduction of ≥50% in two orthogonal projections.

Radiation exposure associated with diagnostic conventional angiography was 6:7 mSv (male:female, respectively).

Statistics

With QCA as the standard of reference, the diagnostic accuracy of CT coronary angiography for the detection of haemodynamically significant lesions in coronary arteries is expressed in terms of the

sensitivity, specificity and the positive and negative predictive values with the corresponding 95% confidence intervals.

The diagnostic performance was calculated on a persegment, per-vessel (presence or absence of at least one significant lesion along each of the major coronary arteries) and per-patient (presence or absence of any lesions in each patient) basis.

Results

Prevalence of Disease and Patient Co-Morbidity

Overall, 67 significant lesions were detected by conventional coronary angiography, resulting in a prevalence of 1.9 lesions per patient.

Conventional angiography revealed no significant stenoses in 10 patients (29%). Ten (29%) patients had 1-vessel disease, 8 (23%) had 2-vessel disease and 7 (19%) had 3- vessel disease. No significant left main disease was found in any patient.

Patient co-morbidity and ongoing medication are reported in Table 2.

TABLE 2. Synopsis of cardiovascular risk factors and medication in the population.

Risk Factors	Frequency (Percentage)
Smoking	7 (20%)
Hypertension	12 (34%)
Dyslipidemia	25 (71%)
Obesity	9 (26%)
Diabetes	7 (20%)
Family history	10 (29%)
Medication	
Long-term beta-blockers	22 (63%)
Calcium-antagonists	6 (17%)
ACE-inhibitors	12 (34%)
Angiotensin II-antagonists	3 (9%)
Lipid lowering therapy	24 (69%)
Previous PCI	3 (9%)

CT Results

Oral metoprolol was administered in 77% (27/35) of the patients. As a result, the average heart rate during the scan was 58±6 beats/min versus 68±9 beats/min before the preparation.

The average scan time was 13±1 seconds (range 11–15 seconds). No significant adverse reactions to the contrast material were recorded.

After the acquisition of the angiographic part of the scan, additional reconstructions in the telesystolic phase were obtained in 31% (11/35) of the CT scans. ECG editing was necessary in 8% (3/35) of the scans.

A total of 494 coronary segments were available for comparison between coronary angiography and CT.

All except for one (66/67) significant coronary stenoses were correctly identified at CT. One false-negative result was scored in the mid-portion of a left anterior descending artery affected by calcification and motion artefacts, and accounting for a 52% stenosis at QCA.

CT image quality was judged to be good, moderate and poor in 92% (455/494), 5% (25/494), and 3% (14/494) of the included segments, respectively. The reasons for poor image quality and for incorrect CT findings are summarized in Figure 1. The reasons for poor image quality affecting the assessability of the right coronary artery were motion artefacts (present in 7/7 segments), whereas a low contrast-to-noise ratio hampered the evaluation of posterior descending and posterolateral arteries (2/2). Bulky calcifications of the vessel wall causing a blooming effect and partial volume averaging were the major detrimental factors for the evaluation of both the left circumflex (2/2) and the left anterior descending (3/3, motion artefacts present in 1/3) arteries with their branches. However, none of the coronary segments were excluded from analysis due to limited image quality.

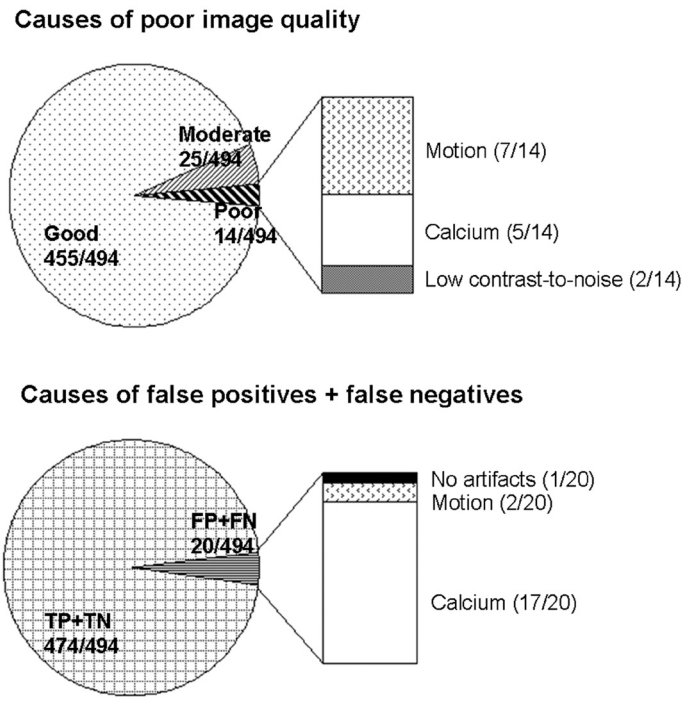

FIGURE 1. Image quality, artefacts and incorrect CT results. Motion artefacts account for half of the cases rated as being of poor image quality, but only for 2/20 cases of incorrect CT findings. Calcification of the vessel wall, either bulky, eccentric or isolated, is associated to 17/20 falsely positive and falsely negative CT results

TABLE 3. Accuracy of CT in individual coronary segments as classified by AHA [13]. Values are reported as ratios and percentages, with in brackets 95% confidence intervals.

	Sensitivity	Specificity	Positive Predictive Value	Negative Predictive Value
Coronary segments				
RCA 1	10/10=100% (72-100)	24/25=96% (80-99)	10/11=91% (62-98)	24/24=100% (86-100)
RCA 2	5/5=100% (54-100)	22/23=96% (79-99)	5/6=83% (42-96)	22/22=100% (85-100)
RCA 3	2/2=100% (29-100)	23/25=92% (75-98)	2/4=50% (15-85)	23/23=100% (86-100)
PDA 4	1/1=100% (16-100)	26/26=100% (87-100)	1/1=100% (16-100)	26/26=100% (87-100)
Distal RCA/PL	2/2=100% (29-100)	18/19¬=95% (75-99)	2/3=67% (19-93)	18/18=100% (82-100)
LM 5	-	35/35=100% (90-100)	-	35/35=100% (90-100)
LAD 6	8/8=100% (66-100)	26/27=96% (82-99)	8/9=89% (55-97)	26/26=100% (87-100)
LAD 7	9/10=90% (59-98)	21/23=91% (73-97)	9/11=82% (52-95)	21/22=95% (79-99)
LAD 8	1/1=100% (16-100)	32/32=100% (89-100)	1/1=100% (16-100)	32/32=100% (89-100)
D 9	6/6=100% (59-100)	22/27=81% (63-92)	6/11=55% (28-79)	22/22=100% (85-100)
D 10	1/1=100% (16-100)	20/21=95% (77-99)	1/2=50% (9-91)	20/20=100% (84-100)
LCX 11	4/4=100% (48-100)	31/31=100% (89-100)	4/4=100% (48-100)	31/31=100% (89-100)
MO 12	7/7=100% (63-100)	26/28=93% (77-98)	7/9=78% (44-93)	26/26=100% (87-100)
LCX 13	5/5=100% (54-100)	27/29=93% (78-98)	5/7=71% (35-91)	27/27=100% (88-100)
MO 14	2/2=100% (29-100)	23/23=100% (86-100)	2/2=100% (29-100)	23/23=100% (86-100)
LCX 15	1/1=100% (16-100)	22/22=100% (85-100)	1/1=100% (16-100)	22/22=100% (85-100)
IB 16	2/2=100% (29-100)	10/11=91% (62-98)	2/3=67% (19-93)	10/10=100% (72-100)

RCA = right coronary artery; PDA = posterior descending artery; PL = postero-lateral artery; LM = left main coronary artery; LAD = left anterior descending artery; D = diagonal branch; LCX = left circumflex artery; MO = marginal obtuse branch; IB = intermediate branch.

Diagnostic Accuracy of 64-Slice CT

The sensitivity, specificity and the positive and negative predictive values of 64-slice CT in the detection of significant coronary artery stenoses were obtained for the 494 coronary segments available for comparison. The values (confidence intervals) obtained on all segments are 99% (92–100), 96% (93–97), 78% (68–85) and 99% (99–100), respectively. On a per-patient basis, the values (confidence intervals) are 100% (87–100), 90% (59–98), 96% (81–99) and 100% (69–100), respectively.

Table 3 details the accuracy of CT in the individual coronary segments according to the AHA classification [13]. The results of all coronary segments, coronary vessels and patients are summarised in Table 4.

TABLE 4. Overall CT accuracy: all segments, per-vessel, per-patient.

	Sensitivity	Specificity	Positive Predictive Value	Negative Predictive Value
All segments (Total 494)	66/67= **99%** (92-100)	408/427= **96%** (93-97)	66/85= **78%** (68-85)	408/409= **99%** (99-100)
Per-vessel				
RCA, PDA, PL (Available 138)	20/20=100% (84-100)	113/118=96% (90-98)	20/25=80% (61-91)	113/113=100% (97-100)
LM (Available 35)	-	35/35= 100% (90-100)	-	35/35= 100% (90-100)
LAD, Diagonal branches (Available 156)	25/26=96% (81-99)	121/130=93% (87-96)	25/34=74% (57-85)	121/122=99% (96-100)
LCX, MO branches, IB (Available 165)	21/21=100% (85-100)	139/144=97% (92-98)	21/26=81% (62-91)	139/139=100% (97-100)
Per-patient (Total 35)	25/25=100% (87-100)	9/10=90% (59-98)	25/26=96% (81-99)	9/9=100% (69-100)

Values are reported in ratios and percentages, with 95% confidence intervals in brackets.
RCA = right coronary artery; PDA = posterior descending artery; PL = postero-lateral artery; LM = left main coronary artery; LAD = left anterior descending artery; LCX = left circumflex artery; MO = marginal obtuse branches; IB = intermediate branch. The left main coronary artery was normal in all patients.

Inter-observer variability for the detection of significant lesions had k-values of 0.73.

Discussion

Earlier generations of multislice CT scanners showed promise for the non-invasive detection of coronary stenoses [1–11]. However, the reported accuracy was obtained on the basis of analysable coronary segments rather than on all coronary segments. A recent study showed promising results of 64-slice CT coronary angiography in the detection of significant stenoses using a CT scanner with a rotation time of 375 ms [14]. Still, coronary branches with a diameter below the threshold of 1.5 mm were excluded from the comparative analysis. Reducing the gantry rotation time to 330 ms provided improvements in the sensitivity and specificity. Two recent papers reported sensitivity and specificity values of 86% and 95% [15] and 73% and 97% [16] in cohorts of patients referred for catheterisation. No calibre threshold was set in those studies. However, 12% of the segments [15] and 4/59 patients [16] were excluded from analysis because of poor image quality. In our population, 64-slice CT coronary

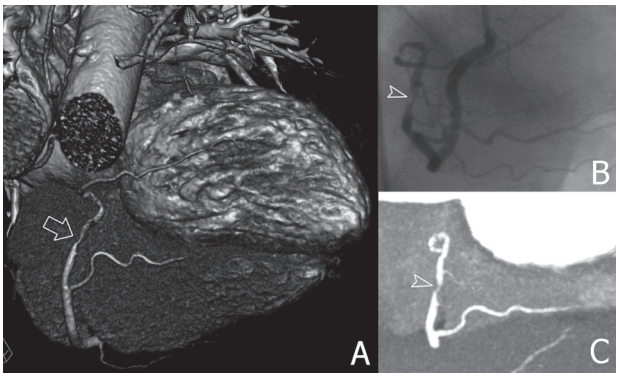

FIGURE 2 (A–C). 68-year-old patient with stable angina pectoris. A) 64-slice CT volume-rendered image. B) Conventional angiogram. C) 1-mm-thick CT maximum intensity projection. A coronary stenosis is seen at the level of the posterolateral artery (arrow and arrowheads). Luminal narrowing determined at QCA was 74%.
(A full color version of this illustration can be found in the color section)

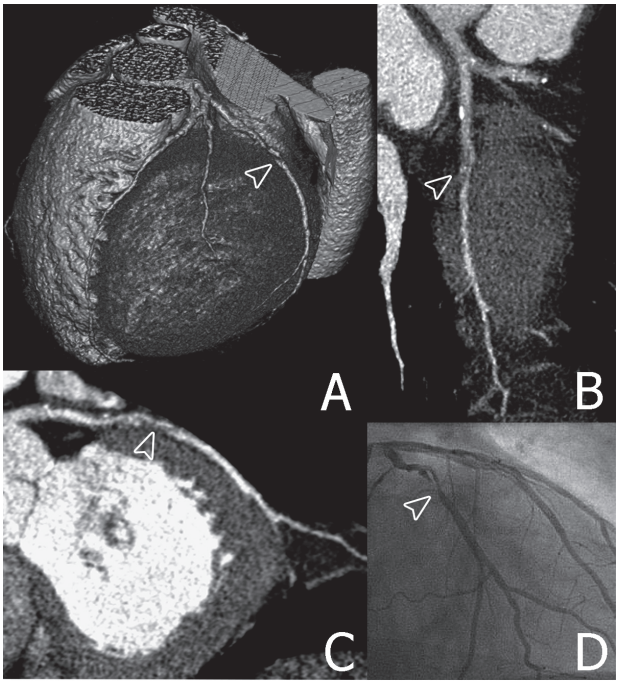

FIGURE 3 (A–D). 54-year-old patient with stable angina pectoris. A) 64-slice CT volume-rendered image. B) 1-mm-thick curved maximum intensity projection. C) 0.75-mm-thick multiplanar reconstruction. D) Conventional angiogram. A lesion is visible in the first marginal obtuse branch (arrowheads). Luminal narrowing determined at QCA was 64%.
(A full color version of this illustration can be found in the color section)

angiography detected significant coronary stenoses of the entire coronary tree with a sensitivity of 99% and a specificity of 96% when compared to conventional invasive coronary angiography. Such results were obtained by including all coronary branches available for visualization at conventional angiography and CT, regardless of the vessel diameter. In addition, none of the coronary segments available were excluded from analysis according to image quality. Thus, our results demonstrate the diagnostic accuracy of the technique to assess the entire coronary tree in the "real" clinical context.

Outcomes

All patients with significant coronary artery disease were correctly diagnosed, and only a single coronary lesion was missed at CT (sensitivity per-patient 100%, per-segment 99%). The missed lesion was found to be responsible for a 52% stenosis at QCA and was localised in the mid-tract of the left anterior descending artery. Dense eccentric

calcifications and motion artefacts were scored as being responsible for poor image quality.

All but one patient with angiographically normal coronary angiograms were correctly identified at CT, which makes the technique reliable for ruling out significant coronary obstructions (specificity per-patient 90%, per-segment 96%). This brings some meaningful implications in a population where 29% (10/35) of the patients had negative angiograms, in that 9/10 unnecessary catheterization procedures could have been avoided on the basis of CT results. This observation also counterbalances to some extent the drawback of a higher radiation dose of multislice CT compared to cardiac catheterisation, standing the periprocedural risk of, sometimes major, complications associated to the latter.

Figures 2 and 3 are examples of coronary artery stenoses detected with 64-slice CT and coronary angiography at the level of the posterolateral artery and first obtuse marginal branch, respectively.

Specifications and Scan Technique Shaping Diagnostic Accuracy

The capability to image the entire coronary tree is conceivably feasible due, in the first instance, to the technical advances of 64-slice CT scanners featuring high x-ray output, smaller individual detectors arranged in wider arrays and faster gantry rotation speed. With the above mentioned scan parameters, an isotropic spatial resolution of 0.4 mm3 is achieved [12]. Likewise, the temporal resolution, obtained from the reconstruction of data acquired during half x-ray tube rotation, is suitable for "freezing" the beating heart.

Indeed, although motion artefacts are a major factor affecting the image quality perceived by the examiner (Figure 1), on the other hand, only one false-negative and 1/19 false-positive CT findings were secondary to motion artefacts in our series, in patients whose heart rates were 68 beats/min and 65 beats/min, respectively. Since motion artefacts deteriorate the quality of a CT data set, the capability to find additional reconstruction windows within the cardiac cycle may allow us to minimise blurring and double-contouring, at least in a portion of the data set, thus providing complementary images suitable for evaluation. In a similar fashion, artefacts induced by mild heart rate irregularities, such as premature beats, can be compensated for with manual ECG editing. The choice of a proper reconstruction window as a key factor to a clinically reliable diagnosis of coronary lesions was also pointed out by Zhang et al. [17] and Hamoir et al. [18]. Conversely, the most common cause of incorrect CT diagnosis in our population

was calcification of the vessel wall, either bulky (4/17), dense and eccentric (9/17) or isolated (4/17). Such findings are in line with the notion that the assessment of significant coronary stenoses with CT is more difficult when many calcifications are present [4]. However, it is also reported that important coronary calcification should not be used as an indication for deferring multislice CT coronary angiography [19].

In order to obtain prominent vascular enhancement, a further prerequisite has to be reproducibly fulfilled for robust coronary CTangiography: the volume, injection rate and concentration of the contrast agent must be optimized into dedicated injection protocols [20–23]. Bolus tracking is a sophisticated synchronisation technique which monitors attenuation changes in the aorta and triggers the CT scan when a threshold value is reached. Hence, the 11–15 s scan window is operated during the expected peak of coronary enhancement to image coronary arteries with optimal contrast resolution.

It is expected that bolus geometry and dynamics considerations differ slightly when applied to tiny coronary side branches. As a rule, distal vessels have a small diameter, contain less blood and, thus, suffer from poor contrast-to-noise resolution. Therefore, we used the contrast agent with the highest iodine concentration available to improve the opacification of smaller vessels and the visualisation of coronary side branches and collateral pathways [24].

The results of diagnostic accuracy reported by Mollet et al. [25], who obtained 95% sensitivity and 98% specificity in a population of stable and unstable patients examined with a 16-slice CT scanner, are not in contrast with the aforementioned considerations. Indeed, the technical parameters featured by the newer generation 16-slice scanner used in that study were gantry rotation speed of 375 ms, detector width of 0.75 mm and high x-ray output. The iodine concentration of the contrast bolus was equally chosen at 400 mgI/ml.

As a matter of fact, the interpretability of coronary images obtained with multislice CT has matched the improvement of hardware equipment and the development of the scanning technique, namely, faster gantry rotation speed, smaller individual detector width, higher x-ray output and optimized protocols for contrast agent administration and synchronization. This created a distance between 4-slice and the first generation of 16-slice scanners on one side and the current CT scanners. Our experience suggests how 64-slice CT scanners, in association with an optimised scanning technique, provide images suitable for reliable interpretation. In association with appropriate operator

training, a role for multislice CT might be shaped as a non-invasive tool capable of assisting management options in selected cardiological patients. In particular, the capability of displaying the extent and morphology of coronary atherosclerosis may help direct treatment options to either conservative therapy, percutaneous intervention or surgery [26].

Limitations of the Study

Nineteen out of 494 lesions scored as being significant at coronary CT revealed to be haemodynamically insignificant at conventional angiography (false-positive findings).

This could, in part, be explained with the fact that, for lesions whose CT interpretation was uncertain, the chance of overestimation of the lesion severity was deemed less undesirable than the risk of underestimation, reflecting a clinical setting where CT plays the role of a decision tool to screen patients for referral to catheterisation. In these settings, where the overestimation of the severity of lesions would refer the patient for coronary catheterisation, overlooking significant stenoses might have much more serious consequences in a symptomatic population. Besides, the positive predictive value of CT rises from 78% to 96% when the patient, not the individual lesion, is considered.

A high pre-test prevalence of disease in the population available for comparison is, somehow, inevitable, since invasive angiography is generally not performed in subjects with suspected or known coronary artery disease in the absence of symptoms. Even in asymptomatic patients with demonstrated inducible ischemia, controversy exists as whether coronary angiography should be performed, unless additional risk factors such as advanced age, diabetes mellitus or lifestyle coexist. According to the American College of Cardiologists/American Heart Association guidelines [27], coronary angiography recommendations in patients with suspected or known stable coronary artery disease are limited to patients with angina pectoris or non-specific chest pain with positive (or contraindicated) stress testing.

We did not perform quantitative CT analysis of the lesions, which is instead reported by Raff et al. [15] and Leber et al. [16]. However, although correlation is reported between quantitative diameter stenosis at multislice CT and QCA, the differences of the percentage diameter stenosis assessed by the two methods show significant variability, thus, suggesting that the quantification of lesions by means of CT cannot reliably substitute QCA at the present time.

Conclusion

Accuracy of coronary CT angiography performed with a 64-slice scanner for the assessment of disease of the entire coronary tree is superior to that of earlier-generation CT scanners.

The sensitivity in the detection of significant lesions is 99% and the specificity is 96%. The predictive value of normal CT findings is also 99%. When referral to catheterisation is questionable, CT coronary angiography may identify subjects with normal angiograms and consistently decrease the number of unnecessary invasive procedures.

References

1. Nieman K, Oudkerk M, Rensing BJ, van Ooijen P, Munne A, van Geuns RJ, de Feyter PJ (2001) Coronary angiography with multi-slice computed tomography. Lancet 357:599–603
2. Knez A, Becker CR, Leber A, Ohnesorge B, Becker A, White C, Haberl R, Reiser MF, Steinbeck G (2001) Usefulness of multislice spiral computed tomography angiography for determination of coronary artery stenoses. Am J Cardiol 88:1191–1194
3. Vogl TJ, Abolmaali ND, Diebold T, Engelmann K, Ay M, Dogan S, Wimmer-Greinecker G, Moritz A, Herzog C (2002) Techniques for the detection of coronary atherosclerosis: multi-detector row CT coronary angiography. Radiology 223:212–220
4. Kuettner A, Kopp AF, Schroeder S, Rieger T, Brunn J, Meisner C, Heuschmid M, Trabold T, Burgstahler C, Martensen J, Schoebel W, Selbmann HK, Claussen CD (2004) Diagnostic accuracy of multidetector computed tomography coronary angiography in patients with angiographically proven coronary artery disease. J Am Coll Cardiol 43:831–839
5. Nieman K, Cademartiri F, Lemos PA, Raaijmakers R, Pattynama PM, de Feyter PJ (2002) Reliable noninvasive coronary angiography with fast submillimeter multislice spiral computed tomography. Circulation 106:2051–2054
6. Heuschmid M, Kuettner A, Schroeder S, Trabold T, Feyer A, Seemann MD, Kuzo R, Claussen CD, Kopp AF (2005) ECG-gated 16-MDCT of the coronary arteries: assessment of image quality and accuracy in detecting stenoses. AJR Am J Roentgenol 184:1413–1419
7. Ropers D, Baum U, Pohle K, Anders K, Ulzheimer S, Ohnesorge B, Schlundt C, Bautz W, Daniel WG, Achenbach S (2003)

Detection of coronary artery stenoses with thin-slice multi-detector row spiral computed tomography and multiplanar reconstruction. Circulation 107:664–666

8. Kuettner A, Trabold T, Schroeder S, Feyer A, Beck T, Brueckner A, Heuschmid M, Burgstahler C, Kopp AF, Claussen CD (2004) Noninvasive detection of coronary lesions using 16-detector multislice spiral computed tomography technology: initial clinical results. J Am Coll Cardiol 44:1230–1237
9. Martuscelli E, Romagnoli A, D'Eliseo A, Razzini C, Tomassini M, Sperandio M, Simonetti G, Romeo F (2004) Accuracy of thin-slice computed tomography in the detection of coronary stenoses. Eur Heart J 25:1043–1048
10. Hoffmann MH, Shi H, Schmitz BL, Schmid FT, Lieberknecht M, Schulze R, Ludwig B, Kroschel U, Jahnke N, Haerer W, Brambs HJ, Aschoff AJ (2005) Noninvasive coronary angiography with multislice computed tomography. JAMA 293:2471–2478
11. Mollet NR, Cademartiri F, Nieman K, Saia F, Lemos PA, McFadden EP, Pattynama PM, Serruys PW, Krestin GP, de Feyter PJ (2004) Multislice spiral computed tomography coronary angiography in patients with stable angina pectoris. J Am Coll Cardiol 43:2265–2270
12. Flohr T, Stierstorfer K, Raupach R, Ulzheimer S, Bruder H (2004) Performance evaluation of a 64-slice CT system with z-flying focal spot. Rofo 176:1803–1810
13. Austen WG, Edwards JE, Frye RL, Gensini GG, Gott VL, Griffith LS, McGoon DC, Murphy ML, Roe BB (1975) A reporting system on patients evaluated for coronary artery disease. Report of the Ad Hoc Committee for Grading of Coronary Artery Disease, Council on Cardiovascular Surgery, American Heart Association. Circulation 51:5–40
14. Leschka S, Alkadhi H, Plass A, Desbiolles L, Grunenfelder J, Marincek B, Wildermuth S (2005) Accuracy of MSCT coronary angiography with 64-slice technology: first experience. Eur Heart J 26:1482–1487
15. Raff GL, Gallagher MJ, O'Neill WW, Goldstein JA (2005) Diagnostic accuracy of noninvasive coronary angiography using 64-slice spiral computed tomography. J Am Coll Cardiol 46:552–557
16. Leber AW, Knez A, von Ziegler F, Becker A, Nikolaou K, Paul S, Wintersperger B, Reiser M, Becker CR, Steinbeck G, Boekstegers P (2005) Quantification of obstructive and nonobstructive coronary lesions by 64-slice computed tomography: a comparative study with quantitative coronary angiography and intravascular ultrasound. J Am Coll Cardiol 46:147–154
17. Zhang SZ, Hu XH, Zhang QW, Huang WX (2005) Evaluation of computed tomography coronary angiography in patients with a high heart rate using 16-slice spiral computed tomography with 0.37-s gantry rotation time. Eur Radiol 15:1105–1109
18. Hamoir XL, Flohr T, Hamoir V, Labaki L, Tricquet JY, Duhamel A, Kirsch J (2005) Coronary arteries: assessment of image quality and optimal reconstruction window in retrospective ECG gated multislice CT

at 375-ms gantry rotation time. Eur Radiol 15:296–304

19. Cademartiri F, Mollet NR, Lemos PA, Saia F, Runza G, Midiri M, Krestin GP, de Feyter PJ (2005) Impact of coronary calcium score on diagnostic accuracy for the detection of significant coronary stenosis with multislice computed tomography angiography. Am J Cardiol 95:1225–1227
20. Cademartiri F, Nieman K, van der Lugt A, Raaijmakers RH, Mollet N, Pattynama PM, de Feyter PJ, Krestin GP (2004) Intravenous contrast material administration at 16-detector row helical CT coronary angiography: test bolus versus bolus-tracking technique. Radiology 233:817–823
21. Bae KT, Heiken JP, Brink JA (1998) Aortic and hepatic contrast medium enhancement at CT. Part II. Effect of reduced cardiac output in a porcine model. Radiology 207:657–662
22. Bae KT, Heiken JP, Brink JA (1998) Aortic and hepatic contrast medium enhancement at CT. Part I. Prediction with a computer model. Radiology 207:647–655
23. Bae KT, Heiken JP, Brink JA (1998) Aortic and hepatic peak enhancement at CT: effect of contrast medium injection rate—pharmacokinetic analysis and experimental porcine model. Radiology 206:455–464
24. Cademartiri F, Mollet NR, van der Lugt A, McFadden EP, Stijnen T, de Feyter PJ, Krestin GP (2005) Intravenous contrast material administration at helical 16-detector row CT coronary angiography: effect of iodine concentration on vascular attenuation. Radiology 236:661–665
25. Mollet NR, Cademartiri F, Krestin GP, McFadden EP, Arampatzis CA, Serruys PW, de Feyter PJ (2005) Improved diagnostic accuracy with 16-row multislice computed tomography coronary angiography. J Am Coll Cardiol 45:128–132
26. Becker CR (2005) Coronary CT angiography in symptomatic patients. Eur Radiol 15(Suppl 2):B33–B41
27. Scanlon PJ, Faxon DP, Audet AM, Carabello B, Dehmer GJ, Eagle KA, Legako RD, Leon DF, Murray JA, Nissen SE, Pepine CJ, Watson RM, Ritchie JL, Gibbons RJ, Cheitlin MD, Gardner TJ, Garson A Jr, Russell RO Jr, Ryan TJ, Smith SC Jr (1999) ACC/AHA guidelines for coronary angiography: executive summary and recommendations. A report of the American College of Cardiology/American Heart Association Task Force on Practice Guidelines (Committee on Coronary Angiography) developed in collaboration with the Society for Cardiac Angiography and Interventions. Circulation 99:2345–2357

CHAPTER 12

Comparison of diagnostic performance of 64-slice computed tomography coronary angiography in women versus men with angina pectoris

Meijboom WB, Weustink AC, Pugliese F, van Mieghem C, Mollet NR, van Pelt N, Cademartiri F, Nieman K, Vourvouri E, Regar E, Krestin GP, de Feyter PJ.

American Journal of Cardiology 2007; 100:1532-1537.

Summary

Purpose: We compared the diagnostic accuracy of 64-slice computed tomographic (CT) coronary angiography to detect significant coronary artery disease (CAD) in women and men.

Materials and methods: The 64-slice CT coronary angiography was performed in 402 symptomatic patients, 123 women and 279 men, with CAD prevalence of 51% and 68%, respectively. Significant CAD, defined as ≥50% coronary stenosis on quantitative coronary angiography, was evaluated on a patient, vessel, and segment level.

Results: The sensitivity and negative predictive value to detect significant CAD was very good, both for women and men (100% vs 99%, p = NS; 100% vs 98%, p = NS), whereas diagnostic accuracy (88% vs 96%; p <0.01), specificity (75% vs 90%, p <0.05), and positive predictive value (81% vs 95%, p <0.001) were lower in women. The per-segment analysis demonstrated lower sensitivity in women compared with men (82% vs 93%, p <0.001). The sensitivity in women did not show a difference in proximal and mid segments, but was significantly lower in distal segments (56% vs 85%, p <0.05) and side branches (54% vs 89%, p <0.001).

Conclusion: In conclusion, CT coronary angiography reliably rules out the presence of obstructive CAD in both men and women. Specificity and positive predictive value of CT coronary angiography were lower in women. The sensitivity to detect stenosis in small coronary branches was lower in women compared with men.

Introduction

Computed tomographic coronary angiography (CTCA) is a rapidly evolving coronary imaging technique, and a potential alternative to established noninvasive tests for coronary artery disease (CAD). The diagnostic accuracy of CTCA in women per se has not been investigated, but is extrapolated from reports that were performed in populations largely consisting of men.1–9 Although earlier data suggested a discrepancy between men and women with regard to the diagnostic performance of ischemia-driven tests, recent reports using contemporary exercise electrocardiographic (ECG) testing, stress echocardiography, and gated single-photon emission computed tomography myocardial perfusion imaging refute these earlier conclusions, and state similar diagnostic results for both women and men.10–16 Apart from varying age, disease prevalence and severity, additional anatomic and physiologic differences, including body composition, heart rate, coronary calcium, and coronary diameter size, between men and women may affect the diagnostic performance of CTCA. The purpose of this study was to ascertain the diagnostic accuracy of CTCA in women versus men with chest pain to detect or exclude the presence of obstructive CAD.

Materials and Methods

During a 24-month period 402 patients with acute or stable chest pain symptoms who were referred for conventional coronary angiography (CCA) were included in the study. No patients with a history of percutaneous coronary intervention or coronary artery bypass surgery, impaired renal function (serum creatinine >120 μmol/L), persistent arrhythmias, and known intolerance to iodinated contrast material were included. CCA was performed before or after CTCA and served as the standard of reference. The institutional review board of the Erasmus MC Rotterdam approved the study, and all subjects gave informed consent.

Patients with a heart rate >65 beats/min received additional ß-blockers (50/100 mg metoprolol) 1 hour before the CT examination. All scans were performed on a 64-slice CT scanner with a gantry rota-

tion time of 330 ms, a temporal resolution of 165 ms, and a spatial resolution of 0.4 mm3 (Sensation 64; Siemens, Forchheim, Germany). For the coronary calcium score, a low-dose, non-enhanced scan was performed with the following, standardized parameters: 32 * 2 slices per rotation; individual detector width of 0.6 mm, 330-ms rotation time, 3.8-mm/rotation table feed, 120-kV tube voltage, 150-mAs tube current, with activated prospective x-ray tube modulation. The CTCA scan was performed with identical parameters except for a higher tube current between 850 and 960 mAs without prospective ECG x-ray tube modulation. The radiation exposure was estimated using dedicated software (ImPACT, version 0.99x, St. George's Hospital, Tooting, London, United Kingdom). A 95-ml bolus of iomeprol (Iomeron, 400 mg/ml; Bracco, Milan, Italy) was injected intravenously into an antecubital vein at 5 ml/s. A bolus-tracking technique was used to monitor the arrival of contrast in the coronary arteries. The scan was started once the contrast material in the ascending aorta reached a predefined threshold of +100 Hounsfield Units.

Datasets were reconstructed immediately after the scan following a stepwise outline. Images were obtained during a half x-ray tube rotation, resulting in an effective temporal resolution of 165 ms. To acquire optimal motion-free images, images were reconstructed by retrospective ECG gating. Initially, a single dataset was reconstructed during the mid-to-end-diastolic phase (350 ms before the next R wave or at 65% of the RR interval). In case of insufficient image quality of ≥1 coronary segments, additional datasets were reconstructed in the diastolic phase (between 250 and 450 ms before the next R wave or between 60% and 70% of the RR interval). In case of persistent artifacts related to coronary motion, a second reconstruction approach was carried out. Datasets were reconstructed during the end-systolic phase using an absolute forward or percentage technique (between 250 and 400 ms after the previous R wave or between 25% and 35% of the RR interval). In 34% of the patients (137 of 402) end-systolic reconstructions were used for image analysis. If necessary, multiple datasets of a single patient were used separately to obtain optimal image quality of all available coronary segments.

All scans were carried out within 1 week before or after CTCA. One experienced cardiologist, who was unaware of the CTCA results, identified and analyzed all coronary segments according to the modified 17-segment American Heart Association classification.17 Regardless of diameter size, all segments were included for comparison with CTCA. Segments were classified as normal (smooth paral-

lel or tapering borders), nonsignificantly stenosed (wall irregularities or <50% narrowed), or significantly stenosed (≥50% narrowed). Stenoses were evaluated in the worst view, and classified as significant if the lumen diameter reduction was ≥50% as measured by a validated quantitative coronary angiographic algorithm (CAAS, Pie Medical, Maastricht, the Netherlands).18

For each patient the total calcium score was measured, and expressed using the Agatston score.17 Two experienced, blinded observers evaluated the CTCA data on an offline workstation (Leonardo, Siemens, Forchheim, Germany). The axial source images, as well as multiplanar or curved reformatted reconstructions and maximum intensity projections, were used to evaluate the CT angiograms and assess the presence of significant segmental stenosis. Segments were scored positive for significant CAD if there was ≥50% diameter reduction of the lumen by visual assessment. Segments distal to an occluded segment were excluded. Interobserver disagreement was resolved by a third reader.

Descriptive statistics were performed for coronary segments, vessels, and patients. The diagnostic performance of CTCA for the detection of significant stenoses in the coronary arteries with quantitative coronary angiography (QCA) as the standard of reference is presented as sensitivity, specificity, positive and negative predictive values. Precision of the diagnostic parameters is presented using a 95% confidence interval (CI). Chi-square tests were performed to show significant differences in diagnostic accuracy. Positive and negative likelihood ratios are given. The likelihood ratio incorporates both the sensitivity and specificity of a test and provides a direct estimate of how much a test result will change the odds of having a disease. Post-test odds can be calculated by multiplying the pretest odds (pretest probability/[1 - pretest probability]) by the positive likelihood ratio (sensitivity/[1 - specificity]) and negative likelihood ratio ([1 - sensitivity]/specificity). Post-test probability can be recalculated by using the following formula: (post-test probability = post-test odds/[1 + post-test odds]).

A subanalysis was performed between the 2 genders. Categorical characteristics are expressed as numbers and percentages, and compared between the 2 groups with the chi-square test. Continuous variables are expressed as mean ± SD and compared with an unpaired 2-sided Student's t test when normally distributed. When not normally distributed, continuous variables are expressed as medians (25th to 75th percentile range) and compared using the nonparametric Mann-Whitney test. p Values <0.05 were considered statistically significant.

TABLE 1. Patient demographics (n = 402)

Variable	Women (n = 123)	Men (n = 279)	p Value
Age (yrs)*	62 ± 11	58 ± 11	<0.01
Calcium score (Agatston score)†	146 (0–373)	207 (18–530)	<0.05
Body mass index (kg/m^2)*	26.7 ± 5.0	27.0 ± 3.6	NS
Heart rate (beats/min)*	61 ± 7	58 ± 8	<0.001
Prevalence of obstructive coronary artery disease	63 (51%)	190 (68%)	<0.01
Atypical angina pectoris	47 (38%)	99 (35%)	NS
Typical angina pectoris	48 (39%)	107 (38%)	
Unstable angina pectoris	14 (11%)	36 (13%)	
Non–ST–segment elevation myocardial infarction	14 (11%)	37 (13%)	
Hypertension‡	78 (63%)	138 (49%)	<0.05
Hypercholesterolemia§	75 (61%)	161 (58%)	NS
Diabetes mellitus#	23 (19%)	28 (10%)	<0.05
Active smoker	30 (24%)	99 (35%)	<0.05
Previous smoker	9 (7%)	20 (7%)	NS
Body mass index ≥30 kg/m^2	34 (28%)	64 (23%)	NS
Previous myocardial infarction	15 (12%)	27 (10%)	NS
Conventional coronary angiography			
Absence of coronary disease	28 (23%)	42 (15%)	<0.05

* Mean ± SD.
† Median and quartiles. Values are numbers (percent), unless otherwise indicated. Categorical variables were tested with chi-square test. Continuous variables were tested with unpaired 2-sided Student's t test. If not normally distributed, continuous variables were compared with the Mann-Whitney test.
p Values are significant if <0.05.
‡ Blood pressure ≥140/90 mm Hg or treatment for hypertension.
§ Total cholesterol >180 mg/dl or treatment for hypercholesterolemia.
# Treatment with oral antidiabetic medication or insulin.

An additional sensitivity analysis was done to investigate the effect of nesting, as repeated assessments within the same patient were made that were not independent observations. Inter- and intraobserver variabilities for the detection of significant coronary stenosis were determined by k statistics.

Results

The analysis comprised 123 women and 279 men (Table 1). On average women were older (62 ± 11 vs 58 ± 11 years, p <0.01). Hypertension and diabetes were more frequent in women, with no significant difference for body mass index. There were more active smokers among

men. Women had lower disease prevalence (51% vs 68%, p <0.01), which was defined as having ≥1 significant stenosis. The severity and extent of obstructive CAD was significantly lower in women compared with men (p <0.05), with fewer cases of multivessel disease (24% vs 35%, p <0.05), and more nonobstructive lesions on CTCA (26% vs 17%, p <0.05). There was a nonsignificant trend toward fewer absence of CAD on CTCA in women (23% vs 15%, p = 0.06). Furthermore, the calcium score was lower in women (146 [0 to 373] vs 207 [18 to 530], p <0.05). During the CT scan, women had a significantly higher heart rate than men: 61 ± 7 vs 58 ± 8 beats/min, p <0.001). Additional ß-blockers before CT scanning were administered to 73% of women (90 of 123) and 70% of men (196 of 279) (p = NS), decreasing the mean heart rate from 69 ± 10 to 61 ± 7 beats/min and from 69 ± 11 to 58 ± 8 beats/min, respectively.

The estimated radiation exposure using prospective x-ray tube modulation for the calcium score in women and men was 1.8 and 1.4 mSv and the estimated radiation exposure for the contrast-enhanced scan without prospective x-ray tube modulation was calculated as 17.0 and 13.4 mSv, which is in line with previous reports.19

The diagnostic performance of CTCA for detecting significant stenoses on a patient-based analysis is detailed in Table 2. All women (63 of 63) and 99% of men (188 of 190) with significant CAD on CTCA were correctly identified by computed tomography (Figures 1 and 2). Fifteen women (25%, 15 of 60) and 9 men (10%, 9 of 89) with nonsignificant CAD were incorrectly classified as having significant coronary stenoses by CT.

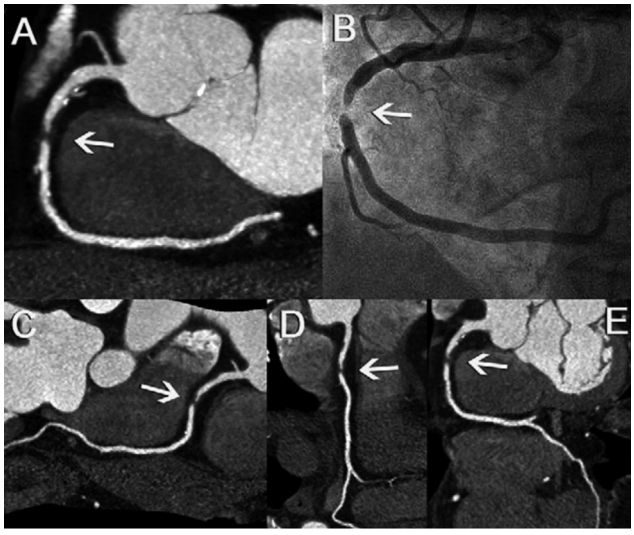

FIGURE 1. A maximum intensity projected CTCA image (A) depicts the anatomy of the right coronary artery. In the mid right coronary artery, a noncalcified obstructive coronary stenosis is visualized (arrow) with proximally and distally nonobstructive calcified plaques. Three curved multiplanar reconstructed images confirm the significant lesions (arrow) from 3 orthogonal projections (C, D, E), which was confirmed by CTCA (B).

In women, specificity (75% vs 90%, p <0.05), positive predictive value (81% vs

95%, p <0.001), and overall accuracy (88% vs 96%, p <0.01) were significantly lower compared with men. Agreement between CTCA and QCA on a per-patient (no or any disease) level for women and men was good (k value 0.75) and very good (k value 0.91).

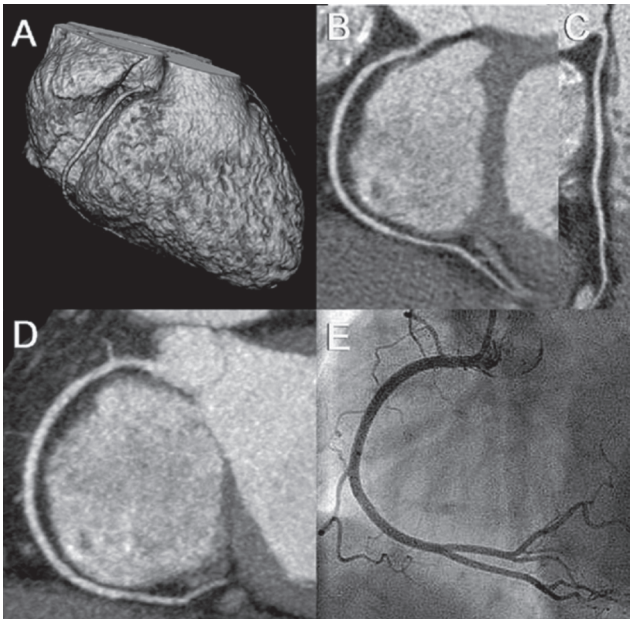

FIGURE 2. A volume-rendered CTCA image (A) reveals the anatomy of the right coronary artery. Two orthogonal curved multiplanar reconstructed images (B, C) and a maximum intensity projected image (D) disclose a normal coronary artery without obstructive or nonobstructive plaques, which was confirmed by CTCA (E).
(A full color version of this illustration can be found in the color section)

The diagnostic performance of CTCA for the detection of significant coronary stenosis on a vessel-based analysis is detailed in Table 2. In women, 2 significantly diseased right coronary arteries, 1 left anterior descending coronary artery, and 3 diseased circumflex coronary arteries were incorrectly classified as nonsignificantly diseased. In men, significant coronary stenosis in 2 right coronary arteries, 2 left anterior descending coronary arteries, and 4 circumflex coronary arteries were missed. Significant left main disease was identified in all patients. Fifty-one and 125 nonobstructive vessels were overestimated in women and men and scored as false positives. The diagnostic accuracy was equal in women and men. Agreement between CTCA and QCA on a per-vessel level was both good for women and men (k value 0.69, 0.74).

After exclusion of anatomically absent segments (833) and segments distal to an occlusion (266), 5,735 of 6,834 potentially available segments (with a maximum of 17 segments per patient) could be included for comparison with QCA. No segments were excluded for reasons of calcification or poor image quality. The overall sensitivity and specificity of CTCA for the detection of significantly stenosed coronary segments was 91% and 93%. Sensitivity was lower in women (82% vs 93%, p <0.001). Also, the specificity (94% vs 92%, p <0.05) and negative predictive value

TABLE 2. Overall diagnostic performance of 64-slice computed tomographic coronary angiography

Variable	Women n% (95% CI), n/n	Men n% (95% CI), n/n	p Value
Patient level			
Sensitivity	100% (93–100) 63/63	99% (96–100) 188/190	NS
Specificity	75% (62–85) 45/60	90% (81–95) 80/89	<0.05
Positive predictive value	81% (70–88) 63/78	95% (91–98) 188/197	<0.001
Negative predictive value	100% (93–100) 45/45	98% (91–100) 80/82	NS
Diagnostic accuracy	88% (82–94) 108/123	96% (94–98) 268/279	<0.01
+ Likelihood ratio	4.00 (2.58–6.20)	9.78 (4.70–14.25)	-
- Likelihood ratio	0 (0-/)	0.01 (0–0.05)	-
Vessel level			
Sensitivity	94% (87–98) 93/99	97% (95–99) 307/315	NS
Specificity	87% (83–90) 342/393	84% (82–87) 676/801	NS
Positive predictive value	65% (56–72) 93/144	71% (66–75) 307/432	NS
Negative predictive value	98% (96–99) 342/348	99% (98–99) 676/684	NS
Diagnostic accuracy	88% (86–91) 435/492	88% (86–90) 983/1,116	NS
+ Likelihood ratio	7.24 (5.58–9.40)	6.25 (5.31–7.34)	-
- Likelihood ratio	0.07 (0.03–0.15)	0.03 (0.02–0.06)	-
Segment level			
Sensitivity	82% (74–88) 111/136	93% (91–96) 400/428	<0.001
Specificity	94% (93–95) 1,551/1,648	92% (91–93) 3,249/3,523	<0.05
Positive predictive value	53% (46–60) 111/208	59% (56–63) 400/674	NS
Negative predictive value	98% (98–99) 1,551/1,576	99% (99–99) 3,249/3,277	<0.05
Diagnostic accuracy	93% (92–94) 1,662/1,784	92% (92–93) 3,523/3,951	NS
+ Likelihood ratio	13.87 (11.25–17.09)	12.02 (10.70–13.50)	-
- Likelihood ratio	0.20 (0.14–0.28)	0.07 (0.05–0.10)	-

Diagnostic performance and predictive value with corresponding likelihood ratios of 64-slice CTCA for the detection of ≥50% stenosis on QCA in women and men. Chi-square test was used for categorical variables. p Values were significant if values <0.05. Values in parentheses represent 95% CIs.

(98% vs 99%, p <0.05) showed a small, but significant difference between men and women (Table 2).

The performance of CTCA was similar between men and women in the proximal and middle segments (Table 3). However, in the distal segments (56% vs 85%, p <0.05) and side branches, more lesions were not detected in women (sensitivity 54% vs 89%, p <0.001; negative predictive value 97% vs 99%, p <0.05).

TABLE 3. Diagnostic performance of 64 slice computed tomography coronary angiography depending on segment location

	Women n% (95% CI), n/n	Men n% (95% CI), n/n	p Value
Analysis of proximal segments			
Sensitivity	96% (84–99) 44/46	98% (93–99) 130/133	NS
Specificity	92% (89–94) 411/446	91% (87–92) 891/983	NS
Positive predictive value	56% (44–67) 44/79	59% (52–65) 130/228	NS
Negative predictive value	100% (98–100) 411/413	100% (99–100) 891/894	NS
Analysis of mid segments			
Sensitivity	93% (81–98) 43/46	96% (90–98) 133/139	NS
Specificity	91% (87–94) 285/314	88% (86–91) 575/650	NS
Positive predictive value	60% (47–71) 43/72	64% (57–70) 133/208	NS
Negative predictive value	99% (97–100) 285/288	99% (98–100) 575/581	NS
Analysis of distal segments			
Sensitivity	56% (31–79) 9/16	85% (74–93) 53/62	<0.05
Specificity	97% (94–98) 364/376	96% (94–97) 754/786	NS
Positive predictive value	43% (23–66) 9/21	62% (51–72) 53/85	NS
Negative predictive value	98% (96–99) 364/371	99% (98–99) 754/763	NS
Analysis of side branches			
Sensitivity	54% (34–72) 15/28	89% (81–95) 84/94	<0.001
Specificity	96% (94–97) 491/512	93% (92–95) 1,029/2,104	<0.05
Positive predictive value	42% (26–59) 15/36	53% (45–61) 84/59	NS
Negative predictive value	97% (96–99) 491/504	99% (98–100) 1,029/1,039	<0.05

Chi-square test was used for categorical variables. p Values were significant if values <0.05. Values in parentheses represent 95% CIs.

The specificity (96% vs 93%, p <0.05) was slightly higher in women. Inter- and intraobserver variabilities for detection of a significant stenosis per segment had k values of 0.70 and 0.72, respectively. Agreement between CTCA and QCA on a per-segment level was good both for women and men (k value 0.61, 0.68). To exclude the possible confounding effect of nesting, random selection of a single segment per patient was done and the diagnostic accuracy for detecting significant artery disease resulted in a sensitivity 92% (44 of 48; 95% CI 79 to 97), specificity 93% (331 of 356; 95% CI 90 to 95), positive predictive value 64% (44 of 69; 95% CI 51 to 75), negative predictive value 99% (331 of 335; 95% CI 97 to 100).

Discussion

We demonstrated that the sensitivity of 64-slice CTCA to detect significant CAD was almost equally high in women and men (100% vs 99%) due to the very low occurrence of false-negative outcomes. Therefore, the diagnostic accuracy of 64-slice CTCA to rule out the presence of significant obstructive CAD was equally high in women and men and a negative CT scan reliably obviates the need for further downstream evaluation with invasive coronary angiography. The lower prevalence of CAD in women, with a trend toward more nonsignificant CAD ($p = 0.06$) likely contributed to the overestimation of coronary stenosis severity and thus resulted in lower specificity (75% vs 90%).

The segment-based diagnostic accuracy of CTCA performed on a site-by-site analysis (segmental analysis) compared with CTCA revealed a more complex outcome. The sensitivity to detect a stenosis was lower in women than in men. The overall reduced sensitivity was mainly caused by the lower sensitivity of CTCA to detect coronary obstructions in distal coronary segments and side branches. This may be partly explained by the combination of a milder stenosis severity and smaller size of the coronary arteries in women than in men. However, this outcome does not affect the reliability to rule out the presence of significant CAD in case of a negative CT scan, because on a segment-based analysis the overwhelming majority of these segments have no significant CAD, and the calculation of the negative predictive value is almost not affected by the higher occurrence of false negative outcomes.

The studied patients were not a prospective, consecutive group of patients. However, selection was not based on particular patient demographics, but rather on the availability of the 64-slice CT scanner for the examination of cardiac patients.

Fundamental limitations of cardiac computed tomography include the use of radiation, potentially nephrotoxic contrast media, and the need to use ß-blockers in patients with a fast heart rate. The substantial radiation exposure of 64-slice CTCA for women (17 mSv) and men (13.4 mSv) compared with CCA (3 to 6 mSv) is of concern.19 In this study prospective ECG x-ray tube modulation, which can significantly reduce radiation exposure, was not applied. This technique limits the possibility of reconstructing images in the end-systolic phase. In our study, end-systolic datasets provided better image quality in 34% of patients. Furthermore, the use of prospective ECG x-ray tube modulation requires a regular heart rhythm throughout the scan. In case of an extra-systole, the use of prospective ECG x-ray tube modulation can miss-trig-

ger the x-ray pulse, limiting the possibility to edit valuable reconstruction window datasets during high-dose scanning.

References

1. Leschka S, Alkadhi H, Plass A, Desbiolles L, Grunenfelder J, Marincek B, Wildermuth S. Accuracy of MSCT coronary angiography with 64-slice technology: first experience. Eur Heart J 2005;26:1482–1487.
2. Raff GL, Gallagher MJ, O'Neill WW, Goldstein JA. Diagnostic accuracy of noninvasive coronary angiography using 64-slice spiral computed tomography. J Am Coll Cardiol 2005;46:552–557.
3. Leber AW, Knez A, von Ziegler F, Becker A, Nikolaou K, Paul S, Wintersperger B, Reiser M, Becker CR, Steinbeck G, Boekstegers P. Quantification of obstructive and nonobstructive coronary lesions by 64-slice computed tomography: a comparative study with quantitative coronary angiography and intravascular ultrasound. J Am Coll Cardiol 2005;46:147–154.
4. Mollet NR, Cademartiri F, van Mieghem CA, Runza G, McFadden EP, Baks T, Serruys PW, Krestin GP, de Feyter PJ. High-resolution spiral computed tomography coronary angiography in patients referred for diagnostic conventional coronary angiography. Circulation 2005;112:2318–2323.
5. Ropers D, Rixe J, Anders K, Kuttner A, Baum U, Bautz W, Daniel WG, Achenbach S. Usefulness of multidetector row spiral computed tomography with 64- _ 0.6-mm collimation and 330-ms rotation for the noninvasive detection of significant coronary artery stenoses. Am J Cardiol 2006;97:343–348.
6. Schuijf JD, Pundziute G, Jukema JW, Lamb HJ, van der Hoeven BL, de Roos A, van der Wall EE, Bax JJ. Diagnostic accuracy of 64-slice multislice computed tomography in the noninvasive evaluation of significant coronary artery disease. Am J Cardiol 2006;98:145–148.
7. Nikolaou K, Knez A, Rist C, Wintersperger BJ, Leber A, Johnson T, Reiser MF, Becker CR. Accuracy of 64-MDCT in the diagnosis of ischemic heart disease. AJR 2006;187:111–117.
8. Fine JJ, Hopkins CB, Ruff N, Newton FC. Comparison of accuracy of 64-slice cardiovascular computed tomography with coronary angiography in patients with suspected coronary artery disease. Am J Cardiol 2006;97:173–174.

9. Ehara M, Surmely JF, Kawai M, Katoh O, Matsubara T, Terashima M, Tsuchikane E, Kinoshita Y, Suzuki T, Ito T, Takeda Y, Nasu K, Tanaka N, Murata A, Suzuki Y, Sato K. Diagnostic accuracy of 64-slice computed tomography for detecting angiographically significant coronary artery stenosis in an unselected consecutive patient population: comparison with conventional invasive angiography. Circ J 2006;70:564 –571.
10. Gibbons RJ, Balady GJ, Bricker JT, Chaitman BR, Fletcher GF, Froelicher VF, Mark DB, McCallister BD, Mooss AN, O'Reilly MG, et al. ACC/AHA 2002 guideline update for exercise testing: summary article: a report of the American College of Cardiology/ American Heart Association Task Force on Practice Guidelines (Committee to Update the 1997 Exercise Testing Guidelines). Circulation 2002;106:1883–1892.
11. Kwok Y, Kim C, Grady D, Segal M, Redberg R. Meta-analysis of exercise testing to detect coronary artery disease in women. Am J Cardiol 1999;83:660–666.
12. Kim C, Kwok YS, Heagerty P, Redberg R. Pharmacologic stress testing for coronary disease diagnosis: a meta-analysis. Am Heart J 2001;142:934 –944.
13. Mieres JH, Shaw LJ, Hendel RC, Miller DD, Bonow RO, Berman DS, Heller GV, Bairey-Merz CN, Cacciabaudo JM, Kiess MC, et al. American Society of Nuclear Cardiology consensus statement: Task Force on Women and Coronary Artery Disease—the role of myocardial perfusion imaging in the clinical evaluation of coronary artery disease in women [correction]. J Nucl Cardiol 2003;10:95–101.
14. Santana-Boado C, Candell-Riera J, Castell-Conesa J, Aguade-Bruix S, Garcia-Burillo A, Canela T, Gonzalez JM, Cortadellas J, Ortega D, Soler-Soler J. Diagnostic accuracy of technetium-99m-MIBI myocardial SPECT in women and men. J Nucl Med 1998;39:751–755.
15. Mieres JH, Shaw LJ, Arai A, Budoff MJ, Flamm SD, Hundley WG, Marwick TH, Mosca L, Patel AR, Quinones MA, et al. Role of noninvasive testing in the clinical evaluation of women with suspected coronary artery disease: consensus statement from the Cardiac Imaging Committee, Council on Clinical Cardiology, and the Cardiovascular Imaging and Intervention Committee, Council on Cardiovascular Radiology and Intervention, American Heart Association. Circulation 2005;111:682– 696.
16. Klocke FJ, Baird MG, Lorell BH, Bateman TM, Messer JV, Berman DS, O'Gara PT, Carabello BA, Russell RO Jr., Cerqueira MD, et al. ACC/ AHA/ASNC guidelines for the clinical use of cardiac radionuclide imaging—executive summary: a report of the American College of Cardiology/American Heart Association Task Force on Practice Guidelines (ACC/ AHA/ASNC Committee to Revise the 1995 Guidelines for the Clinical Use of Cardiac Radionuclide Imaging). J Am Coll Cardiol 2003;42:1318 –1333.
17. Agatston AS, Janowitz WR, Hildner FJ, Zusmer NR, Viamonte M, Jr. Detrano R. Quantification of coronary artery calcium

using ultrafast computed tomography. J Am Coll Cardiol 1990;15:827– 832.

18. Austen WG, Edwards JE, Frye RL, Gensini GG, Gott VL, Griffith LS, McGoon DC, Murphy ML, Roe BB. A reporting system on patients evaluated for coronary artery disease. Report of the Ad Hoc Committee for Grading of Coronary Artery Disease, Council on Cardiovascular Surgery, American Heart Association. Circulation 1975;51:5– 40.

19. Hausleiter J, Meyer T, Hadamitzky M, Huber E, Zankl M, Martinoff S, Kastrati A, Schomig A. Radiation dose estimates from cardiac multislice computed tomography in daily practice: impact of different scanning protocols on effective dose estimates. Circulation 2006;113:1305–1310.

CHAPTER 13

Unusual cause of myocardial ischemia non-invasively assessed with ECG-gated computed tomography coronary angiography

Pugliese F, Meijboom WB, Cademartiri F, Krestin GP.

European Journal of Cardiothoracic Surgery 2006; 29:840.

Summary, Methods and Results

A 71-year-old otherwise healthy woman presenting with atypical chest pain and inconclusive ECG-treadmill test was referred for ECG-gated, 64-detector row computed tomography to study coronary arteries noninvasively (Figures 1 and 2).

Non-ruptured Valsalva aneurysms do not usually cause cardiac dysfunction. However, coronary insufficiency may eventually develop with the expanding sinus.

Supplementary Data

Supplementary data (Video 1) associated with this article can be found, in the online version, at doi:10.1016/j.ejcts.2006.02.028

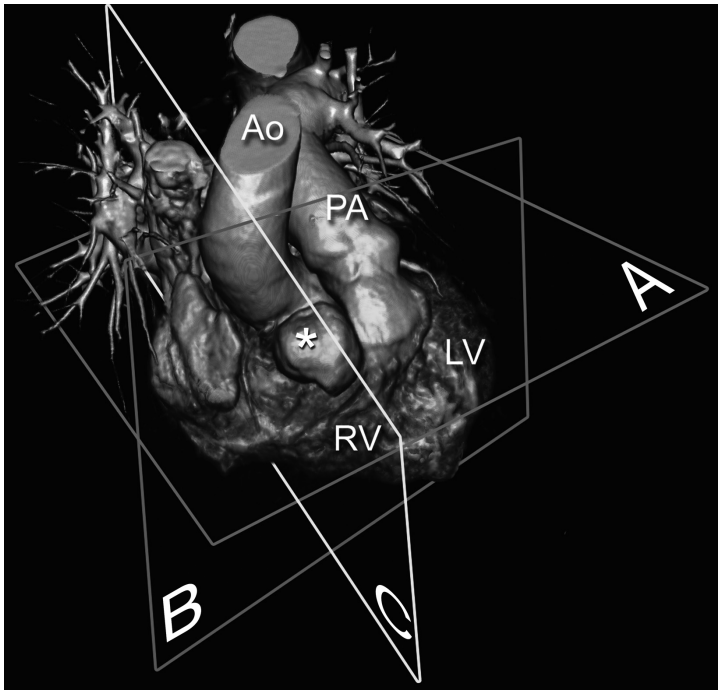

FIGURE 1. Volume-rendered ECG-gated CT image showing a right Valsalva sinus aneurysm (asterisk). Ao: aorta; PA: pulmonary artery; LV: left ventricle; RV: right ventricle.
(A full color version of this illustration can be found in the color section)

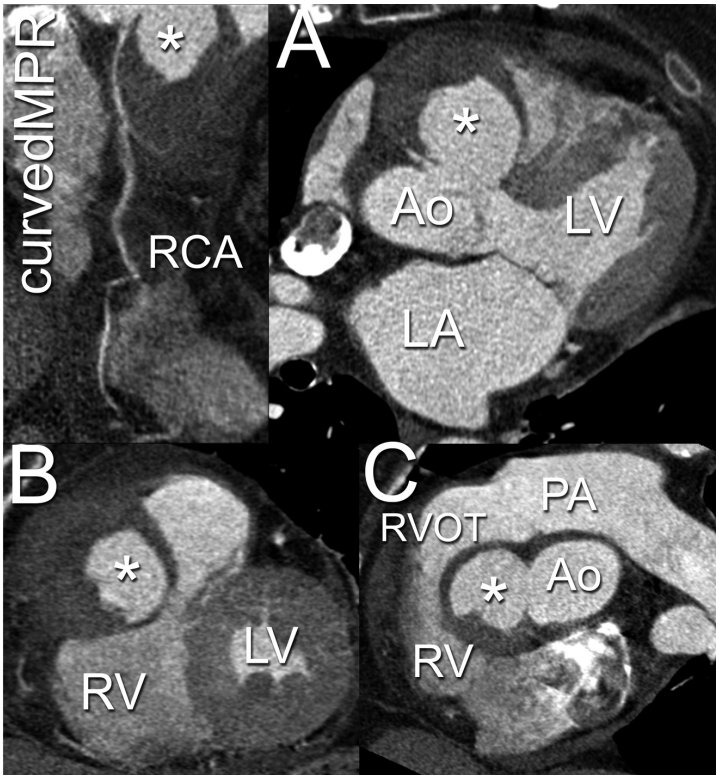

FIGURE 2. Curved multiplanar reconstruction (curved MPR) of the right coronary artery (RCA) and multiplanar reconstructions (A—C) obtained as indicated in Figure 1.On the curved MPR, the proximal RCA is critically narrowed due to the presence of the aneurysm (asterisk), which is seen bulging between the right ventricle (RV) and the aortic root (Ao) on multiplanar reconstructions (A—C). Thick eccentric thrombus is layered on the ectatic walls. As shown in (A), the ostium of the RCA opens at the level of the aneurysmal neck. No signs of rupture can be seen. The patient underwent uneventful surgery. The RCA was revascularized with a venous graft. Asterisk: aneurysm; Ao: aorta; LA: left atrium; LV: left ventricle; RV: right ventricle; RVOT: right ventricular outflow tract; PA: pulmonary artery.

CHAPTER 14

MSCT lesion calcium score to predict stenosis severity of calcified lesions

Pugliese F, Hunink MGM, Meijboom WB, Gruszczynska K, Rengo M, Mollet NR, Weustink AC, Neefjes L, Dijkshoorn ML, Krestin GP, de Feyter PJ.

Manuscript to be submitted.

Summary

Purpose: To develop an algorithm for predicting ≥50% coronary stenoses based on segmental multislice computed tomography calcium score (MSCT CS) and clinical factors.

Materials and Methods: 402 patients underwent MSCT CS and conventional coronary angiography. CS and calcification morphology were assessed in individual coronary segments. In a derivation dataset, we explored the predictive value of segmental CS, morphology, patient's symptoms and risk factors.

Results: Spotty calcifications had an OR for stenosis 2.3-fold ($p < 0.001$) greater than the absence of calcifications, wide calcifications 2.7-fold ($p < 0.001$) greater, diffuse calcifications 4.6-fold ($p < 0.001$) greater. In middle segments, each unit of CS had an OR 1.2-fold ($p < 0.001$) greater than in distal segments; in proximal segments the OR was 1.1-fold greater ($p = 0.021$). The OR was 1.8-fold greater ($p = 0.006$) in patients with typical chest pain, 2-fold ($p = 0.014$) greater in patients with acute coronary syndromes, 2-fold greater ($p < 0.001$) in patients with prior myocardial infarction. The ROC curve area of the prediction rule was 0.795 (0.95 confidence interval: 0.602-0.843). Validation in a validation dataset yielded similar results.

Conclusion: In conjunction with calcification morphology, anatomical location, patient's symptoms and risk factors, MSCT segmental CS can predict coronary stenosis.

Introduction

The quantification of the total amount of coronary calcification (calcium score) by electron beam tomography (EBT) or multislice computed tomography (MSCT) is

useful for predicting the presence of angiographically significant (≥50% diameter reduction) coronary artery stenoses at the patient level (1-4). A calcium score ≥200 provides strong evidence of obstructive coronary artery disease in patients ≥50 years old, and a calcium score of 0 provides strong evidence about the absence of obstructive coronary artery disease (3). However, intermediate calcium scores are less useful in clinical practice. Moreover, the total calcium score does not provide information regarding the probability of stenosis at the level of a specific coronary segment or lesion. In these cases, contrast-enhanced MSCT coronary angiography (MSCT-CA) may be a beneficial next step. Unfortunately, coronary calcifications hinder the visualization of the coronary lumen at MSCT-CA ("blooming effect"), thus the evaluation of stenosis severity in calcified vessels is often impossible using MSCT-CA.

The purpose of this study was to assess the relationship between coronary calcification and the degree of luminal narrowing at the same site. We constructed an algorithm to facilitate the prediction of angiographically significant stenosis in symptomatic patients undergoing MSCT calcium score. The algorithm consists of a multivariable prediction rule which includes the MSCT calcium score measured in a given coronary segment, the patient's symptoms and risk factors in order to calculate the probability of significant coronary artery stenosis in the same coronary segment.

Materials and Methods

Patients

During a 24-month period, 402 patients with stable or acute chest pain were recruited to an ongoing study at our institution comparing 64-MSCT-CA with conventional coronary angiography (CCA). Patients in sinus heart rhythm, able to hold their breath for 15 seconds, and without previous percutaneous coronary intervention or coronary bypass surgery were included. Impaired renal function (serum creatinine >120 μmol/L) and known intolerance to iodinated contrast were exclusion criteria. The study protocol was approved by the Institutional Review Board and was in accordance with the declaration of Helsinki. Particular attention was paid to the additional radiation dose. All patients consented to undergo MSCT before CCA after being informed of the additional radiation dose. They also consented on the use of their data for future retrospective research.

Preparation and Coronary Artery Calcium Scans

Patients with heart rates >65 beats per minute (bpm) received 100 mg metoprolol (Selokeen, Astra Zeneca, London, United Kingdom) orally 1 hour before the scan. Scans were performed with a 64-slice CT scanner with a gantry rotation time of 330 ms, a temporal resolution of 165 ms and a minimal spatial resolution of 0.4 mm3 (Sensation 64; Siemens, Forchheim, Erlangen, Germany). The non-enhanced coronary calcium scans were acquired with a standard spiral low-dose protocol using ECG-gating. Scan parameters were as follows: 32*2 slices per rotation; individual detector width of 0.6 mm, 330 ms rotation time, 3.8 mm/rotation table feed, 120 kV tube voltage, 150 mAs tube current, with activated prospective x-ray tube modulation. Overlapping slices were reconstructed at 65% of the R-R interval (retrospective ECG-gating) using B35f convolution kernel. Reconstructed slice thickness was 3.0 mm with an increment of 1.5 mm. The radiation exposure, estimated using dedicated software (ImPACT, version 0.99x, St. George's Hospital, Tooting, London, United Kingdom), was 1.4 mSv in men and 1.8 mSv in women.

MSCT-CA Scans

For the MSCT-CA studies, 95 ml of contrast agent (iomeprol; Iomeron, 400 mg/ml; Bracco, Milan, Italy) were injected intravenously into an antecubital vein. The injection rate was 5 ml/s. A bolus-tracking technique was used to monitor the arrival of contrast in the coronary arteries (5, 6). Scan parameters were identical to those used for coronary calcium scanning except for a tube current of 900 mAs. Datasets were reconstructed using retrospective ECG gating and a mono-segmental reconstruction algorithm, as previously described (5, 6).

Conventional Coronary Angiography (CCA)

MSCT and CCA were carried out within a time interval of 1 week. A single observer (>10-year experience) identified coronary segments on CCA following a 17-segment modified American Heart Association (AHA) classification model (7). Stenoses were classified as significant if the mean luminal narrowing was ≥50% using validated quantitative coronary angiography (QCA) software (CAAS II®, Pie Medical, Maastricht, the Netherlands).

Segmental Calcium Score (CS) and Morphology

MSCT datasets were analyzed using an off-line workstation (syngo MultiModality Workplace VE25A, Siemens, Erlangen, Germany). Dedicated software (syngo Calcium Scoring VE31H, Siemens, Germany) was used for measuring calcium score (CS) in non-enhanced scans (8). One experienced observer,

unaware of the CCA results, measured CS in individual coronary segments using a standard technique based on seed points and a region growing algorithm. Results were expressed using the Agatston (9), volume (10) and mass (11) scores.

In order to obtain a consistent classification of the coronary tree into segments, contrast-enhanced MSCT-CA axial images were available to the observer (Figure 1). The MSCT-CA images were scrolled using a viewing application (syngo Viewing, Siemens, Erlangen, Germany). Availability of MSCT-CA ensured the visualization of the origin of smaller side branches, especially when they were not calcified. These side branches might have remained undetected on the non-enhanced images. The visualization of the diagonal branches allowed the classification into segments of the left anterior descending coronary artery (LAD); the origin of marginal obtuse branches allowed the classification into segments of the left circumflex artery (LCx), and the origin of acute marginal branches allowed the classification into segments of the right coronary artery (RCA). MSCT-CA was used only for anatomical classification and not for CS measurement. CS was measured on non-enhanced images in accordance to clinical practice (8). To assign calcifications to the corresponding coronary segment, there needed to be separation of connected lesions in a slice (12). To achieve this, calcifications were edited manually slice-by-slice and split using the '3D Edit' function of the software (Figure 2).

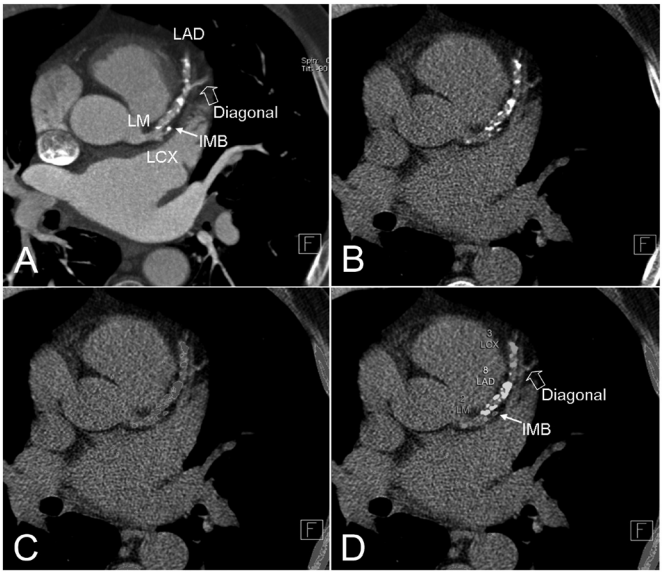

FIGURE 1. Measurement of calcium score at the segment level
To classify coronary segments consistently, contrast-enhanced MSCT-CA axial images (A) were available to the observer. Side branches, especially if non-calcified, could have been difficult to detect on non-enhanced images (B, C). Because the quantification software did not allow labelling of the 17 coronary segments individually, the 4 available labels (named as the 4 major coronary vessels) were used interchangeably and applied to coronary segments (D). LM = left main artery; LAD = left anterior descending artery; LCx = left circumflex; IMB = intermediate branch.
(A full color version of this illustration can be found in the color section)

In each segment, calcification morphology was classified as spotty, wide or diffuse (Figure 3) based on the width and length of the calcification in relation to the coronary segment diameter, following the classification model described in Table 1 (12). In the event of multiple calcifications with different morphology within the same segment, the segment was classified as the calcification with the largest size.

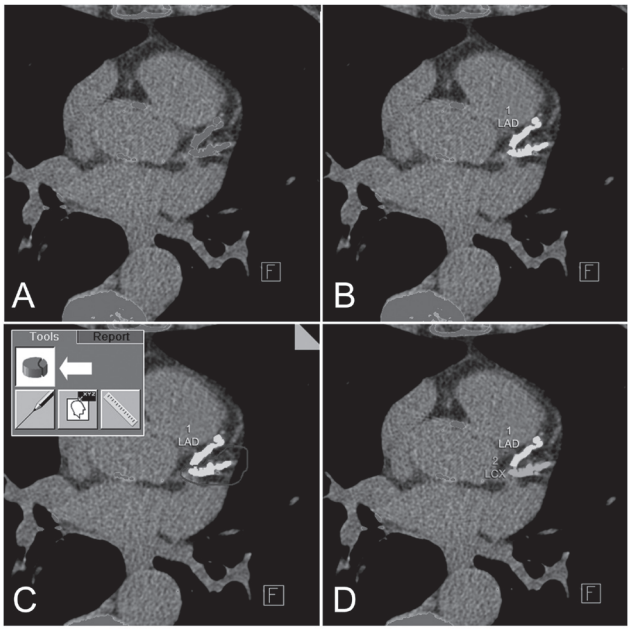

FIGURE 2. Method for separation of connected calcifications in a slice
To assign calcifications to the corresponding individual coronary artery segment, there needed to be separation of connected lesions in a slice (A, B). To achieve this, calcifications were edited manually (C) and split (D) using the '3D Edit' function (C, insert and arrow) of the software (syngo Calcium Scoring).
LAD = left anterior descending artery; LCx = left circumflex.
(A full color version of this illustration can be found in the color section)

Statistical Analysis

Statistical analysis was performed using commercially available software (SPSS, version 12.1. SPSS Inc., Chicago, IL., and STATA/SE 10.0, College Station, TX). Quantitative variables were expressed as means (standard deviations) and categorical variables were expressed as frequencies or percentages. The level of significance was chosen at a p-value <0.05.

The dataset was split into two equal datasets. Data from the first 201 patients were used to identify highly correlated variables, to explore the predictive value of the variables and to derive a multivariable prediction rule. There was a high correlation between the Agatston and the volume score (Pearson r = 0.990; $p < 0.001$), the Agatston and the mass score (r = 0.995; $p < 0.001$) and the volume and the mass score (r = 0.989; $p < 0.001$). We used the Agatston score for further analyses because it has been extensively validated in clinical practice (1-4, 9). Using the derivation dataset, we determined the frequency of significant stenoses at the segment level, according to ranges of segmental CS and calcifica-

TABLE 1. Classification of calcification morphology on non-enhanced MSCT images - modified from (12)

Calcification morphology	Lesion width [a]		Lesion length [b]
Diffuse	≥2/3 of coronary diameter		≥3/2 of coronary diameter
Wide	≥2/3 of coronary diameter	or	<3/2 of coronary diameter
	<2/3 of coronary diameter		≥3/2 of coronary diameter
Spotty	<2/3 of coronary diameter		<3/2 of coronary diameter
None	Undetectable		Undetectable

a Extent of calcification perpendicular to the longitudinal direction of the vessel
b Extent of lesion in the longitudinal direction of the vessel

tion morphology. The natural log transforms of (CS + 1) were used because CS showed a skewed distribution. Categorical variables were compared with the chi-squared statistic. We also obtained receiver-operating characteristic (ROC) curves with luminal narrowing ≥50% at CCA as the reference standard to define positive cases. The prediction rule was then validated in the second set of 201 patients. The outcome of interest was the prediction of angiographically verified significant (≥50% diameter reduction) stenoses at the segment level.

The data was clustered implying that potential correlation existed between the multiple (seventeen) segments analyzed per patient. To adjust for the clustered nature of the data, we used generalized estimating equations (binomial family, logit link function, exchangeable correlation

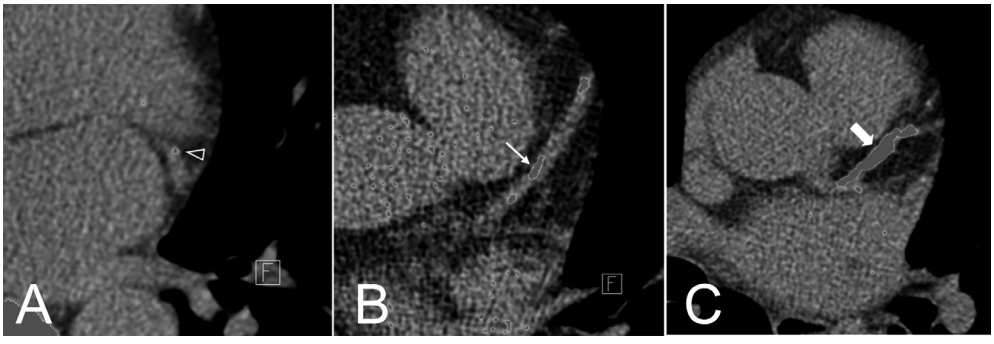

FIGURE 3. Calcification morphology.
Calcification morphology was classified as spotty (A, arrowhead), wide (B, arrow) and diffuse (C, gross arrow) based on the width and length of the calcification in relation to the coronary segment diameter (Table 1).
(A full color version of this illustration can be found in the color section)

matrix, and robust –sandwich– standard errors adjusted for clustering on patient identification). We performed univariable analyses to evaluate the significance of the Agatston CS in each segment, calcification morphology, segment location (proximal, middle, and distal/side branches, as previously described (13)), major coronary vessel (RCA, LAD, LCx, LM), age, gender, patient's symptoms (typical chest pain/atypical chest pain/acute coronary syndrome) and risk factors (obesity, hypertension, smoking, diabetes mellitus, hypercholesterolemia, prior myocardial infarction, family history). Variables with a p-value <0.10 in the univariable analyses were entered in the multivariable model. Interaction terms were explored between morphology and CS, location and CS, location and morphology, vessel and CS, and vessel and morphology. The final multivariable model included all variables with a p-value <0.05 and variables with a p-value<0.10 that were considered to be important based on clinical judgment and internal consistency of the model. Odds ratios (OR) and robust 95% confidence intervals (CI) are reported.

A prediction score was calculated based on the coefficients of the final multivariable model, and was subsequently validated in the second dataset. For both the derivation and validation dataset we report the area under the curve (AUC) with its 95% confidence interval (CI) as summary measure of the performance. To adjust for the clustered nature of the data, the 95% CI of the AUC was obtained with 1000 bootstrap samples using patient identification as clustering variable.

Results

Baseline Characteristics and Angiographic Findings (Table 2)

In the derivation dataset, 126/201 (62.7%) patients had at least one ≥50% stenosis (Table 2). The mean (standard deviation) calcium score was 450.37 (661.23). Thirty/201 (14.9%) patients did not show any detectable calcification. Of these, 4/30 (13.3%) had at least one significant stenosis. A total of 3001 coronary segments were visualized angiographically. Of these, 136/3001 (4.5%) were localized distally to occluded coronary segments and supplied by collateral pathways. These segments were excluded from the analysis. There remained 2865 coronary segments, of which 282/2865 (9.8%) harboured ≥50% stenoses. Among the lesions associated with significant stenosis, 89/282 (31.6%) were in the RCA, 110/282 (39%) in the LAD, 79/282 (29%) in the LCx, and 4/282 (1.4%) in the LM ($p<0.001$).

TABLE 2. Baseline characteristics

Characteristic	Development sample	Validation sample	p-value [e]
No. of patients	201	201	-
Age			
Mean age (sd) [a] (years)	59 (12)	60 (10)	0.52 [f]
Age range	21-87	35-80	-
Age groups: no. (%)	-	-	0.81
≤50	38/201 (19%)	33/201 (17%)	-
51-60	79/201 (39%)	80/201 (40%)	-
61-70	50/201 (25%)	57/201 (28%)	-
>70	34/201 (17%)	31/201 (15%)	-
Men / Women: no. (%)	142 (71%) / 59 (29%)	137 (68%) / 64 (32%)	0.59
Patient clinical presentation: no. (%)			
Typical chest pain [b]	97/201 (48%)	57/201 (28%)	<0.001
Atypical chest pain [c]	71/201 (35%)	76/201 (38%)	0.61
Acute coronary syndrome [d]	33/201 (17%)	68/201 (34%)	<0.001
Cardiovascular risk factors: no. (%)			
Obesity (Body Mass Index ≥30 Kg/m^2)	48/201 (24%)	50/201 (25%)	0.84
Smoking	63/201 (31%)	66/201 (33%)	0.75
Hypertension	106/201 (53%)	110/201 (55%)	0.69
Dyslipidemia (serum cholesterol >200 mg/dL or 5.18 mmol/L)	136/201 (68%)	100/201 (50%)	<0.001
Diabetes mellitus (plasma glucose ≥126 mg/dL or 7.0 mmol/L)	25/201 (12%)	26/201 (13%)	0.88
Family history	90/201 (45%)	106/201 (53%)	0.11
Prior myocardial infarction	43/201 (21%)	21/201 (11%)	0.003
Medication before MSCT and heart rate			
Beta-blockers: no. (%)	142/201 (71%)	135/201 (67%)	0.11
Mean heart rate during scan (sd) [a] (beats/min.)	58 (11)	60 (8)	0.77
Total calcium score (Agatston; patient level)			
Range	0-3839	0-3394	-
Mean (sd) [a]	450.37 (661.23)	346.60 (492.02)	0.70 [f]
Median	198.10	214.70	-
Calcium score groups: no. (%)	-	-	0.79
0-10	50/201 (25%)	47/201 (23%)	-
11-100	32/201 (16%)	32/201 (16%)	-
101-400	59/201 (29%)	68/201 (34%)	-
>400	60/201 (30%)	54/201 (27%)	-

a standard deviation
b retrosternal pain occurring with exercise, relieved by rest and administration of nitrates
c any 2 or 1 features of typical chest pain
d unstable angina or non-ST elevation myocardial infarction
e Chi squared test unless otherwise specified
f Mann-Whitney U test

TABLE 3. Frequency of significant stenoses in relation to segmental CS ranges and morphology (in men and women according to age)

	CS					Calcification morphology				
	0-10	**11-50**	**51-100**	**>100**	**p-value***	**none**	**spotty**	**wide**	**diffuse**	**p-value***
Men										
≤50	16/384 (4.2%)	2/17 (11.8%)	0/2 (0%)	1/4 (25%)	0.114	11/328 (3.4%)	5/58 (8.6%)	1/13 (7.7%)	2/8 (25%)	**0.012**
51-60	43/623 (6.9%)	20/11 (18%)	12/63 (19%)	25/71 (35.2%)	**<0.001**	20/495 (4%)	20/140 (14.3%)	20/113 (17.7%)	40/120 (33.3%)	**<0.001**
61-70	13/260 (5%)	6/59 (10.2%)	9/35 (25.7%)	26/89 (29.2%)	**<0.001**	7/198 (3.5%)	5/63 (7.9%)	14/70 (20%)	28/112 (25%)	**<0.001**
>70	20/162 (12.3%)	8/39 (20.5%)	4/36 (11.1%)	15/49 (30.6%)	**0.016**	12/117 (10.3%)	7/48 (14.6%)	8/57 (14%)	20/64 (31.3%)	**0.003**
Women										
≤50	4/139 (2.9%)	0/6 (0%)	0/2 (0%)	value not observed	0.888	3/130 (2.3%)	1/13 (7.7%)	0/3 (0%)	0/1 (0%)	0.703
51-60	3/234 (1.3%)	0/10 (0%)	2/99 (22.2%)	3/4 (75%)	**<0.001**	3/211 (1.4%)	0/24 (0%)	2/11 (18.2%)	3/11 (27.3%)	**<0.001**
61-70	16/209 (7.7%)	7/39 (17.9%)	1/14 (7.1%)	5/14 (35.7%)	**0.003**	8/170 (4.7%)	6/48 (12.5%)	5/31 (16.1%)	10/27 (37%)	**<0.001**
>70	7/114 (6.1%)	4/35 (11.4%)	2/8 (25%)	8/24 (33.3%)	**0.001**	4/86 (4.7%)	5/37 (13.5%)	4/27 (14.8%)	8/31 (25.8%)	**0.014**

* Chi squared test. Significant p-values are **bolded**

Segmental CS

In the derivation dataset, the range in segmental CS was 0-1370. The mean (standard deviation) was 29.80 (88.40). The median was 0. There were 1735/2865 (60.6%) segments which did not show any detectable calcification (segmental CS = 0). Of these, 68/1735 (3.9%) harboured a significant stenosis.

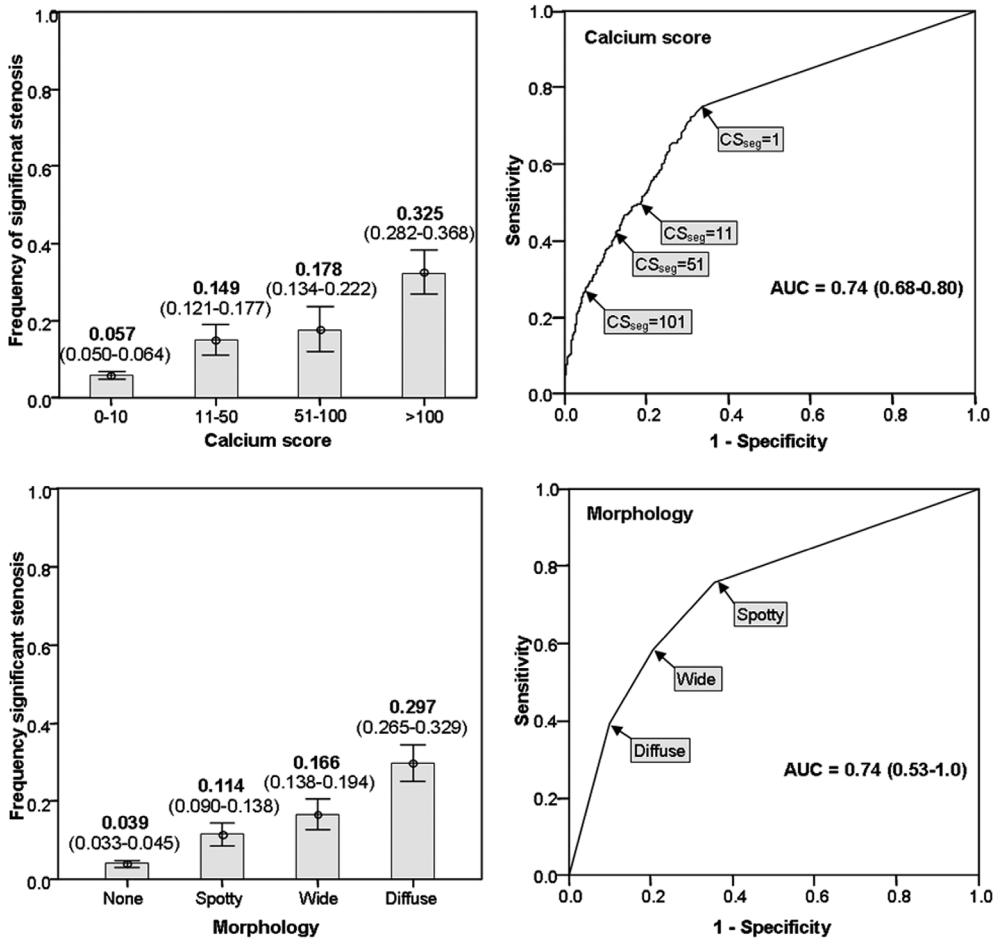

FIGURE 4. Segmental CS and morphology: frequency of associated significant stenoses (left column) and ROC curves (right column)
The frequency of coronary stenosis (left column) increased proportionally with increasing CS. The frequency of stenosis also increased from spotty, to wide, to diffuse morphology. The diagnostic performances of CS and morphology in the detection of significant stenosis (right column) were similar (both AUC's = 0.74). Arrows and labels indicate different thresholds for significant coronary artery stenosis.

TABLE 4. Univariable logistic regression models for the prediction of angiographically proven significant coronary stenosis

Characteristic	Odds Ratio (95% CI)	p-value*
Age	1.032 (1.015-1.0494)	**<0.001**
Gender (male)	1.629 (1.086-2.445)	**0.018**
Typical chest pain	1.694 (1.178-2.438)	**0.005**
Atypical chest pain	0.340 (0.214-0.538)	**<0.001**
Acute coronary syndrome	1.625 (1.068-2.472)	**0.023**
Obesity	0.986 (0.679-1.432)	0.941
Smoking	1.069 (0.755-1.513)	0.708
Hypertension	1.098 (0.763-1.579)	0.615
Dyslipidemia	2.606 (1.523-4.459)	**<0.001**
Diabetes	0.819 (0.513-1.307)	0.402
Family history of CAD	0.781 (0.550-1.108)	0.166
Prior myocardial infarction	2.537 (1.776-3.623)	**<0.001**
Segment location**		
Distal and side branches	odds ratio comparator	
Middle	2.545 (1.913-3.386)	**<0.001**
Proximal	1.777 (1.272-2.483)	**0.001**
Vessel		
RCA	odds ratio comparator	
LAD	0.995 (0.718-1.379)	0.976
LCx	0.722 (0.529-0.984)	**0.039**
LM	0.150 (0.054-0.416)	**<0.001**
CS (ln)	1.500 (1.399-1.604)	**<0.001**
Calcification morphology		
Spotty	2.732 (1.898-3.934)	**<0.001**
Wide	4.269 (2.836-6.427)	**<0.001**
Diffuse	9.144 (6.297-13.277)	**<0.001**

*Significant p-values are bolded
** Proximal segments included segments 1, 5, 6, and 11. Middle segments included segments 2, 3, 7, and 13. Distal and side branches included segments 4a, 4b, 8, 9, 10, 12, 14, 15, and 16 (7, 13).

Calcification Morphology

In the derivation dataset, there were 431/2865 (15%) spotty calcifications, 325/2865 (11.3%) wide calcifications, and 374/2875 (13.1%) diffuse calcifications.

Frequency of Significant Stenoses

The frequency of coronary stenosis increased proportionally with increasing CS (Figure 4, left column), and from spotty, to wide, to diffuse morphology (all p-val-

ues <0.01). The frequency of significant stenoses associated with CS and morphology in men and women according to age is given in Table 3.

The AUCs for the detection of ≥50% coronary stenosis were 0.74 (CI: 0.71-0.77) for CS, and 0.74 (CI: 0.71-0.77) for calcification morphology (Figure 4, right column).

Univariable Analysis (Table 4)

The odds ratio (OR) for significant stenosis was approximately 1.7-fold (p = 0.005) greater for patients with typical chest pain, and 1.6-fold (p = 0.023) greater for patients with unstable angina or non-ST elevation myocardial infarction (acute coronary syndrome). For patients with dyslipidemia, the OR was increased 2.6-fold (p <0.001), and for patients with a prior myocardial infarction the OR was increased 2.5-fold (p<0.001). With distal segments as comparator, the OR for significant stenosis was approximately 1.6-fold (p<0.001) greater for middle segments, and 1.8-fold (p=0.001) greater for proximal segments. With the RCA as comparator, the OR was approximately 0.7-fold (p = 0.039) smaller for the LCx, and 0.2-fold (p <0.001) smaller for the LM; the OR for the LAD was similar. For each unit of natural log of segmental CS, the OR of significant stenosis was 1.5-fold (p <0.001) greater. The presence of spotty calcifications had an OR for stenosis approximately 2.7-fold (p <0.001) greater than the absence of calcification, wide calcifications approximately 4.3-fold (p <0.001) greater, and diffuse calcifications approximately 9.1-fold (p <0.001) greater than the absence of calcification.

Multivariable Analysis (Table 5)

In a multivariable model, the OR for coronary stenosis was approximately 1.8-fold greater (p = 0.006) in patients with typical chest pain, 2-fold (p = 0.014) greater in patients with acute coronary syndrome, and 2-fold greater (p <0.001) in patients with prior myocardial infarction. The presence of spotty calcifications had an OR for stenosis approximately 2.3-fold (p <0.001) greater than the absence of calcification, wide calcifications approximately 2.7-fold (p <0.001) greater, and diffuse calcifications approximately 4.6-fold (p <0.001) greater than the absence of calcification. With distal segments as comparator, each unit of natural log of CS in middle segments corresponded to an OR approximately 1.2-fold (p <0.001) greater; in proximal segments this corresponded to an OR 1.1-fold greater (p = 0.021). The LM coronary artery had an OR for stenosis approximately 0.2-fold (p = 0.001) smaller than the RCA, whereas the remaining coronary vessels were similar.

TABLE 5. Multivariable logistic regression (final) model for the prediction of angiographically proven significant coronary stenosis

Model*	Odds Ratio (95% CI)	p-value**	Coefficient
Clinical presentation			
Typical chest pain	1.755 (1.175-2.622)	**0.006**	0.562
Acute coronary syndrome	1.989 (1.151-3.439)	**0.014**	0.688
Risk factors			
Prior myocardial infarction	1.982 (1.397-2.812)	**<0.001**	0.684
Vessel			
LM	0.169 (0.059-0.482)	**0.001**	-1.776
Calcification morphology			
Spotty	2.303 (1.567-3.384)	**<0.001**	0.834
Wide	2.690 (1.698-4.260)	**<0.001**	0.989
Diffuse	4.614 (2.842-7.491)	**<0.001**	1.529
CS (ln)			
If middle segment	1.189 (1.084-1.304)	**<0.001**	0.173
If proximal segment	1.125 (1.018-1.242)	**0.021**	0.117

*The model Wald chi-square was 226.32 (p <0.001)
**Significant p-values are bolded

Prediction Score (also see Appendix)

Based on the coefficients (multiplied by 100) of the final multivariable model (Table 5), a score for the prediction of significant stenosis in a given segment (SCORE) was calculated as follows:

*SCORE = 12*ln(CS) (if proximal) + 17*ln(CS) (if middle) + 83 (if spotty) + 99 (if wide) + 153 (if diffuse) + 56 (if typical chest pain) + 69 (if acute coronary syndrome) + 68 (if prior myocardial infarction) -178 (if LM) -362*

The probability of significant coronary stenosis increased with the extent (i.e., CS, morphology) of coronary calcification. This probability is related to the SCORE through the following equation:

Probability (significant stenosis) = 1 / [1 + exp (- SCORE)]

(Figure 5) (also see Appendix for an electronic 'SCORE calculator', Figure 6)

Derivation and Validation Datasets

Derivation and validation datasets revealed similar results. The AUC for the derivation set was 0.795 (CI: 0.602-0.843); the AUC for the validation set was 0.783 (CI: 0.598-0.827).

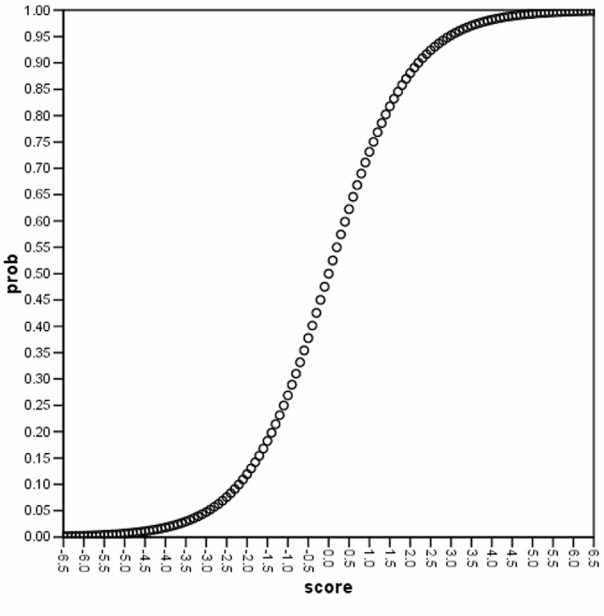

FIGURE 5. Continuous probabilistic prediction of significant coronary artery stenosis.
By entering the SCORE on the x axis, the associated probability of significant stenosis in the same coronary segment can be read on the y axis (see excel spreadsheet – supplemental file, Figure 6). SCORES < (-6.5) (not plotted) are associated with a negligible probability of significant stenosis; SCORES > 6.5 (not plotted) are associated with near certainty of significant stenosis.

Discussion

Calcification overrepresentation is a major limitation to MSCT-CA, which is mainly due to the limited spatial resolution. Calcification overrepresentation is generally referred to as 'blooming effect', and is frequently associated with beam hardening and partial volume artefacts. Calcification overrepresentation limits the visualization of adjacent structures and often yields overestimation of the severity of stenosis (false positive diagnoses). Sharp convolution kernels for image reconstruction partially compensate for the blooming effect, however this comes at the expense of increased image noise. Also several deconvolution filters have been developed with the goal of reducing the blooming effect without increasing image noise (14). These filters are based on iterative measurements, require long computational processing times and have not been validated in clinical practice. The introduction of dual source MSCT scanners and the 'dual energy' scan technique allow the acquisition of separate low- and high-energy images which are then synthesized in order to cancel high-density structures such as calcifications (15). However, the applicability of this technique to coronary imaging has not been evaluated yet. Therefore, MSCT-CA in calcified coronary arteries remains a diagnostic challenge. This study describes a practical approach to overcome such limitation of MSCT-CA,

Location	
Segmental Calcium Score (Agatston)	
Proximal lesion	0
Middle lesion	168
	1/0
Left Main	0
Morphology	
	1/0
Spotty	0
Long or Wide	0
Diffuse	1
Simptoms & Risk Factors	
	1/0
Typical chest pain	1
Acute coronary sindrome	0
Prior myocardial infarction	1
Score	2.208278154
Probability	0.900990433

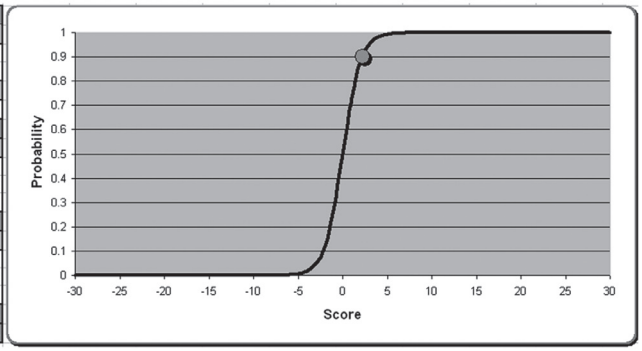

FIGURE 6. Electronic SCORE calculator. Discrete values of Segmental Calcium Score (Agatston) must be entered in the cell corresponding to the appropriate segment location (Proximal or Middle; leave blank if Distal). Location in the LM, calcification morphology, patient's symptoms and risk factors (i.e., history of myocardial infarction) must be selected by filling either 1 = feature applies, or 0 = feature does not apply, in the corresponding cells.

facilitate diagnostic decision making and potentially reduce the number of false positive diagnoses.

We found that the probability of significant coronary stenosis associated to a given coronary calcification increased proportionally with the lesion CS, and from the spotty, to the wide, to the diffuse morphological patterns (Figure 4, left column). This is consistent with the findings of Lau et al. (16) and Kajinami et al.(12). However, our results revealed that for both CS and morphology the use of a high-specificity threshold was associated with a much lower sensitivity for the detection of significant coronary artery stenosis, and a high-sensitivity threshold was associated with a much lower specificity (Figure 4, right column). This implies that the amount and pattern of calcification of a given lesion, when considered per se, are probably rather crude parameters for the presence of an underlying significant stenosis. The most likely mechanism to explain this finding is the compensatory enlargement of atherosclerotic coronary arteries (positive remodeling) (17).

Nevertheless, by combining patient's symptoms, clinical history and lesion location within the coronary tree, the predictive value of CS and calcification morphology observed in a given segment could be improved. The CS is influenced by lesion location because the coronary artery diameter shows a wide variation depending on location. This also suggests the potential merit of morphologic evaluation additional to CS. Characteristics such as the type of chest pain and the history of prior myocardial infarction are important because the way we interpret MSCT-CA studies in daily practice is heavily influenced by the clinical context.

It can be argued that a diagnostic benefit from a complementary use of segmental CS to MSCT-CA cannot be expected in all lesions. Firstly, not all coronary lesions associated with significant stenosis are calcified. Secondly, there will be situations in which segmental CS will yield intermediate probability values. In a hypothetical patient with typical chest pain, prior myocardial infarction, a calcified lesion with diffuse pattern in the middle LAD, and a CS measured in that lesion of 148, the SCORE for the middle-LAD lesion will be:

$$SCORE = [17*ln(148)] + 153 + 56 + 68 - 362 = 0.07 \approx 0$$

A SCORE ≈ 0 corresponds to a probability of significant stenosis of ≈ 50% (Figure 5), which may not be very helpful for clinical decision making (presence and absence of significant stenosis are equally likely). However, because the SCORE proposed in this study was calculated as a function of the natural log transform of lesion CS (skewed distribution), the interval of CS associated to intermediate probabilities of coronary artery stenosis is quite narrow. Indeed, in the same patient, if the lesion had a CS of 158, the probability of significant stenosis would be ≈ 75% (significant stenosis is likely present). If the same lesion had a CS of 118 the probability of stenosis would be <5% (significant stenosis is unlikely present). These probabilities may be more helpful to support decision making.

Limitations of our study include the fact that the Agatston CS is not a physical measurement of calcification (9). However, as opposed to the other scores, the Agatston CS is commonly used in clinical practice. Moreover, we found a very high correlation between the Agatston and the volume/mass scores. Also, CS underestimates coronary plaque burden because it does not include non-calcified plaque. The measurement of coronary plaque burden by MSCT was beyond the purpose of our study. Although early studies (18, 19) have shown that measuring the plaque burden by MSCT is feasible, the robustness and the clinical implications of these methods are to be evaluated.

Conclusion

We developed a practical method which uses a major limitation to MSCT-CA (i.e., coronary calcification) to improve the ability of this technique to predict the presence of significant coronary stenosis and reduce the number of false positives. Further research is warranted to define in which patient population the analysis of segmental CS additional to MSCT-CA may be beneficial for improving the diagnostic performance.

CHAPTER 14

References

1. Budoff MJ, Diamond GA, Raggi P, Arad Y, Guerci AD, Callister TQ, Berman D. Continuous probabilistic prediction of angiographically significant coronary artery disease using electron beam tomography. Circulation 2002; 105(15):1791-1796.
2. Haberl R, Becker A, Leber A, Knez A, Becker C, Lang C, Bruning R, Reiser M, Steinbeck G. Correlation of coronary calcification and angiographically documented stenoses in patients with suspected coronary artery disease: results of 1,764 patients. J Am Coll Cardiol 2001; 37(2):451-457.
3. Bielak LF, Rumberger JA, Sheedy PF, 2nd, Schwartz RS, Peyser PA. Probabilistic model for prediction of angiographically defined obstructive coronary artery disease using electron beam computed tomography calcium score strata. Circulation 2000; 102(4):380-385.
4. Breen JF, Sheedy PF, 2nd, Schwartz RS, Stanson AW, Kaufmann RB, Moll PP, Rumberger JA. Coronary artery calcification detected with ultrafast CT as an indication of coronary artery disease. Radiology 1992; 185(2):435-439.
5. Meijboom WB, Weustink AC, Pugliese F, van Mieghem CA, Mollet NR, van Pelt N, Cademartiri F, Nieman K, Vourvouri E, Regar E, Krestin GP, de Feyter PJ. Comparison of diagnostic accuracy of 64-slice computed tomography coronary angiography in women versus men with angina pectoris. Am J Cardiol 2007; 100(10):1532-1537.
6. Mollet NR, Cademartiri F, van Mieghem CA, Runza G, McFadden EP, Baks T, Serruys PW, Krestin GP, de Feyter PJ. High-resolution spiral computed tomography coronary angiography in patients referred for diagnostic conventional coronary angiography. Circulation 2005; 112(15):2318-2323.
7. Austen WG, Edwards JE, Frye RL, Gensini GG, Gott VL, Griffith LS, McGoon DC, Murphy ML, Roe BB. A reporting system on patients evaluated for coronary artery disease. Report of the Ad Hoc Committee for Grading of Coronary Artery Disease, Council on Cardiovascular Surgery, American Heart Association. Circulation 1975; 51(4 Suppl):5-40.
8. Budoff MJ, Achenbach S, Blumenthal RS, Carr JJ, Goldin JG, Greenland P, Guerci AD, Lima JA, Rader DJ, Rubin GD, Shaw LJ, Wiegers SE. Assessment of coronary artery disease by cardiac computed tomography: a scientific statement from the American Heart Association Committee on Cardiovascular Imaging and Intervention, Council on Cardiovascular Radiology and Intervention, and Committee on Cardiac Imaging, Council on Clinical Cardiology. Circulation 2006; 114(16):1761-1791.
9. Agatston AS, Janowitz WR, Hildner FJ, Zusmer NR, Viamonte M, Jr., Detrano R. Quantification of coronary artery calcium using ultrafast computed tomography. J Am Coll Cardiol 1990; 15(4):827-832.
10. Callister TQ, Cooil B, Raya SP, Lippolis NJ,

Russo DJ, Raggi P. Coronary artery disease: improved reproducibility of calcium scoring with an electron-beam CT volumetric method. Radiology 1998; 208(3):807-814.

11. McCollough CH, Ulzheimer S, Halliburton SS, Shanneik K, White RD, Kalender WA. Coronary artery calcium: a multi-institutional, multimanufacturer international standard for quantification at cardiac CT. Radiology 2007; 243(2):527-538.
12. Kajinami K, Seki H, Takekoshi N, Mabuchi H. Coronary calcification and coronary atherosclerosis: site by site comparative morphologic study of electron beam computed tomography and coronary angiography. J Am Coll Cardiol 1997; 29(7):1549-1556.
13. Pugliese F, Mollet NR, Hunink MG, Cademartiri F, Nieman K, van Domburg RT, Meijboom WB, Van Mieghem C, Weustink AC, Dijkshoorn ML, de Feyter PJ, Krestin GP. Diagnostic performance of coronary CT angiography by using different generations of multisection scanners: single-center experience. Radiology 2008; 246(2):384-393.
14. Rollano-Hijarrubia E, Niessen W, Weinans H, van der Lugt A, Stokking R. Histogram-based selective deblurring to improve computed tomography imaging of calcifications. Invest Radiol 2007; 42(1):8-22.
15. Johnson TR, Krauss B, Sedlmair M, Grasruck M, Bruder H, Morhard D, Fink C, Weckbach S, Lenhard M, Schmidt B, Flohr T, Reiser MF, Becker CR. Material differentiation by dual energy CT: initial experience. Eur Radiol 2007; 17(6):1510-1517.
16. Lau GT, Ridley LJ, Schieb MC, Brieger DB, Freedman SB, Wong LA, Lo SK, Kritharides L. Coronary artery stenoses: detection with calcium scoring, CT angiography, and both methods combined. Radiology 2005; 235(2):415-422.
17. Glagov S, Weisenberg E, Zarins CK, Stankunavicius R, Kolettis GJ. Compensatory enlargement of human atherosclerotic coronary arteries. N Engl J Med 1987; 316(22):1371-1375.
18. Leber AW, Becker A, Knez A, von Ziegler F, Sirol M, Nikolaou K, Ohnesorge B, Fayad ZA, Becker CR, Reiser M, Steinbeck G, Boekstegers P. Accuracy of 64-slice computed tomography to classify and quantify plaque volumes in the proximal coronary system: a comparative study using intravascular ultrasound. J Am Coll Cardiol 2006; 47(3):672-677.
19. Sun J, Zhang Z, Lu B, Yu W, Yang Y, Zhou Y, Wang Y, Fan Z. Identification and quantification of coronary atherosclerotic plaques: a comparison of 64-MDCT and intravascular ultrasound. AJR Am J Roentgenol 2008; 190(3):748-754.

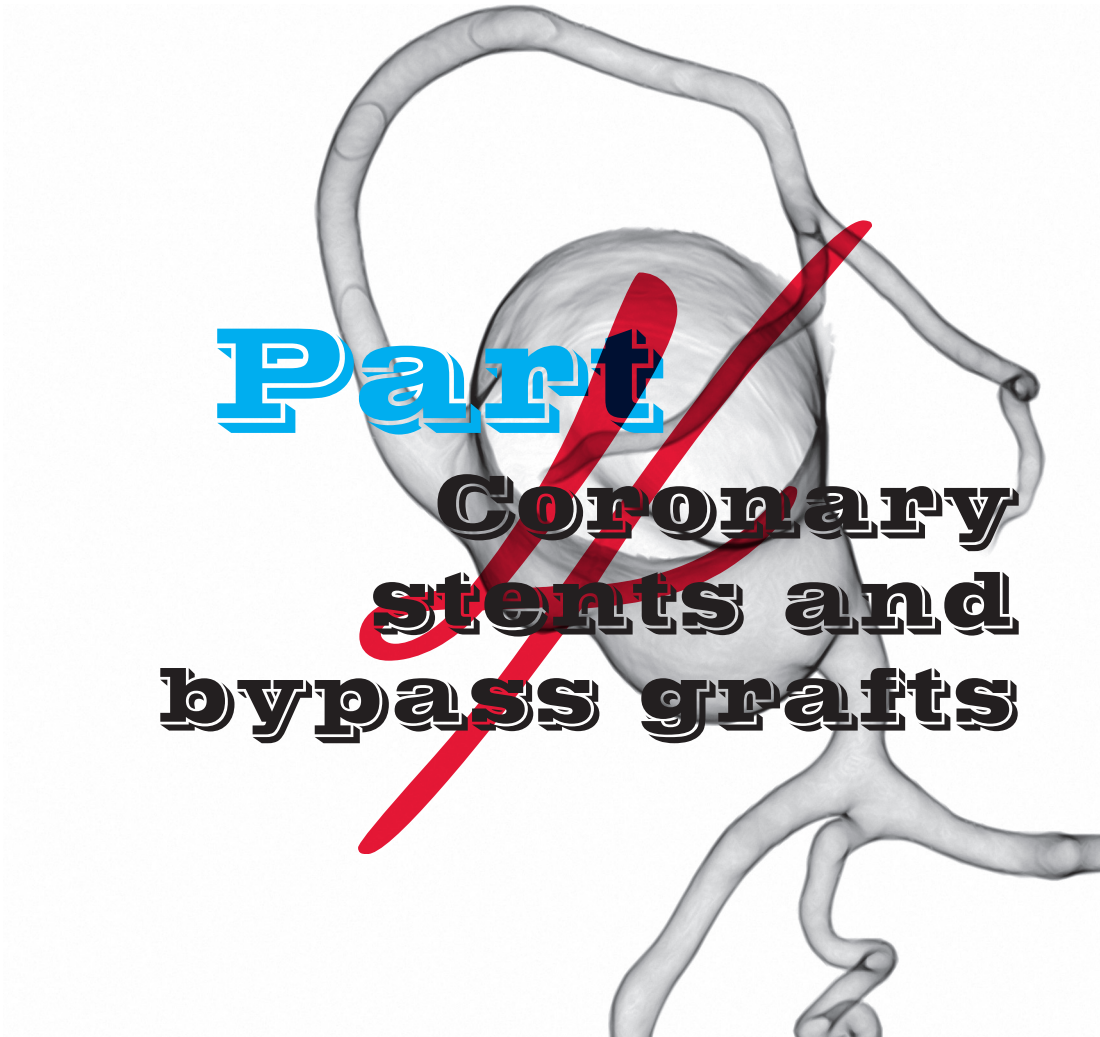

Part II

Coronary stents and bypass grafts

CHAPTER 15

Multislice computed tomography for visualization of coronary stents

Pugliese F, Cademartiri F, van Mieghem C, Meijboom WB, Malagutti P, Mollet NR, Martinoli C, de Feyter PJ, Krestin GP.

RadioGraphics 2006; 26:887-904.

Summary

Whereas the clinical diagnosis of in-stent thrombosis is straightforward, that of in-stent restenosis remains a problem, because although many patients experience chest pain after coronary stent placement, that symptom is secondary to ischemia in only a few. The use of a noninvasive technique to identify such patients for early invasive intervention versus more conservative management is thus highly desirable.

Multidetector computed tomography (CT) performed with 16-section scanners recently emerged as such a technique and has overtaken modalities such as electron-beam CT and magnetic resonance imaging as an alternative to conventional angiography for the assessment of in-stent restenosis.

The improved hardware design of the current 64-section CT scanners allows even better delineation of stent struts and lumen. The more reliable criterion of direct lumen visualization thus may be substituted for the presence of distal runoff, which lacks specificity for a determination of in-stent patency because of the possibility of collateral pathways. However, the capability to accurately visualize the in-stent lumen depends partly on knowledge of the causes of artifacts and how they can be compensated for with post-processing and proper image display settings. In addition, an understanding of the major stent placement techniques used in the treatment of lesions at arterial bifurcations is helpful.

Introduction

Over the past 25 years, catheter-based intervention has become the dominant form of coronary revascularization. Percutaneous coronary interventions are increasingly performed instead of coronary artery bypass graft surgery, even in patients with three-vessel disease or left

main coronary artery disease. The most important advance in the field of percutaneous coronary interventions was the introduction of coronary stent implantation in the 1990s, which led to reductions in both the risk of acute major complications and the incidence of restenosis, compared with the risks after balloon angioplasty (1,2). Although the use of recently introduced drug-eluting stents has resulted in even further reductions in the occurrence of restenosis, in-stent thrombosis and neointimal hyperplasia may still occur and cause partial or complete obstruction.

Whereas the clinical diagnosis of stent occlusion due to thrombosis is usually straightforward in patients with a recent stent implantation and with a subsequent onset of acute myocardial ischemia leading to acute myocardial infarction, the assessment of in-stent restenosis is more challenging. Restenosis occurs in approximately 10%–20% of patients with complex lesion characteristics (3).

Moreover, although several characteristics of high-risk populations have been described as clinical predictors, the likelihood of restenosis in a particular patient remains largely unpredictable (4 –7). For these reasons, conventional coronary angiography is still the technique of choice for the diagnosis of in-stent restenosis, although cardiac catheterization may involve major complications and is associated with moderate to high costs. Magnetic resonance (MR) angiography also can depict the coronary anatomy and help detect stenoses in the proximal segments of coronary arteries (8). However, metallic stents cause magnetic susceptibility artifacts that may prevent visualization of the lumen (9). Electron-beam computed tomography (CT) has been used more successfully to visualize coronary stents (10,11). Electron-beam CT is the modality with the shortest image acquisition times, namely 100 msec for a 3-mm-thick section suitable for morphologic interpretation and 50 msec for an 8-mm-thick section used for flow analysis without direct visualization of the in-stent lumen. However, image noise is extremely high with the first technique, and only severe, flow-limiting stenoses can be detected by using the flow technique. Thus, the occurrence of nonobstructive neointimal hyperplasia remains unnoticed at electron-beam CT. In addition, patients who undergo percutaneous coronary intervention may experience a progression of atherosclerosis in native coronary vessels without a stent implant, but electron-beam CT is suboptimal for monitoring such progression, because it requires the sequential triggered acquisition of multiple 3-mm-thick sections.

Hence, the latest generation of multidetector (multisection) CT scanners, which

offer a smaller voxel size, faster gantry rotation speed, and reconstruction of 64 sections per gantry rotation, provide an appealing alternative for noninvasive luminal assessment in patients with chest pain after coronary stent placement (12). The improved hardware configuration of 64-section CT scanners allows direct visualization of the stent struts and lumen for a more reliable assessment of in-stent patency than is allowed by the visualization of distal runoff. In symptomatic patients, multidetector CT may be used as a complement or a substitute for treadmill testing; because the latter lacks specificity, additional noninvasive investigations such as stress echocardiography and scintigraphy often are required before cardiac catheterization is undertaken. Multidetector CT also can be useful to assess the condition of the whole coronary tree, as it provides information about the number, severity, and location of coronary lesions. In the follow-up of asymptomatic patients after stent implantation, multidetector CT might help overcome the limited accuracy of treadmill testing to rule out restenosis and thus enable a reduction in the number of further examinations (ie, stress echocardiography, scintigraphy) needed because of a positive or inconclusive test result.

In this article, the capability of 64-section CT coronary angiography for the evaluation of in-stent patency is discussed. The authors provide explanatory illustrations of the major stent implantation techniques used to treat lesions at or near arterial branching points. They describe the CT features and artifacts that may be observed in or near stent implants on multiplanar reformatted images and volume-rendered images, the causes of those visual characteristics, and the postprocessing and image display methods that may be used to avoid or minimize artifacts.

Percutaneous Coronary Intervention And Stent Placement

Indications and Outcomes

The clinical indications for percutaneous coronary interventions cover the spectrum of ischemic heart disease, from unstable angina pectoris and acute myocardial infarction to silent ischemia, as summarized in the guidelines of the American College of Cardiologists and the American Heart Association (13). In patients with significant narrowing of a single coronary artery, the main benefit of revascularization is the relief of angina rather than an improvement of the already good prognosis with medical therapy. In contrast, in patients with significant left main coronary artery stenosis or multiple-vessel disease,

revascularization may both relieve angina and improve long-term survival.

Epidemiology

An estimated 1,204,000 inpatients underwent percutaneous coronary interventions in the United States in 2002, and coronary stent placement accounted for 537,000 of such procedures (14–16). More than 80% of percutaneous interventions that were performed in 2004 involved the placement of a drug-eluting stent coated with sirolimus or paclitaxel (17). The procedural success rate of percutaneous revascularization is higher than 90%, and the risk of sudden arterial occlusion and subsequent myocardial infarction is low (13). Despite contradictory reports (18), there is evidence that the long-term survival of patients who have undergone percutaneous revascularization for two- or three-vessel disease is no worse than that achieved with bypass graft surgery (19). Thus, percutaneous coronary intervention has become the preferred coronary revascularization strategy in many countries.

Coronary Stents

Coronary stents are expandable devices that are delivered to the coronary artery via catheter and then expanded to preserve the luminal diameter. The currently available stents are pre-mounted on dedicated delivery systems. Occurrences that may limit the success of stent implantation include in-stent restenosis and thrombosis, which may obstruct the flow through the stent.

Thrombosis

The frequency of in-stent thrombosis is low, with a cumulative incidence of 1.3%–1.7% at 9-month follow-up (20). However, even this incidence is clinically important because in-stent thrombosis is associated with high mortality and morbidity due to acute myocardial infarction. In the era of uncoated metallic stents, in-stent thrombosis typically occurred acutely (less than 48 hours after stent implantation) or sub-acutely (2–30 days after implantation). One of the current concerns about drug-eluting stents is the occurrence of delayed in-stent thrombosis that is manifested more than 30 days after stent implantation. This late manifestation may be related to delayed endothelialization of the stent and typically occurs when antiplatelet therapy is discontinued (21,22). In patients with additional risk factors (eg, renal failure, diabetes mellitus, or low ejection fraction), stents implanted at the level of coronary artery bifurcations are considered to present a higher risk of thrombosis (23). The same applies when very long stents are used, with a reported 1.03 relative risk of thrombosis for each 1-mm increase in length (20).

Restenosis

Restenosis, the major limitation to the long-term outcome of percutaneous coronary intervention, is defined as vessel lumen narrowing of more than 50% after angioplasty, with the resultant recurrence of angina. Restenosis is an iatrogenic process caused by an excessive arterial healing response to vessel injury associated with dilation. It results from the combined effects of elastic recoil (24), vascular remodeling (25), and neointimal hyperplasia (26). Coronary stents represent a mechanical approach to the prevention of restenosis by virtually eliminating elastic recoil and negative remodeling of the vessel after balloon dilation (26). The occurrence of neointimal hyperplasia is mainly responsible for the observed rates of restenosis,

which range from less than 10% with a drug-eluting stent to 40% with an uncoated metallic stent (1,2,27,28). For both stent types, excess stent length is associated with an increased risk of in-stent restenosis (29); thus, the arbitrary use of stents much longer than the actual lesion length is not advisable (30).

Drug-eluting Stents

Drug-eluting stents were developed to help prevent in-stent restenosis. Coating of a conventional metallic stent with an antiproliferative agent helps preserve the mechanical scaffolding properties of the stent; the drug is released locally, at the site of the vascular injury (31). The most extensive accumulated clinical experience to date is that with polymer-coated sirolimus- and paclitaxel-eluting stents. Favorable safety profiles and decreased restenosis rates have resulted in the widespread use of percutaneous coronary interventions and drug-eluting stents since their release in early 2003 (32–34). Ongoing developments in stent design include the creation of biodegradable, nonmetallic, and MR-compatible devices. Theoretically, a biodegradable drug-eluting stent may be the ideal solution to prevent in-stent restenosis. The response to vessel wall damage can be suppressed by the drug, while elastic recoil and negative remodeling are prevented by the stent. Eventually, the stent degrades, and chronic vessel injury related to the metal or polymer is thereby prevented (35).

Multidetector CT For Visualization Of Coronary Stents

Four- and 16-Detector Row CT Scanners

The diagnostic accuracy of electron-beam CT and multidetector CT performed with different generations of scanners is summarized in the Table. Whereas in-stent lumen evaluation with CT was almost impossible with four–detector row scan-

ners (36–38), the introduction of 16–detector row scanners (in combination with dedicated convolution filters) made CT a much more viable modality for the detection of significant in-stent restenosis, with reported sensitivity and specificity values in the ranges of 54%–100% and 88%–100%, respectively (12,39–44) (Table). It is worth noting that the observation of distal runoff cannot be considered an absolute indicator of patency, since the presence of vessel enhancement distal to a stent could also be secondary to retrograde filling. Indeed, whereas in conventional coronary angiography the contrast agent is selectively injected into the coronary artery, CT requires injection into a peripheral vein instead. This allows retrograde flow via collateral branches to the vessel segment distal to an occluded or diseased stent. Attempts also have been made to assess coronary artery stent patency with 16–detector row CT scanners on the basis of contrast enhancement measurements (43) or pixel count methods (44). However, the detection of more subtle degrees of in-stent neointimal hyperplasia was beyond the capabilities of that generation of CT scanners.

Multidetector 64-Section CT Systems

Although the calibers of coronary stents are no smaller than those of the major native coronary arteries and their branches, the depiction of the in-stent coronary lumen at CT is a greater challenge than is that of the native coronary artery lumen because of high-attenuation artifacts secondary to the metallic stent struts. High in-plane and through-plane spatial resolution, optimal contrast resolution, and minimization of high attenuation artifacts are paramount in order to overcome the technical challenges. The superiority of 64-section CT systems over earlier generations of CT scanners with regard to the detection of coronary artery stenoses in native vessels has been demonstrated in recent investigations (45–47). Improvements in CT hardware technology, such as high x-ray output, isotropic voxel size of 0.4 x 0.4 x 0.4 mm (48), acquisition times of 6–14 seconds, and the capability of rendering 64 sections per rotation, can play a valuable role also in the evaluation of the intra–coronary artery stent lumen. Indeed, advances in multidetector CT technology mean that thinner sections can be obtained in a shorter time, with resultant increased spatial resolution along the z-axis and with almost motion-free data sets (49). Temporal resolution depends primarily on a gantry rotation speed faster than those available with earlier scanners. The reduced breath-holding time is better tolerated by patients and contributes to the minimization of motion-related artifacts. Coupled with these improvements in hardware design, electrocardiography (ECG)-based gating techniques and specialized meth-

CT Technique and Study	No. Patients	No. Stents	Stent Location	Stent Caliber (mm)	No. Assessable Stents	Criteria for Patency	Sens (%)	Spec (%)
Electron beam CT								
Pump et al (10)	202	321 (221 vessels)	LM, RCA, LAD, LCX, Bypass grafts		(216 vessels)	Dynamic study distal runoff	78	98
Knollman et al (11)	117	152		2.5–3.0	144	Dynamic study distal runoff	72	60
Four–detector CT								
Kruger et al (36)	20	32	RCA, LAD, LCX		32	Distal runoff		
Maintz et al (37)	29	47		3–5	38	Distal runoff	100	100
Ligabue et al (38)	48	72	RCA, LAD, LCX		53	Distal runoff	100	100
		15		≥3.5	14	Lumen visualization		
		45		3.0–3.4	35			
		12		<3	4			

16–detector CT

Schuijf et al (12)	22	68		2.25–5	50	Distal runoff	78	100
Cademartiri et al (39)	51	76		>2	74	Lumen visualization	84	99
Gilard et al (40)	29	29	LM		27	Lumen visualization	100	92
Gilard et al (41)	143	232	LM, RCA, LAD, LCX		122	Lumen visualization		
		1		4.5	1		86	100
		42		4.0	28			
		61		3.5	41			
		86		3.0	40		56	100
		42		2.5	12			
Kitagawa et al (42)	42	61			42	Lumen visualization		
		15		4.0	14			
		22		3.5	17			
		19		3.0	11			
		5		2.5	0			
Hong et al (43)	19	26		2.25–5	26	Contrast enhancement measurement		
Ohnuki et al (44)	16	20		>3	19	Pixel count method	75	88

Sens = sensitivity, Spec = specificity, LAD = left anterior descending artery, LCX = left circumflex artery, LM = left main coronary artery, RCA = right coronary artery.

ods of image reconstruction are used. Depending on the patient's heart rate, data acquired during one cardiac cycle (monosegmental) or multiple cardiac cycles (multisegmental) can be used for section reconstruction. With these combined advantages, current 64-section CT systems provide better spatial and temporal resolution than do earlier generations of multidetector CT scanners, and higher spatial resolution and a better signal-to-noise ratio than do electron-beam CT scanners (50). In the clinical evaluation of coronary stents, better delineation of the graft struts and of the presence of instent restenosis is possible with 64-section CT technology.

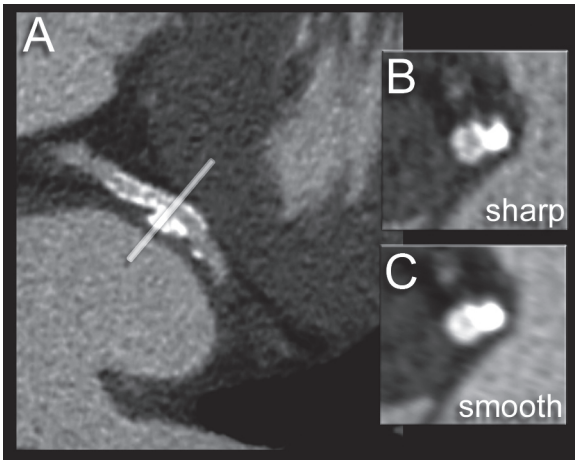

FIGURE 1. Blooming effect on follow-up images obtained with 64-section CT in a patient who underwent stent implantation in the left circumflex coronary artery. (A) Longitudinal multiplanar reformatted image shows, at the outer edge of the stent, a calcified spot that contributes to beam hardening and hampers visualization of the in-stent lumen. Note the insufficient dilation of the stent proximal to the bulky calcification. (B, C) Sharp-kernel-filtered cross-sectional image (B), obtained at the level indicated in A (line), is less affected by blooming than is the smooth-kernel-filtered cross-sectional image (C).

Stent Imaging with Multidetector CT

General Issues

In addition to the specifications of scanner hardware, scanning technique, and dedicated postprocessing (ie, convolution filter), variables such as stent diameter, material, and design as well as patient characteristics may heavily affect the visibility of the in-stent lumen. The earliest experiments to assess the feasibility of coronary stent imaging with multidetector CT were performed in vitro with varying collimations, contrast material concentrations, stent calibers, and stent positions within the gantry (51–53). When imaging is performed in vivo, stent-related beam hardening artifacts are a constant phenomenon, and assessment is further complicated by vessel wall calcifications, poor contrast-to-noise ratios in obese patients, and motion.

Beam Hardening and Blooming Effect

Metallic struts cause a severe CT artifact known as blooming effect. Blooming effect results from beam hardening and causes the stent struts to appear thicker than they are (51) and, often, to overlap the vessel lumen. The result is an under-

estimation of the in-stent luminal diameter (Figure 1A). The energy spectrum of the x-ray beam as it passes through a hyperattenuating structure increases because lower-energy photons are absorbed more rapidly than are higher-energy photons, with the result that the beam is more intense when it reaches the detectors. Calcified spots of the vessel wall near or at the outer surface of an implanted stent also contribute to beam hardening, which further erodes the assessability of the stent lumen (Figure 1B, 1C). Depending on the type of metal and the design of the stent, the magnitude of the artifact varies (Figure 2) (53). As a rule, the depiction of stents with the slimmest profile is least affected by blooming artifacts. Beam hardening is counterbalanced mainly by increasing the spatial resolution (decreasing the voxel size) and performing dedicated data filtering. Tube voltage is usually a constant parameter in cardiac protocols, but the contrast between structures on images also depends on the amount of x-ray energy. At lower-voltage settings, which correspond to lower energy of the x-ray beam, the CT number of metal increases substantially, and, hence, beam hardening artifacts are more likely to occur. Beam hardening artifacts also may be exacerbated by motion or by inappropriate selection of the reconstruction window (54). Conversely, they may be minimized by reducing the amount of motion inherent in the data set and optimizing the reconstruction window.

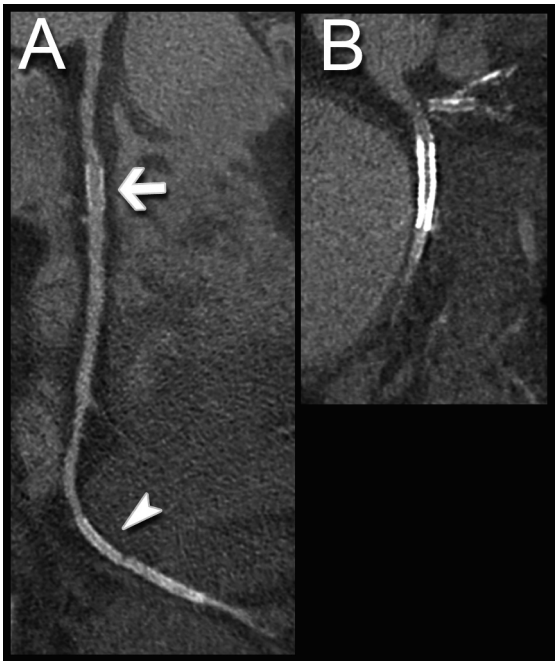

FIGURE 2. Variation in the severity of metal-related artifacts at 64-section CT with variations in metallic content, design, and luminal diameter of the stent. (A) Curved multiplanar reformatted image obtained in a patient with a 4-mm-caliber stent in the proximal right coronary artery (arrow) and 2.50-mm-caliber (arrowhead) and 2.25-mm-caliber stents in the posterolateral artery. Although all three stents consist of the same material, the in-stent lumen in the two stents in the posterolateral artery is not visible because of the small stent caliber. Note the gap between the stents implanted in the posterolateral artery. (B) Image obtained in another patient, who underwent stent implantation (different stent type, 5-mm caliber) in the proximal circumflex artery, shows a more pronounced metal-related artifact than is visible in A.

Partial Volume Averaging and Interpolation

Another obstacle to coronary stent imaging is related to partial volume averaging and interpolation. Inherent in all digital tomographic imaging techniques, partial volume averaging yields a CT number that represents the average attenuation of the materials within a voxel. At stent imaging in vessels with a large diameter, such as the aorta or iliac arteries, beam hardening and partial volume averaging effects are present but are limited to the proximity of the vessel wall. In coronary arteries with smaller diameters, the artifacts are of the same magnitude, but a reliable assessment of the lumen is much more problematic. The smaller the stent, the more detrimental the effect of partial volume averaging on the assessability of the in-stent lumen (Figure 2A).

The thinner detector width on 64-section CT scanners partly solves this problem by reducing the voxel size and thereby the general assessability of the stent lumen (48,55,56).

Optimization of Contrast Enhancement

Prominent contrast enhancement in the lumen is a prerequisite for robust coronary CT angiography (57). It is achieved not only by optimizing the contrast material injection parameters (ie, using a high-concentration contrast agent and a

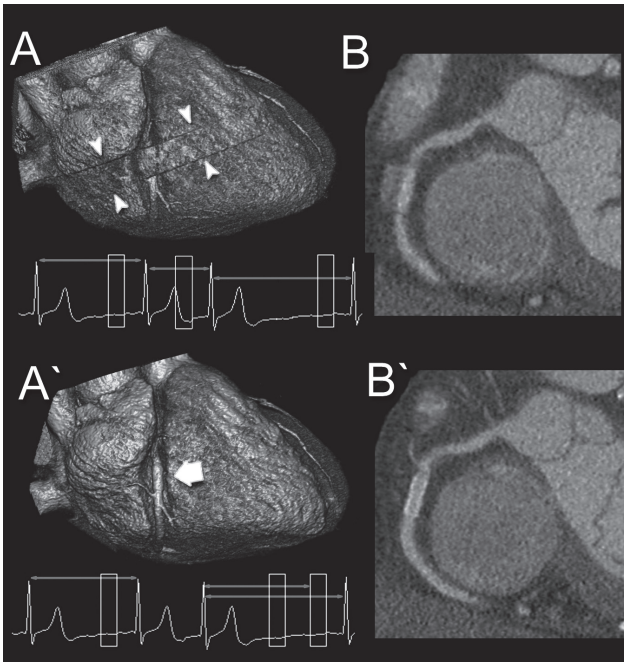

FIGURE 3. Residual cardiac motion exacerbates metal-related artifacts at 64-section CT in a patient with a stent in the midportion of the right coronary artery and with a premature heartbeat recorded at ECG during scanning. (A, B) Images obtained from data acquired during gating with the original ECG tracing. On the volume-rendered image (A), a stepladder artifact (arrowheads) is visible at the level of the midportion of the right coronary artery. On the multiplanar reformatted image (B), a blurring of contours is visible. (A', B') Images obtained with cardiac gating after editing of the ECG tracing. To avoid a gap in the image data, the reconstruction window during the premature heartbeat was deleted and another was added to the subsequent cardiac cycle. This step eliminated the abrupt heart rate change related to the premature beat and allowed a more coherent reconstruction of the data set. On the volume-rendered image (A'), the appearance of the stent (arrow) is unaffected by motion artifacts. Likewise, the in-stent lumen is well depicted on the multiplanar reformatted image (B').
(A full color version of this illustration can be found in the color section)

fast injection rate) but also by accurately synchronizing the CT data acquisition with the passage of the contrast agent by means of bolus tracking or a test bolus. Edge-enhancing convolution filters, which may be used for better delineation of stents, have the drawback of producing noisier data sets. If such a convolution filter is used, the assessability of the in-stent lumen particularly benefits from the presence of a high degree of intraluminal contrast enhancement, which somewhat compensates for the kernel-related noise. A high degree of intraluminal enhancement is recommended especially for the investigation of stent patency in vessels that have a small diameter and thus contain less blood.

Residual Cardiac Motion

Residual cardiac motion is of the utmost importance as a cause of vessel non assessability at multidetector CT coronary angiography. Residual cardiac motion also plays a role in exacerbating metal-related artifacts such as beam hardening and partial volume averaging effects (Figure 3). The use of high gantry rotation speeds, multisegmental reconstruction techniques, and ß-blockers to lower the heart rate consistently improves the interpretability of multidetector CT coronary angiograms. ECG-based editing techniques allow an improvement of image quality for patients with mild irregularities in sinus rhythm, such as premature beats, and for those with bundle-branch block.

Convolution Filters

Once the technical requirements and acquisition parameters for adequate coronary CT angiography have been fulfilled, additional dedicated postprocessing can be performed to optimize the visualization of the stent. The use of a dedicated edge-enhancing convolution kernel allows a significant decrease in the severity of blooming artifacts at the edges of high-attenuation structures. Indeed, the in-stent contrast-enhanced attenuation measured on sharp-kernel images is closer to that measured in the proximal or distal lumen than is the in-stent attenuation measured on smooth-kernel images (43). According to the authors of a recently published article about the effects of reconstruction kernels on the delineation of coronary stents (58), when a medium-smooth filter is applied, as a consequence of the blooming effect an average in-stent lumen narrowing of 37% is observed in comparison with the diameter of the untreated vessel segment, and the measured in-stent attenuation exceeds the aortic attenuation by more than 100 HU because of the partial volume averaging effect. In contrast, the in-stent lumen narrowing is 29% of the diameter of the normal vessel segment on sharp-

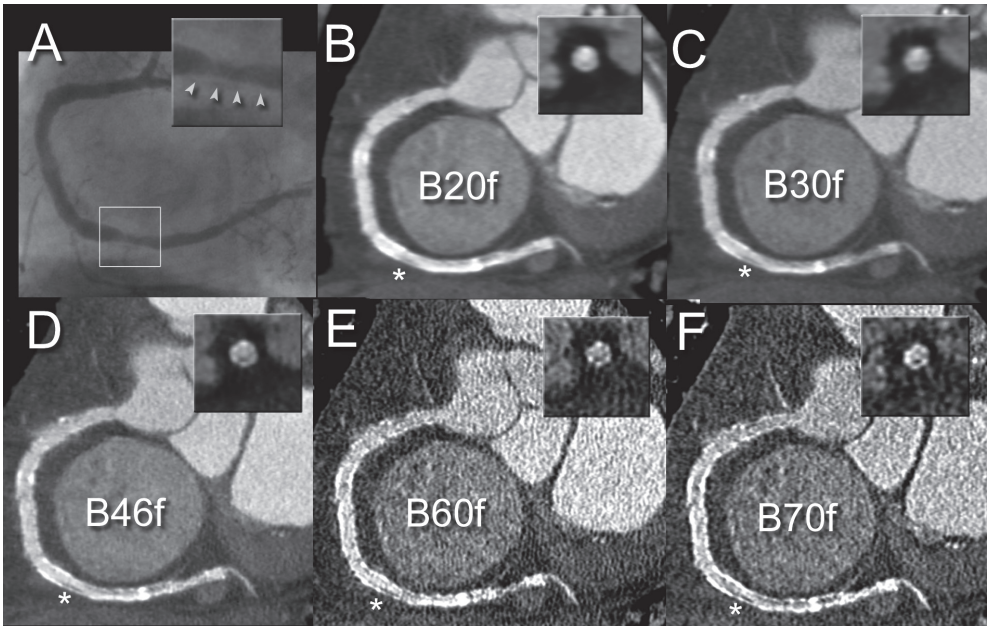

FIGURE 4. Visibility of low-contrast structures with different convolution filters. The most appropriate filter must be chosen so that an advantageous balance is achieved between the visibility of low-contrast structures and the quantity of image noise. (A) Conventional coronary angiogram shows nonsignificant neointimal hyperplasia in the distal portion of the right coronary artery (arrowheads). (B–F) Multidetector 64-section CT angiograms obtained in a patient with multiple stents in the right coronary artery. On the image reconstructed with a smooth convolution filter (B20f) (B), the luminal defect (*) is hardly visible. On the image reconstructed with a medium-smooth convolution filter (B30f) (C), the defect (*) is visible but quite blurred. The image reconstructed with a dedicated edge-enhancing kernel (B46f) (D) allows visualization of in-stent neointimal hyperplasia (*), with good contrast between the defect and the surrounding structures (stent scaffold, enhanced lumen). On the images reconstructed with sharp (B60f) (E) and very sharp (B70f) (F) convolution filters, the edge enhancement does not provide clearer depiction of the defect (*) but, instead, greater amounts of image noise.

filtered images, and the in-stent attenuation exceeds the attenuation in the aorta by only 60 HU. The results of such studies support the superior depiction of the stent lumen with dedicated edge-enhancing convolution kernels in comparison with conventional medium-smooth kernels. While spatial resolution is increased and blooming artifact is reduced by the application of edge-enhancing filters, an increase in image noise has to be accepted as a trade-off. Thus, the most appropriate filter must be chosen so that an advantageous balance is achieved between the visualization of low contrast structures and image noise (Figure 4). In these instances, high intraluminal contrast enhancement is also very helpful to counterbalance the increased image noise. Additional "intelligent" noise-reduction filters may prove beneficial for the depiction of low-contrast structures within the in-stent lumen and therefore may help detect in-stent restenosis (58).

Interpretation of Multidetector CT Data

Display Techniques and Windowing

The clinical evaluation of coronary arteries on CT angiograms is routinely performed by using multiplanar reformation of the data volume. Curved multiplanar reformation, maximum intensity projection, and volume rendering techniques also are often used. The same techniques are applied for the evaluation of coronary stents on CT angiograms. Multiplanar reformatted images and cross-sectional images of the stent are the most useful views on which to assess patency, restenosis, or a minor degree of neointimal hyperplasia. Advances in CT technology have provided 64-section CT scanners with submillimeter spatial resolution of 0.4 x 0.4 x 0.4 mm (43,48). With the very small isotropic voxel size, the assessability of the stent lumen on multiplanar reformatted images remains unaffected by angulation in relation to the z-axis.

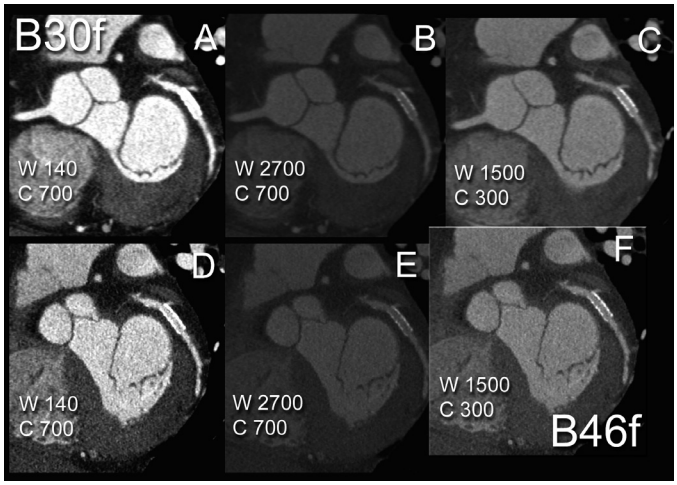

FIGURE 5. Combined effects of the selected filter and window settings on image contrast and noise at 64-section CT coronary angiography. (A–C) Images obtained with a medium-smooth convolution kernel (B30f). (D–F) Images obtained with a dedicated sharp convolution kernel (B46f). Note that D–F more clearly depict the in-stent lumen than do A–C. The standard soft-tissue window width (W) (A, D) is too narrow and accentuates blooming artifacts. On the image filtered with a medium-smooth convolution kernel (A), the blooming effect totally obscures the in-stent lumen. With exaggerated widening of the window (B, E), the blooming effect is decreased, but this occurs at the expense of overall image contrast. Setting the window center (C) at approximately 300 HU and choosing a width (W) of approximately 1500 HU allows a more favorable balance between image contrast and noise (C, F). However, the window settings alone are not sufficient to ensure optimal depiction of the inner lumen (C). The combined use of a dedicated edge-enhancing convolution kernel, which increases image spatial resolution, and appropriate window settings to compensate for filter-related noise allows the most favorable in-stent lumen visualization (F).

CT window settings affect image contrast and noise. If the window is set too narrow, image noise may be significantly increased, and grayscale differentiation of fine structural details may be lost. Wide window settings are necessary for accurate evaluation of the in-stent lumen at CT angiography (window width, 1500 HU; window center, 300 HU) (Figure 5).

Although they are not routinely used to as-

sess CT scans in the clinical setting, other three-dimensional volume rendering techniques are available with current CT scanners. After suitable threshold ranges or transparency settings are selected, an endoscopic view of the internal surface of the vessel can be simulated (Figure 6). This technique may allow visualization of different stent designs (eg, slotted tube and corrugated ring stents) (59). In stents with small diameters, though, the amount of image noise may be too great for such techniques to be reproducibly applied.

In-Stent Lumen Evaluation

As mentioned earlier (39), the direct visualization of the in-stent lumen is important for assessing patency, because collateral vessels may be feeding the vessel segment distal to the occluded stent in a retrograde direction. An accurate intraluminal evaluation can best be performed by means of multiplanar reformation of the CT data volume. The stent may be considered to be occluded if the lumen inside the device appears darker than the contrast-enhanced vessel lumen proximal to the stent.

Unless severe artifacts affect the CT data set, stent evaluation may proceed beyond a judgment of patency or occlusion. Nonocclusive in-stent neointimal hyperplasia is characterized by the presence of a darker rim between the stent and the contrast-enhanced vessel lumen

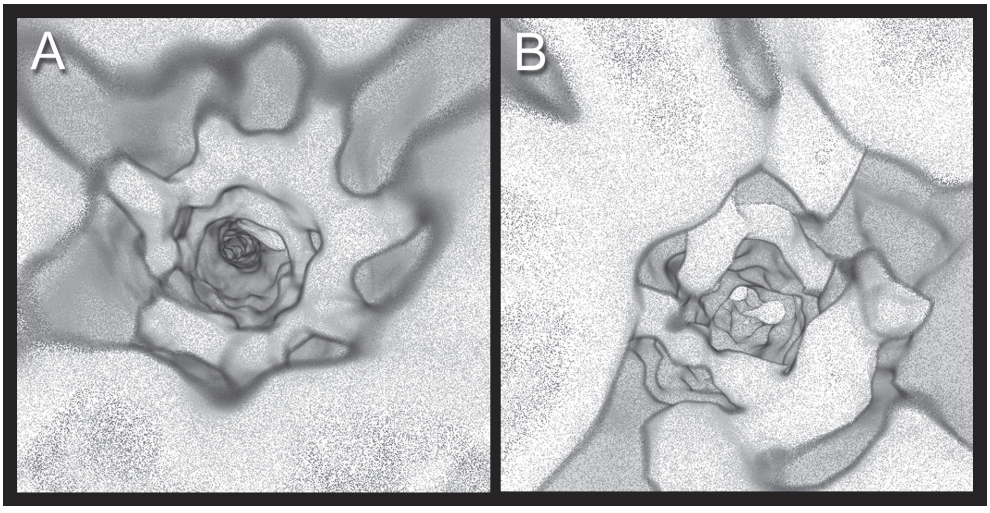

FIGURE 6. Selection of suitable threshold ranges and opacity settings allows simulation of an endoscopic view of the inner vessel surface and makes it possible to recognize different designs of the metal scaffold in stents. A slotted tubular stent (A) and a corrugated ring stent (B) are currently used for the treatment of most coronary lesions. Both stents have a diameter of 3 mm. The amount of image noise may prevent successful application of this technique for depiction of the lumen in stents with very small diameters.
(A full color version of this illustration can be found in the color section)

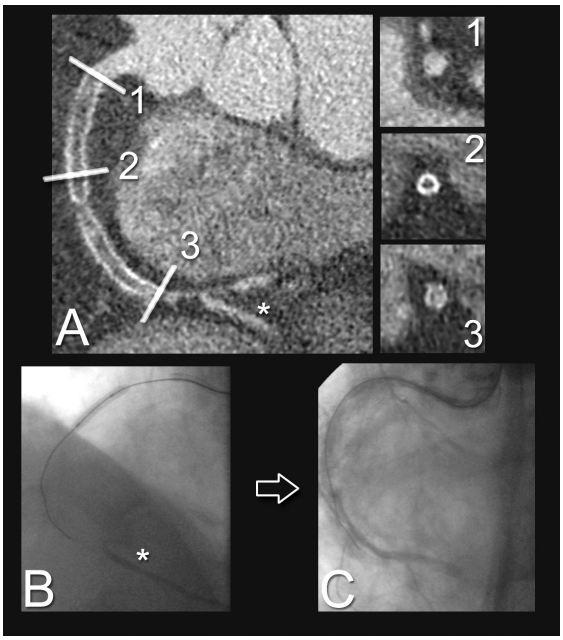

FIGURE 7. In-stent occlusion in a patient with recurrent angina pectoris 18 months after implantation of two stents in the right coronary artery. CT was performed after conventional angiography failed to depict the right coronary artery. (A) Multiplanar reformatted image shows lower attenuation inside the stent lumina than in the proximal untreated tract of the right coronary artery, a gap between the occluded stents, and collateral filling (*). (1–3) Cross-sectional images obtained at the proximal end of the stent (1), in the middle portion (2), and at the distal end (3) show the appearances of patency, occlusion, and patency, respectively. (B, C) Conventional angiograms provide information about the presence of collateral filling (* in B) and the length of the occlusion. This information enabled planning for percutaneous revascularization, which was successful, as evident from a comparison of the pre-treatment image (B) and the post-treatment image (C).

(Figure 4) and is secondary to the healing response to procedure-related vessel injury. If neointimal hyperplasia exceeds a luminal diameter reduction of 50%, the process is consistent with hemodynamically significant in-stent restenosis (Figure 7) (39). In-stent restenosis typically occurs as a localized nonenhancing lesion, often (but not invariably) associated with complex lesion anatomy (ie, ostial lesions) and discontinuity in lesion coverage. It occurs with higher frequency in patients with diabetes mellitus (26). Restenosis may occur either within or adjacent to the stent (within 5 mm of the stent extremities). Edge restenosis might occur because of a decrease in local drug availability, incomplete lesion coverage due to a gap between two stents, procedure-related trauma, or damage to the polymer coating of a stent from calcifications or an overlapping stent (33).

Bifurcation Lesions

Arterial branching points are particularly vulnerable to the atherosclerotic process and its complications. The treatment of lesions located at coronary artery bifurcations, including the left main artery bifurcation, currently accounts for approximately 15% of all percutaneous coronary artery interventions (20,60,61). Stent implantation at coronary artery bifurcations remains technically challenging and is associated with higher restenosis rates than is stent placement for simple lesions (62). An accurate and noninvasive coronary imaging tool thus is highly desirable for the follow-up of these patients.

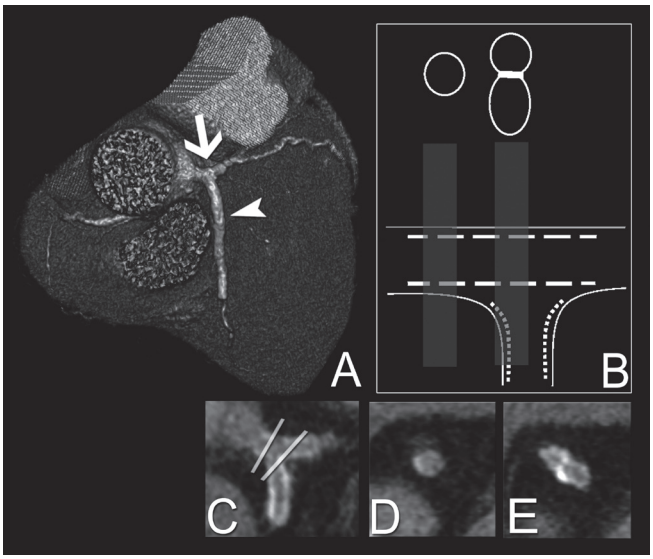

FIGURE 8. T stent implantation at the left main coronary artery bifurcation. (A) Volume- rendered image obtained with 64-section CT shows the left main coronary artery and circumflex artery (arrow), which constitute the main branch, and the anterior descending artery (arrowhead), the side branch for stent implantation. (B–E) T-stent cross-sectional diagram (B), curved multiplanar reformatted image (C), and cross-sectional images (D, E) obtained in the planes indicated in C show overlap of the metal struts only at the bifurcation point.
(A full color version of this illustration can be found in the color section)

Numerous techniques of stent deployment in bifurcation lesions have been described (63–72). The preferred stent implantation strategy depends on the bifurcation anatomy and takes into account the plaque location in relation to the side branch (63–65). In accordance with the strategy applied, different stent configurations may be observed on CT images.

If the lesion anatomy allows it, the provisional stent implantation technique is preferred. This technique consists of stent placement in the main branch first, with subsequent implantation of a second stent in the side branch only if residual stenosis or dissection is present (66). However, in many patients, both the main branch and the side branch are severely diseased. In such cases, the simultaneous implantation of a stent in both branches is favored.

The "T" stent technique (Fig 8) was developed for the treatment of vessels with a bifurcation angle close or equal to 90°. Side branches that originate with a narrower angle (less than 70°) are preferably treated by using one of many available "Y" stent techniques, since incomplete coverage of the side-branch ostium may lead to the recurrence of stenosis at that spot (67,68).

Another variant, the "V" stent technique, involves the implantation of two stents together: one stent is advanced into the side branch; the other, into the main branch. The two stents are in direct contact proximally and form a new bifurcation angle (69). If this angle extends a considerable distance (usually, 5 mm or more) into the proximal part of the main branch, the technique is referred to as "simultaneous

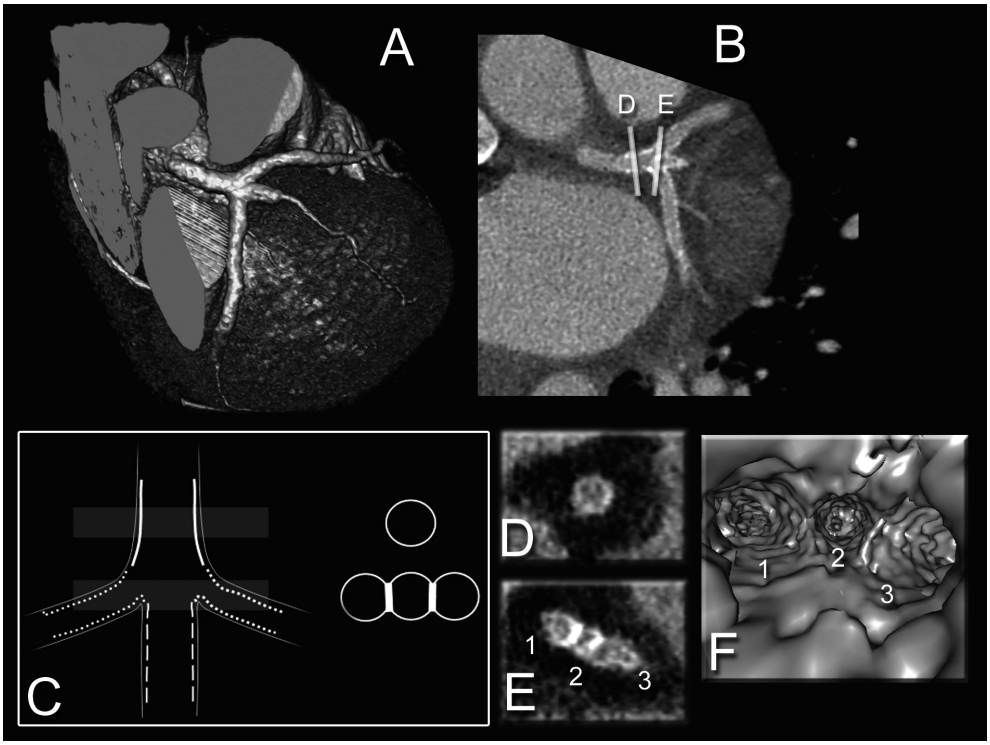

FIGURE 9. V stent implantation in the left coronary artery. (A, B) Volume-rendered image (A) and multiplanar reformatted image (B) show the left main artery and the anterior descending, intermediate, and circumflex branches, in which stents were placed to provide full coverage of the branching point. (C) Diagram of the V stent technique shows overlap of the metal struts only at the trifurcation. (D, E) Cross-sectional images, obtained in the planes shown in B, show the slim and symmetric profiles of the stents, both proximally (D) and at the level of the carina (E). (F) Volume-rendered image obtained for visualization of the vessel lumen provides a simulated endoscopic view of the origin of the three branches (1–3).
(A full color version of this illustration can be found in the color section)

kissing stents" (3,69). V stents and simultaneous kissing stents are suitable for proximal lesions, such as lesions located at the left main coronary artery bifurcation (Figure 9), provided that the part of the main branch that is proximal to the bifurcation is free of disease.

The "culottes" or "trousers" technique (Figure 10) is another well-known Y stent variant that ensures full coverage of the side-branch ostium. First, a stent is deployed across the branch that has the greatest angulation, usually the side branch. Next, a balloon catheter is passed through the struts of the stent, into the other branch, and dilated; a second stent is then delivered into that branch (usually the main branch). This technique is suitable for use at bifurcations of any angulation. The bifurcation itself is fully covered, albeit at the expense of an excess of metal at the proximal end (70,71). This excess of metal produces marked hyperattenua-

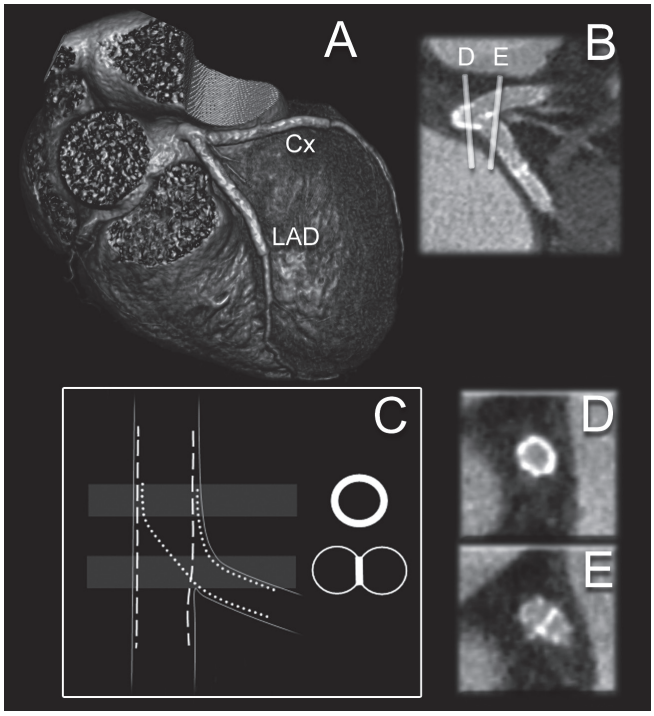

FIGURE 10. Y stent implantation at the bifurcation of the left main coronary artery. (A) Volume-rendered image shows the point of bifurcation, at which two stents were implanted in a configuration resembling a pair of trousers or culottes. Cx = left circumflex artery, LAD = left anterior descending artery. (B) Multiplanar reformatted image shows stent patency at the level of the bifurcation. (C) Diagram shows the concentrically deployed stents, which overlap near the point of bifurcation. (D, E) Cross-sectional images, obtained in the planes shown in B, depict a thicker stent profile in the parent vessel (D) at a level near the side-branch ostium (E).
(A full color version of this illustration can be found in the color section)

tion at the bifurcation on the CT image, an effect that may prevent visualization of the lumen.

The "crush" technique, like the V technique, involves the simultaneous insertion of two stents (Figure 11) (72). The side-branch stent, which protrudes minimally into the main branch, is deployed at the bifurcation. Subsequently, the main-branch stent is deployed across the ostium of the side-branch vessel and causes the protruding side-branch stent to be flattened against the vessel wall (hence the term crush). As a result, three layers of metal are applied to the vessel wall of the main branch immediately upstream of the side-branch ostium, a stent configuration that results in an area of hyperattenuation on one side of the vessel on multidetector CT angiograms.

Conclusion

Considering the high number of percutaneous coronary interventions that involve stent implantation, the development of relatively inexpensive and noninvasive methods for assessing stent patency is an issue of growing interest. Multidetector CT has recently emerged above competing modalities such as electron-beam CT and MR imaging as a practical alternative to invasive coronary angiography. Despite image-degrading effects caused by the metallic scaffold

of the stent, recent experience with the current generation of 64-section scanners suggests improved assessability of the in-stent lumen with the capability to appreciate more subtle degrees of in-stent neointimal hyperplasia. Knowledge of the different

types of artifacts and how they can be compensated for with dedicated postprocessing and appropriate image views and window settings is a prerequisite for reliable depiction of the in-stent lumen and leads to a more robust application of CT findings in the clinical context. In future, the development of biodegradable stents may create optimal conditions for noninvasive post-implantation follow-up with multidetector CT.

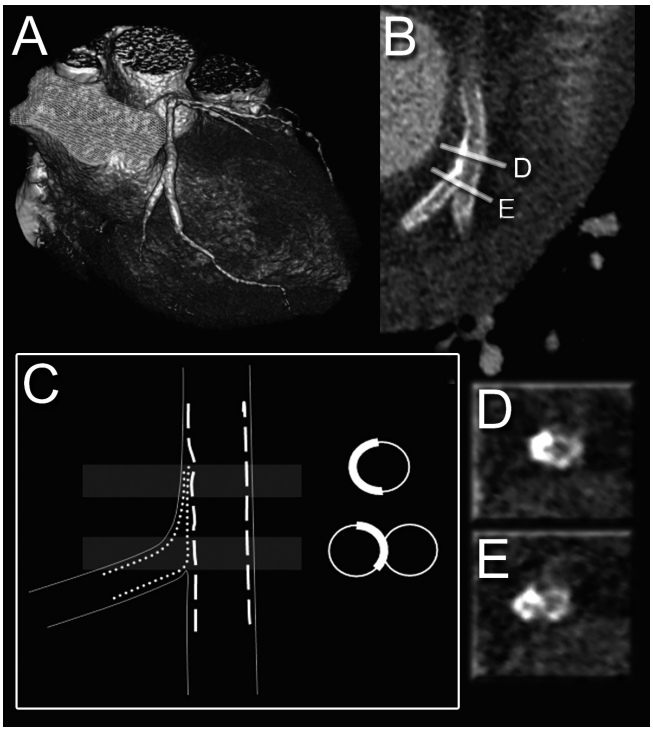

FIGURE 11. Crush stent placement at the circumflex-marginal artery bifurcation. (A, B) Volume rendered image (A) and curved multiplanar reformatted image (B) allow assessment of the stent configuration. (C) Diagram shows the multiple layers of metal that produce an asymmetric appearance of the cross-sectional stent profile. (D, E) Cross-sectional images, obtained in the planes shown in B, show asymmetric high attenuation where the layers of metal overlap, both proximal to the bifurcation (D) and across the ostium of the side-branch vessel (E).
(A full color version of this illustration can be found in the color section)

CHAPTER 15

References

1. Serruys PW, de Jaegere P, Kiemeneij F, et al. A comparison of balloon-expandable-stent implantation with balloon angioplasty in patients with coronary artery disease. Benestent Study Group. N Engl J Med 1994;331:489–495.
2. Fischman DL, Leon MB, Baim DS, et al. A randomized comparison of coronary-stent placement and balloon angioplasty in the treatment of coronary artery disease. Stent Restenosis Study Investigators. N Engl J Med 1994;331:496–501.
3. Sharma SK, Choudhury A, Lee J, et al. Simultaneous kissing stents (SKS) technique for treating bifurcation lesions in medium-to-large size coronary arteries. Am J Cardiol 2004;94:913–917.
4. de Feyter PJ, Kay P, Disco C, Serruys PW. Reference chart derived from post-stent-implantation intravascular ultrasound predictors of 6-month expected restenosis on quantitative coronary angiography. Circulation 1999;100:1777–1783.
5. Mercado N, Boersma E, Wijns W, et al. Clinical and quantitative coronary angiographic predictors of coronary restenosis: a comparative analysis from the balloon-to-stent era. J Am Coll Cardiol 2001;38:645–652.
6. Serruys PW, Kay IP, Disco C, Deshpande NV, de Feyter PJ. Periprocedural quantitative coronary angiography after Palmaz-Schatz stent implantation predicts the restenosis rate at 6 months: results of a meta-analysis of the Belgian Netherlands Stent study (BENESTENT) I, BENESTENT II Pilot, BENESTENT II and MUSIC trials. Multicenter Ultrasound Stent In Coronaries. J Am Coll Cardiol 1999;34:1067–1074.
7. Jeremias A, Kutscher S, Haude M, et al. Nonischemic chest pain induced by coronary interventions: a prospective study comparing coronary angioplasty and stent implantation. Circulation 1998;98:2656–2658.
8. Kim WY, Danias PG, Stuber M, et al. Coronary magnetic resonance angiography for the detection of coronary stenoses. N Engl J Med 2001;345:1863–1869.
9. Hug J, Nagel E, Bornstedt A, Schnackenburg B, Oswald H, Fleck E. Coronary arterial stents: safety and artifacts during MR imaging. Radiology 2000;216:781–787.
10. Pump H, Mohlenkamp S, Sehnert CA, et al. Coronary arterial stent patency: assessment with electronbeam CT. Radiology 2000;214:447–452.
11. Knollmann FD, Moller J, Gebert A, Bethge C, Felix R. Assessment of coronary artery stent patency by electron-beam CT. Eur Radiol 2004;14:1341–1347.
12. Schuijf JD, Bax JJ, Jukema JW, et al. Feasibility of assessment of coronary stent patency using 16-slice computed tomography. Am J Cardiol 2004;94:427–430.
13. Smith SC Jr, Dove JT, Jacobs AK, et al. ACC/AHA guidelines of percutaneous coronary interventions (revision of the 1993 PTCA guidelines)— executive summary. A report of

the American College of Cardiology/American Heart Association Task Force on Practice Guidelines (committee to revise the 1993 guidelines for percutaneous transluminal coronary angioplasty). J Am Coll Cardiol 2001;37:2215–2239.

14. Coronary artery disease statistics—2005 edition [database online]. Oxford, England: British Heart Foundation, 2005. British Heart Foundation Statistics Website. http://www.heartstats.org. Accessed May 28, 2005. Updated June 9, 2005.
15. Health care in America: trends in utilization. Hyattsville, Md: NCHS/CDC, 2004. Centers for Disease Control, National Center for Health Statistics Web site. http://www.cdc.gov/nchs/pressroom/04facts/healthcare.htm. Published January 30, 2004. Accessed May 28, 2005.
16. Heart disease and stroke statistics—2005 update. Dallas, Tex: American Heart Association, 2005. American Heart Association Web site. http://www.americanheart.org. Accessed May 28, 2005. Updated January 11, 2006.
17. Abrams J. Clinical practice. Chronic stable angina. N Engl J Med 2005;352:2524–2533.
18. Hannan EL, Racz MJ, Walford G, et al. Long-term outcomes of coronary-artery bypass grafting versus stent implantation. N Engl J Med 2005;352:2174–2183.
19. de Feyter PJ, Serruys PW, Unger F, et al. Bypass surgery versus stenting for the treatment of multivessel disease in patients with unstable angina compared with stable angina. Circulation 2002;105:2367–2372.
20. Iakovou I, Schmidt T, Bonizzoni E, et al. Incidence, predictors, and outcome of thrombosis after successful implantation of drug-eluting stents. JAMA 2005; 293:2126–2130.
21. McFadden EP, Stabile E, Regar E, et al. Late thrombosis in drug-eluting coronary stents after discontinuation of antiplatelet therapy. Lancet 2004;364:1519–1521.
22. Ong AT, McFadden EP, Regar E, de Jaegere PP, van Domburg RT, Serruys PW. Late angiographic stent thrombosis (LAST) events with drug-eluting stents. J Am Coll Cardiol 2005;45:2088–2092.
23. Ong AT, Hoye A, Aoki J, et al. Thirty-day incidence and 6-month clinical outcome of thrombotic stent occlusion after bare-metal, sirolimus, or paclitaxel stent implantation. J Am Coll Cardiol 2005;45:947–953.
24. Rensing BJ, Hermans WR, Beatt KJ, et al. Quantitative angiographic assessment of elastic recoil after percutaneous transluminal coronary angioplasty. Am J Cardiol 1990;66:1039–1044.
25. Mintz GS, Popma JJ, Pichard AD, et al. Arterial remodeling after coronary angioplasty: a serial intravascular ultrasound study. Circulation 1996;94:35–43.
26. Hoffmann R, Mintz GS, Dussaillant GR, et al. Patterns and mechanisms of in-stent restenosis: a serial intravascular ultrasound study. Circulation 1996;94:1247–1254.
27. Kiemeneij F, Serruys PW, Macaya C, et al. Continued benefit of coronary stenting versus balloon angioplasty: 5-year clinical follow-

up of Benestent-I trial. J Am Coll Cardiol 2001;37:1598–1603.

28. Morice MC, Serruys PW, Sousa JE, et al. A randomized comparison of a sirolimus-eluting stent with a standard stent for coronary revascularization. N Engl J Med 2002;346:1773–1780.
29. Mauri L, O'Malley AJ, Popma JJ, et al. Comparison of thrombosis and restenosis risk from stent length of sirolimus-eluting stents versus bare metal stents. Am J Cardiol 2005;95:1140–1145.
30. Wong SC, Hong MK, Ellis SG, et al. Influence of stent length to lesion length ratio on angiographic and clinical outcomes after implantation of bare metal and drug-eluting stents (the TAXUS-IV Study). Am J Cardiol 2005;95:1043–1048.
31. Lemos PA, Hofma SH, Regar E, Saia F, Serruys PW. Drug-eluting stents for the treatment of coronary disease: state-of-the-art. In: Marco J, Serruys P, Biamino G, et al, eds. EuroPCR textbook. Paris, France: Europa, 2004.
32. Moses JW, Leon MB, Popma JJ, et al. Sirolimus-eluting stents versus standard stents in patients with stenosis in a native coronary artery. N Engl J Med 2003; 349:1315–1323.
33. Lemos PA, Saia F, Ligthart JM, et al. Coronary restenosis after sirolimus-eluting stent implantation: morphological description and mechanistic analysis from a consecutive series of cases. Circulation 2003;108:257–260.
34. Ong AT, Serruys PW, Aoki J, et al. The unrestricted use of paclitaxel- versus sirolimus-eluting stents for coronary artery disease in an unselected population: 1-year results of the Taxus-Stent Evaluated at Rotterdam Cardiology Hospital (T-SEARCH) registry. J Am Coll Cardiol 2005;45:1135–1141.
35. van der Hoeven BL, Pires NM, Warda HM, et al. Drug-eluting stents: results, promises and problems. Int J Cardiol 2005;99:9–17.
36. Kruger S, Mahnken AH, Sinha AM, et al. Multislice spiral computed tomography for the detection of coronary stent restenosis and patency. Int J Cardiol 2003;89:167–172.
37. Maintz D, Grude M, Fallenberg EM, Heindel W, Fischbach R. Assessment of coronary arterial stents by multislice-CT angiography. Acta Radiol 2003;44:597–603.
38. Ligabue G, Rossi R, Ratti C, Favali M, Modena MG, Romagnoli R. Noninvasive evaluation of coronary artery stents patency after PTCA: role of multislice computed tomography. Radiol Med (Torino) 2004; 108:128–137.
39. Cademartiri F, Mollet N, Lemos PA, et al. Usefulness of multislice computed tomographic coronary angiography to assess in-stent restenosis. Am J Cardiol 2005;96:799–802.
40. Gilard M, Cornily JC, Rioufol G, et al. Noninvasive assessment of left main coronary stent patency with 16-slice computed tomography. Am J Cardiol 2005; 95:110–112.
41. Gilard M, Cornily JC, Pennec PY, et al. Assessment of coronary artery stents by 16-slice computed tomography. Heart 2006;92:58–61.
42. Kitagawa T, Fujii T, Tomohiro Y, et al.

Noninvasive assessment of coronary stents in patients by 16-slice computed tomography. Int J Cardiol 2005. doi: 10.1061/j.ijcard.2005.06.012. Published July 14, 2005. Accessed September 15, 2005.

43. Hong C, Chrysant GS, Woodard PK, Bae KT. Coronary artery stent patency assessed with in-stent contrast enhancement measured at multi– detector row CT angiography: initial experience. Radiology 2004; 233:286–291.
44. Ohnuki K, Yoshida S, Ohta M, et al. New diagnostic technique in multi-slice computed tomography for in-stent restenosis: pixel count method. Int J Cardiol 2005. doi:10.1016/j.ijcard.2005.05.013. Published June 27, 2005. Accessed September 15, 2005.
45. Leschka S, Alkadhi H, Plass A, et al. Accuracy of MSCT coronary angiography with 64-slice technology: first experience. Eur Heart J 2005;26:1482–1487.
46. Leber AW, Knez A, von Ziegler F, et al. Quantification of obstructive and nonobstructive coronary lesions by 64-slice computed tomography: a comparative study with quantitative coronary angiography and intravascular ultrasound. J Am Coll Cardiol 2005;46:147–154.
47. Raff GL, Gallagher MJ, O'Neill WW, Goldstein JA. Diagnostic accuracy of noninvasive coronary angiography using 64-slice spiral computed tomography. J Am Coll Cardiol 2005;46:552–557.
48. Flohr T, Bruder H, Stierstorfer K, Simon J, Schaller S, Ohnesorge B. New technical developments in multislice CT. II. Sub-millimeter 16-slice scanning and increased gantry rotation speed for cardiac imaging. Rofo 2002;174:1022–1027.
49. Nakanishi T, Kayashima Y, Inoue R, Sumii K, Gomyo Y. Pitfalls in 16–detector row CT of the coronary arteries. RadioGraphics 2005;25:425–438.
50. Maintz D, Fischbach R, Juergens KU, Allkemper T, Wessling J, Heindel W. Multislice CT angiography of the iliac arteries in the presence of various stents: in vitro evaluation of artifacts and lumen visibility. Invest Radiol 2001;36:699–704.
51. Nieman K, Cademartiri F, Raaijmakers R, Pattynama P, de Feyter P. Noninvasive angiographic evaluation of coronary stents with multi-slice spiral computed tomography. Herz 2003;28:136–142.
52. Mahnken AH, Buecker A, Wildberger JE, et al. Coronary artery stents in multislice computed tomography: in vitro artifact evaluation. Invest Radiol 2004; 39:27–33.
53. Maintz D, Juergens KU, Wichter T, Grude M, Heindel W, Fischbach R. Imaging of coronary artery stents using multislice computed tomography: in vitro evaluation. Eur Radiol 2003;13:830–835.
54. Choi HS, Choi BW, Choe KO, et al. Pitfalls, artifacts, and remedies in multi– detector row CT coronary angiography. RadioGraphics 2004;24:787–800.
55. Mahnken AH, Seyfarth T, Flohr T, et al. Flat-panel detector computed tomography for the assessment of coronary artery stents: phantom study in comparison with 16-slice spiral computed tomography. Invest Radiol 2005;40:8–13.

56. Nieman K, Cademartiri F, Lemos PA, Raaijmakers R, Pattynama PM, de Feyter PJ. Reliable noninvasive coronary angiography with fast submillimeter multislice spiral computed tomography. Circulation 2002; 106:2051–2054.
57. Cademartiri F, Mollet NR, van der Lugt A, et al. Intravenous contrast material administration at helical 16–detector row CT coronary angiography: effect of iodine concentration on vascular attenuation. Radiology 2005;236:661–665.
58. Seifarth H, Raupach R, Schaller S, et al. Assessment of coronary artery stents using 16-slice MDCT angiography: evaluation of a dedicated reconstruction kernel and a noise reduction filter. Eur Radiol 2005; 15:721–726.
59. Colombo A, Stankovic G, Moses JW. Selection of coronary stents. J Am Coll Cardiol 2002;40:1021–1033.
60. Farb A, Burke AP, Kolodgie FD, Virmani R. Pathological mechanisms of fatal late coronary stent thrombosis in humans. Circulation 2003;108:1701–1706.
61. Koller P, Safian RD. Bifurcation stenosis. In: Freed E Sr, Grines C, eds. Manual of interventional cardiology. Birmingham, Mich: Physician Press, 1997; 229–241.
62. Hoye A, van der Giessen WJ. New approaches to ostial and bifurcation lesions. J Interv Cardiol 2004;17:397–403.
63. Lefevre T, Louvard Y, Morice MC, et al. Stenting of bifurcation lesions: classification, treatments, and results. Catheter Cardiovasc Interv 2000;49:274–283.
64. Gobeil F, Lefevre T, Guyon P, et al. Stenting of bifurcation lesions using the Bestent: a prospective dual-center study. Catheter Cardiovasc Interv 2002;55:427–433.
65. Colombo A, Moses JW, Morice MC, et al. Randomized study to evaluate sirolimus-eluting stents implanted at coronary bifurcation lesions. Circulation 2004;109:1244–1249.
66. Melikian N, Di Mario C. Treatment of bifurcation coronary lesions: a review of current techniques and outcome. J Interv Cardiol 2003;16:507–513.67. Al Suwaidi J, Berger PB, Rihal CS, et al. Immediate and long-term outcome of intracoronary stent implantation for true bifurcation lesions. J Am Coll Cardiol 2000;35:929–936.
68. Fort S, Lazzam C, Schwartz L. Coronary 'Y' stenting: a technique for angioplasty of bifurcation stenoses. Can J Cardiol 1996;12:678–682.
69. Schampaert E, Fort S, Adelman AG, Schwartz L. The V-stent: a novel technique for coronary bifurcation stenting. Cathet Cardiovasc Diagn 1996;39:320–326.
70. Khoja A, Ozbek C, Bay W, Heisel A. Trouser-like stenting: a new technique for bifurcation lesions. Cathet Cardiovasc Diagn 1997;41:192–196; discussion 197–199.
71. Chevalier B, Glatt B, Royer T. Kissing stenting in bifurcation lesions [abstract]. Eur Heart J 1996;17:218A.
72. Kobayashi Y, Colombo A, Akiyama T, Reimers B, Martini G, di Mario C. Modified "T" stenting: a technique for kissing stents in bifurcational coronary lesion. Cathet Cardiovasc Diagn 1998;43:323–326.

CHAPTER 16

Coronary computed tomography angiography in patients after percutaneous coronary intervention (PCI): focus on post-processing and visualization techniques

Pugliese F, Gruszczynska K, Alberghina F, Baron J, Mollet NR, de Feyter PJ, Krestin GP.

Medical Science Monitor 2007; 13(Suppl 1):152-157.

Summary

Coronary stent imaging with computed tomography is challenging because of high-density artifacts. However, noninvasive coronary angiography with computed tomography is gaining acceptance as a valid alternative to cardiac catheterization in a broader array of clinical settings, and the work-up of patients after coronary stent implantation represents an application of pressing clinical utility. Only a minority of patients who develop recurrent chest pain after stent implantation have myocardial ischemia, thus a sensitive noninvasive study is desirable. With an awareness of the limitations of the technique, the systematic application of dedicated strategies of data post-processing and display techniques permits partial compensation of the technical limitations brought about by metallic struts.

Introduction

Coronary computed tomography angiography (CTA) performed with the latest-generation equipment has proved to be a reliable technique in the assessment of coronary artery disease [1–6]. Although subject to limitations related to the clinical settings and to the level of expertise with which the studies are interpreted, it is conceivable that the potential applications of coronary CTA might become broader in

the future. In addition to the role for coronary CTA as a gate-keeper prior to catheterization in subjects with an intermediate cardiovascular risk profile, the capability to noninvasively follow-up patients after coronary stenting when symptoms recur or when high risk is present (such as in subjects where a left main artery lesion or a lesion with complex characteristics were treated) might be extremely desirable in terms of patient comfort, procedure-related complications, and costs. Indeed, although many patients experience chest pain after coronary stent placement, that symptom is secondary to ischemia in only a few.

In the first two sections of this article the clinical manifestations of in-stent restenosis and thrombosis will be discussed with their implications in the diagnostic work-up of patients after coronary stenting. Imaging coronary stents with CT is technically very challenging and requires additional post-processing and assessment strategies to be of clinical utility. In the latter part of this article we will review the major limitations of CT in visualizing coronary stents. The steps of image acquisition, reconstruction, and post-processing of peculiar importance in coronary stent imaging will also be addressed.

In-Stent Restenosis

The events that can unfavorably affect the clinical outcome of coronary stenting are in-stent thrombosis and in-stent restenosis. Whereas the diagnosis of in-stent thrombosis is usually straightforward on a clinical basis because the occurrence of total stent obstruction causes acute myocardial infarction, in-stent restenosis is associated with the recurrence of chest pain with variable characteristics. The assessment of in-stent restenosis is therefore more challenging and often requires an imaging tool.

In-stent restenosis occurs as an excessive healing response to vessel injury. Whereas a minor degree of arterial response, the so-called neo-intimal hyperplasia, is a common finding, significant in-stent restenosis is defined by a luminal diameter reduction equal to or greater than 50%. The frequency of in-stent restenosis ranges from below 10% in patients with simple lesions to 20% after the treatment of complex lesions (e.g. coronary bifurcations) [7].

CHAPTER 16

Diagnostic Work-Up of Patients After Coronary Stenting

In patients with recurrent angina after stent placement, treadmill test and additional investigations such as stress echo and scintigraphy are usually undertaken before the decision to perform cardiac catheterization is made. In these settings, coronary CTA might assess the presence of in-stent restenosis and simultaneously detect disease in the native coronary tree in a one-stop study, reducing the number of additional costly investigations. The negative predictive value of coronary CTA is known to be higher than that of treadmill testing [8–13]. This may be of particular clinical utility in subjects with a treated left main artery, whose mortality due to recurrence of disease is particularly high (Table 1). The use of coronary CTA instead of cardiac catheterization for control studies would be advantageous in terms of patient acceptance, procedure-related risks, and costs.

TABLE 1. Hypothesized usage of coronary CTA in patients after PCI

• Chest pain is secondary to ischemia in only a few cases; test with high negative predictive value needed to `screen` patients prior to catheterization: CTA
• In-stent restenosis is relatively rare, symptoms can be secondary to progression of disease in the native coronary arteries; sensitive test needed to check the status of stent and coronary arteries: CTA
• Recurrent disease in the left main artery is associated with high mortality; follow-up needed with sensitive but low-risk, inexpensive test: CTA
• In-stent restenosis is more frequent in simple than in complex lesions; low-risk, inexpensive test: CTA

Modalities for Coronary Stent Imaging

Conventional coronary angiography is the gold standard technique in the assessment of in- stent restenosis. However, cardiac catheterization may involve major complications and is associated with moderate-high costs. Visualization of the in-stent lumen with magnetic resonance angiography is prevented by the metallic scaffold which causes magnetic susceptibility artifacts [14]. Electron beam computed tomography allows the acquisition of 3-mm-thick images suitable for morphological interpretation and 8-mm-thick images used for flow analysis without direct visualization of the instent lumen [15]. However, image noise is high with the former acquisition technique, and only severe, flow-limiting stenoses can be detected using the latter. Current multidetector-row CT technology, featuring almost isotropic voxel size and fast gantry rotation speed and

TABLE 2. Operator-dependent technical parameters to minimize metal-related artifacts in coronary stent imaging with computed tomography angiography

Phase of study	Parameters	Effect
Acquisition (*)	• high contrast agent concentration (e.g. 400 mg/ml)	> luminal enhancement
	• high injection rate (e.g. 5 ml/s)	
Reconstruction	• ECG-editing	compensation for mild heart rate irregularities
	• multisegment reconstruction	> temporal resolution
	• data filtering (edge-enhancement)	> spatial resolution (image noise)
Display technique	• multiplanar reconstructions	compensation for partial voluming due to tortuous coronary anatomy
	• wide window settings (1400/400 HU width/centre)	< image noise after edge-enhencement without in spatial resolution

* mAs can be adapted to patient´s size

allowing the reconstruction of 64 sections per rotation, provides an appealing alternative for non-invasive luminal assessment in patients after coronary stent placement.

Limitations of Coronary CTA for Stent Imaging

Although the diameter of coronary stents is not smaller than that of native coronary arteries, imaging the in-stent lumen with coronary CTA is more challenging than imaging the native coronary artery lumen. This is due in the first instance to metal-related high-density artifacts [16]. We briefly recall that the energy spectrum of the x-ray beam passing through a hyperdense structure increases because lower-energy photons are absorbed more rapidly than higher-energy photons, so the resulting beam is more intense when it reaches the detectors. This phenomenon causes the stent struts to display an exaggerated thickness which superimposes the in-stent lumen and hampers stent interpretability.

The magnitude of high-density artifacts varies depending on stent diameter, type of metal, and scaffold design. As a rule, stents with large diameters and slim metal scaffold show the fewest high-density artifacts. High spatial resolution and minimization of motion are paramount in order to overcome high-density artifacts. Dedicated convolution kernels, interactive volume assessment, and window display settings are equally important in that they allow to optimally exploit the improved

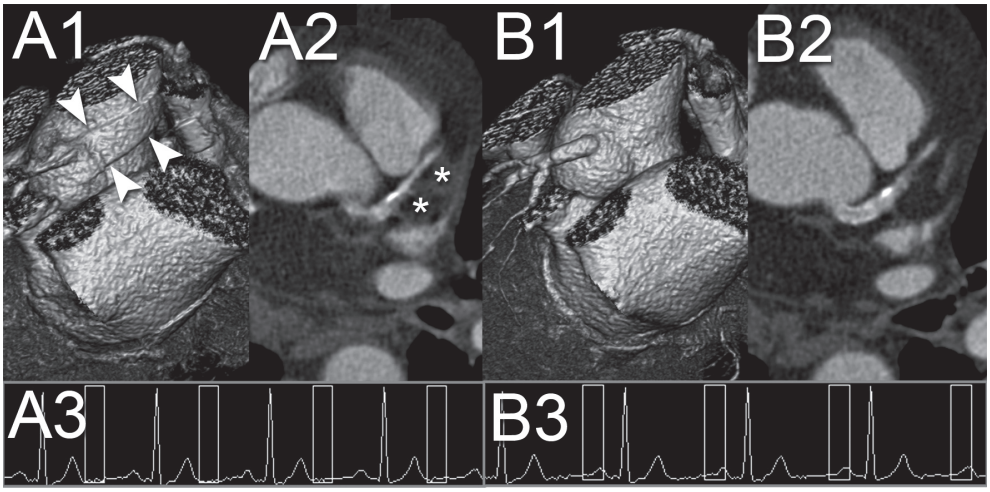

FIGURE 1. Control computed tomography coronary angiography in a patient six months after the placement of a stent in the left main coronary artery. Excessive residual cardiac motion during the reconstruction interval in systole (A3) causes step-ladder artifacts (A1, arrowheads) and stent contour blurring (A2, asterisks). Reconstruction of the volume-data during a more favorable temporal window, in this example the end-diastolic phase (B3), provides images suitable for clinical interpretation (B1,2).
(A full color version of this illustration can be found in the color section)

spatial resolution of current multidetector-row CT systems (Table 2).

Coronary Artery Enhancement

Prominent contrast enhancement in the lumen is a prerequisite for robust coronary CTA [17]. Hence a high-concentration contrast agent (e.g. 400 mg/ml) and a high injection-rate (e.g. 5 ml/s) must be chosen, but also an accurate synchronization of the scan with the passage of contrast agent is required, which can be achieved with the application of sophisticated synchronization protocols such as bolus tracking or test-bolus. The edge-enhancing convolution filters used for better delineation of stents have the drawback of producing noisier data-sets [18]. Thereby the in-stent lumen interpretability particularly benefits from the presence of high intraluminal enhancement to partly compensate for the filter-related image noise.

Direct evaluation of the in-stent lumen patency must be favored over the assessment of distal run-off because subocclusive disease or collateral and retrograde filling pathways might have developed. The presence of enhancement distal to a stent cannot be considered as a reliable criterion of stent patency.

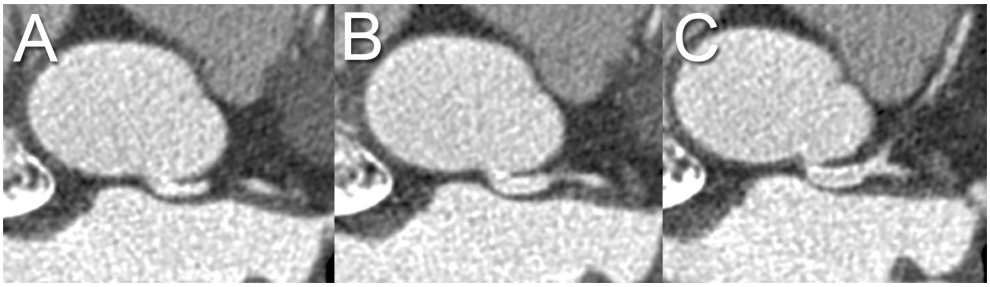

FIGURE 2. When standard axial slices (perpendicular to the z-axis) are browsed in proximal-to-distal (A–C) direction, the stent length is only partially visualized on each image due to its oblique orientation.

Minimization of Motion

In addition to a fast gantry rotation speed, which implies high temporal resolution, the choice of the temporal reconstruction window with the least amount of intrinsic motion is of utmost importance to provide images suitable for clinical interpretation, because metal-related artifacts are exacerbated by motion (Figure 1). ECG-editing techniques may be helpful in patients with mild heart rate irregularities such as premature beats or bundle branch block. Multi-segmental reconstruction algorithms might also increase temporal resolution, but are particularly susceptible to heart rate changes occurring during the scan.

Convolution Kernels

The metal-related blooming effect causes the stent struts to display an exaggerated thickness. With an unchanged image reconstruction thickness, the use of edge-enhancing convolution filters allows a de-

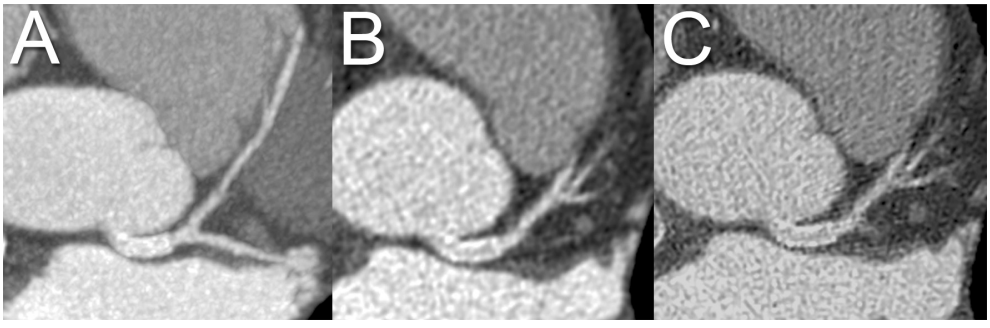

FIGURE 3. The use of the maximum-intensity-projection (MIP) technique (A) allows the entire vessel length to be depicted on the same image. Conversely, in-stent lumen assessment is impossible because the MIP image enhances the visualization of the metallic struts. A multiplanar reconstruction (MPR) image (B) and the addition of a dedicated edge-enhancing convolution kernel (C) allow minimization of high-density artifacts. The application of an edge-enhancing filter causes an increase in overall image noise (C).

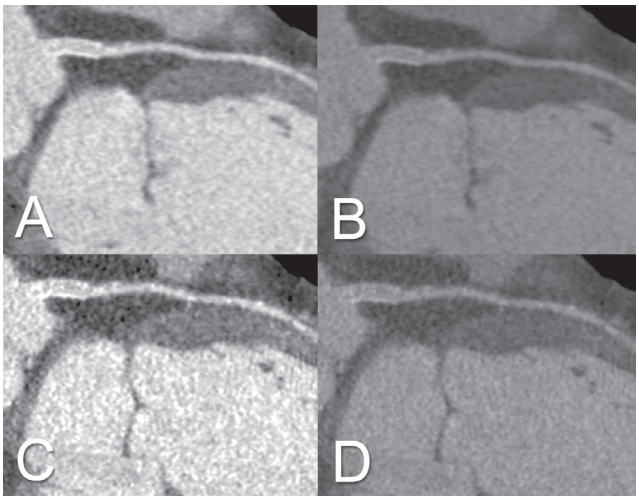

FIGURE 4. Curved MPR images of the left main and anterior descending arteries. The choice of a smooth (A,B) or sharp (C,D) convolution filter affects image contrast and noise in combination with the display window settings (A,C: 800/200 HU width/center. B,D: 1400/400 HU width/center). High-density artifacts are apparent when the standard convolution filter and window settings are chosen (A). Wider window settings with a standard filter (B) decrease the blooming effect, but also decrease overall image contrast. Dedicated edge-enhancing data filtering (C,D) combined with wide window settings (D) can partly compensate for both the blooming effect and image noise into a favorable trade-off for in-stent lumen visualization.

crease in the blooming effect through an increase in spatial resolution. This occurs at the expense of a slight increase in image noise as well. Hence, when coronary stents are present, it is advisable that the data-set reconstructed with the edge-enhancing filter is additional to the data-set obtained with the standard convolution filter for the evaluation of native coronary vessels (Figure 3B,C). Cardiac imaging packages provided by manufacturers include dedicated convolution filters suitable for stent imaging. These filters are extremely helpful also when extensive coronary calcifications are present.

Interactive Assessment and Visualization Techniques

Given their tortuous anatomy, the evaluation of stented coronary arteries requires interactive workstation assessment. When standard transverse images are browsed, the lumen may be only partially visualized due its oblique spatial orientation (Figure 2). The maximum-intensity projection (MIP) technique can increase the vessel length depicted on a single image (Figure 3A), but it is heavily detrimental for in-stent lumen visualization. Owing to the almost isotropic voxel size, multiplanar reconstructions (MPRs) (Figure 3B,C) and curved MPRs (Figure 4) can be tilted and tailored on coronary anatomy while preserving optimal spatial resolution. As a rule, long-axis (Figure 3B,C, Figure 4) and cross-sectional (Figure 5) MPR views of the stent are the most useful key images to assess patency, restenosis, or minor degrees of neo-intimal hyperplasia.

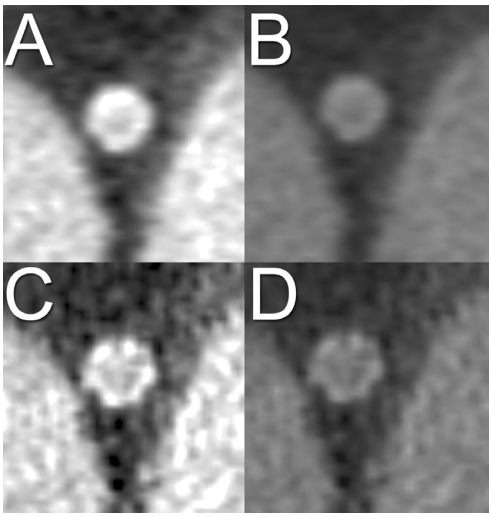

FIGURE 5. Short-axis MPR views of the same left main artery stent obtained with combinations of smooth (A,B) or sharp (C,D) convolution kernels with different window settings (A,C: 800/200 HU width/center. B,D: 1400/400 HU width/center). As in Figure 4, a high-density artifact impairs lumen evaluation if the convolution kernel and display settings are not optimized (A). Widening the window settings only decreases overall image contrast (B). A dedicated convolution kernel increases spatial resolution, but produces a noisier image (C). The combination of a dedicated convolution kernel with wider window settings is helpful to reduce high-density artifacts and image noise (D). The stent in the left main artery is patent, with a minor degree of intimal hyperplasia.

Window Settings

Window settings of the monitor affect image contrast and noise. If the window is set too narrow, image noise can be significantly increased and gray-scale differentiation of fine

structural details may be lost. Coronary CTA of stented vessels requires wide window settings to accurately evaluate the in-stent lumen (1400/400 HU width/center). Dedicated data filtering combined with wide window settings can partly compensate for both the blooming effect and image noise, resulting in a favorable trade-off for in-stent lumen visualization (Figure 4, Figure 5).

Conclusions

Emerged as a practical alternative to invasive angiography in the assessment of coronary artery disease, coronary CTA is timely capable of answering a broader array of clinical questions owing to the tremendous technical advances of current 64-section systems. However, imaging artifacts inherent to metallic stent struts require knowledge of dedicated post-processing and appropriate visualization techniques. With an awareness of the limitations of the technique, this expertise permits exploiting the improvements in technology for the clinical implementation of coronary CTA.

CHAPTER 16

References

1. Leschka S, Alkadhi H, Plass A et al: Accuracy of MSCT coronary angiography with 64-slice technology: first experience. Eur Heart J, 2005; 26: 1482–87
2. Raff GL, Gallagher MJ, O'Neill WW, Goldstein JA: Diagnostic accuracy of noninvasive coronary angiography using 64-slice spiral computed tomography. J Am Coll Cardiol, 2005; 46: 552–57
3. Leber AW, Knez A, von Ziegler F et al: Quantification of obstructive and nonobstructive coronary lesions by 64-slice computed tomography: a comparative study with quantitative coronary angiography and intravascular ultrasound. J Am Coll Cardiol, 2005; 46: 147–54
4. Mollet NR, Cademartiri F, van Mieghem CA et al: High-resolution spiral computed tomography coronary angiography in patients referred for diagnostic conventional coronary angiography. Circulation, 2005; 112(15): 2318–23
5. Pugliese F, Mollet NR, Runza G et al: Diagnostic accuracy of non-invasive 64-slice CT coronary angiography in patients with stable angina pectoris. Eur Radiol, 2006; 16(3): 575–82
6. Ropers D, Rixe J, Anders K et al: Usefulness of multidetector row spiral computed tomography with 64- × 0.6-mm collimation and 330-ms rotation for the noninvasive detection of signifi cant coronary artery stenoses. Am J Cardiol, 2006; 97(3): 343–48
7. Sharma SK, Choudhury A, Lee J et al: Simultaneous kissing stents (SKS) technique for treating bifurcation lesions in medium-to-large size coronary arteries. Am J Cardiol, 2004; 94: 913–17
8. Schuijf JD, Bax JJ, Jukema JW et al: Feasibility of assessment of coronary stent patency using 16-slice computed tomography. Am J Cardiol, 2004; 94: 427–30
9. Cademartiri F, Mollet N, Lemos PA et al: Usefulness of Multislice Computed Tomographic Coronary Angiography to Assess In-Stent Restenosis. Am J Cardiol, 2005; 96: 799–802
10. Gaspar T, Halon DA, Lewis BS et al: Diagnosis of coronary in-stent restenosis with multidetector row spiral computed tomography. J Am Coll Cardiol, 2005; 46(8): 1573–79
11. Hong C, Chrysant GS, Woodard PK, Bae KT: Coronary artery stent patency assessed with in-stent contrast enhancement measured at multidetector row CT angiography: initial experience. Radiology, 2004; 233: 286–91
12. Gilard M, Cornily JC, Rioufol G et al: Noninvasive assessment of left main coronary stent patency with 16-slice computed tomography. Am J Cardiol, 2005; 95(1): 110–12
13. Gilard M, Cornily JC, Pennec PY et al: Assessment of coronary artery stents by 16 slice computed tomography. Heart, 2006; 92(1): 58–61
14. Hug J, Nagel E, Bornstedt A et al: Coronary

arterial stents: safety and artifacts during MR imaging. Radiology, 2000; 216: 781–87

15. Pump H, Mohlenkamp S, Sehnert CA et al: Coronary arterial stent patency: assessment with electron-beam CT. Radiology, 2000; 214: 447–52
16. Seifarth H, Ozgun M, Raupach R et al: 64- versus 16-slice CT angiography for coronary artery stent assessment: in vitro experience. Invest Radiol, 2006; 41(1): 22–27
17. Cademartiri F, de Monye C, Pugliese F et al: High iodine concentration for noninvasive multislice computed tomography coronary angiography. Iopromide 370 versus Iomeprol 400. Invest Radiol, 2006; 41: 349–53
18. Pugliese F, Cademartiri F, van Mieghem C et al: Multidetector CT for visualization of coronary stents. Radiographics, 2006; 26: 887–904

CHAPTER 17

Usefulness of 64-slice multislice computed tomography to assess in-stent restenosis

Cademartiri F, Schuijf JD, Pugliese F, Mollet NR, Jukema JW, Maffei E, Kroft LJ, Palumbo A, Ardissino D, Serruys PW, Krestin GP, Van der Wall EE, de Feyter PJ, Bax JJ.

Journal of the American College of Cardiology 2007; 49:2204-2210.

Summary

Purpose: This study sought to evaluate the diagnostic accuracy of 64-slice multislice computed tomography (MSCT) coronary angiography in the follow-up of patients with previous coronary stent implantation. Recent investigations have shown increased image quality and diagnostic accuracy for non-invasive coronary angiography with 64-slice MSCT as compared with previous-generation MSCT scanners, but data on the evaluation of coronary stents are scarce.

Material and Methods: In 182 patients (152 [84%] male, ages 58 ± 11 years) with previous stent (≥2.5 mm diameter) implantation (n = 192), 64-slice MSCT angiography using either a Sensation 64 (Siemens, Forchheim, Germany) or Aquilion 64 (Toshiba, Otawara, Japan) was performed. At each center, coronary stents were evaluated by 2 experienced observers and evaluated for the presence of significant (≥50%) in-stent restenosis. Quantitative coronary angiography served as the standard of reference.

Results: A total of 14 (7.3%) stented segments were excluded because of poor image quality. In the interpretable stents, 20 of the 178 (11.2%) evaluated stents were significantly diseased, of which 19 were correctly detected by 64-slice MSCT. Accordingly, sensitivity, specificity, and positive and negative predictive value to identify in-stent restenosis in interpretable stents were 95.0% (95% confidence interval [CI] 85% to 100%), 93.0% (95% CI 90% to 97%), 63.3% (95% CI 46% to 81%), and 99.3% (95% CI 98% to 100%), respectively.

Conclusions: In-stent restenosis can be evaluated with 64-slice MSCT with good diagnostic accuracy. In particular, a high negative predictive value of 99% was observed, indicating that 64-slice MSCT may be most valuable as a noninvasive method of excluding in-stent restenosis.

Introduction

Stent implantation is increasingly performed in the treatment of significant coronary artery disease and has significantly reduced the occurrence of restenosis as compared with balloon angioplasty (1,2). Moreover, with the recent introduction of drug-eluting stents, the occurrence of in-stent restenosis has further decreased (3–5). Nonetheless, a subset of patients still presents with recurrent chest pain with possible in-stent restenosis, and frequently evaluation with invasive coronary angiography is required. A noninvasive alternative approach to evaluating these patients may be offered by 64-slice multislice computed tomography (MSCT). In native coronary arteries, sensitivities and specificities of approximately 90% and 96% (6–9) for detection of coronary artery disease have been reported, with a substantial gain in diagnostic accuracy over 4- and 16-slice MSCT. Also the evaluation of coronary stents, which posed still considerable problems with 4- and 16-slice MSCT (10), may have improved with 64-slice MSCT. However, few data are currently available and the routine use of MSCT in patients with a history of stent implantation is at present not recommended (11,12). The purpose of the present study was to evaluate the diagnostic performance of 64-slice MSCT to identify in-stent restenosis (and occlusion) in comparison with the gold standard, invasive coronary angiography.

Materials and Methods

Study Population

The study population consisted of 182 patients who were referred for invasive coronary angiography after previous coronary stent (≥2.5 mm diameter) implantation. Referral of patients for invasive coronary angiography was partially part of an ongoing protocol and partially routine (based on the presence of symptoms, abnormal exercise electrocardiogram [ECG], and/or ischemia on myocardial perfusion imaging). In addition to invasive coronary angiography, 64-slice MSCT was performed. Exclusion criteria were the following: 1) atrial fibrillation, 2) renal insufficiency (serum creatinine >120 mmol/l), 3) known allergy to iodine contrast media, 4) pregnancy, and 5) coronary stent diameter ≥2.5 mm. The study was approved by the ethical committee of

the different centers, and all participating patients gave informed consent.

Scan Protocol and Image Reconstruction

The MSCT angiography was performed with 2 different 64-slice MSCT scanners (Sensation 64, Siemens, Germany n = 150, and Aquilion 64, Toshiba Medical Systems, Japan, n = 32). Thirty-four patients (19%) had a prescan heart rate ≥65 beats/min, and were given a single oral dose of 100 mg metoprolol 1 h before the examination in the absence of contraindications. A bolus of 100 ml iomeprol (400 mg iodine/ml; Iomeron, Bracco, Milan, Italy) was intravenously injected (4 to 5 ml/s) followed by 50 ml of saline at the same rate using a double-head injector (Stellant, MedRAD, Pittsburgh, Pennsylvania). To trigger the start of the scan, a real-time bolus tracking technique was used (13). During the scan, which was performed during an inspiratory breath hold of 8 to 12 s, the MSCT data and ECG trace were acquired. Scan parameters were (for Siemens and Toshiba, respectively): individual detector collimation 32 x 2 x 0.6 mm and 64 x 0.5 mm, tube voltage 120 kV for both, mAs 900 and 712, gantry rotation time 330 and 400 ms. No ECG pulsing was used. Reconstruction parameters (for Siemens and Toshiba, respectively): effective slice width 0.75 and 0.5 mm, increment 0.4 and 0.3 mm, standard and sharp heart view convolution filters for both. For Siemens, B30f and B46f were used, whereas for Toshiba, Q04 was used in addition to Q05 to Q07. Synchronized to the recorded ECG, axial slices were reconstructed from the acquired MSCT data with the use of segmented or half reconstruction algorithms. Image data sets were reconstructed during the mid-to-end diastolic phase, during which coronary artery displacement is relatively small, with reconstruction window positions starting at 400 ms before the next R wave and/or at 75% of the R-to-R interval. If indicated, additional temporal window positions were explored, including the end-systolic phase to obtain images with least motion artefacts.

MSCT Image Interpretation

At each center, 2 observers, both blinded to angiographic and clinical findings but aware of previous cardiac history, evaluated the MSCT examinations using axial slices and multiplanar and curved reconstructions (P.J.F., F.C., J.W.J., and J.D.S.). Of note, different window settings, including 1,500/300 HU, were used for optimal stent assessment. A stent was judged to be occluded when the lumen inside the stent was darker than the contrast-enhanced vessel before the stent and/or when no run-off could be visualized at the distal end of the stent (14,15). Nonocclusive in-stent restenosis was considered when the lumen inside the stent showed a darker rim (eccentric or concentric) between the

stent and the enhanced vessel lumen with a lumen reduction ≥50% (as compared with other portions of the stent). In addition, the presence of reduced run-off distal to the stent was taken into consideration; if reduced distal run-off was observed, this was found to be suggestive of in-stent restenosis. Importantly, the presence of distal run-off was not used as a criterion for the absence of significant in-stent restenosis, because collateral filling may occur (which cannot be detected adequately by MSCT). In Figures 1, 2, and 3, examples are provided of patent and diseased stents.

Invasive Coronary Angiography

Conventional selective coronary angiography was performed with standard techniques and evaluated by a reviewer blinded to the MSCT results with the use of quantitative coronary angiography systems (CAAS II, Pie Medical, Maastricht, the Netherlands, or QCA-CMS version 6.0, Medis, Leiden, the Netherlands). The diameter stenosis, as a percentage of the reference diameter, was determined in 2 orthogonal directions and the average between these 2 values determined the stenosis severity.

Statistical Analysis

Sensitivity, specificity, positive and negative predictive values (including 95% confidence interval [CI]) for the detection of in-stent restenosis ≥50% using conventional angiography in combination with quantitative coronary angiography as the gold standard, were calculated.

All statistical analyses were performed using SPSS software (version 12.0, SPSS Inc., Chicago, Illinois). A value of $p < 0.05$ was considered statistically significant.

Results

Patient Characteristics

In total, 182 patients (152 male, ages 57.8 ± 10.6 years) with a total of 192 coronary stents were enrolled in the study. A total of 4 patients were not enrolled because of the presence of stents with a diameter <2.5 mm. Also, 5 patients were not studied because of a high heart rate in combination with beta-blocker intolerance. Baseline characteristics of the study population are provided in Table 1. The average time interval between stent implantation and 64-slice MSCT coronary angiography was 6.2 ± 1.6 months; 64-slice MSCT and conventional angiography were performed within 1 month of each other (average 9 ± 8 days); MSCT was always performed first. The site of stent implantation was: right coronary artery in 55 (28.6%), left main coronary artery in 11 (5.7%), left anterior descending coronary artery in 113 (58.9%), and left circumflex coro-

TABLE 1. Demographic and Angiographic Characteristics of Patients (n = 182)

	n (%)
Age (yrs), mean ± SD	57.8 ± 10.6
Male	152 (84%)
Previous myocardial infarction	94 (52%)
Previous PCI	182 (100%)
Body mass index (kg/m^2), mean ± SD	28.8 ± 3.8
Diabetes mellitus type II	23 (13%)
Hypercholesterolemia	64 (35%)
Hypertension	57 (31%)
Family history of CAD	88 (48%)
Current smoking	110 (60%)
Angiography	
1-vessel disease	134 (72.5%)
2-vessel disease	34 (18.7%)
3-vessel disease	16 (8.8%)
Stent location	
RCA	55 (28.6%)
LM	11 (5.7%)
LAD	113 (58.9%)
LCx	13 (6.8%)

CAD = coronary artery disease; LAD = left anterior descending coronary artery; LCx = left circumflex coronary artery; LM = left main coronary artery; PCI = percutaneous coronary intervention; RCA = right coronary artery.

nary artery in 13 (6.8%). Average stent diameter was 3.1 ± 0.4 mm (range 2.5 to 4.5 mm), whereas stent length ranged from 8 to 33 mm (average 18 ± 7 mm). Eight different stent types were evaluated, the non–drug eluting stents being Vision (Guidant, Santa Clara, California), Driver (Medtronic, Minneapolis, Minnesota), Ave S7 (Medtronic), Orbus (Orbus Technologies, Hoevelaken, the Netherlands), Bx Velocity (Cordis Corp., Johnson & Johnson, Miami, Florida), and Liberte (Boston Scientific, Boston, Massachusetts). Included drug-eluting stents were Cypher (Cordis Corp.) and Taxus (Boston Scientific). Average heart rate during MSCT data acquisition was 60 ± 7.9 beats/min.

Coronary Stent Analysis

In total, 178 stents were available for evaluation, whereas 14 stents (7.3%) were considered uninterpretable because of residual motion and high-density artefacts (Table 2). No significant differences were observed in interpretability between the different stent diameters; 3 (5.8%) of 52 stents with a diameter <3 mm were uninterpretable, whereas 7 (10%) of 70 and 4 (5.7%) of 70 stents with diameters of respectively 3 mm or >3 mm were uninterpretable (Table 3). The incidence of significant in-stent restenosis (nonocclusive in-stent restenosis and total stent occlusions) was 11.2% (20 of 178), as determined by conventional angiography. Examples of patent stents as well as stents with significant in-stent restenosis are provided in Figures 1, 2, and 3, respectively. All 7 stent occlusions were correctly iden-

TABLE 2. Diagnostic Accuracy of 64-Slice MSCT to Detect Significant In-Stent Restenosis

	≥50% In-Stent Restenosis
Stents (%, 95% CI)	
Assessable	178/192 (92.7%, 89%–97%)
With uninterpretable stents excluded	
Sensitivity	19/20 (95.0%, 85%–100%)
Specificity	147/158 (93.0%, 90%–97%)
Positive predictive Value	19/30 (63.3%, 46%–81%)
Negative Predictive Value	147/148 (99.3%, 98%–100%)
With uninterpretable stents included	
Sensitivity	19/21 (90.5%, 78%–100%)
Specificity	147/171 (86.0%, 81%–92%)
Positive predictive Value	19/43 (44.2%, 29%–59%)
Negative Predictive Value	147/149 (98.7%, 97%–100%)

MSCT = multislice computed tomography.

tified by 64-slice MSCT, whereas 1 stent (located in the second diagonal) of 13 stents with significant but nonocclusive in-stent restenosis remained undetected by MSCT. Of the 158 stents without significant in-stent restenosis, 147 were correctly evaluated by 64-slice MSCT, whereas 11 stents were incorrectly considered positive. Accordingly, the overall sensitivity, specificity, and positive and negative predictive value to detect significant in-stent restenosis were 95.0% (19 of 20, 95% CI 85% to 100%), 93.0% (147 of 158, 95% CI 90% to 97%), 63.3% (19 of 30, 95% CI 46% to 81%), and 99.3% (147 of 148, 95% CI 98% to 100%), respectively. More detailed information is

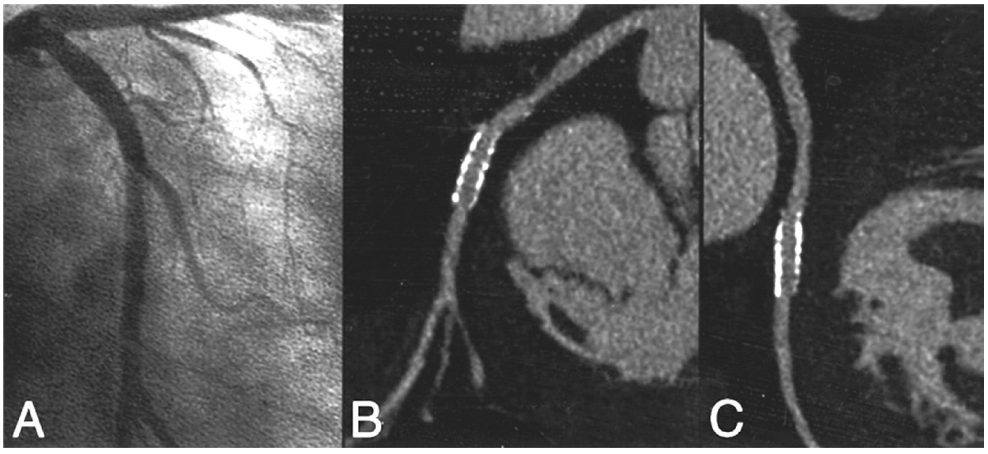

FIGURE 1. Example of a Patent Stent. Conventional coronary angiography (A) showed patency of a stent (Cypher, 3.0 x 18 mm) placed in the left circumflex coronary artery. (B and C) Two orthogonal curved multiplanar reconstructions obtained with 64-slice MSCT (Siemens Sensation, kernel B46f) are provided, also showing patency of the stent. MSCT = multislice computed tomography.

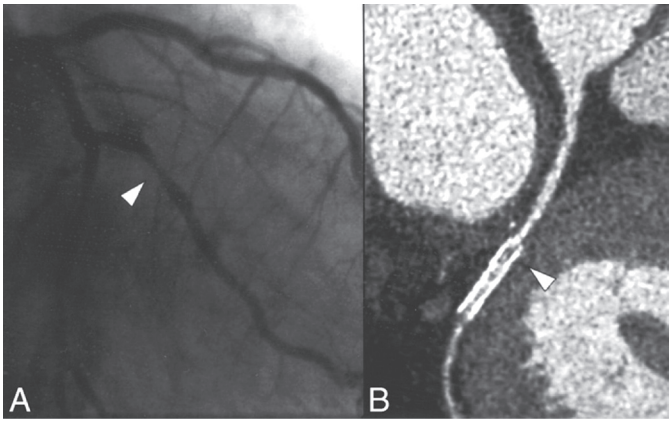

FIGURE 2. Example of In-Stent Restenosis. Conventional coronary angiography (A) showed in-stent restenosis in a stent (Taxus, 2.5 x 20 mm) placed in the second marginal branch of the left circumflex coronary artery (arrowhead). (B) A curved multiplanar reconstruction obtained with 64-slice MSCT (Siemens Sensation, kernel B46f) is provided. In the proximal part of the stent (arrowhead), a hypodense area can be observed, indicating the presence of in-stent restenosis. Abbreviations as in Figure 1.

listed in Table 2. In stents without significant stenosis on conventional angiography, average percentage stenosis as determined by quantitative coronary angiography was significantly higher in stents falsely classified as positive on MSCT as compared with stents correctly classified as negative (36% vs. 25%, $p < 0.05$). Similarly, average percentage stenosis was lower in stents false-negative on MSCT as compared with correct positive stents (65% vs. 73%, p = NS). In a subanalysis, the rate of false diagnosis was evaluated according to stent diameter. In stents with a diameter <3.0 mm, 3 (6.1%) of 49 stents were incorrectly diagnosed. For stents with a diameter of 3.0 mm, this percentage was 1.6% (1 of 63), whereas in stents with a diameter >3.0 mm, incorrect diagnosis was obtained with MSCT in 8 of 66 (12.0%). More details on the rate of false positives and negatives are provided in Table 3. In Table 4, the results from the 2 scanners from the 2 centers are reported separately. At the Leiden center, relatively more stents were deemed uninterpretable as compared with the Rotterdam center (14.3% vs. 5.3%, p

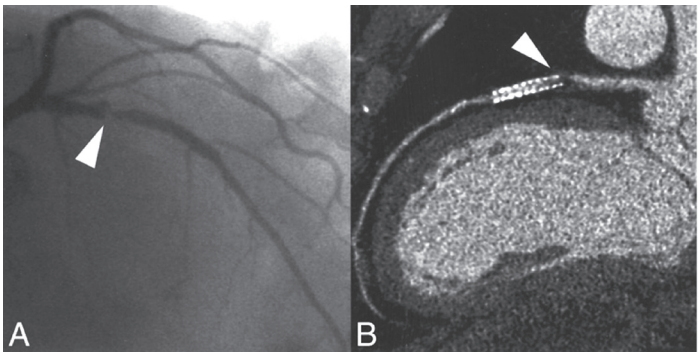

FIGURE 3. Example of High-Grade in-Stent Restenosis. (A) A conventional coronary angiogram is provided showing the presence of high-grade in-stent restenosis in the proximal part of a stent (Taxus, 3.0 x 24 mm) placed in the left anterior descending coronary artery (arrowhead). (B) A curved multiplanar reconstruction obtained with 64-slice MSCT (Siemens Sensation, kernel B46f) shows the presence of a large obstructing hypodense lesion in the proximal part of the stent (arrowhead), indicating the presence of high-grade in-stent restenosis. Abbreviations as in Figure 1.

TABLE 3. Relationship Between Stent Size and Accuracy

	Stent Diameter		
	Stents (%, 95% CI)		
	<3.0	3.0	>3.0
Assessable	49/52 (94.2%, 88%–100%)	63/70 (90.0%, 83%–97%)	66/70 (94.3%, 89%–100%)
False positive	2/49 (4.1%, 0%–9.7%)	1/63 (1.6%, 0%–4.7%)	8/66 (12%, 4.2%–19.8%)
False negative	1/49 (2.0%, 0%–5.9%)	0/63 (0%, NA)	0/66 (0%, NA)

NA = not applicable.

TABLE 4. Results From the 2 Scanners From the 2 Centers Separately

	Rotterdam, Siemens Sensation 64-Slice	Leiden, Toshiba Aquilion 64-Slice
	Stents (%, 95% CI)	Stents (%, 95% CI)
Assessable	142/150 (94.7%, 91%–99%)	36/42 (85.7%, 76%–96%)
Sensitivity	15/16 (93.8%, 82%–100%)	4/4 (100%)
Specificity*	115/126 (91.3%, 86%–96%)	32/32 (100%)
Positive predictive Value	15/26 (57.7%, 39%–77%)	4/4 (100%)
Negative Predictive Value	115/116 (99.1%, 97%–100%)	32/32 (100%)
With uninterpretable stents included		
Sensitivity	15/17 (88.2%, 82%–100%)	4/4 (100%)
Specificity	115/133 (86.5%, 80%–92%)	32/38 (84.2%, 72%–96%)
Positive predictive Value	15/33 (45.5%, 28%–62%)	4/10 (40.0%, 10%–70%)
Negative Predictive Value	115/117 (98.3%, 95%–100%)	32/32 (100%)

*p <0.05 between 2 centers.

= NS). Diagnostic accuracy was slightly lower in the Rotterdam center (91.5% vs. 100%, p = 0.05). However, when all stents (including the uninterpretable stents) were included in the analysis, no significant differences were observed.

Discussion

In the present study, a sensitivity and specificity of respectively 95% and 93% were observed for the noninvasive detection of coronary in-stent restenosis. In addition, a negative predictive value of 99% was observed, suggesting that 64-slice MSCT may allow reliable exclusion of in-stent

restenosis before more invasive procedures such as conventional coronary angiography. During MSCT imaging, visualization of stents is particularly challenging because of the metallic struts resulting in blooming artifacts (16). Accordingly, the stent wall appears enlarged on the MSCT images, which in turn affects the capability to visualize the in-stent lumen. The extent of this artefact depends on the material and design of the stent, with more severe artefacts in stents with high metal content. Although this effect is of minor or no importance in large vessels, such as the aorta and its abdominal branches, it can considerably impair the visualization of the lumen in smaller vessels such as the coronary arteries (16).

Not surprisingly, therefore, visualization of stent lumen could not be achieved in preliminary investigations using 4-slice MSCT scanners (10). In a more recent report, 16-slice MSCT was applied, resulting in a sensitivity and specificity of 78% and 100% (15). Nonetheless, 15 (23%) of the 65 included stents were uninterpretable, indicating still a limited value for MSCT coronary angiography in populations with previous stent implantation (15). More detailed analysis of these 15 uninterpretable stents revealed that stent assessability seems to be highly dependent on stent type and size in particular. These observations were further underlined by Gilard et al. (17), who showed, in 143 patients undergoing 16-slice MSCT, an increase of stent interpretability from 51% for stents ≤3.0 mm to 81% when only stents >3.0 mm were included. More recently, data on stent evaluation using more advanced MSCT technology were reported by Gaspar et al. (18), who evaluated 65 patients with 111 implanted coronary stents using 40-slice MSCT. A considerable improvement in image quality was witnessed in this study because only a small number of stents (n = 5, 5%) were of nondiagnostic image quality. Considering these 5 stents as having restenosis, the investigators reported a sensitivity and specificity for detection of in-stent restenosis of 89% and 81%, respectively. These observations are further underlined by the first ex vivo reports on stent evaluation with 64-slice MSCT, suggesting further improvement in stent visibility as well a reduction of artificial lumen narrowing as compared with 16-slice MSCT (19,20). Also in vivo promising results were reported using 64-slice MSCT by Rist et al. (21), who could evaluate 45 (98%) of 46 stents with a sensitivity and specificity of 75% and 92%, respectively. Nonetheless, somewhat discouraging results were recently reported by Rixe et al. (22), who performed 64-slice MSCT in 64 patients with 102 previously implanted stents. Similar to our study, 64-slice MSCT was shown to be highly accurate, with reported sensitivity and specificity of 86% and 98%, respectively. However, evaluation could be

performed in only 58% of stents, indicating a major limitation of the current technique. In contrast, only 7% of stents were deemed uninterpretable in our present study. To a large extent this discordance may be caused by differences in image interpretation. In our present study, evaluation was performed with the intention to diagnose to allow generalization of results as much as possible to daily clinical routine. Thus, only stents with severely degraded image quality were excluded. In contrast, a more stringent approach was performed by Rixe et al., and in their study, stents were deemed uninterpretable in the presence of any artifact, albeit small. Importantly, both in their study as well as ours, a high negative predictive value was obtained (98% and 99%, respectively), implying a potential role for MSCT to exclude in-stent restenosis in patients presenting with chest pain after stent implantation.

Study Limitations

Several limitations should be addressed. First, only patients having stents with a diameter ≥2.5 mm were included, whereas stents <2.5 mm, which may be encountered in 3% to 5% of patients with previous stent placement, were excluded, because at present they cannot be evaluated accurately with MSCT. Accordingly, the results obtained in the present study may not be generalizable to other populations with different stent characteristics. Second, as previously reported with MSCT coronary angiography, only patients with stable and low heart rates were included in this study, and a high percentage received additional beta-blockers to further reduce heart rate. Accordingly, the results of the present study may not apply to the general population, because in addition to patients with smaller stents, also patients with atrial fibrillation and contraindications to beta-blocking medication were not studied. Third, in-stent restenosis was only present in a small number of stents (11%). However, the findings reflect the current clinical situation, with low in-stent restenosis rates (3–5). In addition, data acquisition was performed in 2 different centers using 2 different 64-slice MSCT systems, which may have influenced the results. Also, no data on interobserver variability were available. Finally, several disadvantages are inherent to the technique itself, including the high radiation exposure (15 to 20 mSv) (23,24) and use of iodinated contrast, which remain a matter of concern for routine use of this technique. Also, an important limitation of MSCT remains the fact that only anatomical information is obtained, whereas the presence or absence of ischemia cannot be established from the MSCT images. Accordingly, in patients with significant restenosis, functional testing remains mandatory to determine further management.

CHAPTER 17

Conclusion

In-stent restenosis can be evaluated with 64-slice MSCT with good diagnostic accuracy. In particular, a high negative predictive value of 99% was observed, indicating that 64-slice MSCT may be most valuable to exclude in-stent restenosis.

CHAPTER 18

Dual source coronary computed tomography angiography for detecting in-stent restenosis

Pugliese F, Weustink AC, Van Mieghem C, Alberghina F, Otsuka M, Meijboom WB, Van Pelt N, Mollet NR, Cademartiri F, Krestin GP, Hunink MGM, de Feyter PJ.

Heart 2008; 94:848-854.

Summary

Purpose: To evaluate the performance of Dual source CT coronary angiography (DSCT-CA) in the detection of in-stent restenosis (≥50% luminal narrowing) in symptomatic patients referred for conventional angiography (CA).

Material and Methods : We prospectively evaluated 100 patients (78 males, age 62 ± 10) with chest pain after coronary stenting. DSCT-CA was performed before CA. Many patients undergo coronary artery stenting; availability of a non-invasive modality to detect in-stent restenosis would be desirable.

Results: Average heart rate (HR) was 67 ± 12 (range 46-106) beats per minute (bpm). There were 178 stented lesions. The interval between stenting and inclusion in the study was 35 ± 41 (range 3-140) months. Thirty-nine/100 (39%) patients had angiographically proven restenosis. Sensitivity, specificity, PPV and NPV of DSCT-CA, calculated in all stents, were 94%, 92%, 77% and 98%, respectively. Diagnostic performance at HR <70bpm (n=69; mean 58 bpm) was similar to that at HR ≥70bpm (n=31; mean 78 bpm); diagnostic performance in single stents (n=95) was similar to that in overlapping stents and bifurcations (n=83). In stents ≥3.5mm (n=78), sensitivity, specificity, PPV, NPV were 100%; in 3mm stents (n=59), sensitivity and NPV were 100%, specificity 97%, PPV 91%; in stents ≤2.75mm (n=41), sensitivity was 84%, specificity 64%, PPV 52%, NPV 90%. Nine stents ≤2.75mm were uninterpretable. Specificity of DSCT-CA in stents ≥3.5mm was significantly higher than in stents ≤2.75mm (OR = 6.14; 99%CI: 1.52-9.79).

Conclusion: DSCT-CA performs well in the detection of in-stent restenosis. Although DSCT-CA leads to frequent false positive findings in smaller stents (≤2.75mm), it reliably rules-out in-stent restenosis irrespective of stent size.

Introduction

Computed tomography angiography is a non-invasive diagnostic tool to visualize coronary arteries 1. The evaluation of stents is however hampered by the occurrence of high-density artifacts ('blooming effect') caused by the stent struts. These artifacts cause an apparent enlargement of the stent and preclude appropriate assessment of the in-stent lumen.

In particular, the lumen of small stents, overlapping stents and bifurcation stents are difficult to assess 2. Motion artifacts may further hinder the evaluation of stents 3. Several investigations have evaluated the diagnostic performance of computed tomography in assessing stent patency or the presence of in-stent restenosis 4-16 ; these studies have included patients with low heart rates and pre-scan preparation with ß-blockers.

The introduction of Dual source 64-slice computed tomography scanners, with an improved temporal resolution 17, may be helpful to more accurately assess coronary stents.

In this study we evaluated the diagnostic performance of Dual source computed tomography coronary angiography (DSCT-CA) for the detection of in-stent restenosis in patients with anginal symptoms after stent implantation.

Materials and Methods

Population

From April 2006 to January 2007, 133 patients with chest pain and prior stent implantation were considered for inclusion in this prospective study. All patients were scheduled for diagnostic conventional angiography. Serum creatinine >120 μmol/l, irregular heart rhythm and known allergy to iodinated contrast agents were exclusion criteria. The recruitment procedure is described in Figure 1. The institutional review board approved the study protocol and all the included patients gave informed consent.

DSCT-CA Protocol

All patients were examined with a Dual source CT scanner (Somatom Definition, Siemens, Forchheim, Germany). The scanner design consists of 2 X-ray tubes and 2 detector arrays mounted at an angle of 90°. Scan parameters were: 120 kV,

330 ms gantry rotation time, 2 x 32 x 0.6 mm collimation with z-flying focal spot for both detectors. Using this scan protocol, spatial resolution was 0.4x0.4x0.4 mm3 17. Pitch values were automatically adapted to the heart rate after an estimation based on the last 10 heart beats preceding the scan, and varied between 0.20 and 0.43. Current X-ray tube modulation was used at full current for 25-70% of the R-R interval. Each tube provided a maximum of 412mAs/rotation. In patients with heart rates <70bpm, X-ray exposure was (mean ± sd) 15.0 ± 4.1mSv in males and 16.7 ± 5.0mSv in females; in patients with heart rates ≥70bpm, X-ray exposure was 12.1 ± 2.6mSv in males and 13.7 ± 4.7 in females (values calculated using ImPACT®, version 0.99x, St. George's Hospital, Tooting, London, UK).

All patients received sublingual Nitroglycerin just before scanning. Contrast agent (Iomeron® 400 mgI/ml, Bracco, Italy) was injected into the antecubital vein at a flow rate of 5.0 ml/s, followed by a saline chaser (40 ml). We calculated the contrast volume with the following equation: estimated scan time + scan delay (7s). The contrast volume varied between 60 and 100 ml depending on the scan time, which in turn varied between 5 and 13 seconds. We used a bolus-tracking technique to synchronize the start of the scan with the arrival of contrast agent in the coronary arteries. A circular region-of-interest (ROI) was positioned in the ascending aorta and the scan was automatically started when a threshold of +100 Hounsfield Units was reached inside the ROI.

Image Reconstruction

Given the scanner geometry, a mono-segmental algorithm using data from a single heartbeat obtained during a quarter gantry rotation was used for reconstruction. This translated into a temporal resolution equal to one fourth of the gantry rotation time, i.e. 330/4 = 83 ms.

First, 0.75 mm-thick images were retrospectively reconstructed during the mid- to end-diastolic phase. The position of the reconstruction window within the R-R interval varied according to the heart rate (from -400 ms before the R wave for low heart rates to -175 ms for high heart rates). Additional data sets were reconstructed during the end-systolic phase (from +400 ms after the R wave for low heart rates to +200 ms for high heart rates). The reconstruction increment was 0.4 mm. The data set with the least motion artifacts was chosen for analysis and reconstructed using a dedicated sharp convolution kernel (B46f, 'Heart View').

Quantitative Coronary Angiography (QCA)

A single observer unaware of the CT results examined the angiograms before

contrast injection to identify the sites of stent implantation. The stents were then located within the coronary tree following a 17-segment modified AHA model, as previously described 18,19. Stents and stent edges, the latters defined as 5 mm-long coronary segments proximally and distally to the stents, were evaluated on multiple projections; luminal narrowing ≥50% was classified as significant (restenosis). A validated quantitative coronary angiography software (CAAS II®, Pie Medical, Maastricht, the Netherlands) was used to determine the minimal lumen diameter and derive the percent diameter stenosis by means of the user-independent method of the interpolated reference diameter, using the angiographic catheter diameter as reference for calibration 20.

DSCT-CA Analysis

Two experienced readers evaluated the DSCT-CA studies independently; the readers were unaware of the findings of conventional angiography. In the event of diverging opinions, a consensus was reached and used in the final analysis.

Using axial images, multi-planar reconstructions (MPR) and curved MPR, the stents were visually screened for the presence of in-stent restenosis (≥50% lumen diameter reduction). When multiple stents were implanted contiguously to treat 1 lesion, they were considered as 1 single lesion. The assessment of restenosis was based exclusively on the visualization of the in-stent lumen. The presence of distal run-off was not considered as an indicator of patency because retrograde or collateral filling in an occluded stent can also give distal contrast enhancement (Figure 2). All stent edges, defined as 5 mm-long coronary segments proximally and distally to the stents, were also included in the evaluation. In the event of bifurcation stenting, each of the 3 branches was evaluated. When the stent lumen was uninterpretable (e.g., obscured by high-density artifacts), and in-stent restenosis could not be excluded by DSCT-CA, stents were considered to have restenosis (worst case scenario) 6,7 for the purpose of the analysis.

Statistics

The statistical analysis was performed with SPSS, version 12.1 (SPSS Inc., Chicago, Ill.). Results are reported in accordance with the STARD criteria 21. Continuous variables are expressed as mean ± standard deviation. Categorical variables are presented as counts and percentages.

Sensitivity, specificity, positive predictive value (PPV), and negative predictive value (NPV) of DSCT-CA for the detection of ≥50% in-stent restenosis, as determined by QCA as reference standard, were computed in 2 subgroups defined as 'low heart rate' and 'high heart rate' ; the

definition of the 2 groups was based on a cut-off heart rate of 70 beats per minute (bpm) as previously described by Leber et al. 22 and Mollet et al.19. The 'low heart rate' subgroup comprised patients with heart rates <70 bpm, the 'high heart rate' subgroup comprised patients with heart rates ≥70bpm.

Sensitivity, specificity, PPV and NPV were then computed in 2 subgroups defined as 'simple configuration' and 'complex configuration': the 'simple configuration' subgroup comprised lesions treated with the deployment of one single stent; the 'complex configuration' subgroup comprised overlapping stents and bifurcation stenting.

We also computed sensitivity, specificity, PPV and NPV in 3 subgroups defined by stent diameters, i.e. ≥3.5mm, 3mm and ≤2.75mm. When multiple stents were employed to treat 1 lesion, the diameter of the proximal stent determined the diameter subgroup. This criterion for sub-classifying lesions with multiple stents was based on the expectation that small stents were more difficult to evaluate than large stents; we preferred to underestimate the diagnostic performance in the larger stent subgroups rather than overestimating the diagnostic performance in the smaller stent subgroup.

Sensitivity, specificity, PPV and NPV were also computed separately for the right coronary artery (RCA), left main (LM) stem, left anterior descending (LAD) and left circumflex (LCx) arteries. Because the accuracy of DSCT-CA to detect occluded stents might be greater than the accuracy to detect restenosis, we performed separate analyses after excluding totally occluded segments. Diagnostic test results are presented with corresponding 95% confidence intervals based on binomial probabilities. The X^2 test was used to compare the frequency of occurrence of restenosis in the different subgroups. The Mann Whitney U test was used to compare the mean stent diameters in the heart rate subgroups and in the configuration subgroups.

We determined the effect of heart rate, stent configuration and stent diameter on sensitivity, specificity, PPV, and NPV using logistic regression analysis including patient identification to correct for possible correlation within the individuals who had multiple stents 23. To compensate for multiple testing, we used a significance level of 0.01 and computed 99% confidence intervals (CI).

Inter-observer and intra-observer agreement for the detection of restenosis were determined by k-statistics.

Results

Baseline Characteristics and Angiographic Findings

Of the 133 patients screened for inclusion in our study, 33 were excluded because of serum creatinine level >120 μmol/l (n=4), known contrast allergy (n=3), irregular heart rate (n=6) and refusal to undergo DSCT-CA (n=20), so that 100 patients underwent DSCT-CA (Figure 1).

DSCT-CA and conventional angiography were performed 35 ± 41 months after stenting (range 3-140 months). Seventy patients were on treatment with ß-blockers; none of the patients received additional ß-blockers before the scan.

The average heart rate during the scan was 67 ± 12 (range 42-106) bpm. Sixty-nine patients had heart rates <70 bpm and were included in the low heart rate subgroup (the average heart rate in this subgroup was 58 ± 6; range 42-69 bpm); 31 patients had heart rates ≥70 bpm and were included in the high heart rate subgroup (the average heart rate in this subgroup was 78 ± 9; range 70-106 bpm).

We examined 178 stented lesions (247 stents used, 1.4 ± 0.8 stents per lesion); 95 lesions consisted of single stents (simple configuration subgroup); the remaining 83 lesions consisted of overlapping stents (n=62) and bifurcations (n=21) (complex configuration subgroup). All but one complex lesions consisted of stents of the same type. One complex lesion was a stent-in-stent implantation consisting of 2 partially

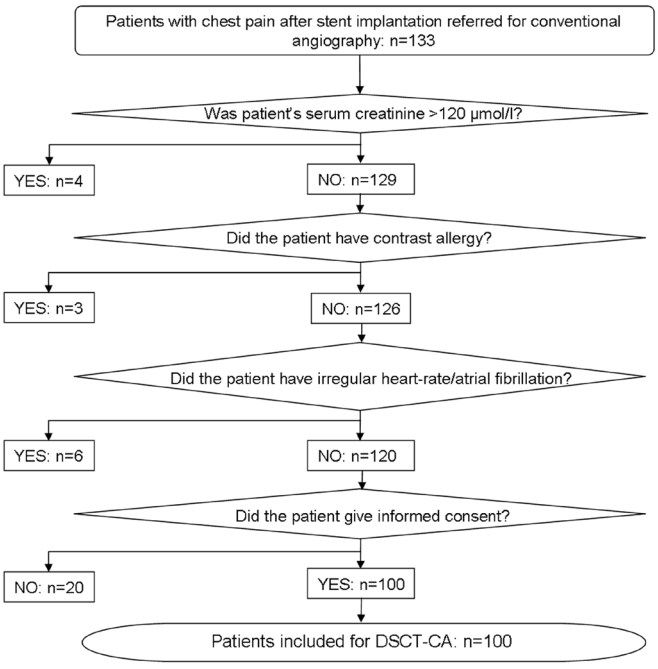

FIGURE 1. Inclusion procedure for the study (from April 2006 to January 2007).

TABLE 1. Baseline characteristics, angiographic findings and stent types

Patient number	100
Age and gender	
Age (yrs): average ± sd	62 ± 10
Men/Women	78/22
Cardiovascular risk factors: no.	
Obesity (Body Mass Index ≥ 30 Kg/m^2)	23
Smoking	25
Hypertension (≥160/95 mmHg or ongoing treatment)	45
Serum cholesterol >200 mg/dL (5.18 mmol/L)	51
Diabetes mellitus	21
Family history	29
Total number of stents used and types	247
Drug-eluting stents	157
Bare-metal stents	90
Frequency of individual diameters and types: no. (%)	
2.25	21/247 (9%)
2.5	31/247 (13%)
2.75	17/247 (7%)
3.0	82/247 (33%)
3.5	63/247 (25%)
4.0	20/247 (8%)
4.5	8/247 (3%)
5.0	5/247 (2%)
Taxus	136/247 (55%)
Cypher	21/247 (8%)
BX Velocity	32/247 (14%)
R Evolution	21/247 (8%)
NIR	7/247 (3%)
Multilink	4/247 (1.5%)
Palmaz-Schaz	4/247 (1.5%)
Other BMS*	22/247 (9%)
Number of lesions and stent types: no. (%) †	178
Drug-eluting stents	113 (63%)
Bare-metal stents	65 (37%)

Vessel implanted: no. (%)		
	RCA	60 (34%)
	LM stem	11 (6%)
	LAD	58 (32%)
	LCx	49 (28%)
Patients diagnosed with ≥50% restenosis (no.)		39
Lesions with ≥50% restenosis: no. (%)		39/178 (22%)
	Restenosis	22/39 (56%)
	Total occlusion	17/39 (44%)
Stent types with restenosis: no. (%)		
	Drug-eluting stents	12/113 (11%)
	Bare-metal stents	27/65 (42%)

* Type not available (implanted before 2003)
† One stent-in-stent implantation consisting of 2 BX Velocity plus 3 Taxus stents was classified as BMS; all other complex lesions consisted of stents of the same type

overlapped BX Velocity stents plus 3 Taxus stents implanted 1 year later (Figure 2); this lesion was classified as a bare metal stent (BMS) lesion. BMS accounted for 37% (65/178) of the stented lesions, drug-eluting stents (DES) accounted for 63% (113/178) of the stented lesions. Restenosis was diagnosed angiographically in 39/178 (22%) stented lesions in 39/100 (39%) patients. Restenosis was found in 27/65 (42%) BMS and in 12/113 (11%) DES. Table 1 summarizes patient baseline characteristics, main angiographic findings and stent types.

The frequency of in-stent restenosis was 23% (29/124) in the low heart rate subgroup and 19% (10/54) in the high heart rate subgroup. In the simple and complex configuration subgroups, frequencies were 18% (17/95) and 26% (22/83), respectively. In the ≥3.5 mm, 3 mm and ≤2.75 mm subgroups, frequencies of restenosis were 19% (15/78), 20% (12/59) and 31% (13/41), respectively. All p-values were not significant ($p > 0.05$).

The mean stent diameter in the entire sample was 3.15 ± 0.58. The mean stent diameters in the simple and complex configuration subgroups were 3.16 ± 0.60 mm and 3.15 ± 0.61 mm, respectively. The mean stent diameters in the low and high heart rate subgroups were 3.17 ± 0.61 mm and 3.15 ± 0.66 mm, respectively. All p-values were not significant ($p > 0.05$).

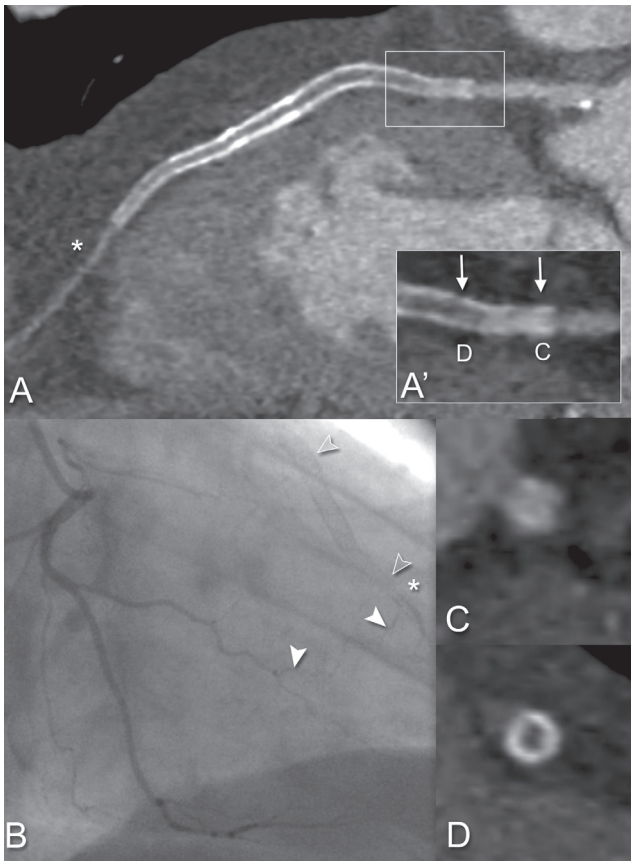

FIGURE 2. Distal run-off as a criterion of patency. The presence of distal run-off is not always associated with stent patency. A: a DSCT-CA curved multiplanar reconstruction shows a stented lesion consisting of 2 BX Velocity stents plus 3 Taxus stents (stent-in-stent) in the left anterior descending artery (LAD). In spite of the presence of distal run-off (asterisk), in-stent total occlusion is seen. C-D: stent cross sections obtained as indicated in A' (magnification of A) show the appearances of a patent stent (C) and of a totally occluded stent (D), respectively. B: the corresponding conventional angiogram demonstrates that, distally to the stents (void arrowheads), the LAD (asterisk) is fed by collateral flow (solid arrowheads). Direct visualization of the stent lumen is therefore mandatory to rule-out in-stent restenosis with DSCT-CA.

Diagnostic Performance of DSCT-CA

All 178 stented lesions were detected by DSCT-CA. The stent lumen was judged interpretable in 169/178 (95%) stents. In the remaining 9 stents (5%), all of which were ≤2.75mm in diameter, the lumen was uninterpretable due to high-density artifacts obscuring the in-stent lumen; these stents were scored as having in-stent restenosis. However, these 9 small stents were angiographically normal (no in-stent restenosis, DSCT-CA false positives).

Sensitivity, specificity, PPV and NPV in detecting ≥50% restenosis, calculated on all stents, were 94%, 92%, 77% and 98%, respectively. The diagnostic performance of DSCT-CA at heart rates <70bpm did not differ significantly from that obtained at heart rates ≥70bpm, as witnessed by widely overlapping confidence intervals. The diagnostic performances obtained in simple stents and overlapping stents/bifurcations were also similar. Likewise, no significant differences were seen between the 4 major coronary vessels. Table 2 gives sensitivity, specificity, PPV and NPV obtained in the heart rate subgroups, in simple and complex con-

TABLE 2. Diagnostic performance of DSCT-CA in detecting ≥50% luminal narrowing – All Lesions and subgroup analysis

	All Lesions	HR<70 Mean=58±6	HR≥70 Mean=78±9	Simple	Complex	≥3.5mm	3.0mm	≤2.75mm	RCA	LM	LAD	LCx
Total	178	124	54	95	83	78	59	41	60	11	58	49
TP	37	28	9	16	21	15	11	11	8	0	15	14
TN	128	88	40	74	54	63	47	18	48	11	38	31
FP	11 (9)*	7	4	4	7	0	1	10 (9)*	4	0	4	3
FN	2	1	1	1	1	0	0	2	0	0	1	1
Sensitivity	37/39 **.94** (.81-.99)	28/29 **.96** (.80-.99)	9/10 **.90** (.54-.99)	16/17 **.94** (.69-.99)	21/22 **.95** (.75-.99)	15/15 **1** (.74-1)	11/11 **1** (.67-1)	11/13 **.84** (.53-.97)	8/8 **1** (.59 -1)	-	15/16 **.93** (.67-.99)	14/15 **.93** (.66-.99)
Specificity	128/139 **.92** (.85-.95)	88/95 **92** (.84-.96)	40/44 **.90** (.77-.97)	74/78 **.94** (.86-.98)	54/61 **.88** (.77-.94)	63/63 **1** (.92-1)	47/48 **.97** (.79-.99)	18/28 **.64** (.44-.80)	48/52 **.92** (.80-.97)	11/11 **1** (.67-1)	38/42 **.90** (.76-.99)	31/34 **.91** (.75-.97)
PPV	37/48 **.77** (.62-.87)	28/35 **.80** (.62-.90)	9/13 **.69** (.38-.89)	16/20 **.80** (.55-.93)	21/28 **.75** (.54-.88)	15/15 **1** (.74-1)	11/12 **.91** (.59-.99)	11/21 **.52** (.30-.73)	8/12 **.66** (.35-.88)	-	15/19 **.78** (.53-.93)	14/17 **.82** (.55-.95)
NPV	128/130 **.98** (.93-.99)	88/89 **.98** (.93-.99)	40/41 **.97** (.85-.99)	74/75 **.98** (.91-.99)	54/55 **.98** (.89-.99)	63/63 **1** (.92-1)	47/47 **1** (.90-1)	18/20 **.90** (.66-.98)	48/48 **1** (.90-1)	11/11 **1** (.67-1)	38/39 **.97** (.84-.99)	31/32 **.96** (.82-.99)
After exclusion of totally occluded stents:												
Total	161	113	48	87	74	70	55	36	57	11	51	42
TP	20	17	3	8	12	7	7	6	5	0	8	7
TN	128	88	40	74	54	63	47	18	48	11	38	31
FP	11	7	4	4	7	0	1	10	4	0	4	3
FN	2	1	1	1	1	0	0	2	0	0	1	1
Sensitivity	20/22 **.90** (.69-.98)	17/18 **.94** (.70-.99)	3/4 **.75** (.21-.98)	8/9 **.88** (.50-.99)	12/13 **.92** (.62-.99)	7/7 **1** (.56-1)	7/7 **1** (.56-1)	6/8 **.75** (.35-.95)	5/5 **1** (.46-1)	-	8/9 **.88** (.50-.99)	7/8 **.87** (.46-.99)
Specificity	128/139 **.92** (.85-.95)	88/95 **.92** (.84-.96)	40/44 **.90** (.77-.97)	74/78 **.94** (.86-.98)	54/61 **.88** (.77-.94)	63/63 **1** (.92-1)	47/48 **.97** (.79-.99)	18/28 **.64** (.44-.80)	48/52 **.92** (.80-.97)	11/11 **1** (.67-1)	38/42 **.90** (.76-.96)	31/34 **.91** (.75-.97)
PPV	20/31 **.64** (.45-.80)	17/24 **.70** (.48-.86)	3/7 **.42** (.11-.79)	8/12 .66 (.35-.88)	12/19 **.63** (.38-.82)	7/7 **1** (.56-1)	7/8 **.87** (.46-.99)	6/16 **.37** (.16-.64)	5/9 **.55** (.22-.84)	-	8/12 **.66** (.35-.88)	7/10 **.70** (.31-.95)
NPV	128/130 **.98** (.93-.99)	88/89 **.98** (.93-.99)	40/41 **.97** (.85-.99)	74/75 **.98** (.91-.99)	54/55 **.98** (.89-.99)	63/63 **1** (.92-1)	47/47 **1** (.90-1)	18/20 **.90** (.66-.98)	48/48 **1** (.90-1)	11/11 **1** (.67-1)	38/39 **.97** (.84-.99)	31/32 **.96** (.82-.99)

*Nine stents had uninterpretable lumen; all these 9 stents were ≤2.75mm in diameter. These were considered positives for the purpose of the analysis.

figuration subgroups and in the 4 major coronary vessels.

In the diameter-based subanalysis, we found that NPV was in the range 90-100% in all subgroups. Sensitivity was 100% in ≥3.5 mm stents and in 3 mm stents, but it dropped to 84% in ≤2.75 mm stents. Specificity and PPV were both 100% in the ≥3.5 mm subgroup; the values for specificity and PPV were 97% and 91%, respectively, in the 3 mm subgroup, and 64% and 52%, respectively, in the ≤2.75 mm subgroup. Table 2 gives the diagnostic performance of DSCT-CA in detecting ≥50% luminal narrowing in the different diameter subgroups.

In the logistic regression analysis predicting specificity, a stent diameter of ≥3.5 mm had an odds ratio of 6.14 (99%CI 1.52-9.79). In predicting the PPV, a stent diameter of ≥3.5 mm had an odds ratio of 3.70 (99%CI 0.98-8.90). All other variables were not significant.

The inter-observer agreement in detecting restenosis was good (k- value = 0.78). The intra-observer agreement was very good (k- value = 0.87).

Discussion

Cardiac catheterization is the technique of choice for the detection of in-stent restenosis. However, it may be involved with life threatening complications and is relatively expensive. The diagnostic accuracy of noninvasive techniques such as exercise testing is known to be suboptimal 24, therefore an alternative noninvasive 'gatekeeper' to invasive coronary angiography would be desirable. The reliability of such technique would have to be demonstrated in various clinical situations (i.e., various stent sizes and configurations, higher heart rates) before it could be routinely used in patients with prior coronary artery stenting.

Feasibility of DSCT-CA at High Heart Rates

This study showed that DSCT-CA was accurate in detecting in-stent restenosis without the use of pre-scan ß-blockers. Although the rate of false positives was slightly higher at high heart rates (PPV=69%) than at low heart rates (PPV=80%), the number of false negatives was low in both subgroups (NPV in the range 97-98%). In addition, the capability to perform DSCT-CA at higher heart rates without the use of ß-blockers may be advantageous in terms of reducing radiation exposure. Table speed increases with increasing heart rates in DSCT-CA, which in turn translates into shorter scan times and reduced radiation exposure.

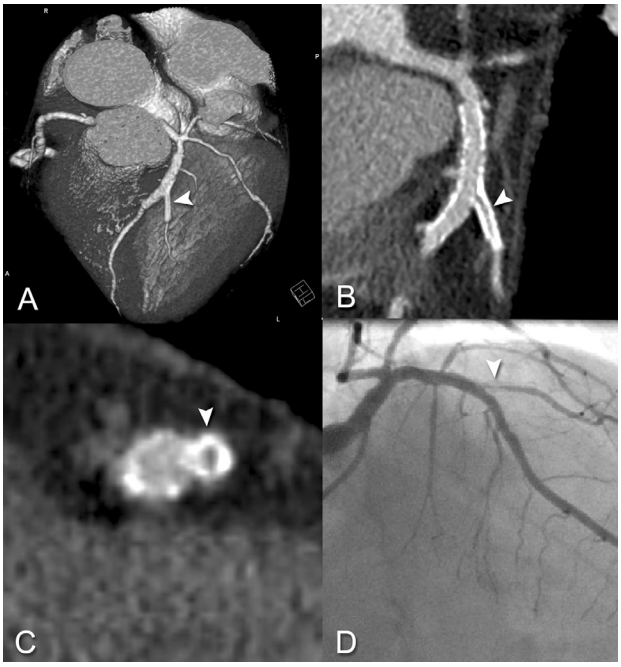

FIGURE 3. Bifurcations. Patient with in-stent restenosis 6 months after crush-stenting. A: a volume-rendered DSCT-CA image shows bifurcation stenting of the left anterior descending artery (LAD) and 2nd diagonal branch. The stent in the diagonal branch (side branch) has a diameter of 2.25 mm, the stent in the LAD (main branch) has a diameter of 4 mm. B: MPR image, C: MPR cross-section obtained at the level of the carina, and D: corresponding conventional angiogram demonstrate restenosis in the diagonal branch (arrowhead); the main branch is patent. In B, note the typical CT appearance of the crush technique, characterized by three layers of metal crushed against the ostium of the side branch.
(A full color version of this illustration can be found in the color section)

in single stents, probably due to the large amount of metal at the ostium of side branches and at overlapping sites. This excess of metal is a major source of high-density artifacts in CT and may lead to lesion overestimation (Figure 3).

It may be argued that restenosis occurs more frequently in patients with complex lesion characteristics than in patients with simple lesions 25. This might have led to an overestimation of sensitivity in our Complex configuration subgroup. However, the difference between the frequency of restenosis in our Simple and Complex configuration subgroups was not statistically significant.

Stent Configurations

To the best of our knowledge, the population evaluated in the present study is the largest available in the literature on coronary CT angiography including overlapping and bifurcation stenting (n=83). Although the differences were not statistically significant, we found that specificity and PPV of DSCT-CA in bifurcation stenting and overlapping stents were slightly lower than those obtained

Stent Diameters

We found that stent diameter was the most important feature influencing the diagnostic performance of coronary CT angiography. This is in keeping with the findings of Gilard et al. 8 and of Rixe et al. 13, who performed 16-slice CT coronary angiography and 64-slice CT coronary angiography, respectively, in patients with low heart rates. In those studies though, up to 50% of the stents were

judged unevaluable. With DSCT-CA, we judged unevaluable only 5% (n=9) of the stents, and found a low rate of false negatives irrespective of stent diameter (NPV in all stents = 98%, NPV in stents ≤2.75mm = 90%). When stent diameter was ≤2.75mm, DSCT-CA had a high rate of false positives (specificity = 64%; PPV = 52%) and could not predict with certainty the presence of restenosis; in particular, the specificity of DSCT-CA in this subgroup was significantly lower than that obtained in stents ≥3.5mm (OR = 6.14; 99%CI: 1.52-9.79). Therefore our study confirms that DSCT-CA is not a suitable gatekeeper to conventional angiography in symptomatic patients with ≤2.75mm stents.

In a recent study, Cademartiri et al.4 reported the relationship between diagnostic accuracy of 64-slice CT and stent size in terms of the rate of false diagnosis (false positives and false negatives). In contrast with our findings, the rate of false diagnosis reported in that study did not decrease with increasing stent diameters. In stents <3mm, the rate of false diagnosis was 6.1%; in 3mm stents, the rate of false diagnosis was 1.6% and surprisingly, in stents >3mm, the rate of false diagnosis was 12%. An explanation of these findings compared to our study is that only patients with stents larger than 2.5mm were included. Secondly, complex stent configurations such as overlapping stents and bifurcation stenting were not included in that study, which may have led to an overestimation of the diagnostic performance in smaller stents. Lastly a 64-slice CT scanner was used as compared to the Dual source CT scanner in this study.

It is conceivable that future developments in CT technology might further increase the diagnostic performance in patients with stents by improvements in spatial (e.g. flat panel technology) and temporal resolution.

Totally Occluded Stents

Totally occluded stents might be easier to recognize on DSCT-CA. In our sample, 17 stents were totally occluded. Overall, the analysis after exclusion of totally occluded segments yielded similar sensitivity, specificity and NPV but lower PPV (Table 2).

Study Limitations

We examined a selected symptomatic patient cohort; applicability to a wider population may therefore yield different results. This limitation was inevitable in order to compare DSCT-CA to the reference technique, i.e., conventional coronary angiography.

X-ray radiation exposure is a general limitation of multi-slice CT coronary angiog-

raphy 26,27. However, using X-ray tube modulation, full dose radiation may be given for a shorter duration of the cardiac cycle than used in this study. Radiation dose is further reduced by automated pitch adaptation with higher heart rates. Other widely accepted imaging techniques, such as technetium sestamibi scans, may deliver radiation doses as high as 20mSv 26,27.

Conclusions

This study shows that in patients with recurrent chest pain after stent implantation, DSCT-CA performs well in the detection of in-stent restenosis. Stent diameter is an important predictor of DSCT-CA diagnostic performance; when stent diameter is ≤2.75mm, the technique is associated with frequent false positives. However, due to the high NPV, DSCT-CA reliably rules-out in-stent restenosis irrespective of stent size.

References

1. Hendel RC, Patel MR, Kramer CM, et al. ACCF/ACR/SCCT/SCMR/ASNC/NASCI/SCAI/SIR 2006 appropriateness criteria for cardiac computed tomography and cardiac magnetic resonance imaging: a report of the American College of Cardiology Foundation Quality Strategic Directions Committee Appropriateness Criteria Working Group, American College of Radiology, Society of Cardiovascular Computed Tomography, Society for Cardiovascular Magnetic Resonance, American Society of Nuclear Cardiology, North American Society for Cardiac Imaging, Society for Cardiovascular Angiography and Interventions, and Society of Interventional Radiology. J Am Coll Cardiol 2006;48(7):1475-97.
2. Pugliese F, Cademartiri F, van Mieghem C, et al. Multidetector CT for visualization of coronary stents. Radiographics 2006;26(3):887-904.
3. Ulzheimer S, Kalender WA. Assessment of calcium scoring performance in cardiac computed tomography. Eur Radiol 2003;13(3):484-97.
4. Cademartiri F, Schuijf JD, Pugliese F, et al. Usefulness of 64-slice multislice computed tomography coronary angiography to assess in-stent restenosis. J Am Coll Cardiol 2007;49(22):2204-10.
5. Cademartiri F, Mollet NR, Lemos PA, Pugliese F, Baks T, McFadden EP, Krestin GP, de Feyter PJ. Usefulness of Multislice Computed Tomographic Coronary Angiography to Assess In-Stent Restenosis. Am J Cardiol

2005;96:799-802.

6. Ehara M, Kawai M, Surmely JF, et al. Diagnostic accuracy of coronary in-stent restenosis using 64-slice computed tomography comparison with invasive coronary angiography. J Am Coll Cardiol 2007;49(9):951-9.
7. Gaspar T, Halon DA, Lewis BS, et al. Diagnosis of coronary in-stent restenosis with multidetector row spiral computed tomography. J Am Coll Cardiol 2005;46(8):1573-9.
8. Gilard M, Cornily JC, Pennec PY, et al. Assessment of coronary artery stents by 16 slice computed tomography. Heart 2006;92(1):58-61.
9. Hong C, Chrysant GS, Woodard PK, Bae KT. Coronary artery stent patency assessed with in-stent contrast enhancement measured at multi-detector row CT angiography: initial experience. Radiology 2004;233(1):286-91.
10. Kitagawa T, Fujii T, Tomohiro Y, et al. Noninvasive assessment of coronary stents in patients by 16-slice computed tomography. Int J Cardiol 2006;109(2):188-94.
11. Ohnuki K, Yoshida S, Ohta M, et al. New diagnostic technique in multi-slice computed tomography for in-stent restenosis: pixel count method. Int J Cardiol 2006;108(2):251-8.
12. Oncel D, Oncel G, Karaca M. Coronary Stent Patency and In-Stent Restenosis: Determination with 64-Section Multidetector CT Coronary Angiography--Initial Experience. Radiology 2007;242(2):403-9.
13. Rixe J, Achenbach S, Ropers D, et al. Assessment of coronary artery stent restenosis by 64-slice multi-detector computed tomography. Eur Heart J 2006;27(21):2567-72.
14. Schuijf JD, Bax JJ, Jukema JW, et al. Feasibility of assessment of coronary stent patency using 16-slice computed tomography. Am J Cardiol 2004;94(4):427-30.
15. Seifarth H, Raupach R, Schaller S, et al. Assessment of coronary artery stents using 16-slice MDCT angiography: evaluation of a dedicated reconstruction kernel and a noise reduction filter. Eur Radiol 2005;15(4):721-6.
16. Van Mieghem CA, Cademartiri F, Mollet NR, et al. Multislice spiral computed tomography for the evaluation of stent patency after left main coronary artery stenting: a comparison with conventional coronary angiography and intravascular ultrasound. Circulation 2006;114(7):645-53.
17. Flohr TG, McCollough CH, Bruder H, et al. First performance evaluation of a dual-source CT (DSCT) system. Eur Radiol 2006;16(2):256-68.
18. Austen WG, Edwards JE, Frye RL, et al. A reporting system on patients evaluated for coronary artery disease. Report of the Ad Hoc Committee for Grading of Coronary Artery Disease, Council on Cardiovascular Surgery, American Heart Association. Circulation 1975;51(4 Suppl):5-40.
19. Mollet NR, Cademartiri F, van Mieghem CA, et al. High-resolution spiral computed tomography coronary angiography in patients referred for diagnostic conventional coronary angiography. Circulation 2005;112(15):2318-23.

20. Foley DP, Escaned J, Strauss BH, et al. Quantitative coronary angiography (QCA) in interventional cardiology: clinical application of QCA measurements. Prog Cardiovasc Dis 1994;36(5):363-84.
21. Bossuyt PM, Reitsma JB, Bruns DE, et al. Towards complete and accurate reporting of studies of diagnostic accuracy: The STARD Initiative. Ann Intern Med 2003;138(1):40-4.
22. L eber AW, Knez A, von Ziegler F, et al. Quantification of obstructive and nonobstructive coronary lesions by 64-slice computed tomography: a comparative study with quantitative coronary angiography and intravascular ultrasound. J Am Coll Cardiol 2005;46(1):147-54.
23. Smith PJ, Hadgu A. Sensitivity and specificity for correlated observations. Stat Med 1992;11(11):1503-9.
24. Zellweger MJ, Weinbacher M, Zutter AW, et al. Long-term outcome of patients with silent versus symptomatic ischemia six months after percutaneous coronary intervention and stenting. J Am Coll Cardiol 2003;42(1):33-40.
25. Sharma SK, Choudhury A, Lee J, et al. Simultaneous kissing stents (SKS) technique for treating bifurcation lesions in medium-to-large size coronary arteries. Am J Cardiol 2004;94(7):913-7.
26. Hoffmann U, Shapiro M. Coronary multidetector computed tomography: a new standard for preoperative risk assessment? J Am Coll Cardiol 2006;47(10):2025-6.
27. Morin RL, Gerber TC, McCollough CH. Radiation dose in computed tomography of the heart. Circulation 2003;107(6):917-22.

CHAPTER 19

Computed tomography coronary angiography and invasive coronary angiography are complementary to assess symptomatic post CABG patients

Weustink AC, Nieman K, Pugliese F, Mollet NR, Meijboom WB, Van Mieghem C, ten Kate G-J, Krestin GP, de Feyter PJ.

Manuscript submitted for publication

Summary

Purpose: To prospectively evaluate whether CT coronary angiography (CTCA) before invasive coronary angiography (ICA) is complementary to ICA for the evaluation of symptomatic post coronary artery bypass graft (CABG) patients.

Materials and Methods: Fifty-two symptomatic patients underwent CTCA. No oral or intravenous beta-blockers were administered prior to the scan. Quantitative coronary angiography was used as the standard of reference.

Results: A total of 63 venous grafts, including 33 jump grafts, representing 102 venous graft segments were evaluated. A total of 48 arterial grafts, including 4 jump grafts, representing 50 arterial graft segments were evaluated. Agreement between CTCA and QCA on a per segment level was very high (k-value: 0.99). A total of 170 coronary arteries (right coronary artery 67%, 35/52; left main 94%, 49/52; left anterior descending artery 96%, 50/52; left circumflex artery 69%, 36/52) including 289 segments were revascularized by bypass grafting. Agreement between CTCA and QCA on a per segment level was good (k-value: 0.79). A total of 38 coronary arteries including 118 segments were not revas-

cularized by bypass grafting. Agreement between CTCA and QCA on the per segment level was good (k-value: 0.85).

Conclusion: CTCA should not be considered as a substitute, but rather as complementary to ICA in the diagnostic work-up of symptomatic post CABG patients. The identification of significant obstructive graft disease did not require further invasive angiographic verification, while invasive coronary angiography is still required to confirm or refute CT evaluation of obstructive native coronary artery disease.

Introduction

Recurrent symptoms after surgical revascularization may be caused by progression of disease either in the nongrafted native coronary arteries or in the venous or more rarely arterial grafts [1]. Therefore, comprehensive assessment of symptomatic patients after bypass surgery should include the native coronary arteries, arterial and venous bypass grafts, and distal runoff vessels.

Invasive coronary angiography (ICA) is often rather cumbersome and requires skilful operators to engage and visualize venous and arterial bypass grafts which frequently prolongs procedure time and is associated with larger contrast use and increased radiation exposure. CT coronary angiography (CTCA) may be useful to reduce the additional extra time, contrast and radiation exposure if it were reliable to evaluate grafts and distal runoffs.

Studies using 64-slice CT scanners reported specificity values of 86% [2] and 76% [3] while up to 9% of nongrafted segments and distal runoffs were unevaluable because of presence of severe coronary calcifications, residual coronary motion or metal clip artefacts [3]. Faster rotating CT scanners may reduce motion artefacts and improve CT-reliability. The Dual Source CT scanner is equipped with two tube–detector systems rotating simultaneously resulting in an improved temporal resolution of 83 ms providing high quality images with less residual motion [4-7]. We hypothesized that high-speed CTCA allows more accurate detection or exclusion of significant stenoses, in particular, in the native coronary arteries and distal runoffs. We sought to evaluate whether CTCA before ICA is complementary to ICA for the evaluation of symptomatic post CABG patients.

CHAPTER 19

Materials and Methods

Study Population

Between July 2006 and February 2008, we prospectively and consecutively enrolled 95 patients after with recurrent anginal symptoms suspected for obstructive graft or coronary artery disease. All patients were scheduled for ICA which was performed within 2 weeks after CTCA. Exclusion criteria were previous percutanous coronary intervention (n=34), known allergy to Iodinated contrast material (n=1), impaired renal function (serum creatinine>120 μmol/l) (n=2), irregular heart rhythm (atrial fibrillation, frequent atrial or ventricular extra systoles) (n=2) and logistic inability to perform a CT scan (n=1) before ICA. Three patients did not consent. A total of 52 patients (41 men, mean age 66.6 ± 13.2 years, range 44-83 years) were included in the study. The institutional review board approved the study and all patients gave informed consent.

Patient Preparation

47 patients (90%) were on long-term beta-blockers. No oral or intravenous beta-blockers or sedation were administered prior to the scan. All patients received Nitroglycerin (0.4mg/dose) sublingually just before scanning.

CTCA Scan Protocol

All patients were scanned using a Dual Source CT scanner (Somatom Definition, Siemens Medical Solutions, Forchheim, Germany). The system is equipped with two X-ray tubes and two corresponding detectors mounted on a single gantry with an angular offset of 90° [8]. CT angiography scan parameters were: number of X-ray sources 2, detector collimation 32 x 0.6 mm with double sampling by rapid alteration of the focal spot in the longitudinal direction (z flying focal spot), rotation time 330 ms, tube voltage 120 kV, ref mAs/rotation 380. The pitch varied between 0.2 for low heart (<40 beats/minute) rates and 0.53 for high heart rates (>100 bpm), with individually adapted pitch values for heart rates >40 and <100 bpm. Automatic tube current modulation in x,y,z-direction (Care Dose 4D®, Siemens Medical Solutions, Forchheim, Germany) was applied in all patients. In patients with left or right internal mammary artery (IMA) grafts, we extended the scan range to the level of the subclavian arteries. In all patients, we used a relative wide ECG pulsing window (30-65% of the R-R-interval) during which full tube current was applied to include both the end-systolic (ES) and end-diastolic (ED) phases. The tube current was reduced to 20% of maximum value outside the ECG pulsing window.

A bolus of Iodinated contrast material (Ultravist® 370 mgI/ml, Schering AG, Germany), which varied between 80-100 ml depending on the expected scan time, was injected (flow rate: 4.0-5.0 ml/s) in an antecubital vein followed by a saline chaser (40 ml; flow rate: 4.0-5.0 ml/s). A bolus tracking technique was applied to synchronize the data acquisition with the arrival of contrast in the bypass grafts and native coronary arteries.

All CTCA datasets were reconstructed using a single-segment reconstruction algorithm: slice thickness 0.75 mm; increment 0.4 mm; medium-to-smooth convolution kernel (B26f); resulting in a spatial resolution of 0.6-0.7 mm in-plane and 0.5 mm through-plane [12]. An additional sharp kernel (B46f) was applied in the presence severe coronary calcifications or vascular clips.

CTCA Image Reconstruction

Images were reconstructed following a stepwise approach depending on patient's heart rate during scanning. Initially, a single dataset was reconstructed during the ED (350 ms before the next R-wave) in patients with low heart rates (<65 beats/min), during both the ED and ES phase (275 after the next R-wave) in patients with intermediate heart rates (65-80 beats/min), and during the ES phase in patients with high heart rates (>80 beats/min). In case of persistent coronary motion artifacts, additional diastolic and systolic datasets were reconstructed, respectively.

CTCA Image Evaluation

Two experienced observers, unaware of the results of ICA, scored all CT datasets. Volume rendered images were initially used to visualize the course of the grafts in relation to the coronary arteries. Axial views and (curved) multi-planar reconstructions were used to identify and to classify lesions into significantly (≥50% lumen diameter reduction) diseased or not (<50% lumen diameter reduction). The CT image evaluation of distal runoffs and native coronary arteries is schematically illustrated in Figure 1. In case of a jump graft (two or more anastomoses per arterial or venous graft), the graft was divided into graft segments. All graft segments between the proximal anastomoses (ascending aorta or subclavian artery) and each coronary insertion were evaluated. Distal runoffs and native coronary arteries were evaluated on a per segment level according to the 17-segment modified American Heart Association (AHA) classification [9]. The distal runoff segments included the segment at which the graft was inserted and all segments located distally to the inserted segment. Native segments were divided into nongrafted and grafted segments. The grafted segments included all segments located proximal to segment at which the

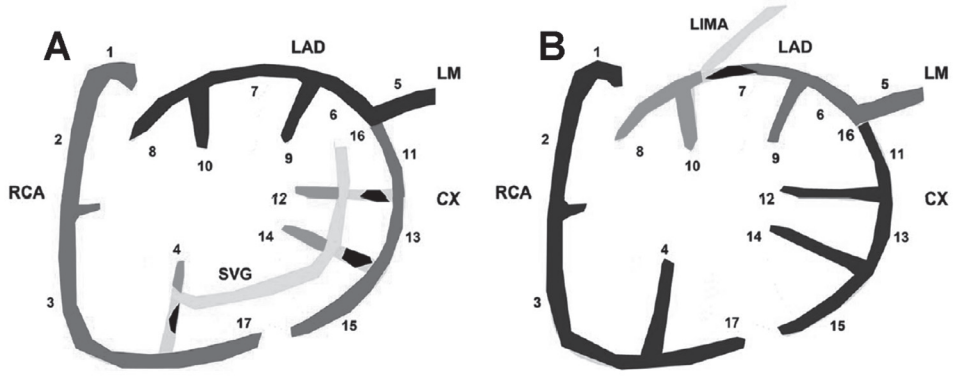

FIGURE 1. Schematic view of CT image evaluation on a per segment level: grafts (yellow), distal runoffs (green), native grafted (red) and nongrafted (blue) coronary arteries were evaluated on a per segment level according to the 17-segment modified American Heart Association (AHA) classification. A, scheme of a venous graft to marginal branches and PDA; B, scheme of a LIMA graft.
(A full color version of this illustration can be found in the color section)

graft was inserted. Distal runoff segments supplied by occluded grafts were classified as native grafted segments. Inter-observer disagreements were resolved by a third reader.

One experienced observer evaluated image quality of all graft segments, distal runoff segments and native coronary segments. Image quality was classified as good (defined as absence of any image-degrading artifacts related to motion, noise, vascular clips), moderate (presence of artifacts but evaluation possible with moderate confidence), or poor (presence of image-degrading artifacts and evaluation possible with low confidence). Coronary calcifications were visually assessed per segment and classified as absent, modest (presence of calcified spots), or severe (presence of extensive calcifications).

Quantitative Coronary Angiography (QCA)

One experienced cardiologist, unaware of the results of CTCA, identified all graft segments, distal runoffs and native coronary segments. Segments were visually classified as normal or luminal irregularities (<20% lumen diameter reduction), or diseased (≥20% lumen diameter reduction). Diseased segments were evaluated using a validated quantitative coronary artery algorithm (QCA) (CAAS®, Pie Medical, Maastricht, the Netherlands). Lesions with ≥50% lumen diameter reduction in two orthogonal planes were considered as significant stenoses. All graft en native coronary segments located distally

TABLE 1. Patient demographics

	n = 52
Male, n (%)	41 (79)
Age, years	66.3 ± 13.2
Body mass index, kg/m^2	27.2 ± 5.8
History	
Family history of CAD, n (%)	21 (40)
Nicotine abuse, n (%)	10 (19)
Hypertension, n (%)	16 (31)
Dislipidaemia, n (%)	31 (60)
Diabetes, n (%)	19 (37)
Previous myocardial infarction, n (%)	22 (42)
Long-term beta-blockers, n (%)	25 (48)
Graft anatomy per patient	
Single graft, n (%)	11 (21)
Two grafts, n (%)	31 (60)
Three grafts, n (%)	9 (17)
More than three grafts, n (%)	1 (2)
Venous and arterial grafts, n (%)	39 (75)
Venous grafts, no arterial grafts, n (%)	6 (12)
Arterial grafts, no venous grafts, n (%)	7 (14)
CT examination	
Heart rate during scanning, beats/min	64.4 ± 14.3
Scan time, sec	15.2 ± 4.3
Pitch	0.26 ± 0.07
Scan length, cm	19.0 ± 5.8
Contrast volume, ml	92.6 ± 17.3
DLP, mGy cm	1726 ± 596

to a total occlusion (100% lumen reduction) and not supplied by collaterals were classified as post-occlusion segments and were excluded from analysis. In addition, native grafted segments with a lumen diameter <1.5 mm were excluded.

Effective Dose

The effective dose (E) for CTCA in each patient was estimated by the following equation as proposed by the European Working Group for Guidelines on Quality Criteria in CT [10]:

$$E = EDLP \bullet DLP$$

DLP; dose-length product (cm), EDLP = 0.017 mSv • mGy^{-1} • cm^{-1}

Statistical Analysis

Continuous variables are expressed as means (standard deviation) and categorical characteristics are expressed as numbers and percentages. The diagnostic performance of CTCA for the detection of significant stenosis as defined by QCA is presented as sensitivity, specificity, and negative and positive predictive values with the corresponding 95% confidence intervals (CIs), and positive and negative likelihood ratios (LRs) were calculated. Comparison between CTCA and QCA was performed on 2 levels: patient-by-patient and segment-by-segment analysis. An additional analysis was performed to explore the effect of nesting since repeated assessments within the same patient were made that

TABLE 2. Diagnostic Performance of CTCA (segment based analysis)

	Prevalence of disease, (%)	N	TP	TN	FP	FN	k	Sensitivity (%)	Specificity (%)	PPV (%)	NPV (%)	ACC (%)	+LR	-LR
Grafts	19	152	29	123	0	0	.99	100	100	100	100	100	-	-
Distal runoffs	13	142	19	122	0	1	.81	95 (91-99)	100	100	99 (98-100)	99 (98-100)	-	0.05
Grafted	59	289	170	11	5	0	.79	100	96 (93-98)	97 (95-99)	100	98 (97-100)	23.4	0
Non-grafted	29	118	33	77	7	1	.85	97 (94-100)	92 (87-97)	83 (76-89)	99 (97-100)	93 (89-98)	11.7	0.03

ACC indicates accuracy; defined as: [TP+TN] / [TP + TN + FP + FN]; +LR, positive likelihood ratio; -LR, negative likelihood ratio; N, number; NPV, negative predictive value; PPV, positive predictive value. Values in parentheses represent upper and lower bound for 95% confidence interval.

were not independent observations. A random selection of a single graft segment, nongrafted and grafted segments, and distal runoff segment per patient was performed, and the diagnostic accuracy for detection of significant lesions was calculated.

To determine the intra-observer variability, one observer evaluated 30 (58%, 30/52) CT datasets twice with a time interval of 8 weeks. Inter- and intra-observer variability for the detection of significant stenosis was determined by k-statistics.

Results

Patient and scan demographics are summarized in Table 1. The mean interval between bypass graft surgery and CTCA was 9.6 ± 7.2 years (range 0-20). The mean interval between CTCA and ICA was 11.5 ± 14.3 days. Mean scan time was 15.2 ± 4.3 seconds (range 9.2–22.9). Mean heart rate during scanning was 64.5 ± 13.2 beats/min (range 48-92). The overall effective dose of CTCA was 22.1 ± 2.8 mSv.

Diagnostic performance of CTCA: segment-by-segment based analysis.

The diagnostic performance of CTCA for the detection of significant lesions in grafts and native coronary arteries on a segment-by-segment based analysis is

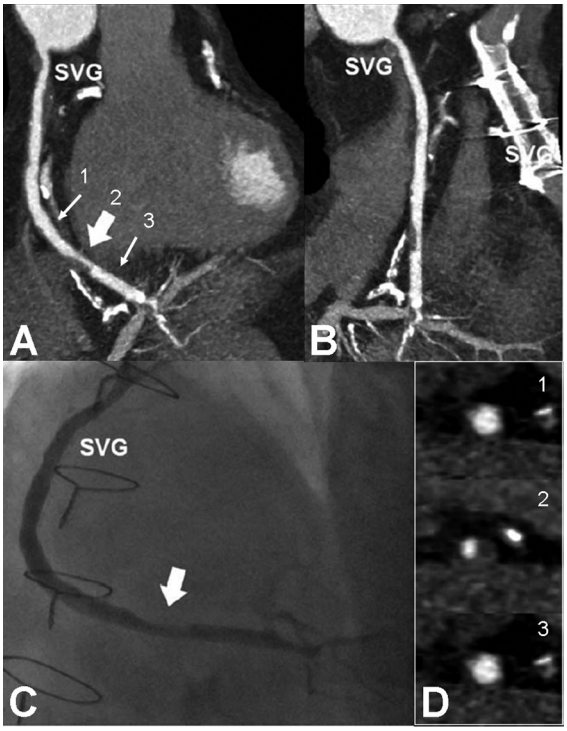

FIGURE 2. 64-year-old man with typical chest pain. Curved multiplanar reconstructed (cMPR) CT images in two orthogonal directions (A and B) and corresponding cross sections (right lower panel, D 1-3, obtained as indicated in A) show a significant obstructive non-calcified plaque (thick arrow) in the saphenous venous graft (SVG) inserted just before the crux. Corresponding coronary angiogram (C) confirms CT findings.

detailed in Table 2.

Grafts

Forty-five (87%, 45/52) patients had venous grafts, and 43 (83%, 43/52) patients had arterial grafts. In one patient, both the right and the left IMA were used. A total of 63 venous grafts, including 33 jump grafts, representing 102 venous graft segments were evaluated. We observed good image quality in 87% (89/102) of venous graft segments, moderate image quality in 11% (11/102), and poor image quality in 2% (2/102). CTCA correctly identified 15/15 occluded venous graft segments and 13/13 significant stenoses (Figure 2). A total of 48 arterial grafts, including 4 jump grafts, representing 50 arterial graft segments were evaluated. We observed good image quality in 90% (45/50) of arterial graft segments, moderate image quality in 8% (4/50), and poor image quality in 2% (1/50). CTCA correctly identified one occluded left IMA graft (Figure 3). Agreement between CTCA and QCA on a per segment level was very high (k-value: 0.99). Analysis on the randomly selected graft segments resulted in a sensitivity of 100% (3 of 3), specificity of 100% (49 of 49), positive and negative predictive value of 100%.

Distal Runoffs

ICA identified 136 patent graft segments, supplying a total of 142 distal runoff segments. The image quality was good in 79% (112/142), moderate in 17% (24/142), and poor in 4% (6/142). CTCA correctly detected all 19 significant stenoses (Figure 4, 5) and one significant stenosis was missed in a marginal obtuse (Figure 6). Agreement between CTCA and QCA on the per segment level was good (k-value:

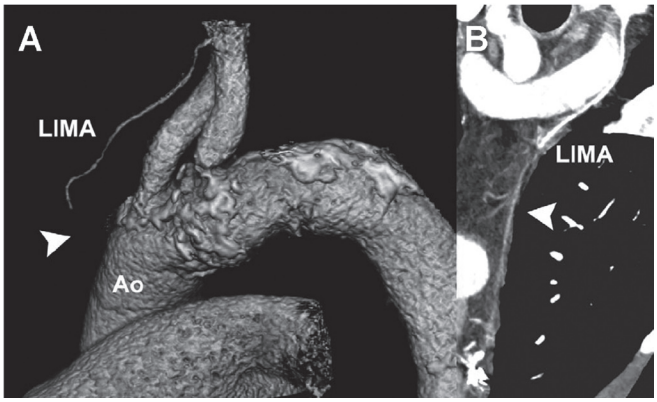

FIGURE 3. 73-year-old man. Volume rendered CT (VRT) image (A) and cMPR (B) show a total occlusion of the left internal mammary artery (LIMA, arrowhead) graft.
(A full color version of this illustration can be found in the color section)

CTCA detected 170 significant stenoses, including 44 (26%, 44/170) total occlusions and 5 lesions were overestimated (Figure 7). A total of 37 post-occlusion segments and 19 segments <1.5 mm were excluded from analysis.

Agreement between CTCA and QCA on a per segment level was good (k-value: 0.79). Analysis on the randomly selected grafted segments was excellent (k-value: 0.81). Analysis on the randomly selected distal runoff segments resulted in a sensitivity of 100% (4 of 4), specificity of 100% (48 of 48), positive and negative predictive value of 100%.

Native coronary arteries – Grafted

A total of 170 coronary arteries (right coronary artery 67%, 35/52; left main 94%, 49/52; left anterior descending artery 96%, 50/52; left circumflex artery 69%, 36/52) including 289 segments were revascularized by bypass grafting. The image quality was good in 73% (211/289), moderate in 22% (64/289), and poor in 5% (14/289) of segments.

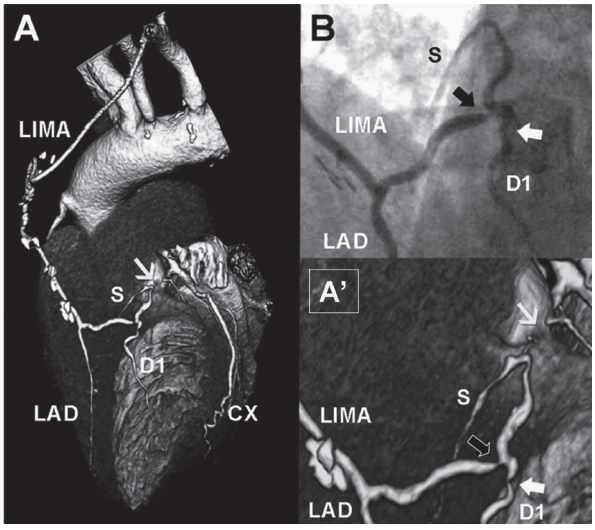

FIGURE 4. 58-year-old man with progressive chest pain and inconclusive stress test. The VRT image (A) shows an occluded proximal left anterior descending coronary artery (LAD, arrow) and a patent LIMA to the distal LAD with a jump to the first diagonal branch (D1). A more detailed view (A', magnification of A) shows a significant stenosis at the anastomosis site of D1 (black thick arrow) with a second significant stenosis in the proximal D1 runoff (white thick arrow). There is retrograde filling of a septal branch (S). The corresponding conventional angiogram (B) confirms the CT findings.
(A full color version of this illustration can be found in the color section)

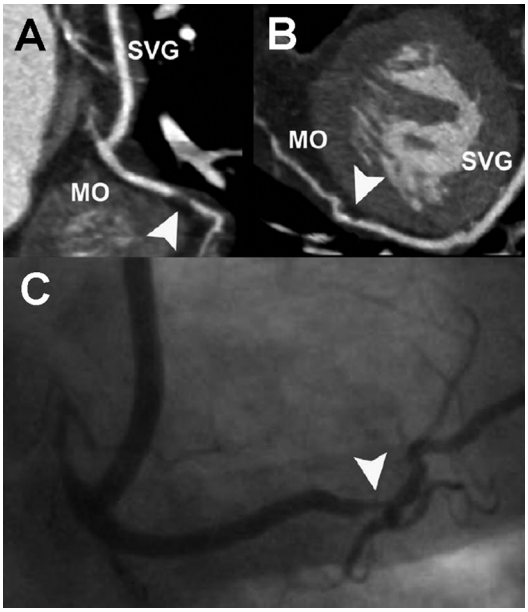

FIGURE 5. 72-year-old woman presenting with typical chest pain and previous myocardial infarction. Curved MPR images (A and B) show a significant lesion (arrowhead) in a venous jump graft segment just before the anastomosis to the marginal (MO) branch. This focal lesion, detected at conventional angiography (C), was missed at CT evaluation and represents a false-negative finding.

ments resulted in a sensitivity of 100% (29 of 29), specificity of 96% (22 of 23), positive predictive value of 97% (30 of 31) and negative predictive value of 100% (22/22).

Native coronary arteries – Nongrafted

A total of 38 coronary arteries including 118 segments were not revascularized by bypass grafting. The image quality was good in 81% (96/118), moderate 16% (19/118), and poor in 3% (3/118). CTCA detected 33 significant stenoses, including 9 (27%, 9/33) total occlusions and 7 lesions were overestimated. A total of 22 post-occlusion segments were excluded from analysis. Agreement between CTCA and QCA on the per segment level was good (k-value: 0.85). Analysis on the randomly selected nongrafted segments resulted in a sensitivity of 100% (16 of 16), specificity of 92% (33 of 36), positive predictive value of 84% (16 of 19) and negative predictive value of 100% (33/33).

The effect of nesting is probably minimal as the result of the sensitivity analysis is very similar to the results shown in the per-segment analysis (Table 2)

Diagnostic performance of CTCA: patient-by-patient based analysis

We observed a very high prevalence (98%, 51/52) of any significant obstructive disease on per patient level. The overall diagnostic accuracy of CTCA for the detection of any significant stenosis was 100% on the per patient level.

Discussion

The diagnostic work-up of patients with recurrent angina after CABG remains challenging and should include complete assessment of bypass grafts and native

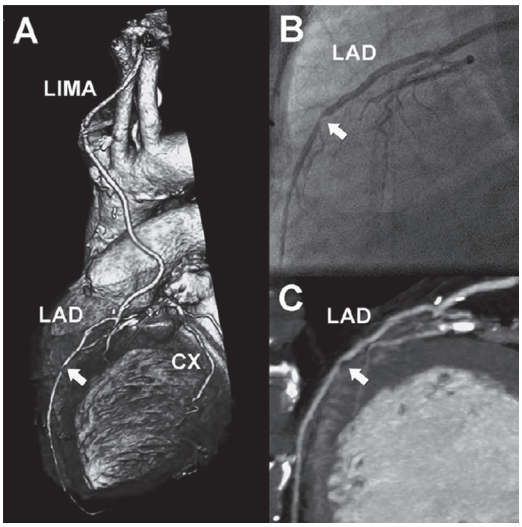

FIGURE 6. 81-year-old man with stable angina pectoris and a positive treadmill test. VRT image (A) shows a patent LIMA to the distal LAD. The proximal LAD is occluded and a lesion is present in the distal runoff (white arrow). The corresponding cMIP image (C) and conventional angiogram (B) confirm the presence of significant stenosis (white arrow).
(A full color version of this illustration can be found in the color section)

coronary arteries. Currently available noninvasive stress tests such as exercise ECG, nuclear MPI and dobutamine stress echocardiography have difficulties to identify significant obstructive graft and native coronary artery disease [11].

Non-invasive multi-slice CT coronary angiography demonstrated a high diagnostic accuracy for the detection of obstructive graft disease [2,3,12-15], but the evaluation of native coronary arteries was limited because of insufficient temporal and spatial resolution. Only few data are available reporting on the diagnostic accuracy of 64 slice CTCA for the detection of significant lesions in native coronary arteries in patients with recurrent angina after CABG. Two studies [2,3] reported a sensitivity of 86% and 89% for the detection of significant stenoses in distal runoffs, and 86% and 97% in nongrafted arteries, respectively. Specificity was 90% and 93% in distal runoffs, and 76% and 86% in nongrafted coronary arteries, respectively, and despite increase in spatial resolution with 64 slice CT, approximately 10% of native segments were unevaluable [3].

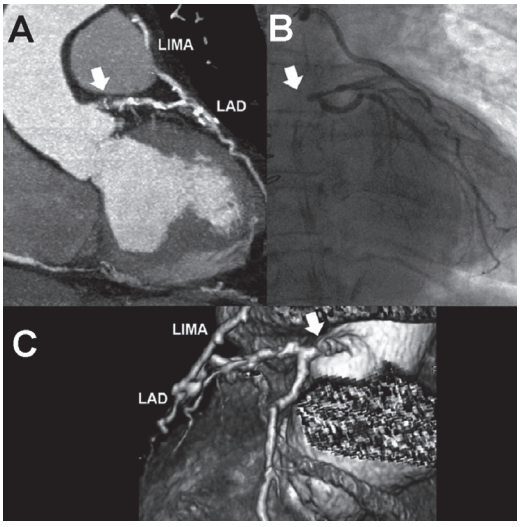

FIGURE 7. 70-year-old woman with typical chest pain and previous myocardial infarction 4 years post CABG. The LIMA and distal runoff vessel are patent. The cMIP (A) and VRT (C) demonstrate a total occlusion of the grafted left main (arrow). The corresponding coronary angiogram (B) confirms the CT findings.
(A full color version of this illustration can be found in the color section)

The Dual Source CT scanner allows acquisition of images during a shorter time window (83 ms) of the heart cycle resulting in images with less residual coronary motion and more precise delineation of stenoses [8]. In addition, fast scanning of the whole thorax can be performed in short manageable breath holds (10-15 s) which is, in particular, important in the assessment of arterial grafts.

In our study, we evaluated whether CTCA, preceding ICA would be helpful not only to facilitate ICA in providing information about the origin and hence catheter engagement of the site of the anastomoses of venous and arterial bypass grafts, but also whether successful reliable noninvasive evaluation of grafts and distal runoffs would obviate the need for invasive angiographic verification which potentially would save time, contrast and radiation exposure during ICA.

For this evaluation we performed a segment-by-segment analysis, rather than a per patient analysis, to provide anatomic information about bypass grafts, grafted and nongrafted native coronary segments. In our evaluation, we included all grafts or native segments in the analysis and did exclude any segment due to motion artifacts or calcifications. We found a 100% sensitivity on a per segment level for the detection of significant obstructive graft disease and a 95% sensitivity for the detection of significant lesions in distal runoffs. Importantly, the majority of graft anastomoses and smaller runoff segments demonstrated good image quality and could be assessed with high confidence.

Our results indicate that a fast CT scanner with 83 ms temporal resolution allows accurate detection of significant stenoses, in particular, in the native coronary arteries. The diagnostic performance of native nongrafted coronary segments was high, irrespective of small vessel size and significant calcifications, which is probably due to the fact that often these vessel segments are totally occluded, which can reliably be detected by CTCA. Furthermore it is noteworthy that on a per patient analysis, all significant obstructive graft disease was correctly identified and no false positives were encountered.

Limitations

The use of retrospective ECG gating or 'spiral' CT scan mode resulted in a relative high effective dose (22.1 mSv) as compared to diagnostic ICA (8.8 mSv) which is usually higher in the angiographic evaluation of venous and arterial bypass grafts. However, patients after CABG are generally older (± 60 years) and this is associated with a lower although not negligible life-time attributable risk of cancer incidence or mortality [16].

Our rather high patient dose was due to the fact that we began our study with a Dual Source CT prototype scanner. However, nowadays patient dose can be significantly reduced by the selection of short windows and the introduction of the possibility to select a very low tube current (4% of maximum tube current; Mindose ®, Siemens Medical Solutions, Forchheim, Germany) outside the ECG pulsing window, which can reduce effective dose up to 64% [17-18] . At that time we used a rather wide ECG pulsing window to be able to select optimal motion-free image reconstruction phases. Recently, it has been shown that prospective ECG triggering or 'step-and-shoot' CT scan mode can significantly reduce radiation exposure, with reported dose values 1.0-3.0 mSv in patients without previous CABG, but requires a very regular heart rhythm [19-20].

Conclusion

We demonstrated that with CTCA preceding ICA, the identification of significant obstructive graft disease did not require further invasive angiographic verification and hence may limit diagnostic ICA to visualization of only native coronary arteries. Moreover, CTCA can facilitate planning of subsequent percutaneous revascularization by providing accurate anatomical site of graft origin saving considerable procedure time, contrast load and radiation exposure. CTCA should not be considered as a substitute, but rather as complementary to ICA in the diagnostic work-up of symptomatic post CABG patients while invasive coronary angiography is still required to confirm or refute CT evaluation of obstructive native coronary artery disease.

References

1. Alderman EL, Kip KE, Whitlow PL, Bashore T, Fortin D, Bourassa MG, Lesperance J, Schwartz L, Stadius M. Native coronary disease progression exceeds failed revascularization as cause of angina after five years in the Bypass Angioplasty Revascularization Investigation (BARI). J Am Coll Cardiol. 2004;44:766-74.
2. Malagutti P, Nieman K, Meijboom WB, van Mieghem CA, Pugliese F, Cademartiri F, Mollet NR, Boersma E, de Jaegere PP, de Feyter PJ. Use of 64-slice CT in symptomatic patients after coronary bypass surgery: evaluation of grafts and coronary arteries. Eur Heart J. 2007;28:1879-85.
3. Ropers D, Pohle FK, Kuettner A, Pflederer T, Anders K, Daniel WG, Bautz W, Baum

U, Achenbach S. Diagnostic accuracy of noninvasive coronary angiography in patients after bypass surgery using 64-slice spiral computed tomography with 330-ms gantry rotation. Circulation. 2006;114:2334-41; quiz 2334.

4. Leber AW, Johnson T, Becker A, von Ziegler F, Tittus J, Nikolaou K, Reiser M, Steinbeck G, Becker CR, Knez A. Diagnostic accuracy of dual-source multi-slice CT-coronary angiography in patients with an intermediate pretest likelihood for coronary artery disease. Eur Heart J. 2007.
5. Weustink AC, Meijboom WB, Mollet NR, Otsuka M, Pugliese F, van Mieghem C, Malago R, van Pelt N, Dijkshoorn ML, Cademartiri F, Krestin GP, de Feyter PJ. Reliable high-speed coronary computed tomography in symptomatic patients. J Am Coll Cardiol. 2007;50:786-94.
6. Achenbach S, Ropers D, Kuettner A, Flohr T, Ohnesorge B, Bruder H, Theessen H, Karakaya M, Daniel WG, Bautz W, Kalender WA, Anders K. Contrast-enhanced coronary artery visualization by dual-source computed tomography--initial experience. Eur J Radiol. 2006;57:331-5.

   Johnson TR, Nikolaou K, Wintersperger BJ, Leber AW, von Ziegler F, Rist C, Buhmann S, Knez A, Reiser MF, Becker CR. Dual-source CT cardiac imaging: initial experience. Eur Radiol. 2006.
8. Flohr TG, McCollough CH, Bruder H, Petersilka M, Gruber K, Suss C, Grasruck M, Stierstorfer K, Krauss B, Raupach R, Primak AN, Kuttner A, Achenbach S, Becker C, Kopp A, Ohnesorge BM. First performance evaluation of a dual-source CT (DSCT) system. Eur Radiol. 2006;16:256-68.
9. Austen WG, Edwards JE, Frye RL, Gensini GG, Gott VL, Griffith LS, McGoon DC, Murphy ML, Roe BB. A reporting system on patients evaluated for coronary artery disease. Report of the Ad Hoc Committee for Grading of Coronary Artery Disease, Council on Cardiovascular Surgery, American Heart Association. Circulation. 1975;51:5-40
10. European Commision. European Guidelines on quality criteria for computed tomography, EUR 16262EN, Luxembourg: Office for Official Publications of the European Communties, 2000. http://www.drs.dk/guidelines/ct/quality/htmlindex.htm (13 June 2008)
11. Chin AS, Goldman LE, Eisenberg MJ. Functional testing after coronary artery bypass graft surgery: a meta-analysis. Can J Cardiol. 2003;19:802-8.
12. Pache G, Saueressig U, Frydrychowicz A, Foell D, Ghanem N, Kotter E, Geibel-Zehender A, Bode C, Langer M, Bley T. Initial experience with 64-slice cardiac CT: non-invasive visualization of coronary artery bypass grafts. Eur Heart J. 2006;27:976-80.
13. Martuscelli E, Romagnoli A, D'Eliseo A, Tomassini M, Razzini C, Sperandio M, Simonetti G, Romeo F, Mehta JL. Evaluation of venous and arterial conduit patency by 16-slice spiral computed tomography. Circulation. 2004;110:3234-8.
14. Schlosser T, Konorza T, Hunold P, Kuhl H, Schmermund A, Barkhausen J.

Noninvasive visualization of coronary artery bypass grafts using 16-detector row computed tomography. J Am Coll Cardiol. 2004;44:1224-9. Chiurlia E, Menozzi M, Ratti C, Romagnoli R, Modena MG. Follow-up of coronary artery bypass graft patency by multislice computed tomography. Am J Cardiol. 2005;95:1094-7.

16. Einstein AJ, Henzlova MJ, Rajagopalan S. Estimating risk of cancer associated with radiation exposure from 64-slice computed tomography coronary angiography. Jama. 2007;298:317-23.
17. Leschka S, Scheffel H, Desbiolles L, Plass A, Gaemperli O, Valenta I, Husmann L, Flohr TG, Genoni M, Marincek B, Kaufmann PA, Alkadhi H. Image Quality and Reconstruction Intervals of Dual-Source CT Coronary Angiography: Recommendations for ECG-Pulsing Windowing. Invest Radiol. 2007;42:543-549.
18. Stolzmann P, Scheffel H, Schertler T, Frauenfelder T, Leschka S, Husmann L, Flohr TG, Marincek B, Kaufmann PA, Alkadhi H. Radiation dose estimates in dual-source computed tomography coronary angiography. Eur Radiol. 2007.
19. Scheffel H, Alkadhi H, Leschka S, Plass A, Desbiolles L, Guber I, Krauss T, Gruenenfelder J, Genoni M, Luescher TF, Marincek B, Stolzmann P. Low-Dose CT Coronary Angiography in the Step-and-Shoot Mode: Diagnostic Performance. Heart. 2008. Epub ahead of print.
20. Husmann L, Valenta I, Gaemperli O, Adda O, Treyer V, Wyss C, Veit-Haibach P, Tatsugami F, von Schulthess G, Kaufmann P. Feasibility of low-dose coronary CT angiography: first experience with prospective ECG-gating. Eur Heart J. 2008;29:191-97.

Part 5

Summary & conclusion

Summary & conclusion

Multislice computed tomography (MSCT) of the coronary arteries has emerged as a non-invasive modality for the diagnostic work-up of coronary artery disease. A complete MSCT study of the coronary arteries (Chapter 2) usually consists of two parts, a non-enhanced scan followed by a contrast-enhanced acquisition. Non-enhanced MSCT is used for measuring coronary artery calcium score. Contrast-enhanced MSCT coronary angiography (MSCT-CA) is used for the detection of coronary artery stenosis, in-stent restenosis, graft pathology and anatomical variants and anomalies of the coronary arteries (Chapters 8-19).

MSCT-CA can yield reliable diagnostic information provided that several technical aspects are optimized (Chapters 3-6). Firstly, high injection rates and iodine concentrations should be used for MSCT-CA to achieve optimal intra-coronary contrast-enhancement. Secondly, the radiation exposure associated with MSCT-CA usually is higher than that associated with catheter angiography, which may restrict clinical use of MSCT-CA. The radiation exposure can be reduced by electrocardiographically-triggered X-ray tube modulation (ECG pulsing). Before the scan, the operator selects the width and timing of the ECG pulsing window in the R-R-interval during which full tube current is given. To minimize motion artifacts, the ECG pulsing window should be positioned in the phase of cardiac cycle with the least amount of heart motion, i.e., end-systole and end-diastole. The tube current outside the pulsing window can be set at 20% (functional analysis possible) or 4% of nominal tube current and hence the total radiation exposure can be greatly reduced without decreasing the quality of the dataset. According to our experience, reconstructions in end-diastole are usually sufficient to ensure high-quality datasets in patients with heart rates $\leq$65 beats/minute. Reconstructions in end-systole are usually sufficient to obtain high-quality datasets in patients with heart rates $\geq$80 beats/minute. Both end-systolic and end-diastolic reconstructions should be obtained in order to optimize image quality in patients with intermediate heart rates.

MSCT-CA is an operator-dependent technique. The performance of MSCT-CA varies substantially according to the level of expertise of the physician interpreting the scans (Chapter 7). We investigated the

learning curve of MSCT-CA following the training guidelines issued by the American College of Cardiology Foundation (ACCF) in conjunction with the American Heart Association (AHA). These guidelines establish that a physician without prior experience in MSCT-CA can achieve three levels of expertise through the mentored interpretation of 50 MSCT-CA cases over a period of 4 weeks (Level 1), 150 MSCT-CA cases over 8 weeks (Level 2), and 300 MSCT-CA cases over 6 months (Level 3), respectively. By including 3 radiologists and 1 cardiologist in a prospective study carried over a period of 1 year, we found that the diagnostic performance could improve significantly only after 1 year of training and exposure to >500 cases. Moreover, the diagnostic performance achieved at the end of our study was lower than expected (sensitivity 66-75%).

The coupling of MSCT-CA with magnetic navigation is a novel approach for performing coronary intervention (Chapter 8). Magnetic navigation is a technology that allows the accurate guidance of a magnetically enabled guidewire through the use of external magnets that generate a precisely directed magnetic field.

Image quality and diagnostic performance of MSCT-CA are strongly correlated (Chapters 9-13). From the retrospective comparison of 4-MSCT, 16-MSCT and 64-MSCT for performing MSCT-CA, we found a decrease in the frequency of unevaluable coronary segments due to motion artifacts, which was associated with an improved diagnostic performance. However, no matter which scanner generation was used, coronary calcifications remained the most common cause of poor image quality and unevaluable coronary segments.

Coronary calcifications hinder the visualization of coronary lumen because high-density structures appear larger than they actually are when imaged with MSCT. These high-density artefacts are also known as the "blooming effect". Because MSCT-CA does not display the dynamic distribution of contrast agent along the vessel (coronary flow) as in catheter angiography, the presence of a stenosis cannot be excluded unless the coronary artery lumen can be directly assessed. Therefore coronary calcifications may cause false positive findings at MSCT-CA. To reduce the number of false positives, we developed a prediction rule (Chapter 14) to calculate the probability of significant coronary artery stenosis underlying a given calcified lesion in patients undergoing both MSCT calcium scoring and MSCT-CA. Based on the lesion calcium score, morphological pattern, location within the coronary tree, patient's symptoms and risk factors, this prediction rule might facilitate diagnostic decision making and reduce the occurrence of false

positive diagnoses due to coronary calcifications.

The blooming effect is also seen when scanning patients with implanted coronary stents for clinical suspicion of in-stent restenosis (Chapters 15-18). Metal stents have hyperdense struts which attenuate the X-ray beam obscuring the visualisation of the in-stent lumen. Layers of metal can also be double or triple such as in overlapping configurations, stent-in-stent, or bifurcation stenting. The detection as well as the exclusion of in-stent restenosis can be very challenging, if not impossible, in these settings. Heart rate control through the administration of beta-blockers before the scan can be advisable because the blooming effect is exacerbated by motion artefacts. The use of appropriate post-processing techniques such as a dedicated convolution kernel (B46f) is also recommended. In our experience however, the key factor influencing the diagnostic performance of MSCT-CA is the stent diameter. In stents with a diameter <3mm, specificity of MSCT-CA is low (64%) and the technique is not effective as a gate-keeper before catheter angiography. The stent diameter should always be used as criterion to select the 'good' candidates for MSCT-CA. A final solution could be the introduction of stents made of MSCT-compatible material, or bio-absorbable stents.

In patients with coronary artery bypass grafts (CABG) (Chapter 19), MSCT-CA can be a helpful diagnostic tool as a substitute, or prior to, catheter angiography. MSCT-CA can provide superior information on the anatomy of the grafts. Moreover, because grafts have a large diameter and are less susceptible to motion artefacts, they are usually easily evaluated by MSCT-CA. Conversely, the native coronary arteries of post-CABG patients, which are usually very extensively calcified, may represent a diagnostic challenge for MSCT-CA.

For the time being, the accepted clinical indications of MSCT-CA include symptomatic patients with intermediate likelihood of coronary artery disease, patients with inconclusive stress test results, pre-operative risk assessment (valve surgery, major non cardiac surgery), acute chest pain (to rule out pulmonary emboli, aortic dissection and coronary artery disease), coronary anomalies, follow-up of bypass graft surgery and stent placement (in selected scenarios) [1, 2]. MSCT-CA can also be used as a planning tool before percutaneous treatment of chronic total occlusions, bifurcation lesions, percutaneous aortic valve replacement, and as a support to magnetic-assisted coronary intervention. In preliminary studies, MSCT-CA is being tested for its ability to quantify coronary plaque burden compared to intravascular ultrasound.

From a technical standpoint, further studies are warranted to reduce patient radiation exposure. The possibility to use "dual energy" acquisition modes to improve plaque tissue characterization will also be explored, although the applicability of this technique to coronary imaging has not been evaluated yet [3]. From a clinical standpoint, further research should aim at determining how MSCT-CA will fit in the diagnostic strategy for patients with coronary artery disease or suspected of having it [4]. Other non-invasive tests such as stress ECG, stress echo and myocardial perfusion imaging provide different and possibly complementary information. For instance, MSCT-CA shows coronary atherosclerosis whereas myocardial perfusion imaging shows myocardial ischemia. The choice of the best first-line technique and potentially the sequential use of these modalities may provide helpful supplemental information in selected patient cohorts. The analysis of cost-effectiveness aspects and of the possibility of organizational structures that will provide for "24/7" availability of competent data acquisition and interpretation will be necessary next steps. The availability of 64-slice scanners and subsequent scanner generations will increase the number of sites able to offer non-invasive imaging of the heart, which creates issues of education, training and quality control.

Samenvatting & conclusie

Multi-slice computer tomografie (MSCT) van de kransslagaders heeft zich in de afgelopen jaren ontwikkeld tot een belangrijke niet-invasieve beeldvormende techniek ten behoeve van de diagnostiek van kransslagaderverkalking. Een complete MSCT studie van de kransslagaders (Hoofdstuk 2) bestaat in het algemeen uit twee gedeelten, een opname zonder contrastmiddel gevolgd door een opname verkregen na toediening van contrastmiddel. De opname zonder contrastmiddel wordt gebruikt om de hoeveelheid kalk in de kransslagaders (calciumscore) te bepalen. De scan met contrastmiddel, de zogenaamde MSCT coronair angiografie (MSCT-CA), wordt gebruikt voor het vaststellen van vernauwingen (stenoses) in de kransslagaders, in-stent re-stenose, afwijkingen van een hartomleiding (bypass), anatomische varianten en/of afwijkingen van de kransslagsaders (Hoofdstuk 8-19).

MSCT-CA kan betrouwbare diagnostische informatie opleveren, mits een aantal technische aspecten van de beeldvorming is geoptimaliseerd (Hoofdstuk 3-6). In de eerste plaats moeten de injectiesnelheid en de jodiumconcentratie van het contrastmiddel bij MSCT-CA hoog genoeg zijn om een optimale aankleuring van de vaten te bewerkstelligen. Ten tweede is de stralingsdosis bij MSCT-CA in de praktijk veelal hoger dan bij conventionele angiografie, hetgeen een beperkende factor zou kunnen zijn voor klinisch gebruik van MSCT-CA. De stralingsdosis kan gereduceerd worden door gebruik te maken van ECG-getriggerde modulatie van de röntgenbuisstroom (ECG pulsing). Hierbij geeft de laborant vóór het onderzoek een periode ("window") aan binnen het R-R-interval (tijdsduur en tijdstip), waarbinnen de röntgenbuis zijn maximale dosis levert. Om bewegingsartefacten te minimaliseren, moet dit "window" geselecteerd worden in de hartfase met de minste hartbeweging; dit is in de eind-systolische of eind-diastolische fase. Buiten het geselecteerde window kan de buisstroom gereduceerd worden tot 20% van de maximale waarde, waarbij functionele analyse van de linker hartkamer nog mogelijk is, of eventueel zelfs tot 4% van de maximale waarde. Op deze wijze kan de totale stralingsdosis fors gereduceerd worden zonder noemenswaardige aantasting van de beeldkwaliteit.

Uit door ons uitgevoerde experimenten blijkt dat reconstructies gemaakt in de eind-

diastolische hartfase normaal gesproken voldoende zijn om beelden van hoge kwaliteit te genereren bij patiënten met een harslag van ≤ 65 slagen per minuut. Reconstructies in de eind-systolische fase zijn voldoende om beelden van hoge kwaliteit te genereren bij patiënten met een hartslag van ≥ 80 slagen per minuut. Bij tussenliggende hartfrequenties is het verstandig zowel eind-systolische als eind-diastolische reconstructies te genereren voor een optimale beeldkwaliteit.

MSCT-CA is een techniek waarbij de kwaliteit sterk afhankelijk is van het expertiseniveau van degene die de het onderzoek uitvoert en interpreteert. (Hoofdstuk 7). We hebben de leercurve van MSCT-CA onderzocht, gebruikmakend van de richtlijnen van de 'American College of Cardiology Foundation (ACCF)' en de 'American Heart Association (AHA)'. Deze richtlijnen laten zien dat een arts zonder MSCT-CA ervaring, drie expertiseniveaus kan bereiken door onder begeleiding van een mentor een interpretatie uit te voeren van 50 MSCT-CA onderzoeken in een periode van vier weken (Niveau 1), 150 MSCT-CA onderzoeken in een periode van acht weken (Niveau 2) of 300 MSCT-CA onderzoeken in een periode van zes maanden (Niveau 3). Aan de hand van een prospectieve studie, waarin drie radiologen en 1 cardioloog deelnamen, hebben wij aangetoond dat de diagnostische kwaliteit van de onderzoeken aanzienlijk vooruitging door een training van circa een jaar waarin meer dan 500 onderzoeken werden geïnterpreteerd. Aan het eind van de studie was de kwaliteit van de diagnostiek echter lager dan wij hadden verwacht (sensitiviteit van 66-75%).

Het koppelen van MSCT-CA aan 'magnetische navigatie' is een nieuwe ontwikkeling in de uitvoering van een dotterbehandeling van de kransslagaderen (Hoofdstuk 8). Magnetische navigatie is een techniek waarbij externe magneten een 'sturend' magnetisch veld creëren, waardoor de katheter in de kransslagader in de juiste richting kan worden gestuurd.

De diagnostische kwaliteit van MSCT-CA is sterk gerelateerd aan de verkregen beeldkwaliteit (Hoofdstuk 9-13). Uit een retrospectieve studie naar CT scanners met een verschillend aantal detector rijen (4-slice, 16-slice en 64-slice; het getal geeft aan hoeveel doorsnedes er per röntgenbuisrotatie maximaal verkregen kunnen worden) bleek dat er een duidelijk omgekeerd verband is tussen het aantal detector rijen en het aantal segmenten van de kransslagvaten dat niet geevalueerd kan worden wegens bewegingsartefacten. De afname van het aantal niet te evalueren segmenten ging samen met een aanzienlijke verbetering van de diagnostische waarde van het CT-onderzoek. Echter, de aanwezigheid van kalk in de

kransslagaders is nog steeds de belangrijkste onafhankelijke oorzaak van een verminderde beoordeelbaarheid van de CT beelden, leidend tot een duidelijke toename van het aantal niet evalueerbare vaatsegmenten en daarmee een verlaging van de diagnostische waarde.

Aderverkalking in de kransslagaders heeft een negatieve invloed op de visualisatie van het lumen van het bloedvat, omdat structuren met een hoge dichtheid op CT-beelden veelal groter afgebeeld worden dan dat ze in werkelijkheid zijn. Beeldartefacten veroorzaakt door gebieden met hoge dichtheid worden ook wel 'blooming effecten' genoemd. MSCT-CA is niet in staat om de dynamiek van de bloeddoorstroming in het vat af te beelden, in tegenstelling tot conventionele angiografie. Hierdoor kan de aanwezigheid van een vernauwing bij blooming effecten niet uitgesloten worden, tenzij de grootte van het lumen van de arterie op directe wijze bepaald kan worden. Dit heeft tot gevolg dat de aanwezigheid van kalk in de kransslagaders kan leiden tot vals-positieve bevindingen bij MSCT-CA. Om het aantal vals-positieven te verminderen, hebben wij een predictie-regel ontwikkeld (Hoofdstuk 14) om een schatting te maken van de kans op een significante vernauwing van een kransslagader, gegeven een aanwezige calcificatie bij patiënten die zowel een MSCT calciumscore als een MSCT-CA onderzoek ondergaan. Gebaseerd op de calciumscore, het morfologische patroon, de lokatie in de vaatboom, de symptomen van de patiënt en de aanwezige risicofactoren, is deze predictieregel in staat om de diagnostische besluitvorming te ondersteunen. Het aantal verkeerde diagnoses (vals-positieven) ten gevolge van de aanwezigheid van kalk kan op deze wijze verminderd worden.

Blooming-effecten kunnen ook worden gezien wanneer patiënten met een geïmplanteerde stent een CT onderzoek ondergaan ten behoeve van de beoordeling van in-stent re-stenose (Hoofdstuk 15-18). Metalen stents bestaan namelijk grotendeels uit structuren met een hoge dichtheid die gesuperponeerd op het lumen worden afgebeeld. Bij overlappende stentconstructies, stent-in-stent plaatsing of bij het aanbrengen van stents in splitsingen van bloedvaten, kunnen er zelfs dubbele of drievoudige stent lagen ontstaan. Onder deze omstandigheden kan het aantonen of het uitsluiten van een mogelijke re-stenose in de stent een uitdagende, soms zelfs onmogelijke, opgave zijn. Aangezien een blooming-effect aanzienlijk versterkt kan worden door bewegingsartefacten, kan het van nut zijn om de hartslag van de patient te verlagen door het geven van hartslagverlagende medicatie (beta-blokkers) vóór het uitvoeren van de scan. Het gebruik van optimale post-processing technieken zoals het gebruik van een specifiek convolutie-filter

(B46f) wordt ook aanbevolen. De diameter van de stent blijkt echter de belangrijkste factor te zijn die van invloed is op de uiteindelijke diagnostische kwaliteit van MSCT-CA. Bij stents met een diameter < 3mm, is de specificiteit van MSCT-CA bijzonder laag (64%) en is deze techniek niet effectief als 'poortwachter' voorafgaand aan een conventionele angiografie. De diameter van de stent dient altijd gebruikt te worden als selectiecriterium voor 'geschikte' kandidaten voor MSCT-CA. Een toekomstige oplossing zou de introductie van stents gemaakt van MSCT-compatibele materialen of van bio-absorbeerbare stents kunnen zijn.

In patiënten met een bypass operatie van een kransslagader (CABG, coronary artery bypass grafting) (Chapter 19), kan MSCT-CA een nuttige radiodiagnostische modaliteit zijn in de plaats van, of voorafgaand aan conventionele angiografie. MSCT-CA is in staat additionele informatie te geven omtrent de anatomie van de bypass. Bovendien kunnen hartomleidingen relatief eenvoudig beoordeeld worden met behulp van MSCT-CA, omdat ze een grotere diameter hebben en minder last hebben van bewegingsartefacten. Daarentegen zijn de oorspronkelijke kransslagaders een diagnostische uitdaging voor MSCT-CA omdat ze veelal uitgebreide kalkophopingen bevatten.

Momenteel wordt MSCT-CA geaccepteerd als klinische diagnostische modaliteit bij symptomatische patiënten met verdenking op kransslagaderverkalking, bij patiënten met twijfelachtige uitkomsten van inspanningstesten, bij het identificeren van mogelijke risico's van een operatie (hartklepchirurgie of een belangrijke niet-hartgerelateerde operatie), bij acute pijn op de borst (om eventuele longembolieën, dissectie van de aorta of kransslagaderverkalking uit te sluiten), bij anatomische afwijkingen van de kransslagaders en bij vervolgonderzoeken van bypass-operaties en stentplaatsingen [1, 2]. MSCT-CA kan ook gebruikt worden ter voorbereiding op en begeleiding van open-hartoperaties zoals de behandeling van chronische totale bloedvatafsluiting en afwijkingen op splitsingen van kransslagaders, het vervangen van een hartklep en als mogelijke ondersteuning bij een ingreep met magnetisch aangestuurde catheters. In eerdere studies is aangetoond dat MSCT-CA de hoeveelheid vettige aderverkalking (plaque) in de bloedvatwand kan kwantificeren, vergelijkbaar met intravasculaire echografie.

Nieuwe technologische ontwikkelingen zijn noodzakelijk om onder andere de stralingsdosis te kunnen verlagen. De recent ontwikkelde 'dual energy' techniek om de compositie van plaque optimaal te karakteriseren, zal verder onderzocht moeten worden. De toepassing

van deze techniek op het gebied van de kransslagaders is nog geheel nieuw en moet nog gevalideerd worden [3]. Vanuit klinisch oogpunt dient toekomstig onderzoek gericht te zijn op de bepaling of en hoe MSCT-CA past in de diagnostische strategie bij patiënten met kransslagaderverkalking of bij patiënten met verdenking daarop [4]. Ander niet-invasieve onderzoeken zoals bijvoorbeeld inspannings-ECG, inspannings-echo en 'myocardial perfusion imaging' leveren andere en wellicht aanvullende informatie op. MSCT-CA toont bijvoorbeeld verkalking aan van de kransslagaders, terwijl perfusie-onderzoek littekenvorming van het hartweefsel kan laten zien. De keuze van een optimale eerstelijns diagnostiek en een eventuele combinatie van genoemde onderzoeksstrategieën kan bij bepaalde patiëntengroepen zeker additionele klinische informatie opleveren. De analyse van de kosteneffectiviteit en het onderzoek naar de mogelijkheden om MSCT op 24x7 uur basis in te zetten, zijn noodzakelijke volgende stappen. De beschikbaarheid van 64-slice scanners en nieuwe scannergeneraties zullen tot een toename leiden van het aantal ziekenhuizen dat niet-invasieve beeldvorming van het hart kan aanbieden. Dientengevolge zal er veel aandacht geschonken moeten worden aan de opleidingsaspecten en trainingsfaciliteiten en moet een gedegen kwaliteitscontrole gewaarborgd worden.

References

1. Hendel RC, Patel MR, Kramer CM, Poon M, Hendel RC, Carr JC, Gerstad NA, Gillam LD, Hodgson JM, Kim RJ, Kramer CM, Lesser JR, Martin ET, Messer JV, Redberg RF, Rubin GD, Rumsfeld JS, Taylor AJ, Weigold WG, Woodard PK, Brindis RG, Hendel RC, Douglas PS, Peterson ED, Wolk MJ, Allen JM, Patel MR (2006) ACCF/ACR/SCCT/SCMR/ASNC/NASCI/SCAI/SIR 2006 appropriateness criteria for cardiac computed tomography and cardiac magnetic resonance imaging: a report of the American College of Cardiology Foundation Quality Strategic Directions Committee Appropriateness Criteria Working Group, American College of Radiology, Society of Cardiovascular Computed Tomography, Society for Cardiovascular Magnetic Resonance, American Society of Nuclear Cardiology, North American Society for Cardiac Imaging, Society for Cardiovascular Angiography and Interventions, and Society of Interventional Radiology. J Am Coll Cardiol 48:1475-97.
2. Schroeder S, Achenbach S, Bengel F, Burgstahler C, Cademartiri F, de Feyter P, George R, Kaufmann P, Kopp AF, Knuuti J, Ropers D, Schuijf J, Tops LF, Bax JJ (2008) Cardiac computed tomography: indications, applications, limitations, and training requirements: report of a Writing Group deployed by the Working Group Nuclear Cardiology and Cardiac CT of the European Society of Cardiology and the European Council of Nuclear Cardiology. Eur Heart J 29:531-56.
3. Achenbach S, Anders K, Kalender WA (2008) Dual-source cardiac computed tomography: image quality and dose considerations. Eur Radiol (2008), in press.
4. Vanhoenacker PK, Heijenbrok-Kal MH, Van Heste R, Decramer I, Van Hoe LR, Wijns W, Hunink MG (2007) Diagnostic performance of multidetector CT angiography for assessment of coronary artery disease: meta-analysis. Radiology 244:419-28.

About the author

Francesca Pugliese was born in Savona, Italy. She graduated at the School of Medicine of University of Genoa in 2000 with a thesis entitled 'Ultrasound in patients with transplanted kidneys'. In 2001, she entered training in Clinical Radiology at University of Genoa. Francesca was trained at University Hospital in Genoa in General Radiology, Ultrasound, CT and MRI, and at Santa Corona Hospital in Pietra Ligure (Italy) in MRI. In 2003, she joined the Department of Radiology at University of California San Diego (UCSD) for a visiting fellowship. In 2004, she was awarded the 'Best Scientific Paper Award' by the European Society of Radiology (ESR) for a scientific paper entitled 'Ultrasound of the peripheral nerves'. In 2004 she started a 6-month fellowship at Uppsala University Hospital, Uppsala, Sweden, where she was trained in cardiac MRI. After being awarded her certificate of completion of specialty training in Clinical Radiology at University of Genoa in 2004 with a thesis entitled 'Gadolinium-enhanced first-pass perfusion MRI', she visited the MRI section of the Russell H. Morgan Department of Radiology at Johns Hopkins University in Baltimore, Maryland. In 2005, Francesca started her training in cardiac CT at Erasmus MC University Medical Centre Rotterdam, and also started her PhD research.

At the present time (2008), Francesca works for the Medical Research Council (Clinical Sciences Centre) at Hammersmith Hospital, London UK, in cardiovascular PET/CT. She also works for the Royal Brompton Hospital in London, under a clinical grant of the European Society of Cardiology.

List of publications

In international peer-reviewed journals

PUGLIESE F, Hunink MGM, Gruszczynska K, Alberghina F, Malago' R, van Pelt N, Mollet NR, Cademartiri F, Weustink A, Meijboom WB, Witteman C, de Feyter PJ, Krestin GP. Multislice Computed Tomography Coronary Angiography: Effect of Experience and Training on Reader Performance. Radiology, accepted for publication.

PUGLIESE F, Mollet NR, Hunink MG, van Domburg R, Nieman K, van Mieghem C, de Feyter PJ, Krestin GP. Diagnostic accuracy of coronary CT angiography with different generation scanners. Single-centre experience. Radiology 2008; 246:384-393.

PUGLIESE F, Weustink AC, Van Mieghem C, Alberghina F, Otsuka M, Meijboom WB, Van Pelt N, Mollet NR, Cademartiri F, Krestin GP, Hunink MGM, de Feyter PJ. Dual-source coronary computed tomography angiography for detecting in-stent restenosis. Heart 2008; 94:848-854.

PUGLIESE F, Mollet NR, Runza G, van Mieghem C, Meijboom WB, Malagutti P, Baks T, Krestin GP, deFeyter PJ, Cademartiri F. Diagnostic accuracy of non-invasive 64-slice CT coronary angiography in patients with stable angina pectoris. Eur Radiol 2006; 16(3):575-82.

PUGLIESE F, Cademartiri F, van Mieghem C, Meijboom WB, Malagutti P, Mollet NR, Martinoli C, de Feyter PJ, Krestin GP. Multidetector CT for visualization of coronary stents. RadioGraphics 2006; 26(3):887-904.

PUGLIESE F, Gruszczynska K, Alberghina F, Baron J, Mollet NR, de Feyter PJ, Krestin GP. Coronary computed tomography angiography in patients after percutaneous coronary intervention (PCI): Focus on post-processing and visualization techniques. Med Sci Monit, 2007; 13(Suppl 1):152-157.

Tagliafico A, **PUGLIESE F**, Bianchi S, Bodner G, Padua L, Rubino M, Martinoli C. High-resolution sonography of the palmar cutaneous branch of the median nerve. AJR Am J Roentgenol. 2008 Jul;191(1):107-14

Cademartiri F, Schuijf JD, **PUGLIESE F**, Mollet NR, Jukema JW, Maffei E, Kroft LJ, Palumbo A, Ardissino D, Serruys PW, Krestin GP, Van der Wall EE,

de Feyter PJ, Bax JJ. Usefulness of 64-slice multislice computed tomography coronary angiography to assess in-stent restenosis. J Am Coll Cardiol 2007; 49:2204-10.

Meijboom WB, Weustink AC, **PUGLIESE F**, van Mieghem CA, Mollet NR, van Pelt N, Cademartiri F, Nieman K, Vourvouri E, Regar E, Krestin GP, de Feyter PJ. Comparison of diagnostic accuracy of 64-slice computed tomography coronary angiography in women versus men with angina pectoris. Am J Cardiol 2007; 100:1532-1537.

Meijboom WB, van Mieghem CA, Mollet NR, **PUGLIESE F**, Weustink AC, van Pelt N, Cademartiri F, Nieman K, Boersma E, de Jaegere P, Krestin GP, de Feyter PJ. 64-slice computed tomography coronary angiography in patients with high, intermediate, or low pretest probability of significant coronary artery disease. J Am Coll Cardiol. 2007; 50:1469-75.

Van Mieghem CA, Cademartiri F, Mollet NR, Malagutti P, Valgimigli M, Meijboom WB, **PUGLIESE F**, McFadden EP, Ligthart J, Runza G, Bruining N, Smits PC, Regar E, van der Giessen WJ, Sianos G, van Domburg R, de Jaegere P, Krestin GP, Serruys PW, de Feyter PJ. Multislice spiral computed tomography for the evaluation of stent patency after left main coronary artery stenting: a comparison with conventional coronary angiography and intravascular ultrasound. Circulation 2006; 114(7):645-53.

Cademartiri F, La Grutta L, Malaga R, Alberghina F, Meijboom WB, **PUGLIESE F**, Maffei E, Palumbo AA, Aldrovandi A, Fusaro M, Brambilla V, Coruzzi P, Midiri M, Mollet NR, Krestin GP. Prevalence of anatomical variants and coronary anomalies in 543 consecutive patients studied with 64-slice CT coronary angiography. Eur Radiol. 2008 Feb 2 [Epub ahead of print]

Cademartiri F, de Monye C, **PUGLIESE F**, Mollet NR, Runza G, van der Lugt A, Midiri M, de Feyter PJ, Lagalla R, Krestin GP.High iodine concentration contrast material for noninvasive multislice computed tomography coronary angiography: iopromide 370 versus iomeprol 400. Invest Radiol 2006; 41(3):349-53.

Meijs MF, Meijboom WB, Cramer MJ, **PUGLIESE F**, Prokop M, Doevendans PA, De Feyter PJ. Computed tomography of the coronary arteries: an alternative? Scand Cardiovasc J 2007; 41(5):277-86.

Meijboom WB, Mollet NR, Van Mieghem CA, Weustink AC, **PUGLIESE F**, Van Pelt N, Cademartiri F, Vourvouri E, de Jaegere P, Krestin GP, de Feyter PJ. 64-slice computed tomography coronary

angiography in patients with non-ST elevation acute coronary syndrome. Heart 2007; 93:1386-92.

Mollet NR, Cademartiri F, Van Mieghem CA, Meijboom B, **PUGLIESE F**, Runza G, Baks T, Dikkeboer J, McFadden EP, Freericks MP, Kerker JP, Zoet SK, Boersma E, Krestin GP, de Feyter PJ. Adjunctive value of CT coronary angiography in the diagnostic work-up of patients with typical angina pectoris. Eur Heart J 2007; 28:1872-78.

Meijboom WB, Mollet NR, Van Mieghem CA, Kluin J, Weustink AC, **PUGLIESE F**, Vourvouri E, Cademartiri F, Bogers AJ, Krestin GP, de Feyter PJ. Pre-operative computed tomography coronary angiography to detect significant coronary artery disease in patients referred for cardiac valve surgery. J Am Coll Cardiol 2006; 48(8):1658-65.

Malagutti P, Nieman K, Meijboom WB, van Mieghem CA, **PUGLIESE F**, Cademartiri F, Mollet NR, Boersma E, de Jaegere PP, de Feyter PJ.Use of 64-slice CT in symptomatic patients after coronary bypass surgery: evaluation of grafts and coronary arteries. Eur Heart J 2007; 28:1879-85.

Weustink AC, Mollet NR, Meijboom WB, Otsuka M, van Mieghem C, **PUGLIESE F**, Malago' R, Van Pelt N, Cademartiri F, Krestin GP, de Feyter PJ. Diagnostic Accuracy of High-speed Coronary Computed Tomography in Symptomatic Patients. J Am Coll Cardiol, 2007; 50:786-94.

Cademartiri F, Malagò R, Grutta LL, Alberghina F, Palumbo A, Maffei E, Brambilla V, **PUGLIESE F**, Runza G, Midiri M, Mollet NR, Krestin GP.Coronary variants and anomalies: Methodology of visualisation with 64-slice CT and prevalence in 202 consecutive patients. Radiol Med 2007; 112:1117-1131.

Cademartiri F, Malagutti P, Belgrano M, Runza G, **PUGLIESE F**, Mollet NR, Meijboom WB, Krestin GP, De Feyter PJ.Non-invasive coronary angiography with 64-slice computed tomography. Minerva Cardioangiol 2005; 53(5):465-72.

Cademartiri F, Aldrovandi A, Palumbo A, Maffei E, Fusaro M, Tresoldi S, Messalli G, Rossi A, Rengo M, **PUGLIESE F**, Salamousas BV, Reverberi C, Meijboom WB, Mollet NR, Ardissino D, De Feyter PJ. Multislice
Multislice computed tomography coronary angiography: clinical applications. Minerva Cardioangiol. 2007; 55:647-658.

Cademartiri F, Mollet N, Lemos PA, **PUGLIESE F**, Baks T, McFadden EP,

Krestin GP, de Feyter PJ.Usefulness of multislice computed tomographic coronary angiography to assess in-stent restenosis. Am J Cardiol 2005; 96(6):799-802.

Cademartiri F, La Grutta L, Palumbo A, Malagutti P, **PUGLIESE F**, Meijboom WB, Baks T, Mollet NR, Bruining N, Hamers R, de Feyter PJ. Non-invasive visualization of coronary atherosclerosis: state-of-art. J Cardiovasc Med 2007: 8:129–137

Cademartiri F, La Grutta L, Palumbo AA, Maffei E, Runza G, Bartolotta TV, **PUGLIESE F**, Mollet NRA, Midiri M, Krestin GP. Coronary plaque imaging with multislice computed tomography: technique and clinical applications. Eur Radiol Suppl (2006) 16 [Suppl 7]: M44-M53

Cademartiri F, Palumbo A, Maffei E, La Grutta L, Runza G, **PUGLIESE F**, Midiri M, Mollet NRA, Meijboom WB, Menozzi A, Vignali L, Reverberi C, Ardissino D, Krestin GP. Diagnostic accuracy of 64-slice CT in the assessment of coronary stents. Radiol Med 2007; 112(4):526-37

Cademartiri F, La Grutta L, Palumbo A, Maffei E, Aldrovandi A, Malagò R, Alberghina F, **PUGLIESE F**, Runza G, Belgrano M, Midiri M, Cova MA, Krestin GP. Imaging techniques for the vulnerable coronary plaque. Radiol Med 2007; 112:637-59.

Sallam BMH, Pilch-Kowalczyk J, Gruszczynska K, Baron J, **PUGLIESE F**. Diagnostic performance of CT colonography in a population with a high prevalence of large bowel disease. Med Sci Monit, 2007; 13(Suppl 1): 105-110.

Martinoli C, Bianchi S, **PUGLIESE F**, Bacigalupo L, Gauglio C, Valle M, Derchi LE.Sonography of entrapment neuropathies in the upper limb (wrist excluded). J Clin Ultrasound 2004; 32(9):438-50.

Martinoli C, Bianchi S, Prato N, **PUGLIESE F**, Zamorani MP, Valle M, Derchi LE.US of the shoulder: non-rotator cuff disorders. Radiographics 2003; 23(2):381-401; quiz 534.

Serafini G, Gandolfo NG, Gandolfo N, **PUGLIESE F**, Pretolesi F, Martinoli C.Use of the sonographic contrast medium in the study of pelvic masses: preliminary remarks. Radiol Med (Torino) 2002; 104(5-6):459-65. English, Italian.

Martinoli C, Bianchi S, Santacroce E, **PUGLIESE F**, Graif M, Derchi LE.Brachial plexus sonography: a technique for assessing the root level. AJR Am J Roentgenol 2002; 179(3):699-702.

Martinoli C, Bianchi S, Dahmane M, **PUGLIESE F**, Bianchi-Zamorani MP, Valle M.Ultrasound of tendons and nerves. Eur Radiol 2002; 12(1):44-55.

Martinoli C, Bianchi S, Giovagnorio F, **PUGLIESE F**.Ultrasound of the elbow. Skeletal Radiol 2001; 30(11):605-14.

Case-reports

PUGLIESE F, Meijboom WB, Cademartiri F, Krestin GP. Unusual cause of myocardial ischemia noninvasively assessed with ECG-gated computed tomography coronary angiography. Eur J Cardiothorac Surg 2006; 29(5):840

PUGLIESE F, Dahlman P, Radecka E, Wassberg C, Wikstrom J. Why such a different appearance? MR imaging of metastases from neuroendocrine tumors before and after treatment. Available online, www.eurorad.org

PUGLIESE F, Alberghina F, Meijboom WB, Malago' R, Gopalan D, de Feyter PJ. Post-processing using multislice CT coronary angiography improves image interpretability in patients with fast heart-rates and heart-rate variations: a case-report. J Cardiovasc Med 2007; 8(12):1088-90.

Bize P, **PUGLIESE F**, Bacigalupo L, Bianchi S.Unrecognized bilateral posterior shoulder dislocation diagnosed by ultrasound (2003:11b). Eur Radiol 2004; 14(2):350-2.

Books

Medical text translation: Bonomo L, **PUGLIESE F**. Gurney J (ed). Chest. Pocket Radiologist. W. B. Saunders Ed. (Elsevier Science), Philadelphia 2003.

Medical text translation: Rollandi GA, **PUGLIESE F**. Federle MP, Fishman E, Jeffrey RB, Anne VS (ed). Abdomen. Pocket Radiologist. W. B. Saunders Ed. (Elsevier Science), Philadelphia 2003.

Book Chapters

PUGLIESE F, de Feyter PJ. Multi-slice computed tomography of coronary arteries. In Di Mario C, Dangas G, Barlis P (ed). Interventional cardiology: principles and practice. Wiley-Blackwell Ed, Oxford. In press.

Cademartiri F, **PUGLIESE F**, Mollet N, de Feyter P, Krestin G. Contrast enhancement in MDCT coronary angiography. In deFeyter P, Schoenhagen P, Hammerstingl R, Feragalli B (ed). Advances in MDCT. Atlas Medical Publishing Ed, Oxford 2005. Volume 2 Number 1, Chapter 3.

Cademartiri F, Palumbo A, La Grutta L, Malagò R, Alberghina F, **PUGLIESE F**, Maffei E, Aldrovandi A, Mollet N. Valutazione non invasiva dell'aterosclerosi coronarica con TC e RMN. In Prati F (ed). Le coronarie viste dall'interno. Pharma Project Group Edizioni Scientifiche Ed, Varese 2007. Chapter 11, pp. 137-148.

Martinoli C, **PUGLIESE F**, Gauglio C, Bacigalupo L, Derchi LE. Strumentazione ecografica e tecnica d'esame. In Lagalla R, Latteri MA, Attard M, Midiri M (ed). Tiroide. Diagnostica per immagini e approccio clinico ragionato. Idelson-Gnocchi Ed, Napoli 2004. Cap. 8, pp. 105-115.

Other publications

PUGLIESE F, Krestin GP. CTA has triage role in patients with unstable angina, non ST-elevated MI. Diagnostic Imaging, January 2008, pp. 21-27.

PUGLIESE F. Which contrast agent for coronary CT angiography? RAD Magazine 2008, in press

Acknowledgements

This book would not exist without its co-authors.

Professor Gabriel Krestin wanted this project and made it possible. Professor Pim de Feyter had the unique ability (and patience) to speak the languages of cardiology and radiology. He turned the 'project' into the 'thesis'. Professor Myriam Hunink helped me with study design, data analysis, and so much more. Myriam, as I told you once, I wouldn't have reached the end of the PhD without your help. The biggest thank you is for each of these three people. I am so happy and honored we have worked together.

I feel privileged for having other brilliant co-authors: Nico Mollet, Filippo Cademartiri, Koen Nieman, Carlos van Mieghem, Bob Meijboom, Annick Weustink and more recently Lisan Neefjes. Annick, Bob, Lisan and I shared long hours in Erasmus MC scanning patients, scoring CT studies, analyzing data, reading and writing. Their help was key with patient recruitment. My thesis is also theirs. Moreover, thank you Bob for introducing the world of water-skiing to me!

I cannot forget the great team of radiographers of Erasmus MC headed by Marcel Dijkshoorn. Marcel, thank you so much for your continuous teaching. Thanks also to Ronald, Berend and Anne-Marie. Big thanks to Marja Thijse and the staff of the Radiology secretariaat. Thanks to Ton Everaers, Linda Everse, Karin ten Wolde, Frans Sebus and Erik-Jan Schoonen.

The list of fellows, scientists, clinicians and friends I met in Rotterdam is long, and the chances of not leaving anyone out are rather slim. Giuseppe Runza, Manuel Belgrano, Empar Rollano-Hjarrubia, Patrizia Malagutti, Marco Valgimigli, Paola Pontrelli and Stefano Mona were the very first people I met. Then came Oscar Lao Grueso and Gianluca Trifirò. Thank you Gianluca for your time, constant support, for your heart-warming risotto, and for everything you did for me (including your help when I moved to Britain). Then I met Eleni Vourvouri, Gaston Rodriguez-Granillo and his wife Inès, Hector Garcia and his wife Lulu, Ludovico La Grutta, Alessandro Palumbo, Danijela Vukadinovic and Masato Otsuka. Masato taught me the basics of the Japanese greeting: 45 degrees, twice. It was then the time of Niels van Pelt, Gert-Jan ten Kate, Roberto Malagò, Deepa Gopalan, Ernesto Luna-Cardenas and Riccarda Failo. A special thank you is for Filippo Alberghina: for his hard work and for his friendship. Then came Katarzyna (Kate) Gruszczynska,

Alexia Rossi, Marco Rengo and Hui-Lin (Kei) Li. Kate, I don't know how to thank you for your dedication, hard work and friendship. Alexia and Marco, all the best for your future in research. Kei, thank you for the Japanese pic-nics when I was overworked and the Japanese cooking classes. You are unique.

Thanks to Jurgen Ligthart, Carl Schultz, Steve Ramcharitar and Robert-Jan van Geuns for their cooperation. There are two very nice 'blokes' in Erasmus MC that I cannot forget: Henri Vrooman, physicist/computer scientist, and Piotr Wielopolski, MRI scientist.

Professor Lorenzo Derchi and Professor Carlo Martinoli of University of Genoa can neither be forgotten. They never run out of enthusiasm (even when I did) and encouraged me throughout.

Last but not least, I would like to thank my family and friends. My Father Franco, my cousin Laura and her husband Felice, my Aunts and Uncles and my friends who supported me from Italy. I regret I cannot hug my Mother Giovanna. She is however always with me.

Part 6

Color section

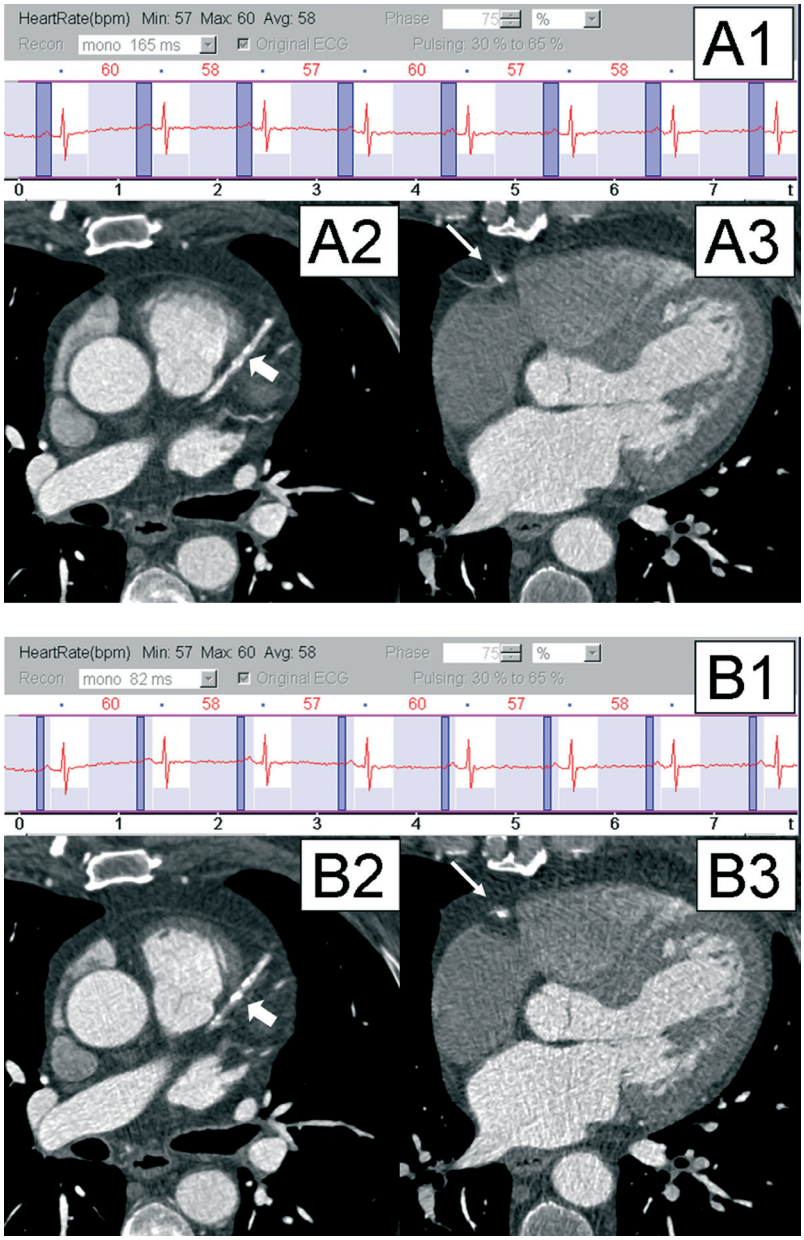

FIGURE 4. MSCT images display the average cardiac motion over the reconstruction window. A 165mm-wide reconstruction window (A1-A3) averages MSCT views obtained during 180° gantry rotation. This is the reconstruction algorithm employed in 64-MSCT. An 83mm-wide reconstruction window (B1-B3) averages MSCT views obtained (by 2 detector arrays) during 90° gantry rotation. This is the reconstruction algorithm employed in DSCT. Reconstruction using 180° data (A2) might improve image contrast when compared to reconstruction using 90° data (B2) because more MSCT views are averaged for the reconstruction of the same image (gross arrow=LAD). However, a wider reconstruction window worsens temporal resolution and may cause more blurring (A3) than the use of the narrowest reconstruction window (B3) (thin arrow=RCA)

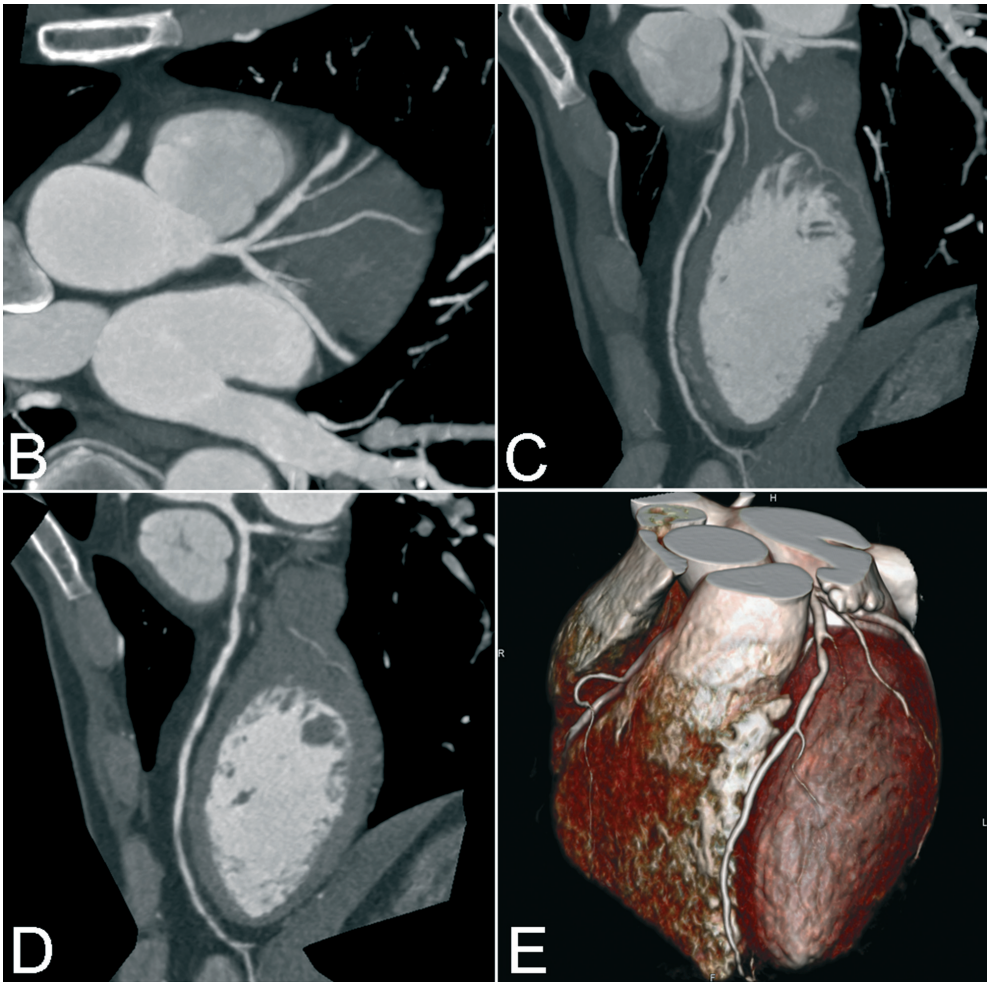

FIGURE 5B-E. Axial images are reconstructed to form a volume. Post-processing is performed on this volume data set. Multiplanar reconstructions (B) cut this volume according to planes arbitrarily tilted in any orientation. When the cut plane is not flat but curved, the result is a curved multiplanar reconstruction (C, D). This image is a flattened representation of the curved plane (D). Maximum intensity projection is an algorithm that visualizes only the structures with the highest attenuation along the observation line (C).
Volume rendering (E) displays the volume based on the density of the structures. Color attribution is arbitrary, therefore the appearance will change when the operator changes the colors of the algorithm.

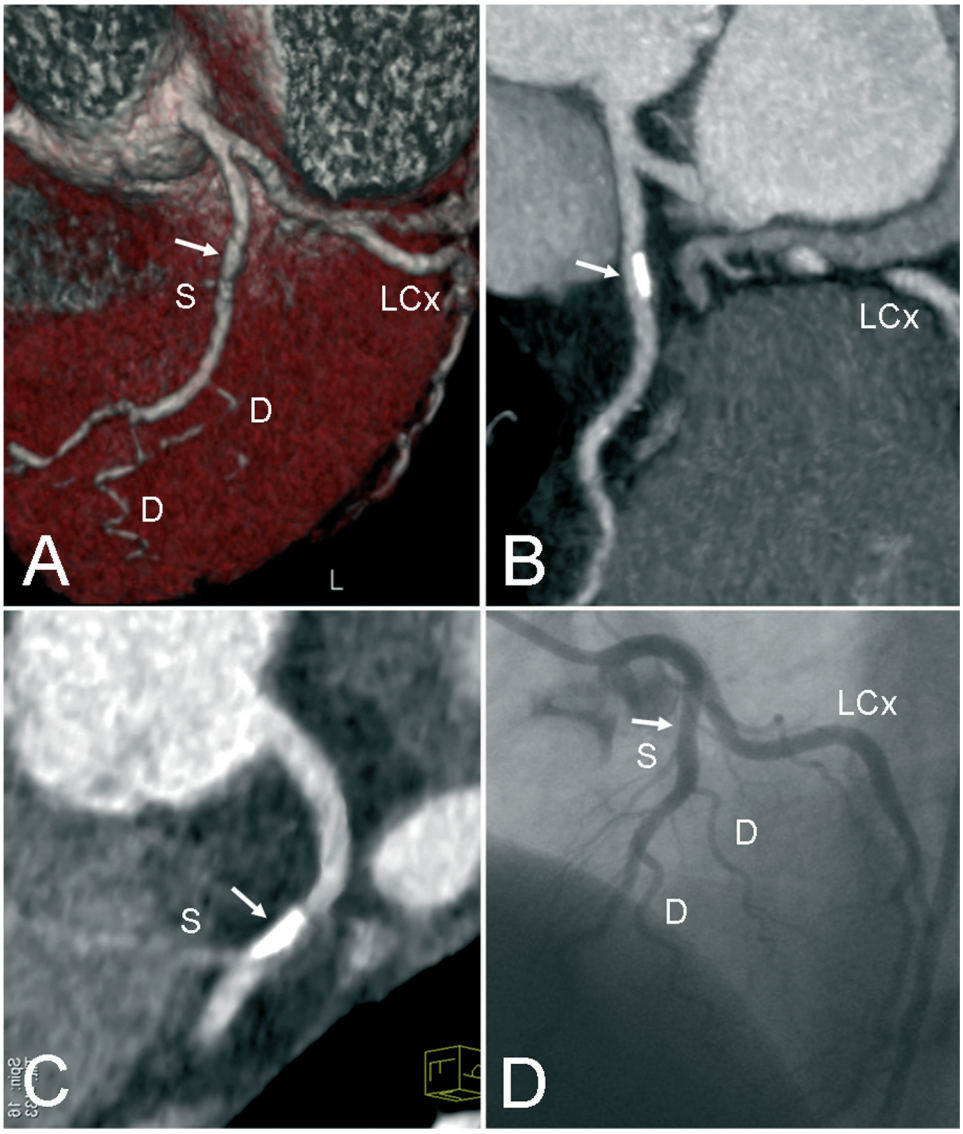

FIGURE 7. Volume rendered image (A), curved maximum intensity projection (B) and multiplanar reconstruction (C) show a calcified plaque (arrow) located in the LAD just proximal to the origin of a septal branch (S). The size of structures with high X-ray attenuation such as calcifications is overestimated in MSCT due to partial voluming. This calcification superimposes most of the coronary artery lumen. The conventional angiogram (D) shows a normal LAD.

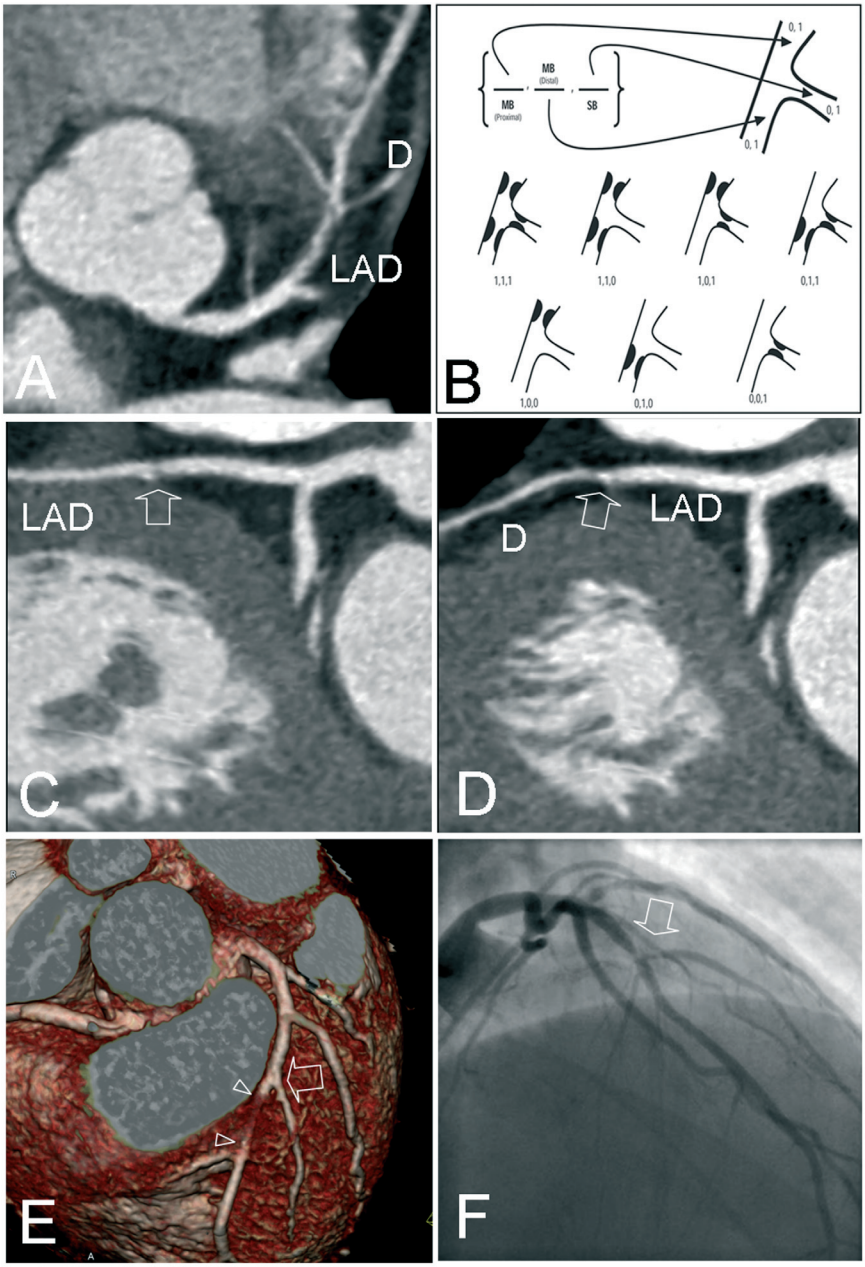

FIGURE 9. The DSCT multiplanar reconstruction (A) shows a proximal bifurcation lesion (arrows) in the LAD artery, also seen on the curved multiplanar reconstructions of the LAD (C) and diagonal branch (E). The lesion is confirmed by the conventional angiogram (F). According the Medina classification system (B), the lesion involves proximal main branch and side branch whereas the distal main branch is unremarkable (1,0,1). The lesion is not clearly detectable in the volume rendered image (E); distally to the bifurcation, the LAD has intramyocardial course (arrowheads).

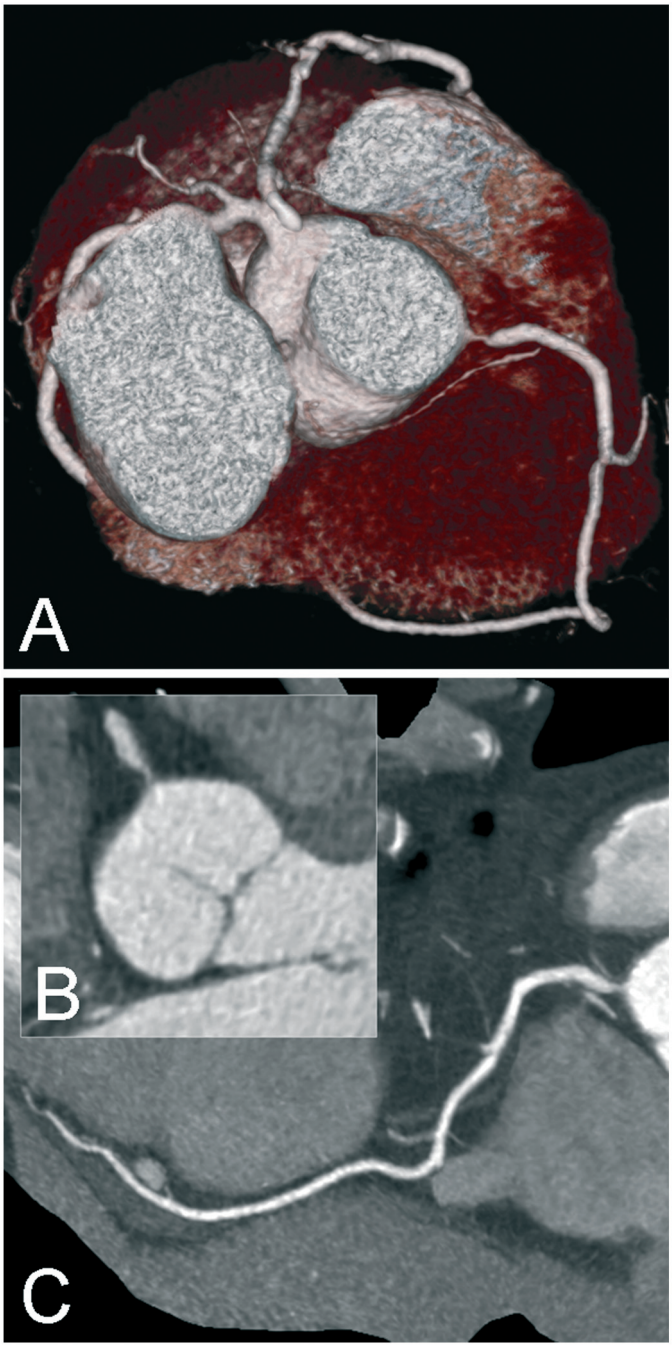

FIGURE 10. The volume rendered view after removal of the right atrium (A), axial image (B) and curved multiplanar reconstruction (C) demonstrate an ostial lesion of the RCA.

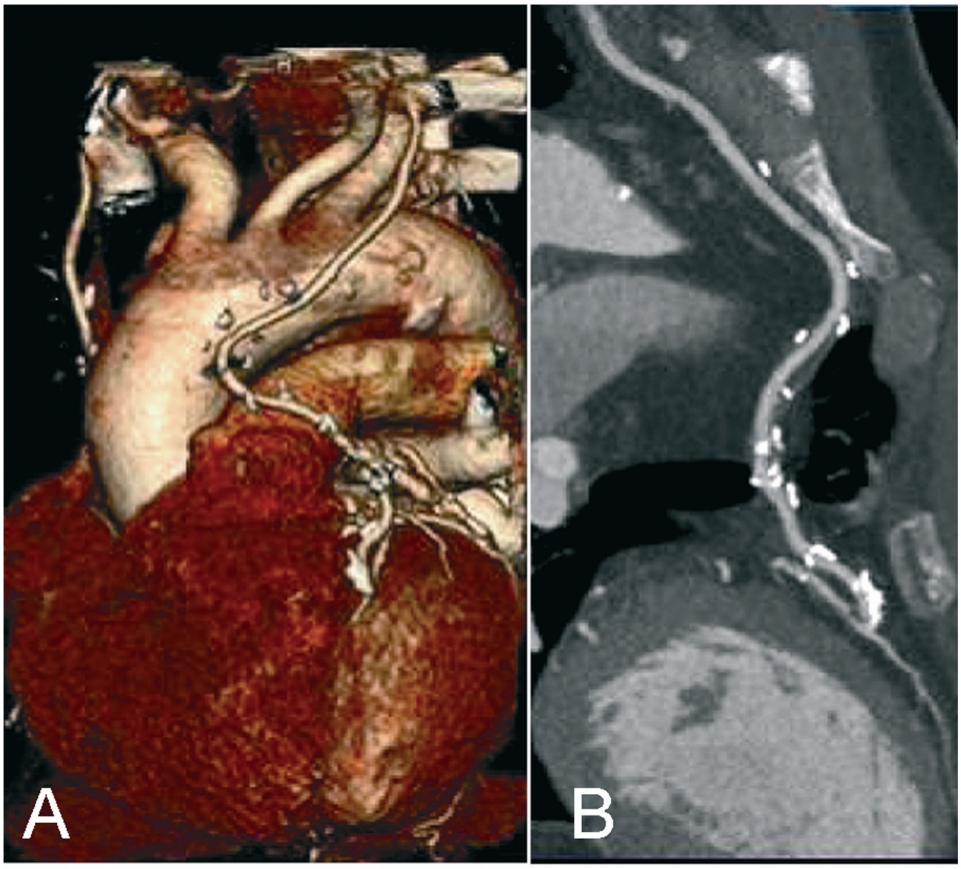

FIGURE 15. In a patient after coronary artery bypass graft surgery, the DSCT volume rendered image (A) and the curved multiplanar reconstruction (B) show patency of the left internal mammary artery graft and of the anastomosis of the graft onto the LAD. Notice the hyper-dense appearance of the surgical clips.

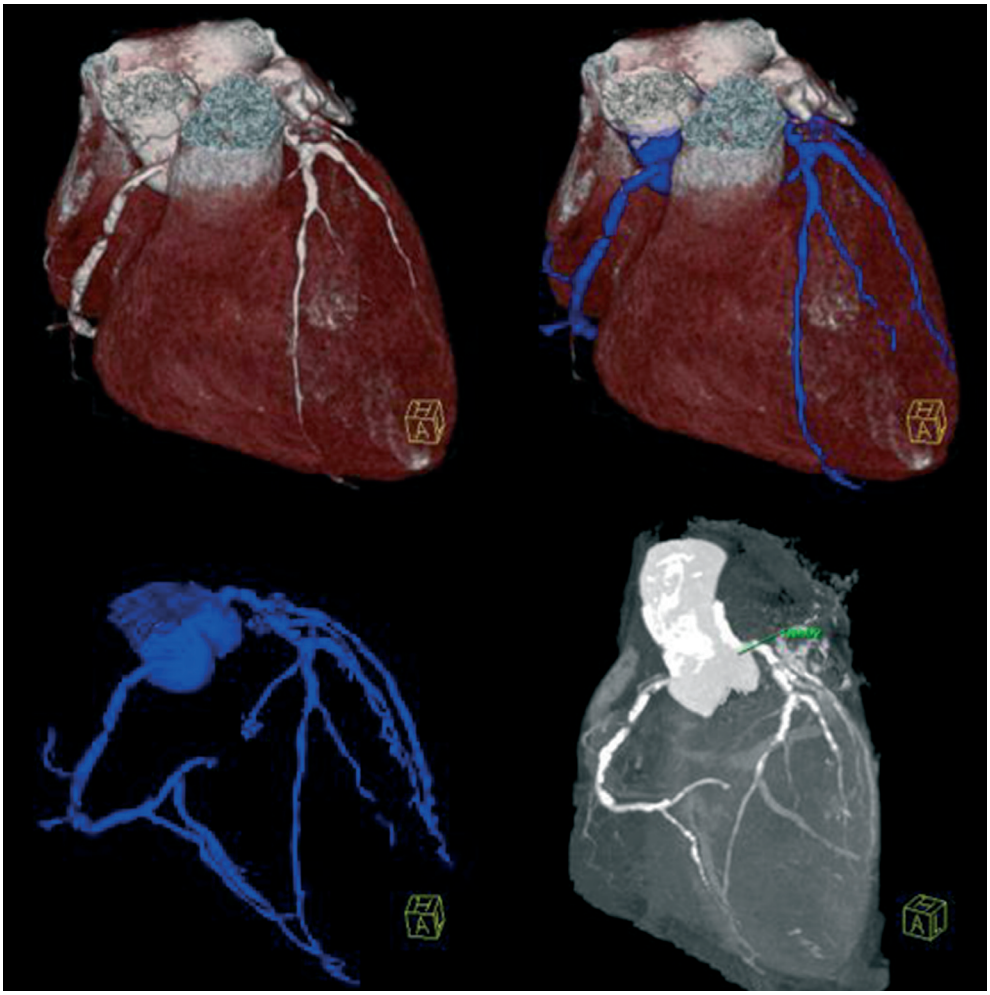

FIGURE 2. Volume-rendered MSCT image with coronary segmentation is displayed in blue with vessel calcification shown in bottom right image.

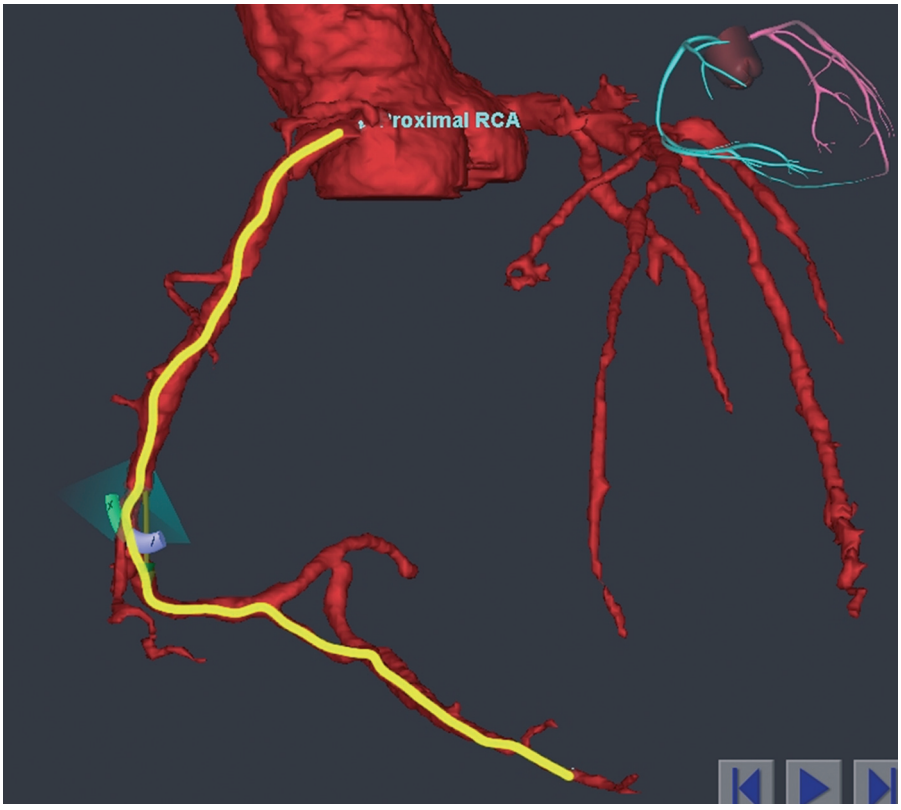

FIGURE 3. Volume-rendered coronary tree with the automatically computed pathway and the tangent magnetic vector.

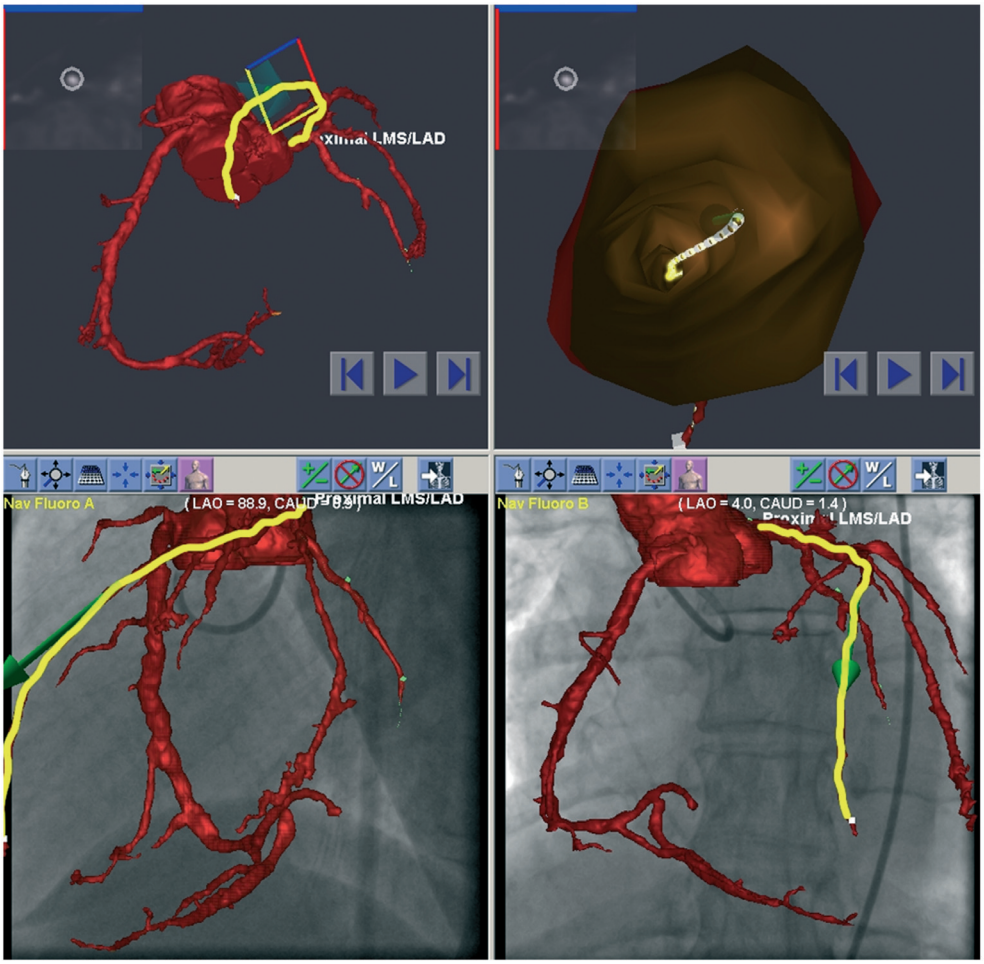

FIGURE 4. Volume-rendered navigation and tools for the operator.

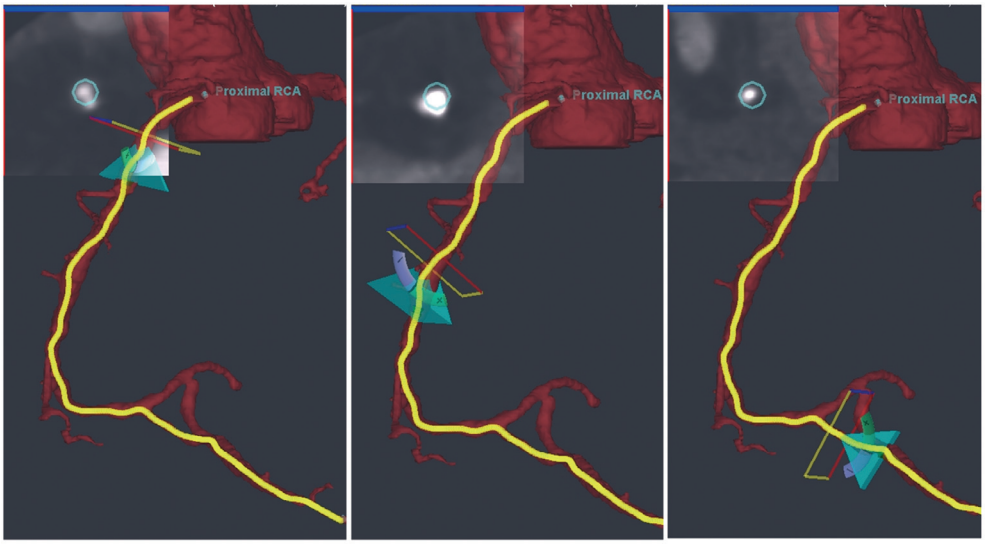

FIGURE 5. Volume-rendered automated vessel sequencing. MPR slices are in the upper left quadrants.

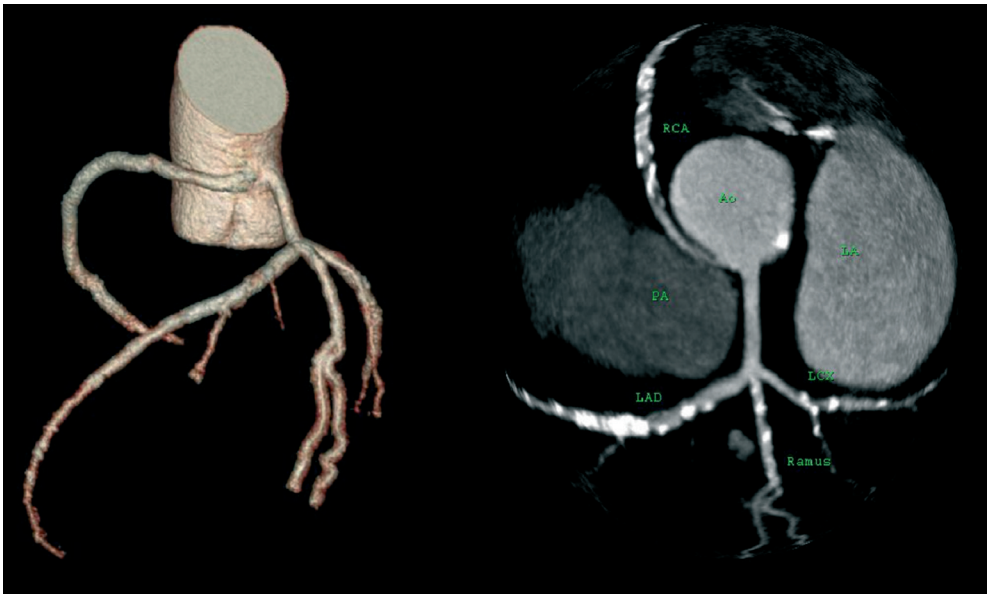

FIGURE 1. Right coronary artery arising from the left sinus of Valsalva, with a interarterial (between the aorta and the pulmonary artery) course, an acute angle take-off, and ostial stenosis without evidence of atherosclerosis at the proximal segment.

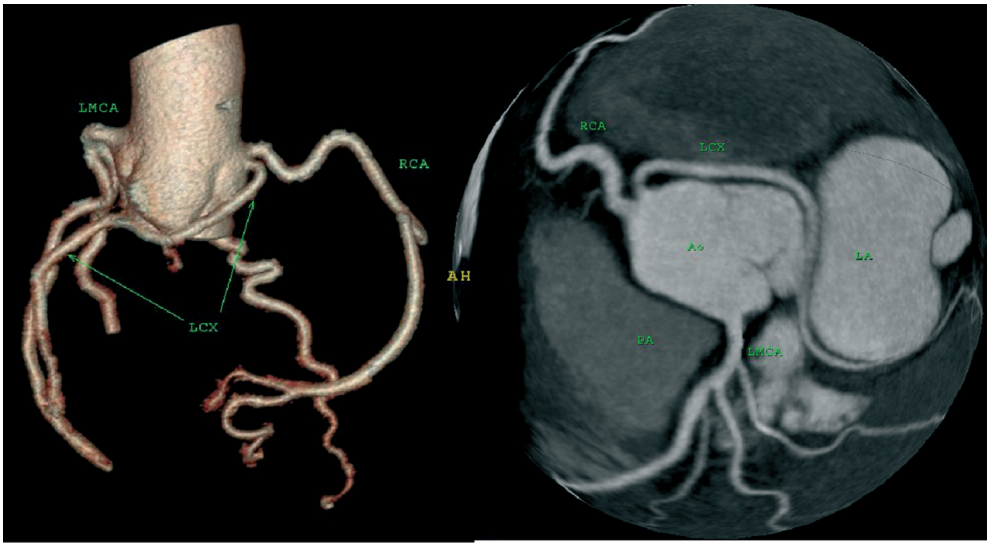

FIGURE 2. Left circumflex arising from the right sinus of Valsalva, with a retroartic course, ostial stenosis, and no evidence of coronary atherosclerosis along the coronary tree. This patient had a previous angiogram deemed as normal, where a prominent diagonal was probably mistaken with the left circumflex.

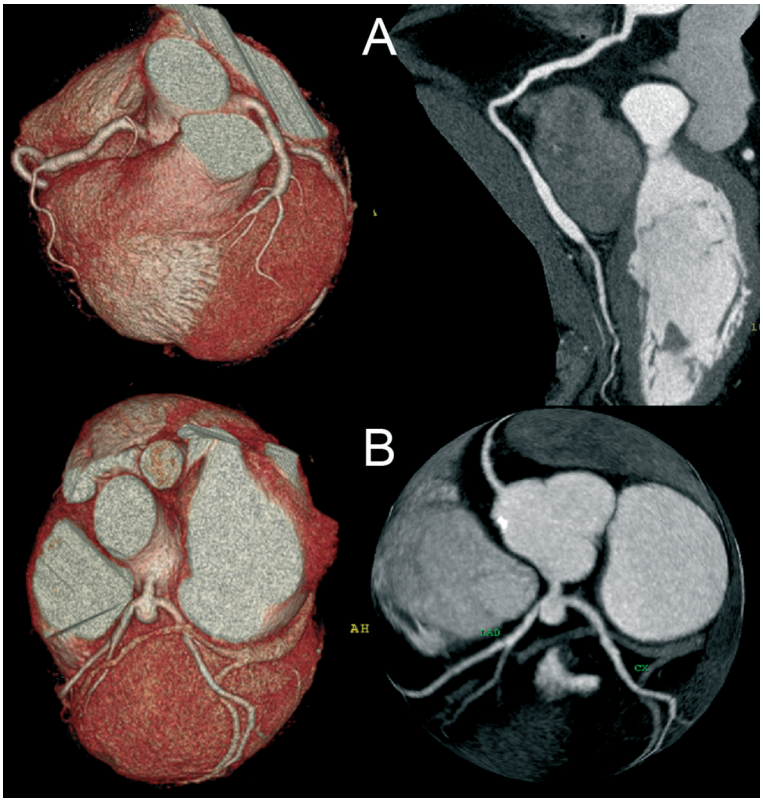

FIGURE 3. Coronary ectasia or aneurysms: A) Bilateral fusiform coronary ectasia ("dilated coronaropathy"). On the right panel, a curved multiplanar reconstruction shows difuse ectasia of the distal right coronary artery. B) Saccular aneurysm of the distal left main coronary artery with ostial stenosis of the left anterior descending.

FIGURE 6. Absence of left main coronary artery. The left anterior descending and the the left circumflex clearly arise from independent ostia at the left sinus of Valsalva.

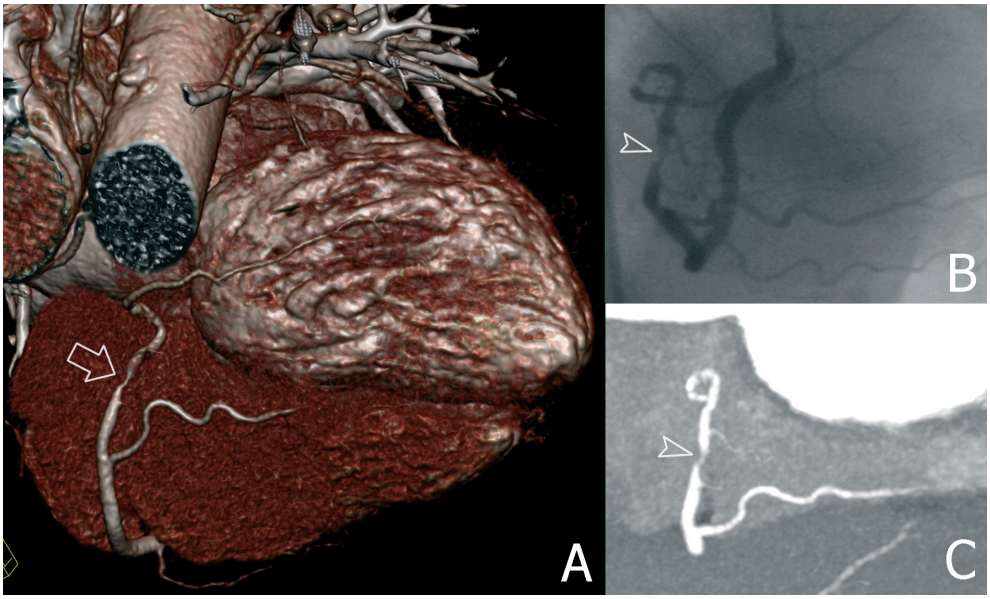

FIGURE 2 (A–C). 68-year-old patient with stable angina pectoris. A) 64-slice CT volume-rendered image. B) Conventional angiogram. C) 1-mm-thick CT maximum intensity projection. A coronary stenosis is seen at the level of the posterolateral artery (arrow and arrowheads). Luminal narrowing determined at QCA was 74%.

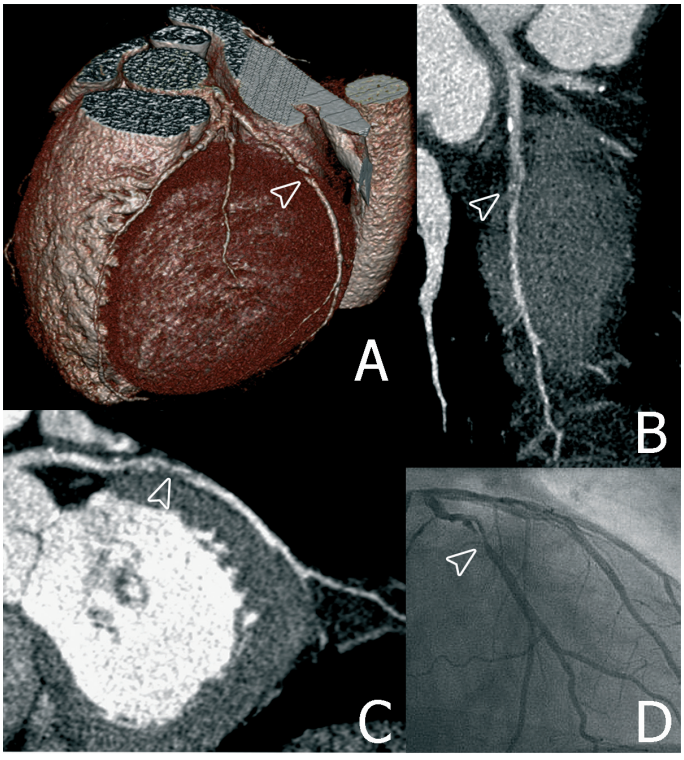

Figure 3 (A–D). 54-year-old patient with stable angina pectoris. A) 64-slice CT volume-rendered image. B) 1-mm-thick curved maximum intensity projection. C) 0.75-mm-thick multiplanar reconstruction. D) Conventional angiogram. A lesion is visible in the first marginal obtuse branch (arrowheads). Luminal narrowing determined at QCA was 64%.

Chapter 13

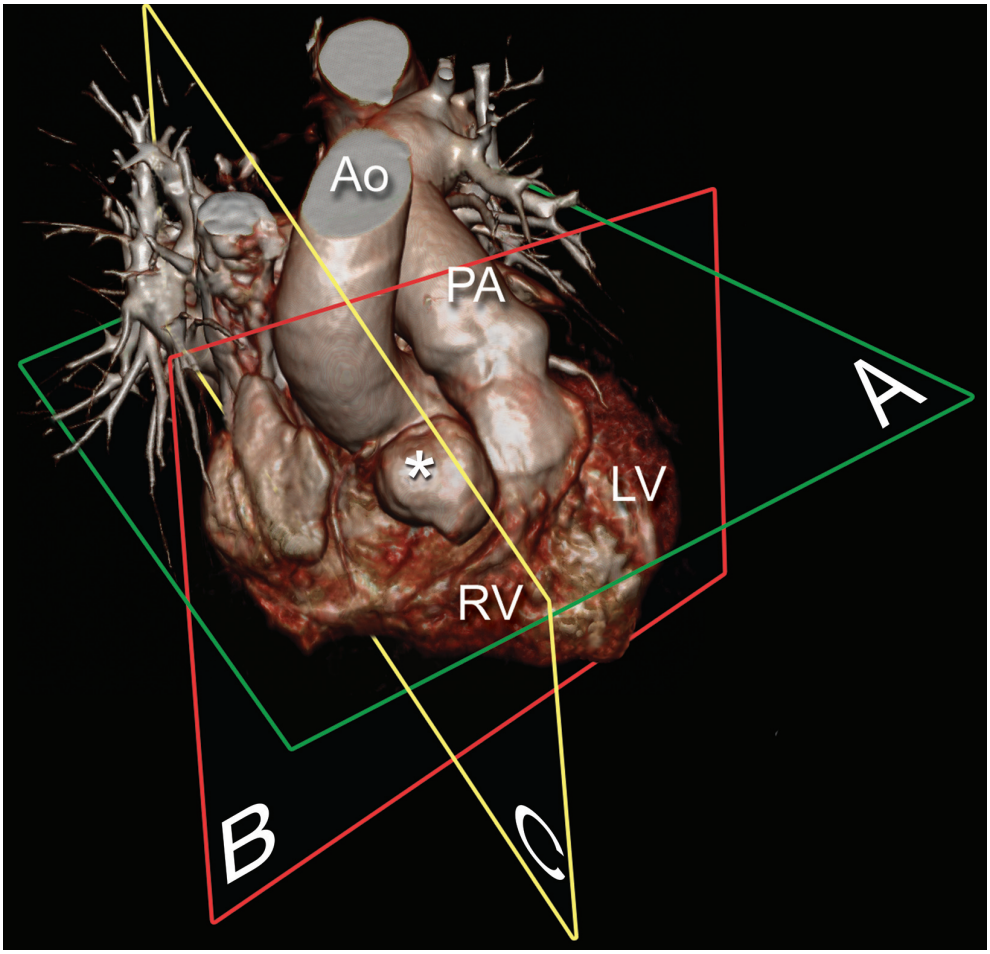

FIGURE 1. Volume-rendered ECG-gated CT image showing a right Valsalva sinus aneurysm (asterisk). Ao: aorta; PA: pulmonary artery; LV: left ventricle; RV: right ventricle.

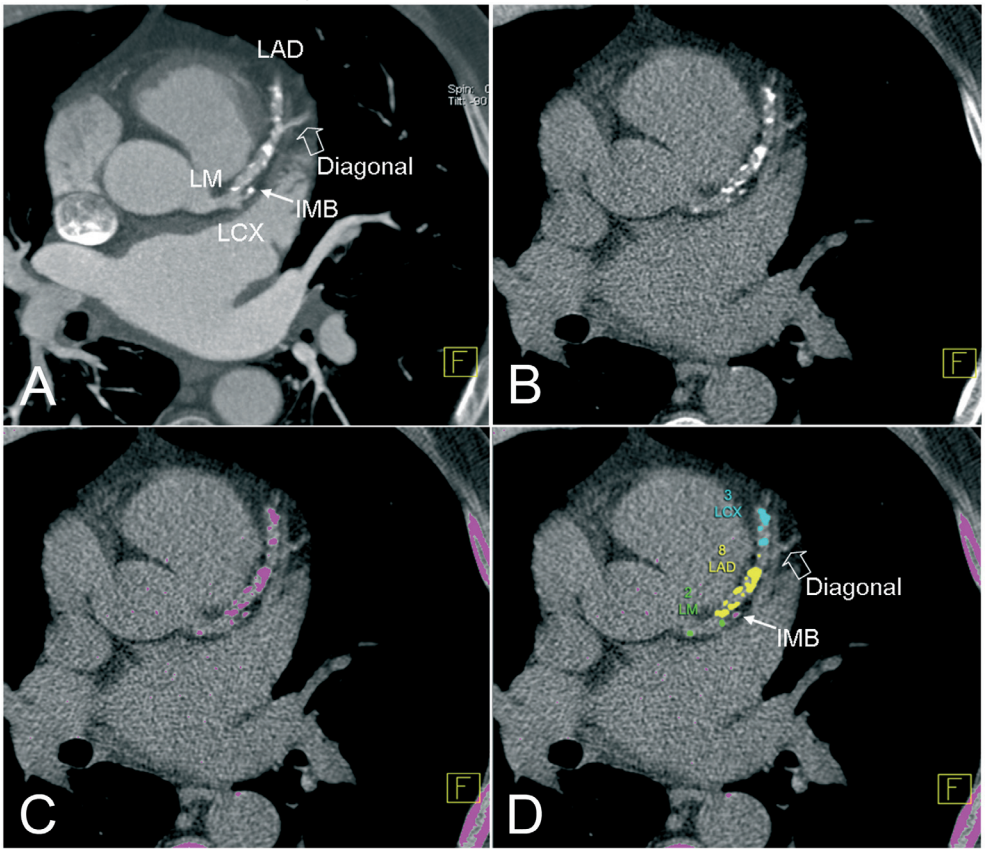

FIGURE 1. Measurement of calcium score at the segment level
To classify coronary segments consistently, contrast-enhanced MSCT-CA axial images (A) were available to the observer. Side branches, especially if non-calcified, could have been difficult to detect on non-enhanced images (B, C). Because the quantification software did not allow labelling of the 17 coronary segments individually, the 4 available labels (named as the 4 major coronary vessels) were used interchangeably and applied to coronary segments (D).
LM = left main artery; LAD = left anterior descending artery; LCx = left circumflex; IMB = intermediate branch.

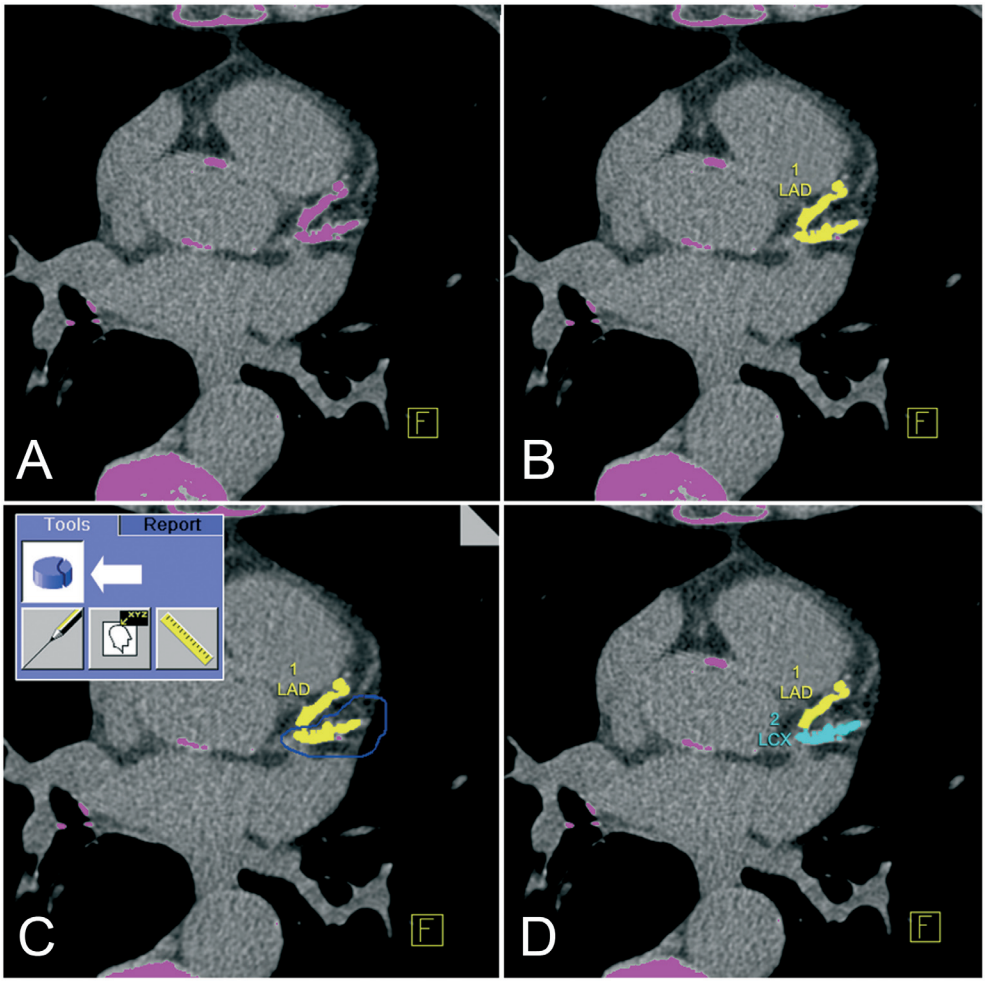

FIGURE 2. Method for separation of connected calcifications in a slice
To assign calcifications to the corresponding individual coronary artery segment, there needed to be separation of connected lesions in a slice (A, B). To achieve this, calcifications were edited manually (C) and split (D) using the '3D Edit' function (C, insert and arrow) of the software (syngo Calcium Scoring).
LAD = left anterior descending artery; LCx = left circumflex.

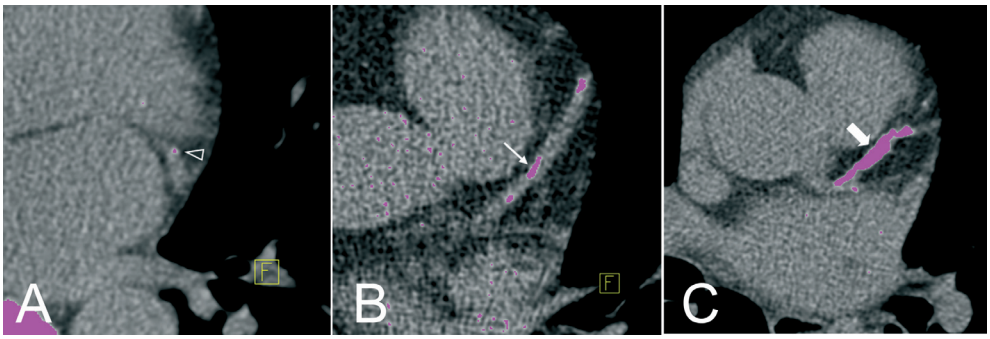

FIGURE 3. Calcification morphology
Calcification morphology was classified as spotty (A, arrowhead), wide (B, arrow) and diffuse (C, gross arrow) based on the width and length of the calcification in relation to the coronary segment diameter (Table 1).

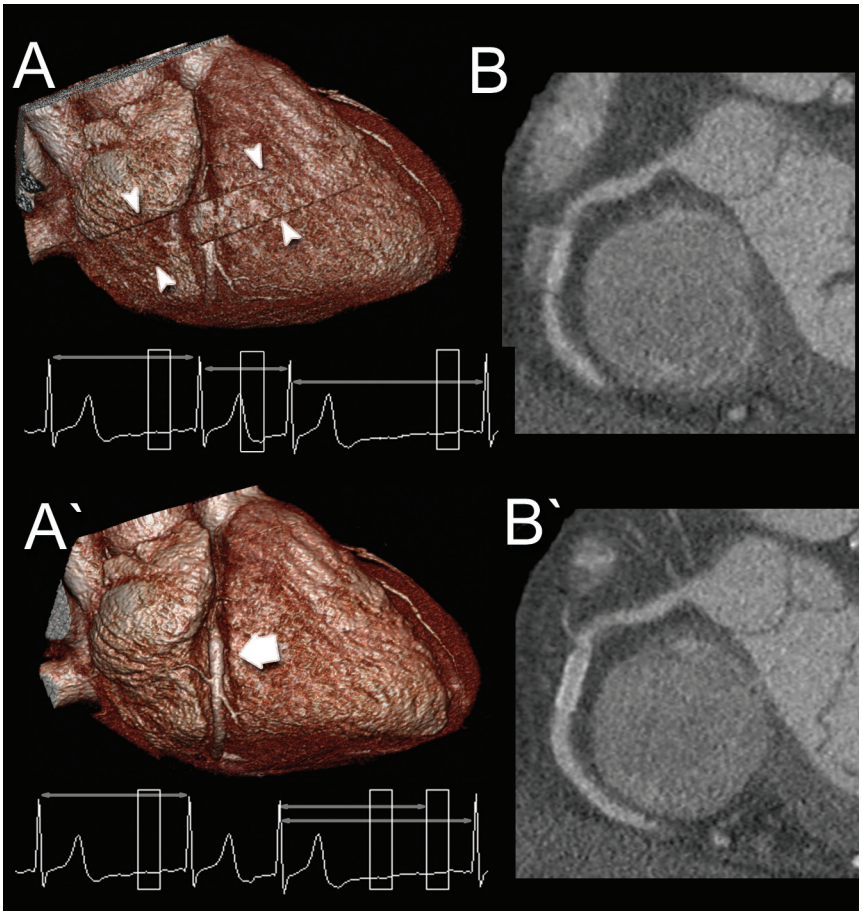

FIGURE 3. Residual cardiac motion exacerbates metal-related artifacts at 64-section CT in a patient with a stent in the midportion of the right coronary artery and with a premature heartbeat recorded at ECG during scanning. (A, B) Images obtained from data acquired during gating with the original ECG tracing. On the volume-rendered image (A), a stepladder artifact (arrowheads) is visible at the level of the midportion of the right coronary artery. On the multiplanar reformatted image (B), a blurring of contours is visible. (A′, B′) Images obtained with cardiac gating after editing of the ECG tracing. To avoid a gap in the image data, the reconstruction window during the premature heartbeat was deleted and another was added to the subsequent cardiac cycle. This step eliminated the abrupt heart rate change related to the premature beat and allowed a more coherent reconstruction of the data set. On the volume-rendered image (A′), the appearance of the stent (arrow) is unaffected by motion artifacts. Likewise, the in-stent lumen is well depicted on the multiplanar reformatted image (B′).

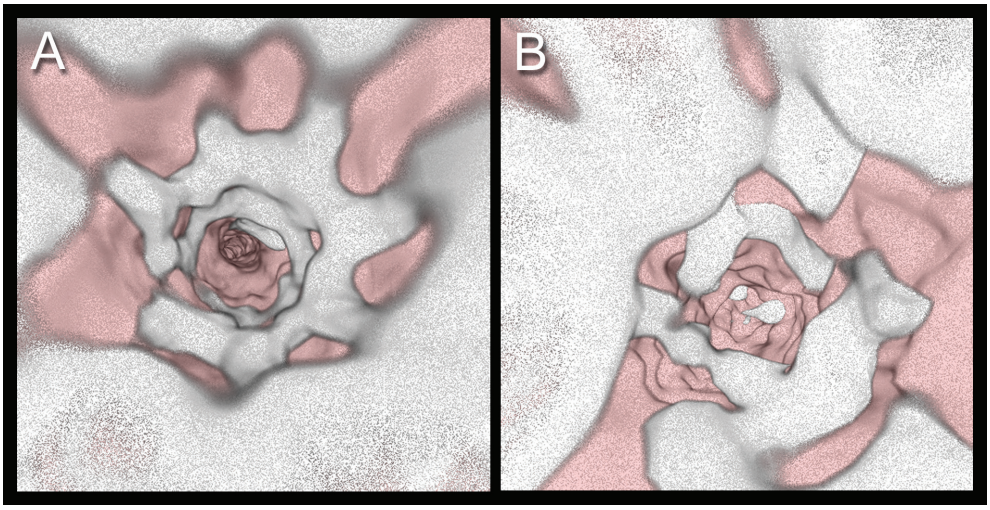

FIGURE 6. Selection of suitable threshold ranges and opacity settings allows simulation of an endoscopic view of the inner vessel surface and makes it possible to recognize different designs of the metal scaffold in stents. A slotted tubular stent (A) and a corrugated ring stent (B) are currently used for the treatment of most coronary lesions. Both stents have a diameter of 3 mm. The amount of image noise may prevent successful application of this technique for depiction of the lumen in stents with very small diameters.

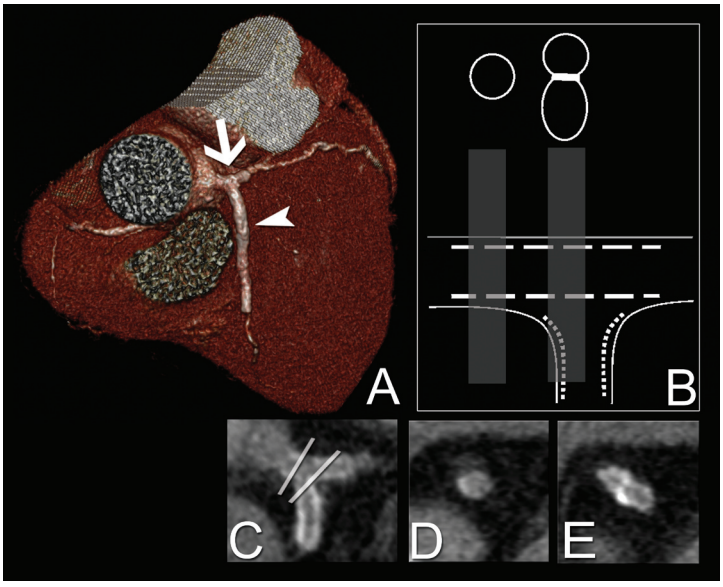

FIGURE 8. T stent implantation at the left main coronary artery bifurcation. (A) Volume-rendered image obtained with 64-section CT shows the left main coronary artery and circumflex artery (arrow), which constitute the main branch, and the anterior descending artery (arrowhead), the side branch for stent implantation. (B–E) T-stent cross-sectional diagram (B), curved multiplanar reformatted image (C), and cross-sectional images (D, E) obtained in the planes indicated in C show overlap of the metal struts only at the bifurcation point.

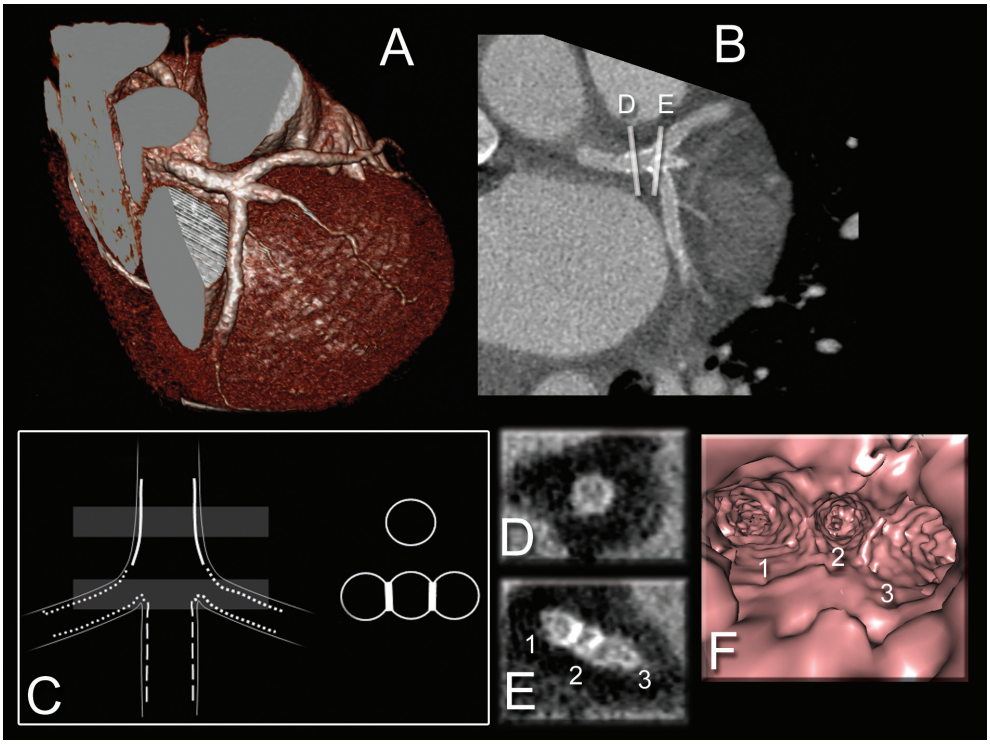

FIGURE 9. V stent implantation in the left coronary artery. (A, B) Volume-rendered image (A) and multiplanar reformatted image (B) show the left main artery and the anterior descending, intermediate, and circumflex branches, in which stents were placed to provide full coverage of the branching point. (C) Diagram of the V stent technique shows overlap of the metal struts only at the trifurcation. (D, E) Cross-sectional images, obtained in the planes shown in B, show the slim and symmetric profiles of the stents, both proximally (D) and at the level of the carina (E). (F) Volume-rendered image obtained for visualization of the vessel lumen provides a simulated endoscopic view of the origin of the three branches (1–3).

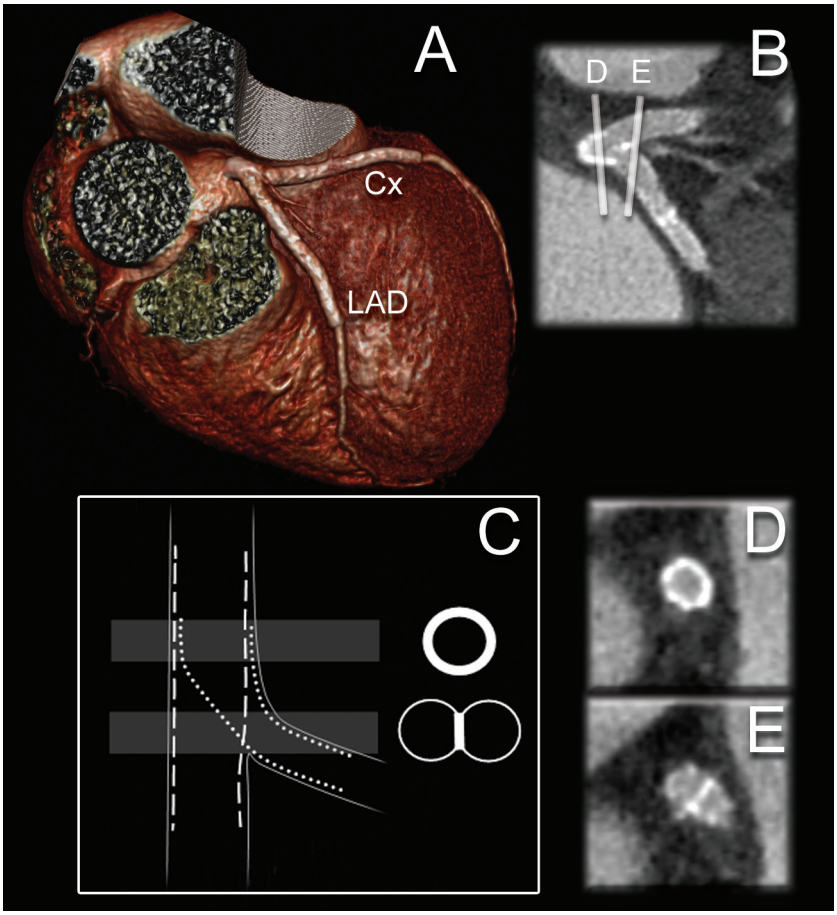

FIGURE 10. Y stent implantation at the bifurcation of the left main coronary artery. (A) Volume-rendered image shows the point of bifurcation, at which two stents were implanted in a configuration resembling a pair of trousers or culottes. Cx = left circumflex artery, LAD = left anterior descending artery. (B) Multiplanar reformatted image shows stent patency at the level of the bifurcation. (C) Diagram shows the concentrically deployed stents, which overlap near the point of bifurcation. (D, E) Cross-sectional images, obtained in the planes shown in B, depict a thicker stent profile in the parent vessel (D) at a level near the side-branch ostium (E).

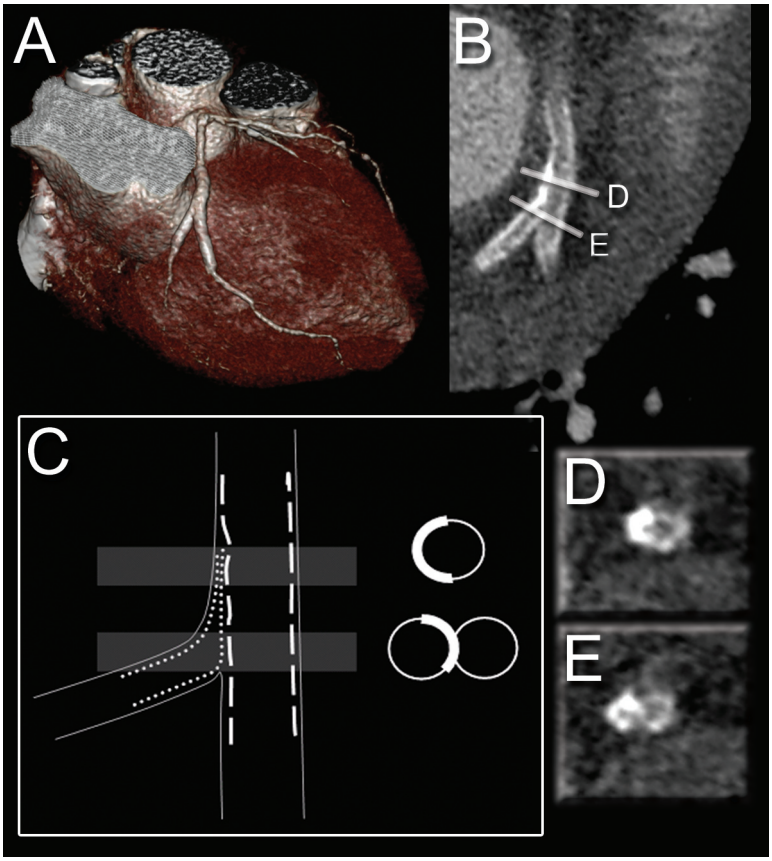

FIGURE 11. Crush stent placement at the circumflex-marginal artery bifurcation. (A, B) Volume rendered image (A) and curved multiplanar reformatted image (B) allow assessment of the stent configuration. (C) Diagram shows the multiple layers of metal that produce an asymmetric appearance of the cross-sectional stent profile. (D, E) Cross-sectional images, obtained in the planes shown in B, show asymmetric high attenuation where the layers of metal overlap, both proximal to the bifurcation (D) and across the ostium of the side-branch vessel (E).

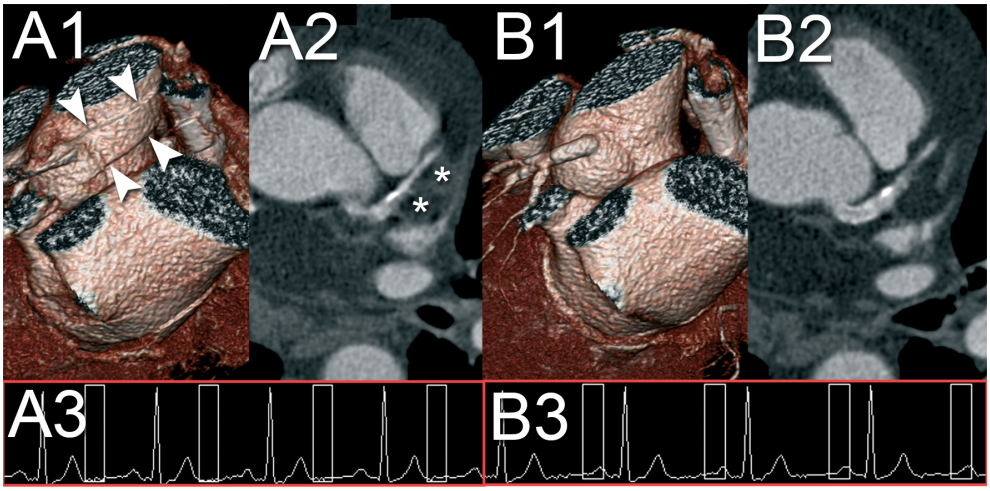

FIGURE 1. Control computed tomography coronary angiography in a patient six months after the placement of a stent in the left main coronary artery. Excessive residual cardiac motion during the reconstruction interval in systole (A3) causes step-ladder artifacts (A1, arrowheads) and stent contour blurring (A2, asterisks). Reconstruction of the volume-data during a more favorable temporal window, in this example the end-diastolic phase (B3), provides images suitable for clinical interpretation (B1,2).

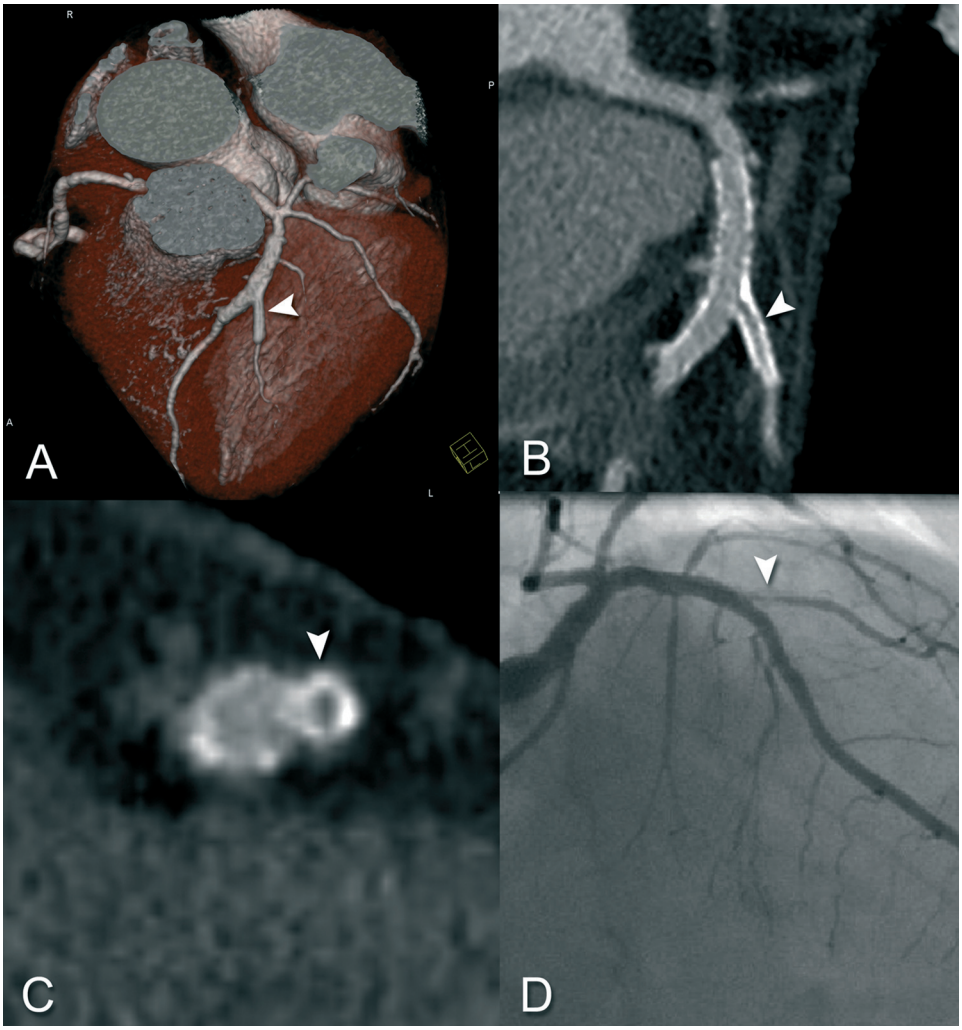

FIGURE 3. Bifurcations
Patient with in-stent restenosis 6 months after crush-stenting. A: a volume-rendered DSCT-CA image shows bifurcation stenting of the left anterior descending artery (LAD) and 2nd diagonal branch. The stent in the diagonal branch (side branch) has a diameter of 2.25 mm, the stent in the LAD (main branch) has a diameter of 4 mm. B: MPR image, C: MPR cross-section obtained at the level of the carina, and D: corresponding conventional angiogram demonstrate restenosis in the diagonal branch (arrowhead); the main branch is patent. In B, note the typical CT appearance of the crush technique, characterized by three layers of metal crushed against the ostium of the side branch.

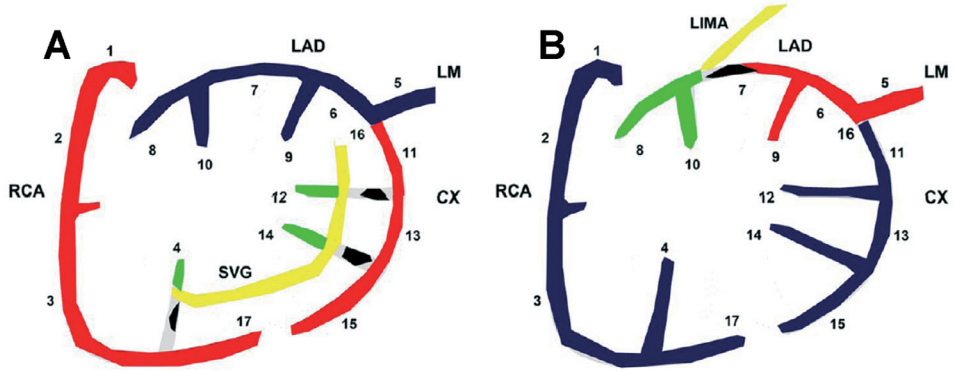

FIGURE 1. Schematic view of CT image evaluation on a per segment level: grafts (yellow), distal runoffs (green), native grafted (red) and nongrafted (blue) coronary arteries were evaluated on a per segment level according to the 17-segment modified American Heart Association (AHA) classification. A, scheme of a venous graft to marginal branches and PDA; B, scheme of a LIMA graft.

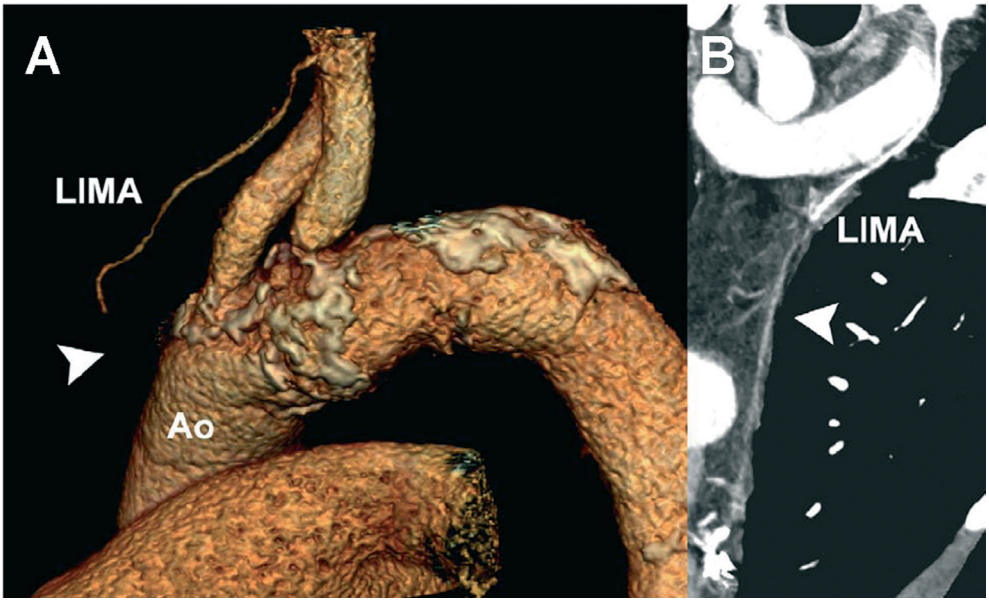

FIGURE 3. 73-year-old man. Volume rendered CT (VRT) image (A) and cMPR (B) show a total occlusion of the left internal mammary artery (LIMA, arrowhead) graft.

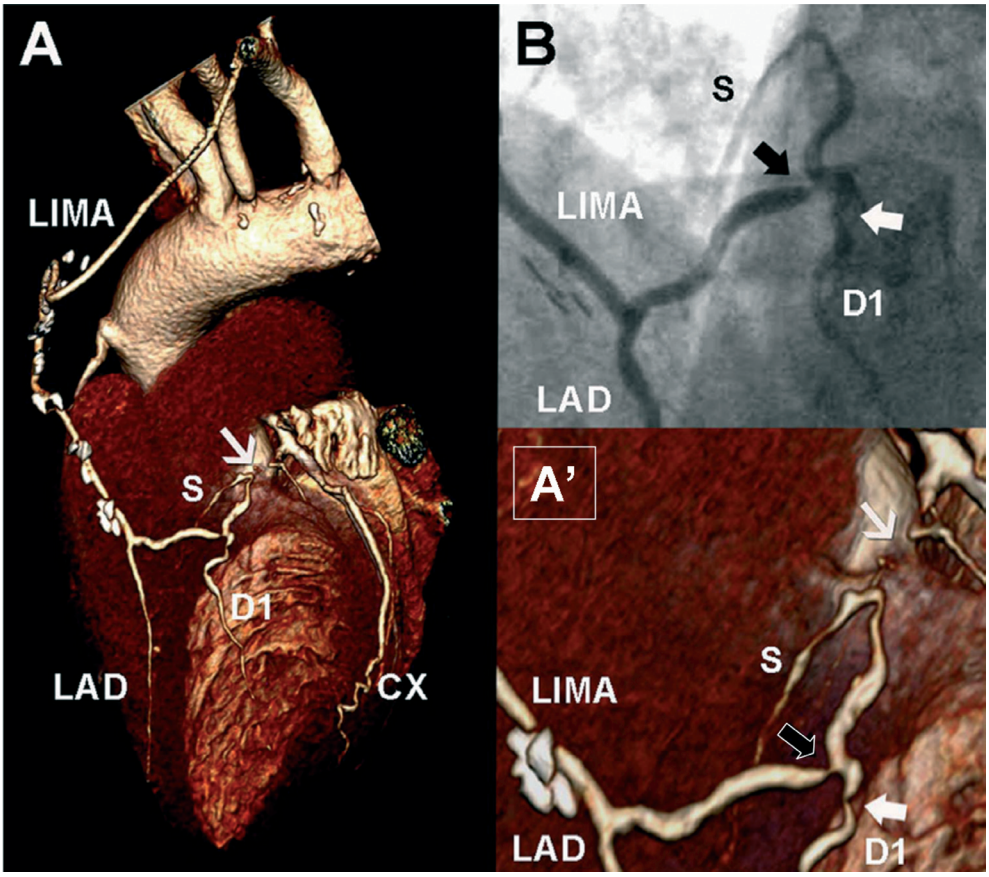

FIGURE 4. 58-year-old man with progressive chest pain and inconclusive stress test. The VRT image (A) shows an occluded proximal left anterior descending coronary artery (LAD, arrow) and a patent LIMA to the distal LAD with a jump to the first diagonal branch (D1). A more detailed view (A', magnification of A) shows a significant stenosis at the anastomosis site of D1 (black thick arrow) with a second significant stenosis in the proximal D1 runoff (white thick arrow). There is retrograde filling of a septal branch (S). The corresponding conventional angiogram (B) confirms the CT findings.

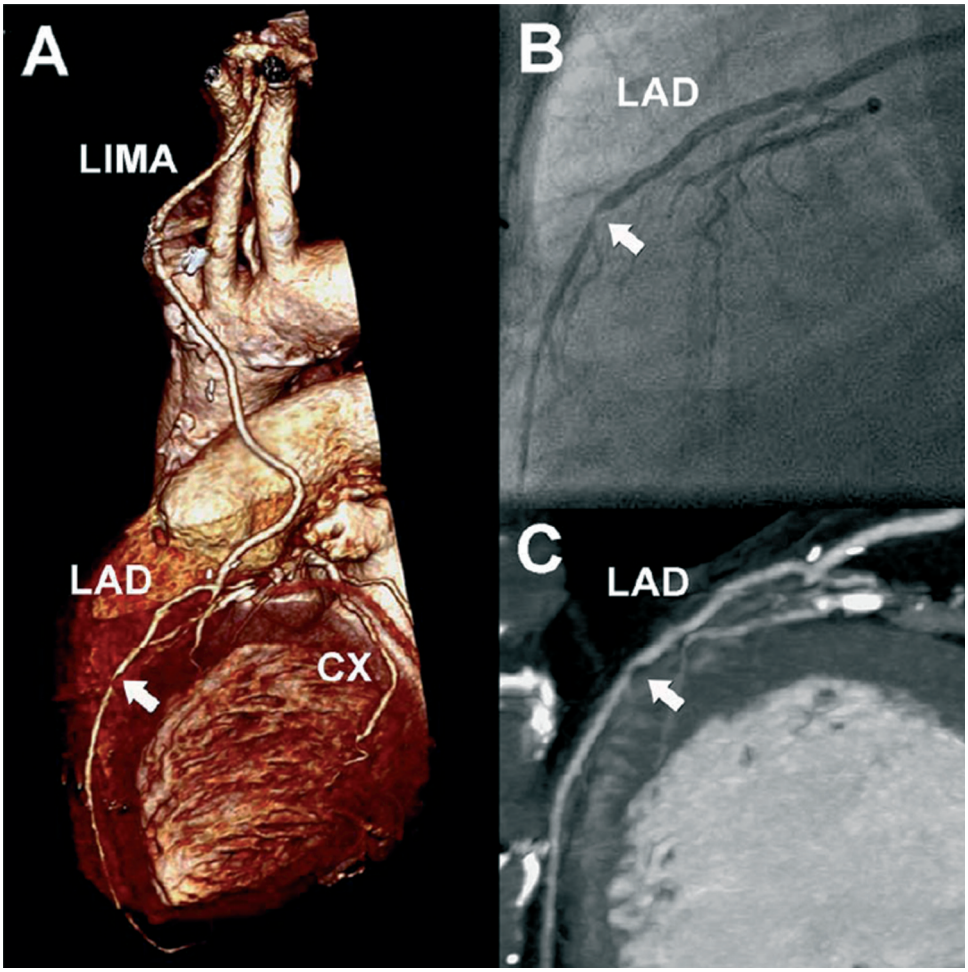

FIGURE 6. 81-year-old man with stable angina pectoris and a positive treadmill test. VRT image (A) shows a patent LIMA to the distal LAD. The proximal LAD is occluded and a lesion is present in the distal runoff (white arrow). The corresponding cMIP image (C) and conventional angiogram (B) confirm the presence of significant stenosis (white arrow).

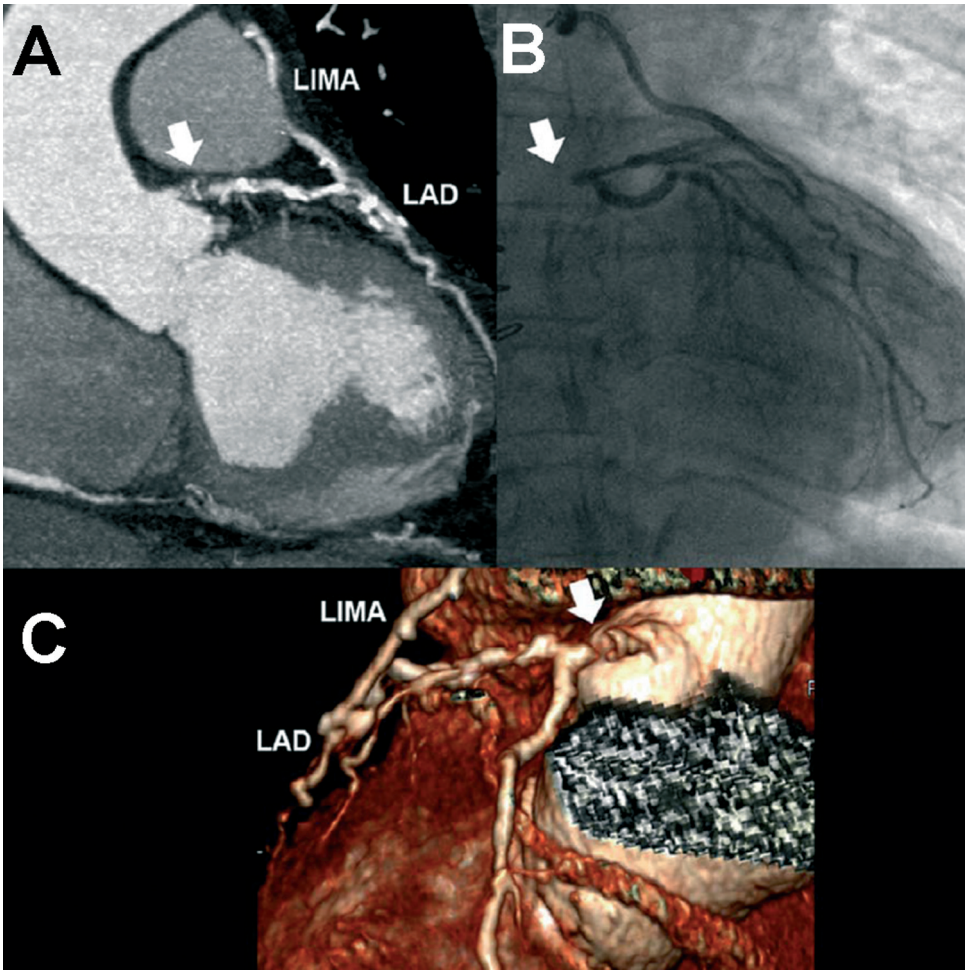

FIGURE 7. 70-year-old woman with typical chest pain and previous myocardial infarction 4 years post CABG. The LIMA and distal runoff vessel are patent. The cMIP (A) and VRT (C) demonstrate a total occlusion of the grafted left main (arrow). The corresponding coronary angiogram (B) confirms the CT findings.